

UNCLASSIFIED

AD **4 5 8 8 5 4**

DEFENSE DOCUMENTATION CENTER

FOR

SCIENTIFIC AND TECHNICAL INFORMATION

CAMERON STATION ALEXANDRIA, VIRGINIA



UNCLASSIFIED

DISCLAIMER NOTICE

THIS DOCUMENT IS BEST QUALITY PRACTICABLE. THE COPY FURNISHED TO DTIC CONTAINED A SIGNIFICANT NUMBER OF PAGES WHICH DO NOT REPRODUCE LEGIBLY.

NOTICE: When government or other drawings, specifications or other data are used for any purpose other than in connection with a definitely related government procurement operation, the U. S. Government thereby incurs no responsibility, nor any obligation whatsoever; and the fact that the Government may have formulated, furnished, or in any way supplied the said drawings, specifications, or other data is not to be regarded by implication or otherwise as in any manner licensing the holder or any other person or corporation, or conveying any rights or permission to manufacture, use or sell any patented invention that may in any way be related thereto.

SACRAMENTO PLANT

INVESTIGATIONS OF THE MECHANISMS
OF DECOMPOSITION, COMBUSTION, AND DETONATION
OF SOLIDS

Contract AF 49(638)-851, Supplemental
Agreement No. 4 (64-475)

March 1964 through February 1965

Report 0372-01F

15 March 1965

DDC
MAR 23 1965



458854

CATALOGED BY: DDC
AS AN MO

458854

Report 0372-01F

INVESTIGATIONS OF THE MECHANISMS
OF DECOMPOSITION, COMBUSTION, AND DETONATION
OF SOLIDS

Contract AF 49(638)-851, Supplemental
Agreement No. 4 (64-475)

Period Covered: March 1964 through February 1965

To

Director of Aeronautical Sciences
Air Force Office of Scientific Research
Air Research and Development Command
United States Air Force
Washington, D. C.

Aerojet-General Corporation

PREPARED BY:


F. J. Cheselske
Principal Investigator

APPROVED BY:


C. J. Strickler
Program Manager, Advanced Propellants
Solid Propellant Research Division

This is the final report of technical progress accomplished under this
program and is submitted in fulfillment of the contract.

OSR Project No. 9750, Task 37501
ARPA Order No. 24-60, Project No. 4759

Report 0372-01F

PREFACE

The Aerojet-General Corporation has for several years been engaged in fundamental research dealing with the mechanisms of decomposition, combustion and detonation of solids. During the 1958-1959 period, these subjects were studied separately under Contracts AF 49(638)-573, AF 49(638)-566, and Nonr 2804(00), respectively. Since these programs were interdependent, they were combined into a single study under Contract AF 49(638)-851. This report describes the important results of these studies which have been carried out during the period from February 1960 to February 1965, and is submitted in partial fulfillment of the contract.

Report O372-01F

ABSTRACT

This report summarizes the results of research on the mechanisms of decomposition, detonation and combustion of solids.

Extensive kinetic studies have been made on 1) linear surface regression rates of solid high explosives (TNT, RDX, etc.), 2) sublimation of ammonium halides, 3) thermal decomposition of anhydrous perchloric acid, and 4) apparent flame strength measurements on NH_3 with O_2 , Cl_2 , NO and N_2O in the opposed-jet diffusion flame reactor.

Preliminary phenomenological studies have been carried out on the decomposition of pure or nearly pure single crystals of ammonium perchlorate.

Theoretical studies were made on reactions in opposed-jet diffusion flames. New models were developed to explain extinction phenomena in solid rocket motors and a low pressure deflagration limit (P_{DL}).

Report O372-01F

TABLE OF CONTENTS

	<u>Page</u>
I. Introduction and Summary	1
II. Technical Discussion	4
A. Mechanism of Detonation Processes	4
1. Introduction and Background	4
2. Summary of Results	8
B. Mechanism of Decomposition of Solids	9
1. Introduction	9
2. Sublimation of Ammonium Halides	10
3. Decomposition of Single Crystals	12
C. Mechanism of Combustion: Reaction Processes in Combustion of Propellants Containing Ammonium Perchlorate	17
1. Reaction Processes in Combustion of Solid Propellants	17
2. Thermal Decomposition of Anhydrous Perchloric Acid Vapor	24
3. Opposed-Jet Diffusion Flame Studies	26
III. Recommendations for Future Work	54
IV. Project Personnel	54
V. Publications	55
References	56

Report 0372-01F

Figure List

	<u>Figure</u>
High Pressure Pyrolysis Apparatus	1
Ammonium Perchlorate Microscopic Decomposition	2
Crystal No. 1 - Original Surface Before Heating 1000X Bright Field	3
Crystal No. 1 - Surface After Heating for 30 Minutes at 190°C. Same areas as Figure 3. 1000X Bright Field	4
Crystal No. 1 - After Heating for 90 Minutes at 190°C. Same area as Figure 3. 1000X Bright Field.	5
Crystal No. 2 - After Heating for 15 Minutes at 220°C. 1000X Bright Field.	6
Crystal No. 2 - After Heating for 45 Minutes at 220°C. 1000X Bright Field	7
Crystal No. 3 - After Heating for 9 Minutes at 250°C. 1000X Polarized Light	8
Distribution of Major Gaseous Products From the Deflagration of One Mole of Solid Ammonium Perchlorate	9
Decomposition of Perchloric Acid at 200°C	10
Reactor for Study of $\text{HClO}_4\text{-NH}_3$ Flames	11
Flow Reactor System	12
Conditions of Opposed-Jet Reactions Between HClO_4 and NH_3	13
Opposed-Jet Reactor System	14
Ammonia - Oxygen Diffusion Flame at Extinguishment	15
Reaction Conditions for Opposed-Jet Flames Between Ammonia and Oxygen	16
Ammonia-Oxygen Flames	17
Reaction Products From Ammonia-Oxygen Flames	18
Stoichiometry of the Ammonia-Oxygen Flame Reaction in the Opposed-Jet at Extinguishment	19

Report 0372-01F

Figure List (Continued)

	<u>Figure</u>
Reaction Conditions for Opposed-Jet Flames Between Ammonia and Chlorine	20
Ammonia-Chlorine Flames	21
Reaction Products From Ammonia-Chlorine Flames	22
Ammonia-Oxygen-Chlorine Flames, AFS, Laminar Flow	23
Ammonia-Oxygen-Chlorine Flames	24
Reaction Conditions for Opposed-Jet Flames Between Ammonia and Nitric Oxide	25
Ammonia-Nitric Oxide Flames	26
Reaction Products From Ammonia-Nitric Oxide Flames (Mass Spectrographic Analyses)	27
Reaction Conditions for Opposed-Jet Flames Between Ammonia and Nitrous Oxide	28
Ammonia-Nitrous Oxide Flames	29
Reaction Products from Ammonia-Nitrous Oxide Flames (Mass Spectrographic Analyses)	30
Reaction Conditions for Opposed-Jet Flames Between Ammonia and Nitrogen Dioxide	31
Ammonia-Nitrogen Dioxide Flames	32
Opposed-Jet Reaction Parameters for Ammonia at 1 Atmosphere Pressure	33
Ammonia Oxidation in Opposed-Jet Diffusion Flames (Summary of Results)	34

APPENDICES

	<u>Appendix</u>
Surface Rate Processes and Sensitivity of High Explosives	A
Rate of Sublimation of Ammonium Halides	B

Report 0372-01F

APPENDICES (Continued)

Appendix

Analysis of the Sublimation of Ammonium Halides	B-2
Kinetics of the Decomposition of Anhydrous Perchloric Acid	C
On the Extinction of Opposed-Jet Diffusion Flames: A Physical Criterion for Extinction	D
A Model for Low Pressure Extinction of Solid Rocket Motors	E
Implications of a Steady-State Solid Propellant Combustion Model to a Low Pressure Deflagration Limit	F
List of Pertinent Publications	G

Report 0372-01F

I. INTRODUCTION AND SUMMARY

Over the past several years, Aerojet-General Corporation has been engaged in fundamental studies dealing with the mechanisms of decomposition, combustion and detonation of solids. The objective of these studies has been to advance the understanding of the kinetics of solid phase reactions and the mechanism of deflagration and detonation. These investigations have led to significant advances and a continual increase in our understanding of the processes of evaporation sublimation, decomposition of solids and combustion of propellants. A number of technical notes and publications have resulted from these and related studies. Much of this work has been summarized in contributions which appear at the end of the report.

This report is concerned with a discussion of essentially all phases of the studies mentioned above, and, in addition, with the mechanisms of the gas-phase reactions deemed important to ammonium perchlorate deflagration.

Rates of linear surface regression of TNT, RDX, tetryl and PETN were studied by means of the (hot-plate) linear pyrolysis technique. The primary surface process appeared to be an endothermic melt-flow, which, when used as a measure of surface heat dissipation, correlated well with measured values of impact sensitivity.

Extensive studies of the rates of sublimation of the ammonium halides were carried out using two different experimental techniques - isothermal weight loss (quartz balance) and the hot-plate pyrolysis method. The results were in fair agreement with the Schults-Dekker mechanism for ammonium halide sublimation.

Report 0372-01F

Preliminary phenomenological studies were carried out on the thermal decomposition of single crystals of ammonium perchlorate using continuous microscopic observation and metallographic techniques. The results tend to corroborate the postulate concerning the decomposition of the intermosaic structure.

An overall reaction scheme (based upon the work at Aerojet and other laboratories) has been proposed for ammonium perchlorate deflagration.

It has been found that NH_3 catalyzes the thermal decomposition of anhydrous perchloric acid, and is believed to have important implications in connection with ammonium perchlorate deflagration.

An extensive investigation has been made on the thermal decomposition of anhydrous perchloric acid. The results indicate that the decomposition does not take place by a simple reaction scheme. Initially the reaction occurs by a mechanism which is second-order in perchloric acid, and, after 50% reaction, a first order mechanism is rate controlling. Both mechanisms were sensitive to surfaces. Water has been found to inhibit the first-order reaction on Pyrex surfaces. A hydrated Cl_2O_7 species has been postulated as the activated complex for the second-order reaction.

Experimental studies have been carried out on NH_3 oxidation by O_2 , Cl_2 , NO and N_2O in the opposed-jet diffusion flame reactor. Apparent flame strength measurements indicate the order of reactivity at 1 atmosphere pressure is $\text{N}_2\text{O} > \text{O}_2 > \text{Cl}_2 > \text{NO}$. However, overall reaction orders (pressure dependencies) of these flame reactions are $\text{Cl}_2 (2.3) > \text{N}_2\text{O} (2.0) > \text{O}_2 (1.7) > \text{NO} (1.56)$ indicating that at higher pressure, chlorine may govern the rate of heat release if the same reaction mechanism is operative.

Report 0372-01F

Theoretical studies were made on reactions in opposed-jet diffusion flames. A physical criterion for extinction in counter-flow diffusion flames has been developed which differs from that given by Spalding. In the new treatment, maximum reaction rates are determined by means of physical extinction criteria which are imposed on the flame process rather than previous or assumed chemical kinetic information as required by Spalding's treatment.

A model of low pressure extinction of solid rocket motors, involving the coupling of propellant flame kinetics and rocket nozzle exhaust time, has been developed.

Also, the thermal layer treatment of steady-state combustion has been applied to the problem of a low pressure deflagration limit. The hypothesis relating extinguishability and low pressure burning stability to PDL appears to be in satisfactory agreement with the available experimental data.

II. TECHNICAL DISCUSSION

The following discussion briefly summarizes the important results of studies dealing with investigations of mechanisms of detonation, decomposition and combustion which have been conducted under Contract AF 49(638)-851. For more extensive discussions of various phases of this program the reader is referred to the appendices (A through F) at the end of the report. The results of experimental studies on opposed-jet diffusion flames are discussed in greater detail in the body of this section since the publication covering this work was not completed at the writing of this report.

A. MECHANISM OF DETONATION PROCESSES

1. Introduction and Background

The kinetic processes involved in the initiation, deflagration, and (non-ideal) detonation of solid high explosives (e.g., TNT, PETN, RDX, etc.) have never been ascertained with certainty. Experimental and theoretical investigations which have been conducted for many years have yielded sufficient information to enable formulation of hypotheses regarding the interpretation of much observable explosive phenomena. It is only within recent years that these studies have become sufficiently quantitative to allow some definitive elaboration of these hypotheses; however, much of the picture is still highly speculative.

A thorough understanding of the fundamental processes involved in the deflagration and detonation of solid explosives takes on new importance in view of recent interest in such materials as HMX and RDX. Previous studies at Aerojet-General Corporation on such propellant ingredients as ammonium nitrate and ammonium perchlorate have led to significant advances in the knowledge of combustion and detonation of propellants and explosives. It was believed that similar studies on solid high explosives such as PETN,

Report 0372-01F

RDX, TNT, etc., would provide the information needed to elucidate the kinetic processes involved in the combustion and detonation of propellants containing high explosives.

There is strong evidence that, for all conventional high explosives, the initiation process is thermal in origin. Mechanical energy, such as a blow or friction, must be transformed into heat in order to ignite the explosive. Like-wise, the energy of the shockwave preceding a detonation front in a solid explosive is converted into heat by the work the shock does (by compression) on the explosive through which it is moving. On the assumption, then, that the initiation of an explosive is a thermal process, the overall characteristics of the initiation and propagation of detonation in explosives rest upon the balance between the rate of release of thermal energy by chemical reaction, and the rate of loss of energy by gas expansion and thermal conductivity.

The mechanism of detonation in solid explosives may be conveniently considered from two broad aspects--viz., the surface properties and the bulk properties of the explosive. The various possible detonation-reaction mechanisms then include the following:

Grain Burning

- (1) Gaseous diffusion is rate determining.
- (2) Bulk decomposition is rate determining.
- (3) Surface decomposition, evaporation, or sublimation is rate determining.

Unimolecular Bulk Decomposition From Shock Compression

- (1) Unimolecular, first-order, bulk decomposition is rate determining.
- (2) Gaseous diffusion is rate determining.

Report 0382-01F

In the grain burning theory (originally due to Eyring and co-workers, Reference 1), the initiation and propagation of detonation in heterogeneous explosives is considered on a microscopic scale to proceed through a mechanism whereby chemical reaction is induced in and spreads from "hot-spots" produced by localized stress from impact (e.g., shock or mechanical impact). The detonation reaction time (τ) is then given by the equation

$$\tau = \frac{\bar{R}}{Lk_p} \text{ sec} \quad (1)$$

where \bar{R} is the average grain radius of the explosive particles, L is the effective diameter of a molecule on the surface of the grain, and k_p is the specific rate constant of the rate controlling reaction. The detailed mechanism of energy release in the grain burning theory need not be known to evaluate detonation reaction times; it is only necessary to isolate the rate determining step. Eyring and co-workers (Reference 1) concluded that k_p had only a small temperature dependence and thus involved a smaller activation energy than would normally be expected for first- or second-order kinetics. They suggested that a diffusion process, either of heat or matter, was possibly rate controlling. Unfortunately, it has never been possible to numerically calculate k_p with any confidence using this suggestion.

Cook and co-workers (Reference 2) describe a grain burning model in which the rate-controlling kinetics of the reacting surface layer of the explosive particles corresponds to the exothermic bulk decomposition kinetics obtained from low temperature isothermal measurements. In general, reaction times calculated from these data are much greater (by 10 to 50 times) than those estimated from the curved front (Reference 1) and nozzle (Reference 3) theories, which relate detonation reaction times

Report 0372-01F

to observable detonation velocities. Unfortunately, unambiguous experimental absolute reaction times have never been obtained for heterogeneous explosives, and the validity of the various diameter theories is not known.

In contrast to the grain-burning theory of relatively recent origin, the concept of unimolecular first-order bulk decomposition arising from shock compression has been discussed since the early history of detonation studies. It has, for example, long been the accepted mechanism of gaseous detonation. There appear to be at least two reasons why a grain-burning detonation theory need be considered. The first of these is that a particle size influence on the non-ideal detonation characteristics of heterogeneous explosives is almost always observed experimentally. The second reason is that at low-charge densities the detonation shock is relatively weak and can produce but little temperature rise through bulk compression of the explosive.

Evidence that compressional bulk heating is a possible mechanism of propagation of detonation in conventional high explosives has been obtained in investigations at Los Alamos (Reference 4). It was demonstrated that under suitable conditions of initiation, large single crystals of TNT, PETN and tetryl can be made to detonate. The apparent lack of heterogeneity in single crystals thus seems to exclude grain burning in these cases.

The general picture suggesting a grain-burning mechanism for the detonation of low-energy heterogeneous explosives and low-density high-energy explosives, and an unimolecular bulk decomposition mechanism for shock compression of high-density, high explosives appears to be qualitatively consistent with many known experimental facts. However, much of the picture is still highly speculative and additional studies both theoretical and

experimental are needed to clarify the situation.

2. Summary of Results

On this basis of these considerations, the mechanism of detonation studies of low density high explosives (such as TNT, RDX, etc.) carried out on this program were initially based upon a model similar to that proposed for low-energy, low-density granular explosives such as ammonium nitrate (AN) and ammonium perchlorate (AP) (Reference 5). This model incorporated Eyring's grain burning detonation theory and stipulated that the rate controlling reaction in grain-burning detonation was the linear endothermic surface gasification rate of the explosive particles. Thus, the linear pyrolysis rate, B , is considered to be the proper value for Lk_p in Equation 1.

Accordingly, linear pyrolysis (hot-plate) studies were made on the four common high explosives (TNT, RDX, tetryl and PETN) utilizing the high-pressure apparatus shown in Figure 1. The results indicated that over the range of surface heating conditions employed, the rate of linear surface regression was governed by a melt-flow process rather than an evaporative or sublimation process. Therefore, the data were not compatible with the grain-burning detonation model proposed at the outset of this work.

Consequently, a theoretical treatment of steady-state surface melting of materials which are pressed against a heated surface has been developed to explain the experimental hot-plate data for the high explosive strands. The rate of surface regression of the solid strands was attributed to viscous flow in a molten layer which separated the solid strand surface from the hot-plate surface.

Report O372-01F

This theoretical treatment of a viscous flow process at the heated surface of high explosives has made possible a quantitative description of Bowden's concept of hot-spot ignition of explosives by impact and frictional heating. The results of the analyses presented (Appendix A) are consistent with a mechanism for initiation of pure solid high explosives which involves the rate of dissipation of kinetic energy of impact by endothermic surface melting, and not by the melting temperature alone. From the observed energy balance versus temperature relationship, the rate at which kinetic energy can be dissipated by melting is $TNI > Tetryl > RDX > PETN$, which is the order of increasing sensitivity of these explosives. The results demonstrate the importance of melting in determining the initial rate of heating of solid high explosives by external stimuli such as impact and friction.

Also, by means of this treatment and the hot-plate technique, it should be possible to obtain surface melting rates, viscosity-temperature relationships and heats of fusion for materials (ex., high explosives) which are normally unstable in the molten state. Such information could be useful in determining equations of state for such materials.

A detailed discussion of the results of these studies and of their importance to impact sensitivity is presented in Appendix A.

B. MECHANISM OF DECOMPOSITION OF SOLIDS

1. Introduction

This section of the report summarizes the results of studies concerned with the processes involved in the decomposition of solids, with particular emphasis being placed on surface decomposition phenomena. These relatively fundamental studies were designed to serve as forerunners for investigations of the more complex problems associated with the decomposition of solid propellant components.

Report O372-01F

An extensive kinetic study of the sublimation of the ammonium halides has been carried out by means of linear pyrolysis (hot-plate) and bulk heating techniques. The sublimation studies were undertaken to gain fundamental knowledge on prototype ammonium salts with the object of applying such knowledge to the decomposition of oxidizers such as ammonium perchlorate.

In addition, a study of the decomposition of single crystals of solids was undertaken. However, due to a decrease in funding, this phase of the program was dropped before definitive results could be obtained.

2. Sublimation of Ammonium Halides

a. Introduction

Application of the Eyring activated complex theory to sublimation of both molecular and ionic solids by workers at Aerojet (References 6-10) has resulted in a number of significant advances in the understanding of the basic theories of decomposition at solid-gas interfaces. The most recent studies dealing with surface decomposition phenomena involve the rates of sublimation of the ammonium halide series.

The studies of the sublimation of ammonium halides which have been carried out in these laboratories have been of special value in helping to understand the mechanism of evaporative processes which involve endothermic dissociative decomposition.

The rates of evaporation of such solids appear to be characterized by an apparent activation energy which is considerably less than the heat of vaporization, and an apparent accommodation coefficient for evaporation which is approximately 10^{-4} (as compared to 0.1 - 1.0 for many non-dissociative molecular evaporation rates).

Report 0372-01F

Prior to the present studies, a considerable amount of work had been carried out on the rate of sublimation of ammonium chloride; however, two different mechanisms were postulated to explain the sublimation data. In view of the conflicting concepts concerning the sublimation mechanism, studies were initiated with the idea that data on the sublimation of the other ammonium halides might resolve the problem.

b. Summary of Results

The rates of sublimation of ammonium chloride, bromide, iodide and fluoride have been determined by two different experimental techniques over the temperature range of 100 to 600°C, corresponding to an increase in sublimation rate of 10^4 . The two experimental methods employed were the measurement of isothermal rate of weight loss using a quartz spring balance, and the hot-plate linear pyrolysis method. Using these techniques, it was possible to determine linear rates of sublimation ranging from 10^{-6} to 10^{-2} cm/sec. These rates corresponded to a change in surface temperature of approximately 200°C for ammonium fluoride and approximately 400°C for the other three halides.

The unusually low values for the Arrhenius frequency factor and activation energy observed by other investigators for NH_4Cl have been verified in these studies and found to extend to the other halides. In all cases, the measured apparent activation energies were approximately one-third of the heat of sublimation. Except for ammonium fluoride, which has a frequency factor of 10 to 100 times greater than the other halides, the frequency factor increases with increasing molecular weight.

By applying the Schultz-Dekker transition-state treatment of NH_4Cl sublimation, it was possible to calculate linear rates of sublimation which are in reasonable agreement with the experimental results.

A detailed discussion of these studies are presented in Appendix B.

3. Decomposition of Single Crystals

a. Introduction and Analysis

Considerable effort has been expended in many laboratories on studies of the mechanisms of decomposition of ammonium perchlorate (References 11-14). However, it appears that certain abnormal behavior in the crystal still exists which is unexplained.

It has long been assumed that a simple first order transition from orthorhombic to a cubic structure takes place at approximately 240°C (References 13, 14) with ammonium perchlorate. Changes in the decomposition rate at 240°C have been ascribed to the formation of the new cubic structure.

However, investigations at the Aerojet laboratories of the crystal transitions of ammonium perchlorate in the same temperature range by X-ray diffraction techniques suggested that this picture of the crystal transition may be inaccurate. The X-ray data indicated that an irreversible transition occurred at 240°C which was separate and distinct from the reversible orthorhombic-cubic transition which occurs at a higher temperature. At 240°C, it was not possible to show a structural change by X-ray diffraction, although significant intensity changes did appear in the diffractogram. At 270°C, the cubic structure was evident. It disappeared on cooling, returning to the pattern obtained at 240°C. Thus, it appears that the abnormal decomposition behavior of ammonium perchlorate in the neighborhood of 240°C may be caused by an irreversible second order phase transition.

This picture receives some support from the earlier work of Bircumshaw, Newman and Phillips (References 11, 12) who observed that,

Report 0372-01F

although the rate of decomposition of ammonium perchlorate went through a maximum at a temperature slightly below 240°C , there was a continuously decreasing decomposition rate up to temperatures of approximately 250°C . A continuously varying rate would be expected for second order phase transitions. However, first-order structural transitions, such as the orthorhombic to cubic change, should occur sharply, resulting in nearly discontinuous properties. Second order transitions have been observed in other ammonium salts (Reference 15). This type of transition is known to give rise to a specific heat anomaly which would be expected to cause a modification of the decomposition behavior of the solid (Reference 16).

Experimenters who have analyzed the data of ammonium perchlorate decomposition have concluded that the mechanism consists of two steps in which changes in the physical structure of the solid are rate determining. The conclusions of Galwey and Jacobs (References 13, 14) are that the low temperature reaction (to 300°C) represents the decomposition of strained material in intermosaic configurations, while the high temperature reaction represents the decomposition of unstrained material formed by mosaic blocks. They also conclude that the low temperature reaction is confined to the intergranular material, although nucleation occurs at the boundaries of the mosaic blocks from which the reaction grows until all of the intergranular material is consumed.

On the basis of the preliminary findings at the Aerojet laboratories, it was felt that a re-evaluation of the crystal surface processes was needed in order to establish the cause of the variations in decomposition rates which occur in the neighborhood of 240°C for ammonium perchlorate. It was believed possible that a second order phase transition which took place at temperatures below the known structural change was the

real cause of the decomposition rate change.

b. Summary of Results

An experimental program was initiated to study the reaction kinetics of single crystals of oxidizers. Ammonium perchlorate was examined initially in order to develop the necessary experimental techniques without undue hazard; and, of course, because of its importance to the theoretical aspects of the problem.

Relatively large single crystals of ammonium perchlorate were used in these studies and were prepared by means of a temperature-differential technique described by Dreyfus and Levy (Reference 17). Single crystals of AP were decomposed under continuous microscopic observation. A Zeiss Ultraphot II microscope, with a Leitz hot-stage attachment, and a Bausch and Lomb metalograph were used in these investigations. The results of these studies are shown in Figures 2 through 8.

Two views of a decomposing NH_4ClO_4 crystal are shown in Figure 2. This photo shows the orthorhombic-to-cubic transition in a single crystal. It was noted that the transition was accompanied by the appearance of a large number of surface cracks and an apparent sudden increase in surface reaction (i.e., growth of reaction nuclei). The photo on the right (Figure 2) shows the transition in the process of occurring. This is depicted by an irregular boundary line which was photographed as it moved from the top to the bottom of the crystal. The increase in reactivity at this point is in agreement with the postulate concerning the decomposition of the intermosaic structure.

It was anticipated that shadow-cast replica techniques would be required to obtain the necessary detail to study the crystal surfaces at various stages of decomposition. However, metallographic examination gave

Report 0372-01F

sufficient magnification for these studies.

A series of three well-formed crystals was photographed with the Bausch and Lomb metallograph using three magnifications, 100X, 500X, and 1000X. These original pictures were selected in order to show some identifying feature of the crystal surface which could be used as a reference point. Each of the crystals was then heated under vacuum (5×10^{-5} mm Hg), using a Nichrome heating element situated ~ 4 mm above the surface of the crystal. The temperature was determined by a chromel-alumel thermocouple held against the crystal surface by its own tension, and the emf was read on a potentiometer. The crystals were heated according to the following schedule: Crystal No. 1 was heated at 190°C for three separate intervals of 30 min each; Crystal No. 2 was heated at 220°C for three intervals of 15 min each; and Crystal No. 3 was heated at 250°C for three intervals of 3 min each. After each of the heating intervals, the resulting crystal surface was photographed using some unique surface detail to identify the original area.

A study of the completed series of photographs resulted in several generalized observations. The original crystal surfaces were smooth with some wrinkling and showed a number of cleavage planes. This behavior is illustrated in Figure 3. Upon heating, the surfaces changed radically and took on a mottled, amorphous, quasi-liquid appearance, punctuated with numerous very small irregularities (Figure 4).

The observations with each of the crystals may be summarized:

Crystal No. 1 (190°C): An amorphous layer of unknown thickness formed on the surface, appeared to loosen from the crystal substrate, and then separated into many clumps of various sizes, which upon further heating, formed single rhombic crystallites. The larger crystallites

Report O372-01F

grew faster than the smaller ones; after the final heating, the amorphous material was gone, having been replaced by crystalline structures. The entire surface was then covered with individual rhombic crystals. (Figure 5).

Crystal No. 2 (220°C): The same result was noted with this crystal as was described for Crystal No. 1, except that the transition took place more rapidly, being completed within the first heating interval of 15 min. (Figure 6). However, after the last heating period (total heating time, 45 min) the crystallites seemed to degenerate somewhat, and their outlines became less clearly defined (Figure 7).

Crystal No. 3 (250°C): None of the crystallite growth observed at lower temperatures was detected. Continued heating of this crystal only resulted in a darkening and rapid deterioration of the original surface characteristics. After the final heating period, the surface of the crystal exhibited a mottled, appearance lacking in structure (Figure 8). This crystal appeared milky and opaque as contrasted with Crystal No. 1, which was still fairly clear, and Crystal No. 2, which was beginning to appear slightly milky.

These studies indicate the need to determine whether the amorphous layer, which first appears to form on the large crystal surface, is transformed into crystallites or decomposes (or sublimes), leaving behind the observed structures. It is thought that the points on the surface where the tiny crystals form are defect sites, but the cause of the process is still speculative.

To date, these studies have been primarily phenomenological in nature. However, the results obtained thus far clearly show the need for this type of study. It is firmly believed that such data, when compared with kinetic decomposition data for particulate samples of

Report 0372-01F

the same material will help elucidate the decomposition mechanisms involved and the importance of crystal imperfections on rates of reactions in crystalline solids.

This phase of the program was discontinued at this point due to a decrease in funding of the program.

C. MECHANISM OF COMBUSTION: REACTION PROCESSES IN COMBUSTION OF PROPELLANTS CONTAINING AMMONIUM PERCHLORATE

1. Reaction Processes in Combustion of Solid Propellants

a. General Considerations

The fundamental experimental and theoretical studies on solid propellant combustion which have been carried out at Aerojet, as well as in other laboratories, have led to a concept of combustion in which the solid ingredients gasify under the thermal influence of a flame to form reactive species which then undergo gas-phase redox reactions to propagate that flame. The mass-flow and energy of each reaction step in the burning process are of necessity coupled to each other by the conservation equations. Suitable mathematical models of varying complexity have been developed to describe this coupling process, and have been tested with some success against burning rate data for ammonium nitrate (AN) and ammonium perchlorate (AP) composite propellants. In spite of the overall agreement between these mathematical treatments and experimental burning rate data, relatively little headway has been made in predicting, by one of these models, the effects of specific propellant binders and additives on the combustion properties. In this connection, the failure of the models is due primarily to the lack of information on the specific chemical reaction mechanisms which give rise to the burning process, and the attendant kinetic data under burning conditions.

The primary purpose of the combustion research being carried out under the present contract is the study of the chemical

Report O372-01F

reactions which are deemed important in determining the burning properties of solid propellants. The basic problems associated with such an approach are essentially three-fold, viz;

- 1) the design and analysis of experiments to elucidate the chemical nature of the combustion process;
- 2) the development of experimental and theoretical methods suitable for obtaining the necessary specific reaction rate data;
- 3) the development and testing of mathematical combustion models based upon the proposed chemical mechanisms.

These problems must be attacked simultaneously since, more often than not, the advances made in each problem area are interdependent. Also, the relatively unusual reaction conditions (e.g., high pressure and temperature, surface heating, etc.) have often required the examination of the applicability of the existing basic theories of reaction rates themselves.

The progress made at Aerojet towards the goals of the present contract (and its predecessors) is well documented in various reports and publications (see Appendix G), particularly in the area of the nature of the solid phase reactions and their relationship to the burning rates of AN and AP composite propellants. More recently, research efforts have delved in greater detail into the kinetics of the gas-phase redox reactions which give rise to the flame processes near the burning propellant surface. It is believed that the effects of pressure, binders and other additives on propellant burning are due primarily to changes in the specific rates and/or nature of these redox reactions. Considerable progress has been made in elucidating the nature of some of these gas-phase reactions, and in developing techniques for determining

Report 0372-01F

their kinetics under flame conditions. At present, particular emphasis is being placed on reactions involving ammonia and oxidizers of the chlorine-oxygen and nitrogen-oxygen types. These advancements are discussed in a following section.

The following sections are devoted to a discussion of the concepts behind the formulation of the current program of research and the pertinent results of the work completed on the contract.

b. Solid Propellant Combustion Model

The combustion model taken is that developed at Aerojet, and is based upon the concepts of the two temperature postulate and thermal layer theory of propellant combustion.* These concepts have been described extensively in the literature (21, 22, 23) and are summarized in Section II in Appendix F.

Briefly, it is believed that the major surface reaction processes in AP propellant combustion involve the gasification of ammonium perchlorate to gaseous HClO_4 and NH_3 , which then undergo a rapid exothermic redox reaction resulting in a primary flame close to the oxidizer surface (within a distance of about 100μ). This flame zone is essentially the thermal layer. Under the influence of this redox flame, the polymeric binder in the vicinity of the oxidizer vaporizes (probably by a surface thermal degradation process) and diffuses away from the surface. The reaction between the pyrolysis products of the binders and the oxidizer redox flame

* This model is somewhat at divergence with the Granular Diffusion Flame model of Summerfield (Reference 18). However, it is in accord with the model of ammonium perchlorate strand deflagration described by Friedman (Reference 19) and with the model Vandekerckhove (Reference 20) has used in describing resonant burning.

is diffusion controlled, and its influence upon the propellant burning rate depends upon the extent of diffusion into the thermal layer. It is possible that at elevated pressures (>100 psi), most of the binder oxidation occurs too far from the oxidizer particle surface to influence the surface temperature gradient to any significant degree. However, at lower pressures this does not appear to be the case.

The effect of pressure on the rate processes has been considered to be two-fold: (1) to change the rate of the $\text{NH}_3\text{-HClO}_4$ gaseous redox reactions; (2) to alter the rate of diffusion of the binder and oxidizer pyrolysis products.

It is evident that the role of burning-rate catalysts could be to increase the rate of the $\text{NH}_3\text{-HClO}_4$ redox reaction. Thus, it appears that the rates of surface decomposition of solid oxidizer and polymeric binder; the rates of reaction of HClO_4 with NH_3 and binder degradation products; and the rates of diffusion of binder and oxidizer gases are the basic parameters which define the propellant burning characteristics.

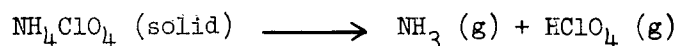
Much of the recent research on the present contract has been devoted to a study of the rates of the oxidizer gas-phase reactions.

c. Surface Decomposition of Ammonium Perchlorate

Utilizing the hot-plate linear pyrolysis technique, the linear rate of surface decomposition, B , for ammonium perchlorate has been reported to be:

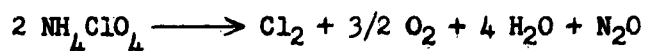
$$B = 4600 \exp(-22000/RT_s) \text{ cm/sec}$$

corresponding to a sublimation process,



B is the linear regression rate of the surface measured as a function of surface

temperature, T_s . The sublimation process probably involves a proton transfer at the solid surface followed by desorption of HClO_4 and NH_3 from the surface. Upon combustion of the ammonium perchlorate, rapid decomposition of the HClO_4 occurs (catalyzed by NH_3) making the above reaction irreversible. Preceding the surface evaporation, partial decomposition ($\sim 30\%$) by the following exothermic solid-phase reaction occurs (References 24, 25, 26, 27):



This reaction is believed to occur by means of an electron transfer process in the so-called intermosaic (defect lattice) material, and results in an apparent lowering of the endothermicity of the overall surface sublimation. The extent to which the intermosaic reaction affects the ammonium perchlorate deflagration rate has yet to be studied.

d. The Gaseous Reaction of Ammonia With Perchloric Acid

The experimental study of the reaction between NH_3 (g) and HClO_4 (g) is severely complicated by the highly reactive nature of the system, even at low temperature and pressure. Early exploratory studies under Contract AF 49(638)-566 demonstrated that NH_3 (g), at initial gas temperatures as low as 25-40°C, could be oxidized to NH_4Cl almost instantaneously upon admixture with HClO_4 . The same result was found to occur in attempts to establish an $\text{NH}_3 + \text{HClO}_4$ flame in the opposed-jet reactor. The solid product NH_4Cl can be explained by the decomposition of HClO_4 to Cl_2 followed by oxidation of NH_3 by Cl_2 to NH_4Cl (g) + N_2 . These exploratory studies led to an intensive study of the isothermal decomposition of HClO_4 at temperatures as high as 250°C (Appendix C).

A salient feature of the isothermal decomposition studies was the relatively slow rate of decomposition of HClO_4 as compared with

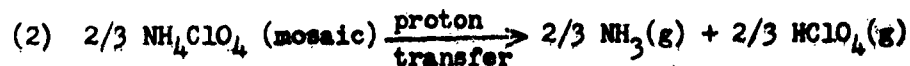
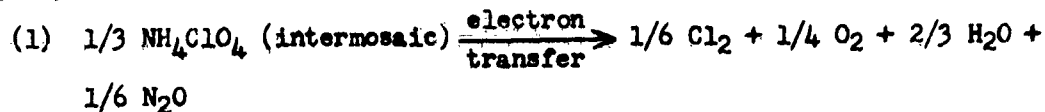
Report O372-01F

the rapid NH_3 oxidation reaction. However, it was observed (Reference 28) that the sudden addition of ~10 mole % of NH_3 to slowly decomposing pure HClO_4 ($T = 230^\circ\text{C}$) caused the reaction to become vigorous and led to a rapid decomposition. Thus, it would appear that small amounts of NH_3 "catalyze" the HClO_4 decomposition at elevated temperatures. This observation has important implications in connection with the AP deflagration reaction mechanism which is proposed in the following section.

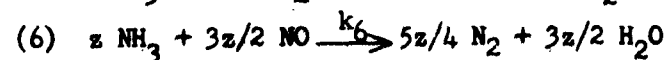
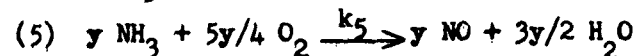
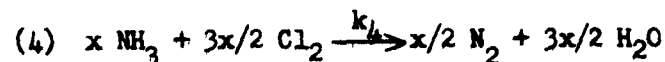
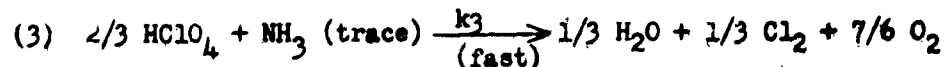
e. A Proposed Reaction Scheme for Solid Ammonium Perchlorate Deflagration

The available information on ammonium perchlorate decomposition, its deflagration products and the reactions of NH_3 with HClO_4 , O_2 and Cl_2 , which has been accumulated by Aerojet and others agrees with the following proposed reaction scheme which is based upon the burning of one mole of NH_4ClO_4 (solid):

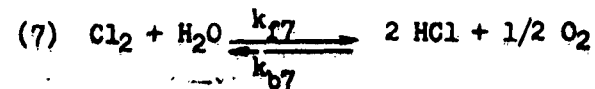
Solid Phase

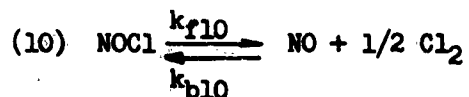
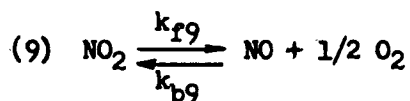
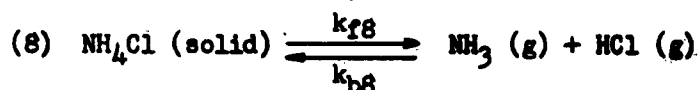


Gas Phase (Irreversible)



Gas Phase (Reversible) - Reactions are written so that high temperature favors the right hand side.



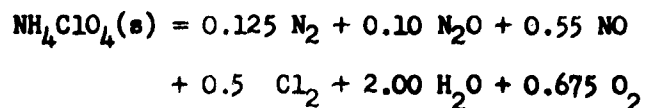


It may be seen from this scheme that the gas phase oxidation of ammonia involves the competing reactions (4) through (6), with the reversible reactions (7) through (10) acting as buffers to control the concentrations of reactants and products.

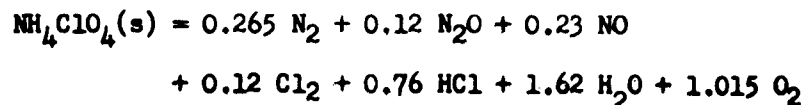
It should be pointed out that the total amount of NH_3 (g) available for oxidation by this scheme is only $2/3$ mole per mole of NH_4ClO_4 (i.e., $x + y + z = 2/3$). Inasmuch as the only source of NO considered is reaction (5), this sets an upper limit to the amount of NH_3 (g) that can be oxidized by reaction (6) (i.e., $Z_{\text{max}} = 2y/3 = 4/15 - 2x/5$).

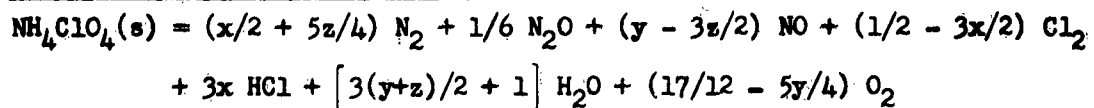
It is interesting to compare the distribution of deflagration products which would be expected by summing reactions (1) through (6) in the above reaction scheme, with the distribution determined by J. Levy and R. Friedman (Reference 19) from sampling measurements on burning strands of solid ammonium perchlorate. Their results at 1 atm and 70 atm pressure applied to the sum of reactions (1) through (6) above gives:

1 atm ($T_f = 1240^\circ\text{K}$)



70 atm ($T_f = 1260^\circ\text{K}$)



Sum of Reactions (1) through (6)

By assuming values for x and z to match the experimental values of HCl and N_2 , it is possible to calculate the remaining product distribution. The results of these calculations, shown in Figure 9, are in striking agreement with the experimental values.

It is evident from the preceding discussion that the proposed reaction scheme has afforded a good deal of insight into the nature of AP propellant combustion, and that there is growing evidence that the overall kinetic behavior of the $\text{NH}_3\text{-HClO}_4$ redox flame reaction is governed by at least two, and perhaps three competing ammonia oxidation reactions, viz; by O_2 , Cl_2 and NO . Thus, the kinetics problem of determining the rate of heat release near a burning oxidizer surface would involve the determination of the parameters in the expression

$$\dot{Q}_+ = \sum_i k_i H_i [\text{NH}_3]^{a^i} [X_i]^{b^i} \quad (2)$$

where \dot{Q}_+ = the volumetric rate of heat release

i refers to the various ammonia oxidation reactions.

X_i is the oxidant of the i^{th} reaction.

H_i = the heat of i^{th} reaction per mole of NH_3 consumed.

k_i = the specific rate constant of the i^{th} reaction.

$a^i + b^i$ = the overall reaction order of the i^{th} reaction.

2. Thermal Decomposition of Anhydrous Perchloric Acid Vapor

a. Introduction

Under Contract No. AF 49(638)-566 a brief attempt was made to study the reaction between ammonia and perchloric acid in a static

Report 0372-01F

system. The reaction occurred too rapidly to obtain rate data even at low temperatures (25 - 40°C) and pressures. Mass spectrographic analysis of the reaction products indicated that decomposition of the perchloric acid probably played an important part in the reaction. For this reason, a study of the kinetics of the thermal decomposition of gaseous, anhydrous perchloric acid was undertaken. Work on this phase of the program was initiated under Contract AF 49(638)-566 and has been completed under the present Contract, AF 49(638)-851.

b. Experimental

The decomposition of anhydrous perchloric acid samples was studied between 165° and 250°C using two types of systems. In one, acid samples were decomposed in an all-glass apparatus immersed in an opaque oil bath and pressure changes, indicated by a glass Bourdon gage and a pressure balancing system, were used to follow the rate of the reaction. A second system allowed an intermittent determination of chlorine concentration by use of a photoelectric colorimeter while simultaneous pressure readings were obtained.

In the course of these studies, the effects of a wide variation in initial perchloric acid pressure were studied; pressures between 8 and 280 mm were used. In addition, the surface-to-volume ratio in the reactors were varied between 1.7 and 12 cm²/cm³ by the addition of Pyrex beads, in selected experiments. (See Appendix C for details.)

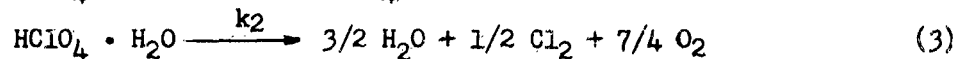
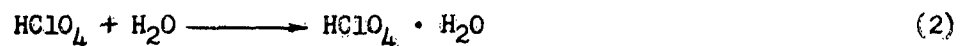
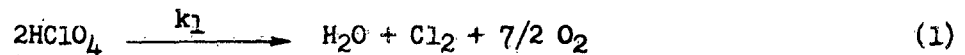
c. Summary of Results

The experimental data indicated that the decomposition of anhydrous HClO₄ does not take place by a simple reaction scheme. Initially the reaction occurs by a mechanism which is second-order in perchloric acid. However, after approximately 50% of the acid has been destroyed, a first-order mechanism is rate controlling. Both reaction mechanisms were found to be

Report 0372-01F

extremely sensitive to the presence of surface, whether added or the original reactor walls.

The amount of chlorine evolved was found to be directly proportional to the amount of decomposed acid at all times. By use of a Runge-Kutta Gill program on an IBM 7090 computer system a demonstration of the fit of the data to the reactions



has been carried out. A portion of the results of such computations are compared to experimental data in Figure 10.

The rate of reaction (3) on the Pyrex surface is inhibited by one of the reaction products, almost certainly, water. Apparent activation energies of 13.4 and 33.8 Kcal/mole were obtained for reactions (1) and (3), respectively, where the latter value takes into account the heat of adsorption of water. A hydrated Cl_2O_7 species has been postulated as the activated complex for reaction (1). It is believed that a competitive adsorption mechanism best satisfies the requirements of the data on reaction (3). See Appendix C for a detailed discussion of this work.

3. Opposed-Jet Diffusion Flame Studies

a. Introduction

The study of gas phase reactions between reactive gaseous species associated with the combustion of solid composite propellants has been handicapped, until recently, by the lack of a suitable technique which could be employed at flame temperatures. The development of the opposed-jet reactor by Potter and Butler (Reference 29) makes possible the study of highly

Report O372-01F

reactive components such as those which are desorbed from the surface of a subliming or decomposing surface of a solid propellant. An analysis of this type of experiment has been made by Spalding (Reference 30) who, within the limits of a set of simplifying assumptions, has shown the relationships between chemical kinetic theory and the flame properties measured by the opposed-jet diffusion flame reactor. Pandya and Weinberg (Reference 31) have demonstrated the use of the technique to study temperature distributions across flat, premixed flames to make possible the measurement of heat release rates.

Earlier theoretical studies by Zeldovich (Reference 32) and by Spalding (Reference 33) demonstrated the existence of a fundamental property of diffusion flames which could be made the basis of a combustion measurement. These workers showed that when the flow of fuel and oxidant into the reaction zone of a diffusion flame exceeded a critical value the chemical reaction could not keep pace and the reaction ceased. In the opposed-jet technique, the mass flows of fuel and oxidant are increased until the critical flows are reached at which the flame is extinguished in a region surrounding the jet axis. Potter, et. al. (References 29, 34, and 35) defined the highest mass flow rate at which the flame remained unbroken as the "apparent flame strength." This value was obtained from the average of the sum of the mass flows of fuel and oxidant divided by the cross sectional area of the jet so as to give a value of the mean mass flow per unit area. This result, when multiplied by the theoretical ratio of axis to mean flow velocity (2.0), gave the mass flow rate per unit area at the jet axis.

During the current contract period, the opposed-jet technique was used to determine the apparent flame strength of several of the reactions deemed important in the combustion of solid composite propellants containing ammonium perchlorate. These results are described in subsequent sections.

b. Theory of the Opposed-Jet Diffusion Flame Reactor

In this section, the results of the theory of extinguishment of diffusion flames supported from opposed-jets will be outlined. Spalding (Reference 32) has developed a mathematical theory which shows the relationships between the fluid mechanic, mass transfer and chemical kinetic factors of the opposed-jet reactor system.

As a basis for this development, it was assumed that jet diameters, gas density and gas velocity of the oxidizer and fuel streams are equal. (A parallel theoretical development appears required for variations in gas density and velocity, if this technique is to achieve maximum value). Using as a model the impingement of an inviscid fluid jet on a flat plate, the solution of the equation of motion of the gas stream requires that a flat flame be obtained in which the flame thickness is not greater than 0.2 D. D is the diameter of the jet approaching the impingement zone. The diagram shown on the next page indicates the situation between the jet nozzles.

Applying the mass conservation principle to the impingement region, it was possible to solve for the flame location and the burning rate in the flame. The position of the flame was defined by

$$f_{\text{stoich}} \equiv \frac{m_{\text{ox},-\infty}/r}{m_{\text{fu},\infty} + m_{\text{ox},-\infty}/r} = 1/2 \left[1 + \text{erf}(Y_{\text{stoich}} \sqrt{R_{\infty} U / \gamma_{\infty} D}) \right] (3)$$

where $m_{\text{ox},-\infty}$ = the mass fraction of the oxidizer in the oxidizer stream

$m_{\text{fu},\infty}$ = the mass fraction of the fuel in the fuel stream

r = the mass of oxidizer consumed per unit mass of fuel

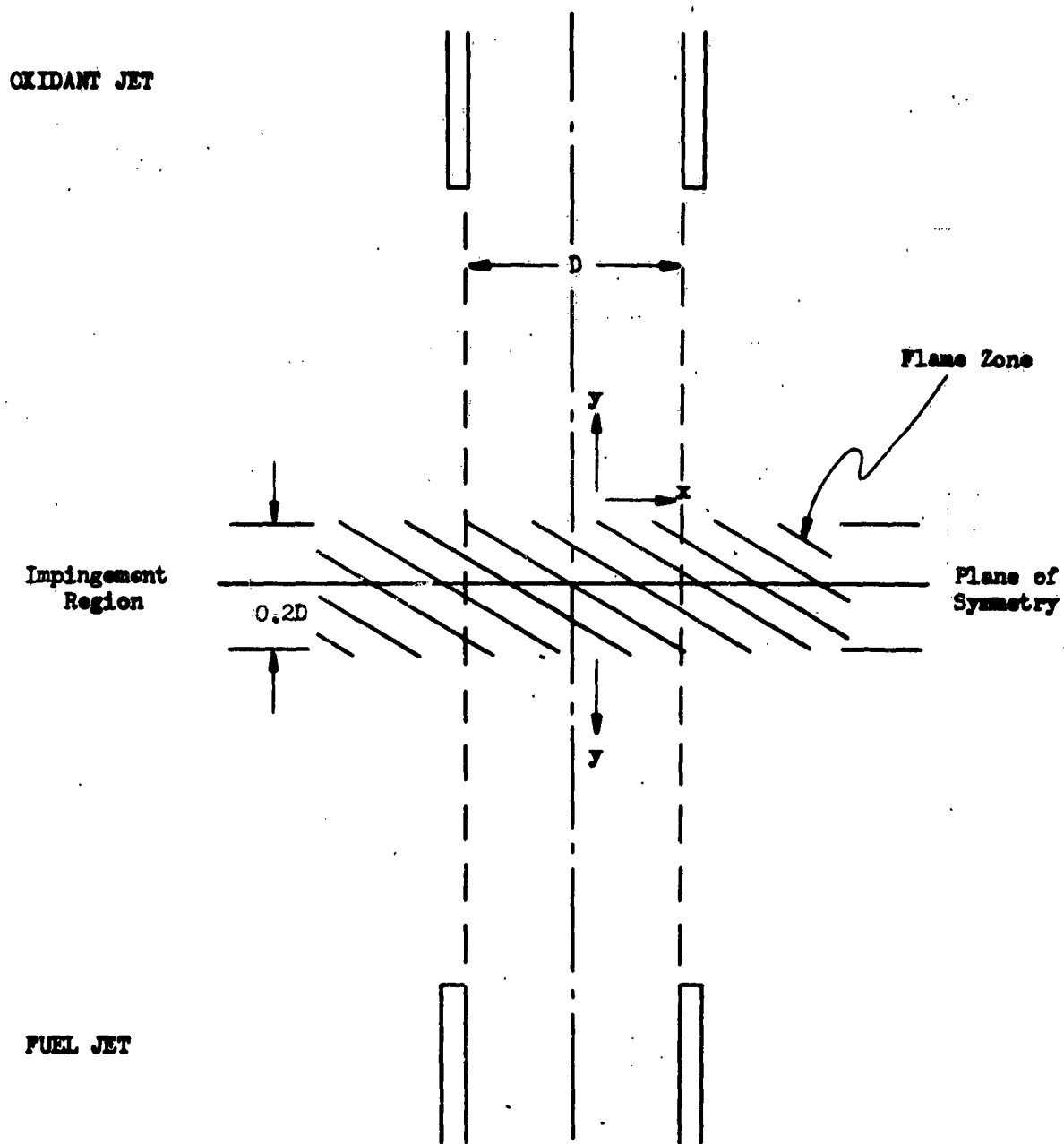
R_{∞} = the fuel gas density

U = the jet velocity approaching the impingement area

γ_{∞} = the exchange coefficient (defined as the thermal conductivity of the mixture divided by the specific heat at constant pressure)

MODEL OF OPPOSED-JET SYSTEM (Spalding)

Axis of Symmetry

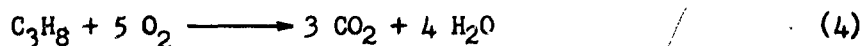


In this figure: D = The diameter of the jet approaching the plate
 x = The radial distance from the axis of symmetry
 y = The distance from the plane of symmetry to the fuel jet
 U = The velocity in the jet approaching the plate

and Y_{stoich} = the distorted distance along the y axis which indicates the location of the flame under stoichiometric conditions.

Values of $Y \sqrt{\rho_{\infty} U / \gamma_{\infty} D}$ against f_{stoich} have been computed and are available for use.

Thus, computation of f_{stoich} , the mass fraction of material derived from the fuel stream at stoichiometry permits the determination of the flame coordinate, $Y_{\text{stoich}} \sqrt{\rho_{\infty} U / \gamma_{\infty} D}$. For example, for a propane-air system where the following reaction is assumed:



$$r = 3.63 \text{ lb oxygen/lb propane}$$

$$m_{\text{ox}, -\infty} = 0.222$$

$$m_{\text{fu}, \infty} = 1.0$$

and $f_{\text{stoich}} = 0.057$

The resulting value of $Y \sqrt{\rho_{\infty} U / \gamma_{\infty} D} \approx -1.0$ indicates that the flame lies well on the oxidant side of the stagnation point.

The burning rate in the flame, Ω can be defined in terms of the mass fraction f , of material derived from the fuel stream which is present in the local mixture.

$$\Omega_{\text{stoich}} = \left\{ \frac{\dot{m}_{\text{fu}}}{m_{\text{fu}, \infty} \rho_{\infty} U} \right\} \sqrt{\frac{D \rho_{\infty} u}{\gamma_{\infty}}} \frac{\exp\left(-\frac{\rho_{\infty} U}{\gamma_{\infty} D} Y_{\text{stoich}}^2\right)}{1/2 (1 - f_{\text{stoich}})} \quad (5)$$

Ω is defined by Equation (3) and by

$$\Omega = \frac{\exp\left[-\frac{\rho_{\infty} U Y^2}{\gamma_{\infty} D}\right]}{\pi^{1/2} (1 - f)} \quad (6)$$

where \dot{m}_{fu} is the mass burning rate of the fuel per unit area of diffusion flame and the other terms have the meanings indicated above.

Values of Ω have also been computed as a function

of f and are available.

The chemical kinetic aspects of the theory have been obtained by solution of the differential equation for the fuel concentration m_{fu} :

$$\rho v \frac{dm_{fu}}{dy} - \frac{d}{dy} \left(\gamma \frac{dm_{fu}}{dy} \right) = \dot{m}_{fu}''' \quad (7)$$

v = the velocity of gas in the y direction

where \dot{m}_{fu}''' = the rate of creation of the fuel by chemical reaction per unit volume. Other notation remains as indicated previously.

The volumetric reaction rate \dot{m}_{fu}''' is a function only of the reactants, pressure, local temperature and the local mass fractions of fuel and oxidant, provided that the chemical reaction is a single step or proceeds by specified classes of chain reactions (Reference 36).

Employing a variable change, the rate expression may be put in the following form:

$$\frac{d^2 m_{fu}}{df^2} = \Lambda \frac{\Psi}{(1-f)^2 \Omega^2} \quad (8)$$

$$\text{where } \Lambda \equiv \frac{DR_{\max}}{\rho_{\infty} v} \quad (9)$$

In these equations,

$R_{\max} = R(f, m_{fu})$ is the maximum rate of consumption of fuel at extinction

Ψ = a non-dimensional reaction rate defined as R/R_{\max}

Numerical integration of Equation (8) to obtain the lowest value of Λ under the restraint that Λ must approach unity, gives the extinction coefficient of the flame. The value of Λ depends on the activation energy of the reaction, reaction order and the values of f in the originating jets.

The value of Λ_{\min} when applied to Equation (9)

permits the calculation of R_{\max} from the jet velocity at extinction, U_{ext} .

Thus, the relationship between U_{ext} and R_{\max} depends uniquely on chemical properties.

It can now be shown that the extinction condition takes the form

$$\frac{\rho_{\infty} U_{\text{ext}}}{DR_{\max}} \approx \frac{2\Psi_{\text{stoich}} f_{\text{stoich}}}{\Omega_{\text{stoich}}^2 m_{\text{fu}, \infty}} \quad (10)$$

Applying the Zeldovich, Frank-Kamenetsky approximation:

$$m_{\text{fu}, \infty} f_{\text{stoich}} G \approx \sqrt{2 \int_0^{m_{\text{fu}, \infty} f_{\text{stoich}}} \gamma_{\text{fu}}^{\text{fu}} dm_{\text{fu}}} \quad (11)$$

where G is the mass flux normal to a laminar, premixed flame propagating through a stoichiometric mixture formed from the fuel and oxidant stream.

$$\text{Then, } m_{\text{fu}, \infty} f_{\text{stoich}} G \approx \sqrt{2 \gamma_{\infty} m_{\text{fu}, \infty} f_{\text{stoich}} \Psi_{\text{stoich}} R_{\max}} \quad (12)$$

Eliminating $\Psi_{\text{stoich}} R_{\max}$ from Equation (10)

$$\frac{\rho_{\infty} U_{\text{ext}} D}{\gamma_{\infty}} / \left(\frac{GD}{\gamma_{\infty}} \right)^2 \approx \frac{f_{\text{stoich}}^2}{\Omega_{\text{stoich}}^2} \quad (13)$$

Equation (5) allows the elimination of U and D from this expression so that $m_{\text{fu}, \text{ext}}^{\text{fu}} \approx m_{\text{fu}, \infty} f_{\text{stoich}} G$ (14)

This equation indicates that the flame strength is approximately equal to the burning rate of the fuel component per unit area for a laminar flame propagating through a stoichiometric mixture of the gases of the diffusion flame.

Making use of this development, the rate of creation (negative of the rate of destruction) of the fuel by chemical reaction per unit volume may be expressed as:

$$\dot{m}_{fu, \max}'' = \frac{\rho}{\rho_{\infty}} \frac{\rho_{\infty} U_{\text{ext}}}{D} \cdot \frac{m_{fu, \infty} \Omega_{\text{stoich}}^2}{2 \bar{\Psi}_{\text{stoich}} f_{\text{stoich}}} \quad (15)$$

This may be evaluated from the experimental data and the computed numerical values of Ω as a function of f . An assumed value of $\bar{\Psi}$, the average reaction rate, must be applied. $\bar{\Psi}_{\text{stoich}}$ is a number smaller than unity, normally with a value lying between 0.33 and 0.17. It may be evaluated by construction of contours on the m_{fu-f} plane. $\bar{\Psi}$ is the average value Ψ along the line $f = f_{\text{stoich}}$. For propane-air at atmospheric conditions $\Psi \approx 0.25$. Spalding has reported that exact values of the Ψ function are being computed.

The volumetric heat release rate may also be obtained by multiplying \dot{m}_{fu}'' by the specific heat of combustion of the fuel.

Three valuable results are implied in this theory.

(1) From Equation (10), $\rho_{\infty} U_{\text{ext}}$ (AFS), the mass flow rate per unit jet cross sectional area at extinguishment, is shown directly proportional to R_{max} , the modified rate of consumption of fuel per unit volume. From this proportionality it should be possible to determine the total dependence of the volumetric rate upon pressure and to gain some insight into the mechanism of the flame reaction, since both R and $\rho_{\infty} U_{\text{ext}}$, the experimentally determined quantity, will have the same pressure dependence.

(2) From the same equation, it appears that the "flame strength" is independent of the transport properties of the gases. Thus, this technique will permit a study of the kinetic factors of the flame processes without requiring detailed knowledge of diffusion coefficients of individual gases in the mixture or of thermal conductivity properties of the mixture.

(3) From Equation (13), at constant values of D and γ_{∞} , it may be shown how the mass burning rate of fuel in a laminar flame

and "flame strength" are related.

$$\rho_{\infty} U_{\text{ext}} \propto \frac{(m_{\text{fu}, \infty} f_{\text{stoich}} G)^2}{(m_{\text{fu}, \infty} \Omega_{\text{stoich}})^2} \quad (16)$$

In this expression, the product $m_{\text{fu}, \infty} f_{\text{stoich}} G$ is the mass burning rate in a laminar flame. $\rho_{\infty} U_{\text{ext}}$ is, of course, the mass velocity/unit area of the "flame strength" measurement.

A number of experimental limitations have been pointed up by the theoretical results outlined above.

(1) The solutions hold for flame thicknesses of approximately 0.2 D. Translated into the terms of a Peclet number,

$$\frac{\rho_{\infty} U D}{\gamma_{\infty}}$$

a value > 1000 is required.

(2) The derivation also requires that the incident gas jets remain uncontaminated until they reach the impingement zone.

In conclusion, it is believed that the opposed-jet diffusion flame reactor technique has an adequate initial theoretical background for establishing the method as a major tool in the examination of high-temperature and flame reactions between highly reactive components. For general use, the theory requires study in terms of unequal gaseous densities from the two jets, gas velocity variations and chemical kinetic system which cannot be considered to occur in terms of single steps.

c. Combustion of Ammonia In Opposed-Jet Diffusion Flames

(1) Reaction Between HClO_4 and NH_3

During the current contract period, a number of studies of the perchloric-acid-ammonia system have been carried out with the

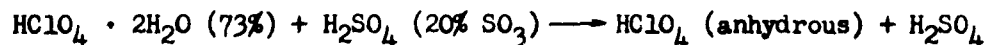
Report 0372-01F

objectives of establishing a diffusion flame in an opposed-jet reactor and of determining the "apparent flame strength" ($\rho_{\infty} U_{\text{ext}}$) of the flame.

Exploratory studies of this system carried out previously under Contract AF 49(638)-566 at temperatures between ambient and 60°C have indicated that these highly reactive components cannot be premixed for study as a laminar flame. The gaseous products of this extremely rapid reaction were oxygen, hydrogen and nitrogen and small quantities of nitrogen oxides. Simultaneously NH_4Cl and NH_4ClO_4 were deposited as solids. In view of these results, studies of the diffusion flame reaction between these components was initiated. Figures 11 and 12 are schematic diagrams of the apparatus which was constructed to examine the flow reactions between perchloric acid and ammonia.

The glass system consists of four functional sections (1) gas preparation and flow rate controllers, (2) the reaction zone, (3) sample collection and analysis and (4) vacuum and pressure control sections.

In the gas preparation and control section (Sections A, B, C, F-L of Figure 12), ammonia gas passes directly from a gas cylinder through a drying train, a calibrated glass rotameter and a flow rate controlling section of 1/2 mm capillary to the orifice within the reactor. Provision has also been made for dilution and mixing of this gas with helium for examination of the effects of diluents on the burning velocity. Anhydrous perchloric acid is prepared under vacuum in an all-glass train without stopcocks by the reaction:



The anhydrous oxidizer is passed over magnesium perchlorate and sealed in a five liter reservoir which is also connected to the reaction cell through a glass rotameter and a flow-controlling capillary. However, this portion of the system is closed off from the reaction zone by interposition of a glass breakseal

tube, K, in the line. At the start of a reaction, after ammonia flow into the reactor has been stabilized, the break-seal is ruptured by a sealed-in magnetic breaker to initiate flow of the anhydrous acid through its nozzle into the reactor.

The reactor (Section E) consists of a 12 inch section of 50 mm square Pyrex tubing which is mounted vertically. The oxidizer and fuel enter from opposite ends of the cell and are metered through 1/2 mm capillary orifices which were separated by 5 cm in the initial experiment. An electrically heated platinum wire is positioned approximately 3 mm above the perchloric acid outlet for igniting the gases.

The exit from the reactor leads directly to a trapping system (Sections M and N) and a gas chromatograph (Section O). In the traps, condensible reaction products are removed from the gas stream. At the end of an experiment these gases can be revaporized and passed directly into the chromatograph for analysis. During the reaction, gaseous products can also be analyzed by a direct sampling of the gas stream. The chromatographic unit contains three columns for separation of the product gases which are expected to include N_2O , NO , NO_2 , Cl_2 , HCl , H_2O , H_2 , NH_3 , O_2 , $NOCl$ and N_2 . The columns are 30% Kel-F on powdered fire brick, 13-X Molecular Sieve and 10% Carbowax on teflon.

The final section of the apparatus consists of standard manifolds (Section P), a vacuum system (Section U), three pressure measuring devices, a McLeod gage (Section T), a differential manometer (Section S) which is read by a cathetometer, and a glass sickle gage (Sections Q and R) for measuring pressures within the perchloric acid reservoir. A Precision manostat is also connected to control the pressure in the reactor.

Experiments have been carried out under

Report 0372-01F

varied experimental conditions. Figure 13 catalogues the conditions of the experiments. All experiments were conducted at reduced pressures. The effect of pressure from 1.0 to 60 torr was examined while HClO_4 flow rates were varied between 4.3×10^{-6} to 2.6×10^{-4} moles/min. Mole ratios of $\text{HClO}_4:\text{NH}_3$ were varied from 0.05 to 7.7 with corresponding mass ratios between 0.3 and 46.2. Nozzle geometry was also varied: Initial trials used a 0.5 mm capillary orifice while 2.0 mm nozzles were used for all experiments at pressures from 9.0 mm upwards. Nozzle separation was 2.0 cm with the exception of the first trial. Finally, gas inlet temperatures were varied between ambient and 180°C .

Despite the relatively large range in variation of conditions, no stable flames were obtained. In two runs, No's 8 and 10, a small flame envelope was observed to form at the perchloric acid jet initially. However, when the spark igniter system was turned off, the flame disappeared and could not be reestablished. It is believed possible that the flame was caused by perchloric acid decomposition, rather than the reaction with ammonia. In all cases in which the transient flame was not observed, a rapid build-up of a white deposit was observed at the HClO_4 nozzle. In the cases where the flame appeared, the deposit formed immediately on extinguishment. Analysis of the deposit indicated its composition to be exclusively ammonium chloride.

In order to ascertain whether it was possible that NH_3 might catalyze or trigger the decomposition of HClO_4 , a test of the effect of ammonia on perchloric acid at 230°C was carried out. In this experiment, perchloric acid vapor, whose pressure was monitored by use of a glass sickle gage, and ammonia were brought to thermal equilibrium in a two-compartment reactor. After establishing the rate of decomposition of the acid, a membrane between the two compartments was broken, allowing the gases to mix.

Report O372-01F

Instantaneously the pressure rose to a high level, followed by a slight decline to a fixed plateau. Although analysis of the gaseous products are not available, some preliminary observations are warranted. From a measure of the relatively large quantity of gases which were not condensible at liquid nitrogen temperatures, it is reasonable to conclude that the presence of a relatively small amount of ammonia appeared sufficient to induce the instantaneous decomposition of perchloric acid.

In any case, this experiment makes it appear unlikely that a flame can be established between gaseous perchloric acid and ammonia. Instead, it appears that ammonia reacts with the decomposition products of HClO_4 (oxygen and chlorine) after initiating decomposition of the acid. The analysis of the jet deposit as 100% NH_4Cl appears to be consistent with these findings.

(2) Reaction Between O_2 and NH_3

Following the unsuccessful attempts to establish a stable $\text{NH}_3 - \text{HClO}_4$ flame in the opposed-jet reactor, experimental work was initiated on the flame reactions between NH_3 and two of the decomposition products of HClO_4 , i.e., O_2 and Cl_2 . A new opposed-jet reactor was constructed for these investigations in order to permit higher mass flow rates of reactants and better heat dissipation. Figure 14 is a schematic diagram of the apparatus.

This apparatus is basically similar to that used by Potter et. al. The burner tubes were mounted in a large glass chamber which in turn was connected to a vacuum system. The pressure was maintained by means of a manostat which operates on the principle of leaking into the system the amount of an inert gas required to maintain any vacuum less than the ultimate the vacuum pump will pull. In order to start the diffusion flame, the following procedure was followed. Helium or argon was blown through the fuel

Report 0372-01F

and oxidant lines for a sufficient length of time to ensure that the entire system was free of fuel and oxidant. The pressure was then set at the desired value and fuel turned on until the reactor was fuel-filled. Finally the oxidant stream was started and the reactants ignited by means of a Tesla coil attached to and grounded through the metal burner tubes.

To make a measurement, the fuel and oxidant flows were alternately increased, keeping the flame centered between the two jets until a hole was observed at the center of the flame. The flame strength was calculated from the experimental data as follows: The mass flows (gr/sec) of fuel and oxidant at flame breaking were averaged and the result divided by the cross-sectional area of the jet to give the mean mass flow per unit area ($\text{gr}/\text{cm}^2\text{-sec}$). Since the flame always broke at the center, the mean flow was multiplied by the ratio of axial to mean flow velocity to give the mass flow rate per unit area (apparent flame strength) at the jet axis. This factor is 1.22 for turbulent flow and 2.0 for laminar flow in straight tubes.

The opposed-jet flame reaction between ammonia and oxygen has been investigated at pressures ranging from 200 torr to 1 atm. Figure 15 is a photograph of a typical flame as it appears at extinguishment. The photograph was taken from below at an angle of approximately 45° . In this case the experiment was carried out at atmospheric pressure with a 2 cm jet separation. As the pressure was decreased the combustion zone became increasingly thin and, at 250 torr, the flame had very little thickness and appeared to be nearly linear (planar). Changes of less than 5% in the gas flow rates were sufficient to create or destroy the axial flame-quenching phenomenon.

The experimental data are summarized in Figures 16 and 17. Figure 17 shows the effect of pressure on the apparent flame strength of the ammonia-oxygen system. Since there is an effect of nozzle

Report O372-01F

or jet diameter on the apparent flame strength all data must be referred to a single diameter (0.77 cm in this case). The plotted data are linear and have a slope of 1.70. According to Spalding (Reference 30) the slope should be the order of the reaction since the apparent flame strength is directly proportional to the maximum reaction rate in the flame. J. Verwimp and A. Van Tiggelen (Reference 37) studied the reaction by another technique and reported an activation energy ($490^{\circ}\text{C} < T < 540^{\circ}\text{C}$) of approximately 50 kcal/mole, with an overall reaction order of 1.7 (1.4 order in NH_3 and 0.3 order in O_2). The agreement obtained by these two independent methods is excellent.

A sample calculation of AFS is given below for the $\text{NH}_3\text{-O}_2$ flame reaction, using Equation (15) from Spalding's analysis.

$$\dot{m}_{\text{fu, max}}''' = \frac{\rho}{\rho_{\infty}} \cdot \frac{\rho_{\infty} U_{\text{ext}}}{D} \cdot \frac{m_{\text{fu, } \infty} \Omega_{\text{st}}^2}{2 \Psi_{\text{st}} f_{\text{st}}}$$

- where $\dot{m}_{\text{fu, max}}''' =$ the maximum volumetric rate of consumption of the fuel, (g/cm³-sec)
- $\rho_{\infty} =$ density of the fuel (g/cm³)
- $\rho/\rho_{\infty} =$ fractional density of the fuel in the local mixture (0.50)
- $U_{\text{ext}} =$ linear velocity of the jet streams upstream of the reaction at extinguishment (cm/sec)
- $\rho_{\infty} \cdot U_{\text{ext}} =$ apparent flame strength (2.20 g/cm²-sec)
- $m_{\text{fu, } \infty} =$ mass fraction of fuel in the fuel stream (1.0)
- $f_{\text{st}} =$ the stoichiometric mass fraction of the material derived from the fuel stream in the local mixture (0.47)
- $\Omega =$ a dimensionless function of f indicative of the burning rate in the flame ($\Omega_{\text{st}} = 1.08$)
- $\Psi_{\text{st}} =$ an average dimensionless reaction rate (≈ 0.25)

$$f_{\text{st}} = \frac{m_{\text{ox, } \infty}/r}{m_{\text{fu, } \infty} + m_{\text{ox, } \infty}/r}$$

where $r =$ mass of oxidant reacting with unit mass of fuel.

Report 0372-01F

Spalding (Reference 30) has plotted values of Ω as a function of f ; values of $\bar{\Psi}_{st}$ have been estimated. Substitution of the appropriate values* in the above equation yields $\dot{m}'''_{fu, max} \approx 7.1 \text{ g/cm}^3\text{-sec}$ for the ammonia reaction at one atmosphere. Using a value of 3410 cal/g as the specific heat of combustion, a volumetric heat release rate of $q'''_{max} \approx 2.42 \times 10^4 \text{ cal/cm}^3\text{-sec}$ is obtained. More exact calculations will become possible when exact values of Ψ become available.

On the basis of the approximate theory of laminar flame propagation derived by Zeldovich (Reference 32), calculated values of the mass burning rate, G , of a stoichiometric mixture of NH_3 and O_2 as obtained from the apparent flame strength data at 1 atm were compared with the mass burning rate of ammonia in a laminar flame using Van Tiggelen's experimentally determined value ($S_{\mu} = 113 \text{ cm/sec}$ at 1 atm) of the flame speed. Using this value for S_{μ} , the mass burning rate $G (m_f \rho_{\infty} S_{\mu})$ was found to be $12.8 \times 10^{-3} \text{ g/cm}^2\text{-sec}$ at 70°F . The equivalent value derived from the experimentally determined value of the apparent flame strength is $23.7 \times 10^{-3} \text{ g/cm}^2\text{-sec}$. These values differ by a factor of two, however, this comparison is considered reasonable in view of the estimations involved in Zeldovich's treatment.

One aspect of the kinetics problem of determining the rate of heat release from the redox-zone of burning AP involves the determination of the stoichiometry of the pertinent gas-phase reactions. Consequently, product analyses have been carried out to determine the stoichiometry (and exothermicity) of the ammonia-oxygen flame reactions in the immediate region of flame extinguishment.

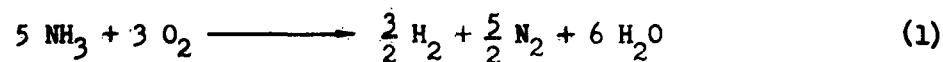
* The opposed-jet reaction parameters used in these and subsequent calculations and the values of $\dot{m}'''_{fu, max}$ and q'''_{max} for all the flame reactions are summarized in Figures 33 and 34, respectively.

Report 0372-01F

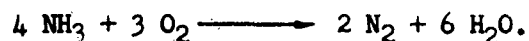
Figure 18 lists the results of mass spectrographic analyses of the reaction products sampled from the effluent streams of several of these ammonia-oxygen flames. The sampling and analytical techniques are such that the values for H_2O concentration are inaccurate; therefore, it is the hydrogen-nitrogen ratio that is utilized in determining the overall stoichiometry of the reaction. Such a procedure is valid since the data indicate that essentially all of the oxygen in the reaction products appears in the water. Also, the data indicate that the H_2/N_2 ratio exhibits a small pressure dependency (decreasing with increasing pressure); however, it appears that the product distribution of the NH_3-O_2 flame reaction in this pressure region is characterized by a H_2/N_2 ratio of approximately 0.5 to 0.6. This conclusion is substantiated by the results of Gaydon and Wolfhard (Reference 38) who have calculated the equilibrium compositions and temperatures of NH_3-O_2 flames for various mixture strengths. Their calculations showed that, for a fuel-oxidant ratio of 5/3, the equilibrium H_2/N_2 ratio in the flame was 0.55. This would seem to indicate that chemical equilibrium was attained in the NH_3-O_2 flames examined by means of the opposed-jet technique.

One of the chief features of the opposed-jet technique is that it provides information concerning the fuel oxidant ratio (in the flame) at extinguishment, where the reaction rate is at its maximum. This information has also been used to determine the overall stoichiometry of the NH_3-O_2 flame reaction. The results of an analysis based upon both combustion product analyses and NH_3/O_2 ratios at extinguishment are presented in Figure 19. This table lists calculated coefficients for the reactants (based upon product analyses) and for the products, based upon the measured NH_3/O_2 ratios at extinguishment. An examination of the data reveals a slight disparity between the calculated and measured values of the NH_3/O_2 and H_2/N_2 ratios; however, it

is clear that the overall stoichiometry of the $\text{NH}_3\text{-O}_2$ flame reaction is best represented by the equation



Actually the "true" overall stoichiometry for this reaction (as determined in non-flame systems using static reactors) is



It appears, therefore, that some of the NH_3 is undergoing thermal decomposition before it reaches the stoichiometric plane in the flame zone.

(3) Reaction Between Cl_2 and NH_3

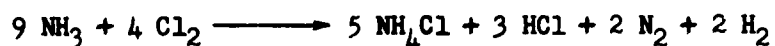
The flame reaction between ammonia and chlorine has been studied by means of the opposed-jet reactor at pressures ranging from 300 torr to 1 atmosphere. It was observed that the $\text{NH}_3\text{-Cl}_2$ flame was considerably more difficult to establish than $\text{NH}_3\text{-O}_2$ flames, and was too unstable at pressure below 300 torr (nozzle diameter = 0.77 cm) for accurate apparent-flame-strength (AFS) measurements. The results of the AFS measurements are summarized in Figures 20 and 21. A log-log plot of the data is linear and indicates that the overall reaction order for the $\text{NH}_3\text{-Cl}_2$ flame is 2.3 in this pressure range.

A comparison of these data with those obtained for the $\text{NH}_3\text{-O}_2$ flame reaction in the same pressure range shows that the apparent flame strength (at 1 atmosphere) of the $\text{NH}_3\text{-O}_2$ system is approximately 70% greater. This result was unexpected since it was previously postulated on the basis of the work of R. Mattair and H. Sisler (Reference 39) that chlorine would oxidize ammonia more rapidly than oxygen. It should be pointed out, however,

Report 0372-01F

that at higher pressures (>2 atmospheres) chlorine may be a better oxidant since the overall reaction order for the $\text{NH}_3\text{-Cl}_2$ system (2.3) is larger than that (1.7) for the $\text{NH}_3\text{-O}_2$ system. This is based upon the assumption that the same mechanisms are operative at the higher pressures. This system requires further investigation.

The flame reaction between ammonia and chlorine has also been investigated by means of the opposed-jet technique in conjunction with a mass spectrometer in order to determine the overall stoichiometry of this reaction. Figure 22 lists the reaction products of flame reactions carried out at pressures ranging from 300 to 745 torr. The data in Figure 20 clearly indicate that the mole ratio of ammonia to chlorine, in the vicinity of flame extinguishment, is approximately 9/4 (2.25) in the pressure region of 350 to 650 torr. The mole ratio values at 300 and 745 torr differ somewhat from the average value of 2.25 because of inaccurate flow rate data. The inaccuracy of these latter data is due primarily to the instability of the ammonia-chlorine flame at these pressures. On the basis of these results (Figure 20), the overall stoichiometry could be represented by the equation



which accounts for the measured NH_3/Cl_2 ratio of 2.25. However, the results of products analyses (Figure 22) indicate that the H_2/N_2 ratio in the above equation is too high by a factor of about 30. An overall stoichiometry which is in better agreement with the analytical results (neglecting Run No. 41) is represented by the equation



Report 0372-01F

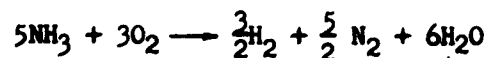
The ammonia-chlorine ratio for this equation is 2.33, which lies within the experimental error of the extinction measurements. The small amount (~2%) of hydrogen detected in the reaction products is probably due to incomplete reaction of the hydrogen formed in the flame as a result of thermal breakdown of NH_3 to N_2 and H_2 .

The volumetric rate of reaction of ammonia per unit volume for this equation ($\text{NH}_3/\text{Cl}_2 = 7/3$) has been calculated on the basis of Spalding's analysis to be $3.39 \text{ g/cm}^3\text{-sec}$. This value corresponds to a volumetric heat release rate of $\dot{q}_{\text{max}}''' = 9.17 \times 10^3 \text{ cal/cm}^3\text{-sec}$. (See Figure 33 for opposed-jet parameters.)

It appears that no quantitative data are available in the literature regarding the flame reaction of ammonia with chlorine. R. Mattair and H. Sisler (Reference 39) studied the reaction in a flow system with the object of forming hydrazine by condensing the products in liquid ammonia. Consequently, the results of these apparent flame strength studies represent the only quantitative information currently available for the ammonia-chlorine flame reaction.

(4) Reaction of $\text{O}_2\text{-Cl}_2$ Mixtures with NH_3

The kinetics of proposed mechanism for the gas-phase reactions above burning ammonium perchlorate is believed to be dependent kinetically upon the competition between two primary irreversible reactions:



and



In order to further test this hypothesis, preliminary experiments on the flame reaction between ammonia and a mixture of oxygen and chlorine was studied by the opposed-jet technique. The flames were considerably less stable than those

Report 0372-01F

to which chlorine had not been added, however, they were more stable than the ammonia-chlorine flames. Figure 23 is a tabulation of representative data on the apparent flame strength for the ammonia-oxygen-chlorine mixture as a function of reactor pressure and chlorine content of the oxidizer stream.

These data clearly show the inhibiting effect of the chlorine on the AFS of these flames. The results indicate that the AFS of $\text{NH}_3\text{-O}_2\text{-Cl}_2$ flames is inversely proportional to the mass fraction of chlorine in the initial unreacted mixture. This fact is further born out by the data shown in Figure 24.

An unusual feature about these curves is that the slopes are constant over the indicated range of chlorine mass fractions (0.1 to 0.3). Furthermore, the overall reaction order (2.0) falls midway between the values found for $\text{NH}_3\text{-O}_2$ flames (1.7) and $\text{NH}_3\text{-Cl}_2$ flames (2.3).

Since product analyses could not be obtained with the present apparatus, no volumetric reaction or heat release rate data are available for these flame reactions.

(5) Reaction Between NO and NH_3

Although it is believed that the overall kinetics of ammonium perchlorate deflagration is governed primarily by the competition between O_2 and Cl_2 for the NH_3 , other irreversible reactions which may enter into the overall reaction involve oxidation of the NH_3 by NO, N_2O and possibly NO_2 . Consequently, experiments were initiated to investigate these flame reactions in the opposed-jet reactor.

The $\text{NH}_3\text{-NO}$ counterflow diffusion flame was found to be quite stable and easily ignited; however, at pressures below 150 torr, the flame exhibited some instability and AFS measurements were not feasible for a nozzle diameter of 0.77 cm. Figure 25 tabulates the conditions and

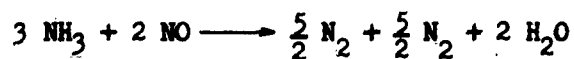
Report 0372-01F

apparent flame strength data for the NH_3 -NO system. A log-log plot (Figure 26) of the AFS versus pressure data is linear and indicates that the overall reaction order is 1.56 at pressures ranging from 150 to 745 torr. This value is in good agreement with that found by Wise and Frech (Reference 40) who investigated this reaction by another technique and reported an overall reaction order of 1.5; first order with respect to NH_3 and one-half order with respect to NO. Volders and van Tiggelen (Reference 41) on the other hand report the reaction to be 1.3 order with respect to NO and 0.5 order with respect to NH_3 (1.8 overall). Although there is mild disagreement concerning the overall order of this reaction, there appears to be considerable disparities among the results of the various studies regarding the reaction orders with respect to NH_3 and NO.

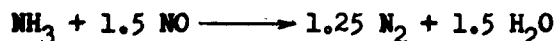
Initial studies have been made to determine the overall stoichiometry of the NH_3 -NO flame reaction. Figure 27 lists the results of mass spectrographic analyses of representative samples of the reaction products sampled downstream from the flames. The sampling techniques are such that the values for H_2O concentrations are inaccurate; consequently, the hydrogen-nitrogen ratio has been utilized in determining the overall stoichiometry. This procedure is valid since all of the oxygen in the reaction products appears in the water. The H_2/N_2 ratio (Figure 27) does not exhibit a pressure dependency indicating constancy of flame temperature over this pressure range (150 to 745 torr). However, the observed ratio of ≈ 0.7 is not in complete agreement with the value (1.0) predicted on the basis of the stoichiometry determined from the NH_3/NO ratio (≈ 1.5) at flame extinguishment. An overall stoichiometry based on the H_2/N_2 of 0.7 predicts an NH_3/NO ratio of 1.0 with unreacted oxygen appearing in the products in order to give a correct mass balance. In as much as no oxygen was detected in the

Report O372-01F

products and an NH_3/NO ratio of 1.0 involves too great an error in the NH_3/NO measurement, it is believed that the stoichiometry based upon the NH_3/NO ratio at extinguishment is the more accurate one and that the measured H_2/N_2 ratio is in error. The overall stoichiometry of the NH_3 -NO counterflow diffusion flame (at extinguishment) can be represented by the following equation.



Actually, in such an NH_3 rich flame, the stoichiometry of combustion can be represented by a combination of two reactions.

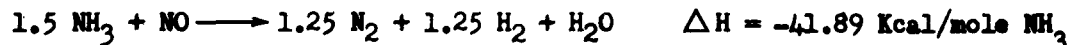


and



These equations indicate that the stoichiometric proportion of NH_3 was oxidized and the excess NH_3 (1.25 moles) decomposed into N_2 and H_2 . A significant result of the AFS measurements is that the NH_3/NO ratio (at extinguishment) in counterflow diffusion flames does not correspond to the ratio (0.828) for the mixture giving the maximum laminar flame speed (S_u).

The volumetric rate of reaction of ammonia for the reaction



has been calculated on the basis of Spalding's analysis. Substitution of the appropriate values (See Figure 33) in Equation (15) yields a value for $\dot{M}_{fu, \max}''' \approx 2.73 \text{ g/cm}^3\text{-sec}$ for the NH_3 -NO reaction at 1 atmosphere. The heat release ratio (\dot{q}_{\max}''') corresponding to this volumetric rate is $6.73 \times 10^3 \text{ cal/cm}^3\text{-sec}$.

(6) Reaction Between N_2O and NH_3

The NH_3-N_2O counterflow diffusion flame was also quite stable, down to pressure as low as 100 torr (for a nozzle diameter of 0.77). Figures 28-30 summarize the results for this flame reaction. The usual plot of AFS versus pressure is quite linear, giving an overall reaction order of 2.0 at pressures ranging from 100 to 745 torr.

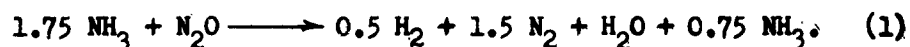
A comparison of these data with those obtained for the NH_3-NO reaction shows that the apparent flame strength (at 1 atmosphere) of the NH_3-N_2O flame is approximately 3.5 times that for the NH_3-NO flame. Considering their respective adiabatic flame temperatures (2580 and 2710°K), this is somewhat surprising. Also of considerable interest is the fact that the AFS of the NH_3-N_2O flame is of the same order of magnitude as the NH_3-O_2 flame.

Experimental studies were carried out on the determination of the stoichiometry and exothermicity of the ammonia-nitrous oxide diffusion flame in the immediate region of flame extinguishment. The results of mass spectrographic analyses of representative samples or reaction products are presented in Figure 30. The samples were taken downstream from the flames and the sampling techniques are such that the values for H_2O concentration are inaccurate. This presents no problem for the reasons indicated previously.

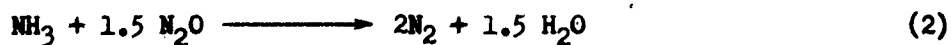
The data indicate that unusually large amounts of unreacted ammonia passed through the reaction zone of these flames. This finding was unexpected, since this phenomenon was not observed in other counter-flow diffusion flames between ammonia and oxidants such as O_2 , Cl_2 and NO . Also burning velocity measurements by other workers on binary mixtures of NH_3 with N_2O gave no indication of any unusual behavior which might distinguish

Report 0372-01F

this flame from those between NH_3 and the oxidants mentioned above. The only unusual feature of the $\text{NH}_3\text{-N}_2\text{O}$ counter-flow diffusion flame that distinguished it from those studied previously is that the flame had a bell shape rather than the usual flat disc shape. Furthermore, the flame extended downward from the mouth of the oxidant jet rather than remaining suspended between the two jets as was normally observed for counter-flow flames. Whether or not these phenomena have any bearing or effect on the nature of the reaction zone, and consequently, on the passage of NH_3 through it remains to be demonstrated. However, the fact remains that the analytical results are in agreement with the results obtained for the fuel/oxidant ratio as determined from reaction parameters in apparent flame strength (AFS) measurements. The average value of the fuel/oxidant ratio deduced from the H_2/N_2 and NH_3/N_2 ratios listed in Figure 30 is 1.75 which agrees with the value of 1.74 determined from AFS measurements (see Figure 28). On the basis of these results and the data listed in Figure 30, the complete reaction is best represented by the equation



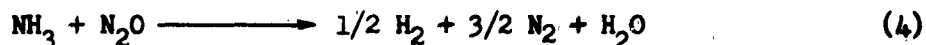
However, subtracting out the unreacted NH_3 leaves an overall stoichiometry for the $\text{NH}_3\text{-N}_2\text{O}$ counter-flow flame that can be represented by the sum of reactions (2) and (3).



These equations (1, 2, and 3) would seem to indicate that the stoichiometric proportion (1 mole) of NH_3 was oxidized to the expected products, excess NH_3 (0.5 mole) was decomposed into N_2 and H_2 , and finally, that 0.75 mole of NH_3 did not react. Thus, the exothermicity of the flame reaction is governed

Report O372-01F

by the overall reaction



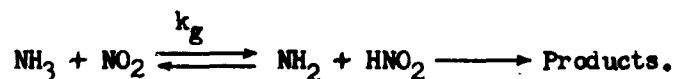
with a corresponding $\Delta H = -3898$ cal/gm NH_3 . The volumetric rate of reaction of ammonia for reaction (4) is 1.95 gm/cm³-sec at 1 atm pressure. This value corresponds to a volumetric heat release rate of 7.6×10^3 cal/cm³-sec.

(See Figures 33 and 34 for summary of opposed-jet parameters).

(7) Reaction Between NO_2 and NH_3

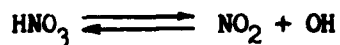
A cursory examination of the reaction

between ammonia and nitrogen dioxide was initiated with the objective of comparing known kinetic data with apparent flame strength data obtained by the opposed-jet technique. Such a study should facilitate a theoretical analysis of the theory of flame strength because of the availability in the literature of kinetic data for this reaction. Furthermore, it has been postulated (Reference 22) that the rate controlling step of the gas phase reactions occurring over ammonium nitrate propellants involves the reaction



This provides an additional incentive for the investigation of this system.

W. A. Rosser and H. Wise (Reference 42) have suggested that NO_2 is produced by the relatively rapid decomposition:



These workers studied the kinetics of the NH_3 - NO_2 reaction in the temperature range of 600 to 800°K and reported an activation energy of 27.5 kcal/mole. They found that approximately the first third of the reaction was second order. On the other hand, F. Falk and R. N. Pease (Reference 43) reported an overall reaction

Report 0372-01F

order of 3 for this reaction in the temperature range of 150 to 200°C at total pressures up to 200 torr. They also observed a gradual change in the reaction order.

The results of the initial studies in these laboratories on the effect of pressure on the apparent flame strength of $\text{NH}_3\text{-NO}_2$ flames is shown in Figures 31 and 32. The flames were readily established and were stable at pressures ranging from 300 to 745 torr. The plotted data are linear and the slope of the line indicates that the overall reaction order is 2.43. This value falls approximately midway between the values reported by the aforementioned workers. These studies need to be extended in order to provide additional data for carrying out a theoretical analysis of the flame strength data in terms of standard kinetic units.

(8) Theoretical Studies

Although the opposed-jet diffusion flame reactor technique had an adequate theoretical background for the preliminary studies completed on this program, the experimental work has progressed to the point where there is a need to obtain actual kinetic rate constants from apparent flame strength data. Spalding's approximate theoretical treatment in its present stage of development is not adequate since it requires prior kinetic knowledge or assumptions about the flame reactions we are attempting to investigate. This shortcoming in Spalding's treatment was recognized when attempts were made to obtain the necessary kinetic constants required for the solution of Equation (2) (Section II, 1., e.). Accordingly, theoretical studies were undertaken to examine the theory with the objective of expanding its development for use with practical systems.

As a result, a physical criterion for extinction in opposed-jet flames has been developed and differs somewhat from

Report 0372-01F

that given by Spalding. In this treatment, maximum reaction rates are determined by means of physical extinction criteria which are imposed on the flame process rather than previous or assumed chemical kinetic information.

This criterion, when used in conjunction with the Spalding Theory of mixing in opposed gas jets enables the apparent flame strength to be related to (1) the effective maximum chemical reaction rate in the opposed-jet flame, and (2) the laminar flame speed of an equivalent pre-mixed diffusion flame. The derived relationships differ somewhat from similar relationships given by Spalding's earlier treatment of the phenomena in the thin flame approximation, but do yield quantitatively similar results.

A detailed discussion of the new treatment is given in Appendix D. Also in the Appendix (D) is a discussion and evaluation of some of the results from the opposed-jet diffusion flame experiments.

Two additional theoretical studies were carried out, in part, during the present contract period. In one of these studies, a new model was developed to explain the extinction process in solid rocket motors. In the other theoretical study, the thermal-layer theory of steady-state combustion has been applied to the problem of a low pressure deflagration limit.

The results of these studies are presented in Appendices E and F.

III. RECOMMENDATIONS FOR FUTURE WORK

It is recommended that future work be directed along two general lines:

(1) a continued effort to develop the opposed-jet technique (and theory) for investigating fast-burning mixtures and high temperature kinetics; and (2) investigate the mechanisms of decomposition of single crystals, particularly with respect to the effect of defects, impurities, etc., on the decomposition rate.

The opposed-jet technique is particularly useful for investigating high temperature kinetics of highly reactive or hypergolic materials. Furthermore it permits studies, (particularly, structure determinations) to be made of reactive mixtures under certain conditions that would be impossible to obtain in corresponding premixed flames. It is believed that flame structure determinations in conjunction with the new theoretical treatment developed on this program could provide the means of determining kinetic rate constants for highly reactive systems.

IV. PROJECT PERSONNEL

The following is a list of personnel who were engaged, in whole or in part, in carrying out the investigations described in this report:

F. J. Cheselske	Research Chemist, Principal Investigator (June 1963 to March 1965)
D. J. Sibbett	Senior Chemist, Principal Investigator (October 1961 to May 1963)
R. F. Chaiken	Technical Specialist, Principal Investigator (February 1960 to September 1961) Later Consultant to the program (October 1961 to February 1965)
A. Wheeler	Technical Specialist
I. Geller	Research Chemist
J. M. Lobato	Research Chemist

Report O372-01F

J. E. Sutherland	Research Chemist
D. K. Van de Mark	Senior Laboratory Technician
R. S. Godds	Senior Laboratory Technician
R. L. Carter	Senior Laboratory Technician
P. A. Kees	Senior Laboratory Technician

V. PUBLICATIONS

The following is a list of publications which describe the experimental and theoretical research achievements of this program, Contract AF 49(638)-851. The disposition of these papers are indicated below.

1. R. F. Chaiken, D. J. Sibbett, J. C. Sutherland, D. K. Van de Mark and A. Wheeler, "The Rate of Sublimation of Ammonium Halides"; published in J. Chem. Phys., 37, 2311 (1962).
2. D. J. Sibbett and I. Geller, "Kinetics of the Decomposition of Anhydrous Perchloric Acid"; accepted for publication in the Journal of Physical Chemistry (1965).
3. R. F. Chaiken and F. J. Cheselske, "Surface Rate Processes and Sensitivity of High Explosives"; submitted for publication in the Journal of Chemical Physics.
4. R. F. Chaiken, "A Model for Low Pressure Extinction of Solid Rocket Motors"; accepted for publication in AIAA Journal (1965).
5. F. J. Cheselske, R. F. Chaiken and D. J. Sibbett, "Oxidation of Ammonia in Opposed-Jet Diffusion Flames"; in preparation.
6. R. F. Chaiken, "On the Extinction of Opposed-Jet Diffusion Flames: A Physical Criterion for Extinction"; in preparation.
7. R. F. Chaiken, "Implications of a Steady-State Solid Propellant Combustion Model to a Low Pressure Deflagration Limit"; in preparation.

REFERENCES

1. H. Eyring, R. E. Powell, G. H. Duffey and R. B. Parlin, Chem. Rev., 45, 69 (1949).
2. M. A. Cook, "The Science of High Explosives", Reinhold Publishing Corp., New York, N.Y., 1958
3. H. Jones, Proc. Roy. Soc., 189A, 415 (1947).
4. A. W. Campbell, M. C. Malin, and T. E. Holland, "Second ONR Symposium on Detonations", Office of Naval Research, Washington, D.C. (February 1955).
5. W. H. Andersen and R. F. Chaiken, ARS Journal, 27, 49 (1959).
6. R. D. Schultz and A. O. Dekker, "The Absolute Normal Decomposition Rates of Solids", Part I, Fifth Symposium (International) on Combustion, Reinhold, New York (1955), p. 260.
7. R. D. Schultz and A. O. Dekker, "The Absolute Decomposition Rates of Solids", Part II, J. Chem. Phys., 23, 2133-38 (1955).
8. R. D. Schultz and A. O. Dekker, "The Effect of Physical Adsorption on the Absolute Decomposition Rates of Crystalline Ammonium Chloride and Cupric Sulfate Trihydrate", J. Phy. Chem., 60, 1095 (1956).
9. R. D. Schultz and A. O. Dekker, "Transition-State Theory of the Linear Rate of Decomposition of Ammonium Perchlorate", Sixth Symposium (International) on Combustion, Reinhold, New York (1957), p. 618
10. R. F. Chaiken, D. J. Sibbett, J. E. Sutherland, D. K. Van de Mark, and A. Wheeler, "Rate of Sublimation of Ammonium Halides", J. Chem. Phys., 37, 2311 (1962).
11. L. L. Bircumshaw and B. H. Newman, Proc. Roy. Soc., A227, 115; (1954); ibid., A227, 228 (1955).
12. L. L. Bircumshaw and T. R. Phillips, J. Chem. Soc., 1957, 4741.
13. A. K. Galwey and P. W. M. Jacobs, Proc. Roy. Soc., A254, 455 (1960).
14. A. K. Galwey and P. W. M. Jacobs, J. Chem. Soc., 1959, 837.
15. J. C. Slater, "Introduction to Chemical Physics", McGraw-Hill Book Co., New York, 1939, p. 293.
16. H. N. V. Temperley, "Changes of State", Interscience Publishers, New York, 1956, Chapter II.
17. R. W. Dreyfus and P. W. Levy, Proc. Roy. Soc., 246A, 233 (1958).

Report 0372-01F

REFERENCES (Cont'd)

18. D. W. Blair, E. K. Bastress, C. E. Hermance, K. P. Hall and M. Summerfield, Progress in Astronautics and Rocketry, Volume I, Solid Propellant Rocket Research, Academic Press, New York, 1960, p. 183-206.
19. J. Levy and R. Friedman, Eighth Symposium (International) on Combustion, Williams and Wilkins Co., Baltimore, 1962, p. 663.
20. J. Vandekerckhove and A. Jaumotte, ibid. p. 689.
21. W. H. Andersen, K. W. Bills, E. Mishuck, G. Moe, and R. D. Schultz, "A Model Describing Combustion of Solid Composite Propellants; Application to Ammonium Nitrate", Combustion and Flame, 3, 301 (1959).
22. R. F. Chaiken, "A Thermal Layer Mechanism of Combustion of Solid Composite Propellants; Application to Ammonium Nitrate Propellants", Combustion and Flame, 3, 285 (1959).
23. R. F. Chaiken and W. H. Andersen, "The Role of Binder in Composite Propellant Combustion", Progress in Astronautics and Rocketry, Volume I, Solid Propellant Rocket Research, Academic Press, New York, 1960, p. 227-249.
24. P. W. M. Jacobs and A. R. Tarig Kureishy, Eighth Symposium (International) on Combustion, Williams and Wilkins Co., Baltimore, 1962, p. 672.
25. L. L. Bircumshaw and B. H. Newman, Proc. Roy. Soc., A227, 115 (1954); A227, 228 (1955).
26. A. K. Galwey and P. W. M. Jacobs, J. Chem. Soc., 1959, 837
27. A. K. Galwey and P. W. M. Jacobs, Proc. Roy. Soc., A254, 455 (1960).
28. Aerojet-General Corporation Quarterly Project Report No. 0372-01-12, Contract AF 49(638)-851, 31 December 1962 (Unclassified).
29. A. E. Potter and J. N. Butler, "A Novel Combustion Measurement Based On the Extinguishment of Diffusion Flames", ARS Jour., 29, 54-56 (1959).
30. D. B. Spalding, "Theory of Mixing and Chemical Reaction in the Opposed-Jet Diffusion Flame", ARS Jour., 31, 763-771 (1961).
31. T. P. Pandya and F. J. Weinberg, "A Study of the Structure of Laminar Diffusion Flames by Optical Methods", Ninth Symposium (International) on Combustion, Academic Press Inc., New York, 1963, p. 587.
32. Y. B. Zeldovich, "On the Theory of Combustion of Initially Unmixed Gases", NACA Technical Memorandum No. 1296, Translated from Zhur. Tek. Fiz., 19, 1199-1210 (1949).
33. D. B. Spalding, "A Theory of the Extinction of Diffusion Flames", Fuel, 33, 255-273 (1955).

Report O372-01F

REFERENCES (Cont'd)

34. Evelyn Anagnostou and A. E. Potter, "Flame Strength of Propane-Oxygen Flames at Low Pressures in Turbulent Flow", Ninth Symposium (International) on Combustion, Academic Press Inc., New York, 1963, p. 1-6.
35. A. E. Potter, J. HeimeI, and J. N. Butler, "Apparent Flame Strength", Eighth Symposium (International) on Combustion, Williams and Wilkens Co., Baltimore, 1962, p. 1027-34.
36. D. B. Spalding, "One-Dimensional Laminar Flame Theory for Temperature - Explicit Reaction Rates", Combustion and Flame, 1, 296-307 (1957).
37. J. Verwimp and A. Van Tiggelen, Bull. soc. chim. Belges, 62, 205 (1953).
38. A. G. Gaydor and H. G. Wolfhard, "Flames, Their Structure, Radiation, and Temperature", Chapman and Hall Ltd., London, 1960, p. 297.
39. R. Mattair and H. H. Sisler, J. Amer. Chem. Soc., 73, 1619 (1951).
40. H. Wise and M. W. Frech, J. Chem. Phys., 22, 1463 (1954).
41. A. Volders and A. Van Tiggelen, Bull. Soc. Chim. Belg., 63, 542 (1954).
42. W. A. Rosser and H. Wise, Jet Propulsion Laboratory Progress Report No. 20-273, California Institute of Technology, 15 September 1955.
43. F. Falk and R. N. Pease, J. Amer. Chem. Soc., 76, 4746 (1954).



HIGH PRESSURE PYROLYSIS APPARATUS

FIGURE 1

AMMONIUM PERCHLORATE MICROSCOPIC DECOMPOSITION

Hot-Stage Heating Rate, $\dot{T}_h, \sim 30^\circ\text{C}/\text{min}$



$T_h \sim 240^\circ\text{C}$

$\Delta t \sim 1 \text{ min}$



$T_h \sim 270^\circ\text{C}$

FIGURE 2



Figure 3. Crystal No. 1 - Original Surface before Heating. 1000X Bright Field.



Figure 4. Crystal No. 1 - Surface after Heating for 30 Min. at 190°C. Same Area as Figure 3. 1000X Bright Field.

Figures 3 - 4



Figure 5. Crystal No. 1 - After Heating for 90 Min. at 190°C. Same Area as Figure 3. 1000X Bright Field.



Figure 6. Crystal No. 2 - After Heating fo 15 Min. at 220°C. 1000X Bright Field.

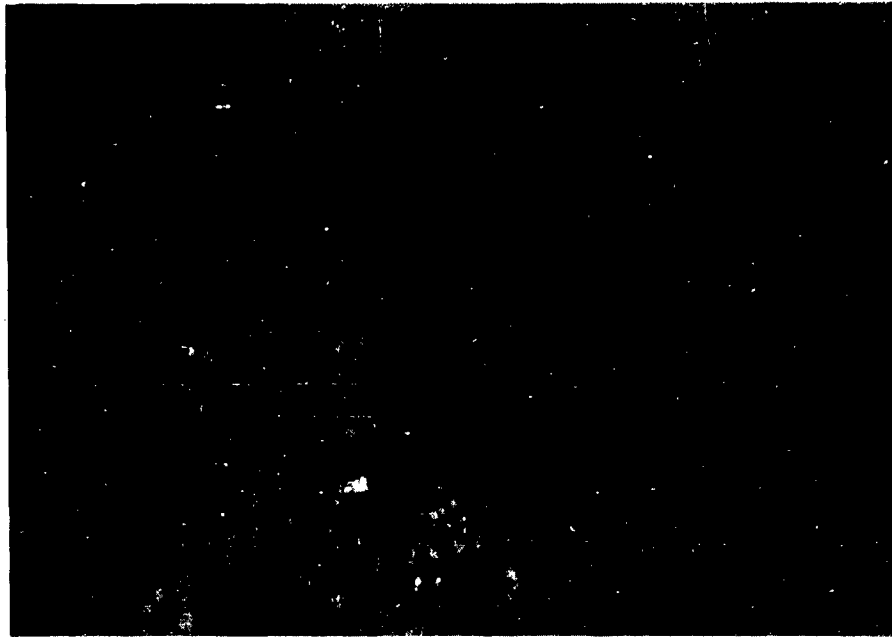


Figure 7. Crystal No. 2 - After Heating for 45 Min. at 220°C. 1000X Bright Field.

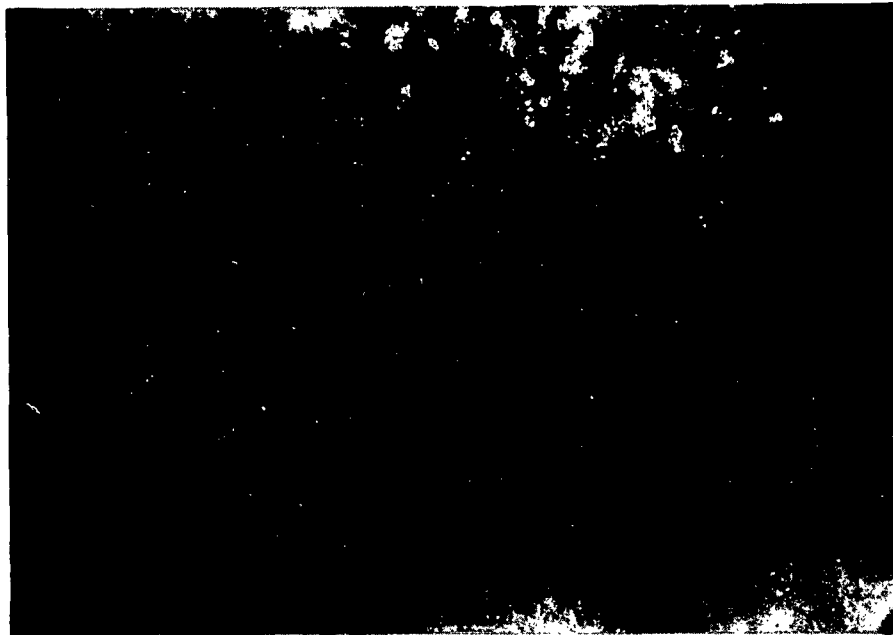


Figure 8. Crystal No. 3 - After Heating for 9 Min. at 250°C. 1000X Polarized Light.

DISTRIBUTION OF MAJOR GASEOUS PRODUCTS FROM THE DEFLAGRATION
OF ONE MOLE OF SOLID AMMONIUM PERCHLORATE*

	Moles, Calculated		Moles, Experimental*	
	$x = 0^{**} (1 \text{ atm})$ $y = \frac{2}{3} - z$	$x = \frac{1}{4^{**}} (70 \text{ atm})$ $z = 0.10^{**}$	1 atm	70 atm
N_2	$\frac{5}{4} z$	0.125	0.125	0.265
N_2O	$\frac{1}{6}$	0.167	0.10	0.12
NO	$\frac{2}{3} - \frac{5}{2} z$	0.417	0.55	0.23
Cl_2	$\frac{1}{2}$	0.500	0.50	0.12
HCl	0	0	0	0.76
H_2O	2	2.000	2.00	1.62
O_2	$\frac{5}{4} z + \frac{7}{12}$	0.708	0.675	1.015

* Based upon a comparison of the proposed reaction scheme with the experimental results reported by J. Levy and R. Freidman (Reference 19).

** $x + y + z = \frac{2}{3}$ where x, y, z refer to the moles of NH_3 oxidized by Cl_2, O_2 and NO , respectively. The value of x and z is chosen so that the calculated values match the experimental HCl and N_2 data of Levy and Freidman.

Figure 9

DECOMPOSITION OF PERCHLORIC ACID AT 200°C
 -- Comparison of Experimental and Computed Results

Time (min)	Experimental Pressure (mm)	Calculated Pressure (mm)	HClO ₄ Pressure (mm)	Cl ₂ Pressure (mm)	H ₂ O Pressure (mm)	O ₂ Pressure (mm)
0	218.5	218.5	0	0	0	0
20	278.7	281.2	182.7	17.9	17.9	62.7
40	333.7	327.2	156.4	31.1	31.1	108.7
60	370.2	362.2	136.4	41.0	41.0	143.7
80	392.2	389.5	120.8	48.9	48.9	171.0
100	410.2	411.5	108.2	55.2	55.2	193.0
120	426.5	429.6	97.9	60.3	60.3	211.1
140	441.0	444.7	89.3	64.6	64.6	226.2
160	453.5	457.4	81.9	68.3	68.3	238.9
180	465.5	468.4	75.7	71.4	71.4	249.9
200	475.7	477.9	70.3	74.1	74.1	259.4
220	484.3	486.2	65.5	76.5	76.5	267.7
240	492.5	493.6	61.3	78.6	78.6	275.1
260	500.0	500.1	57.6	80.5	80.5	281.6
280	505.5	505.9	54.2	82.1	82.1	287.5
300	511.0	511.2	51.2	83.6	83.6	292.7
320	516.2	515.9	48.5	85.0	85.0	297.5
340	520.6	520.3	46.0	86.2	86.2	301.8
360	524.8	524.2	43.8	87.4	87.4	305.7
380	528.2	527.8	41.7	88.4	88.4	309.4
400	532.0	531.2	39.8	89.3	89.3	312.7

Figure 10

REACTOR FOR STUDY OF HClO_4 - NH_3 FLAMES

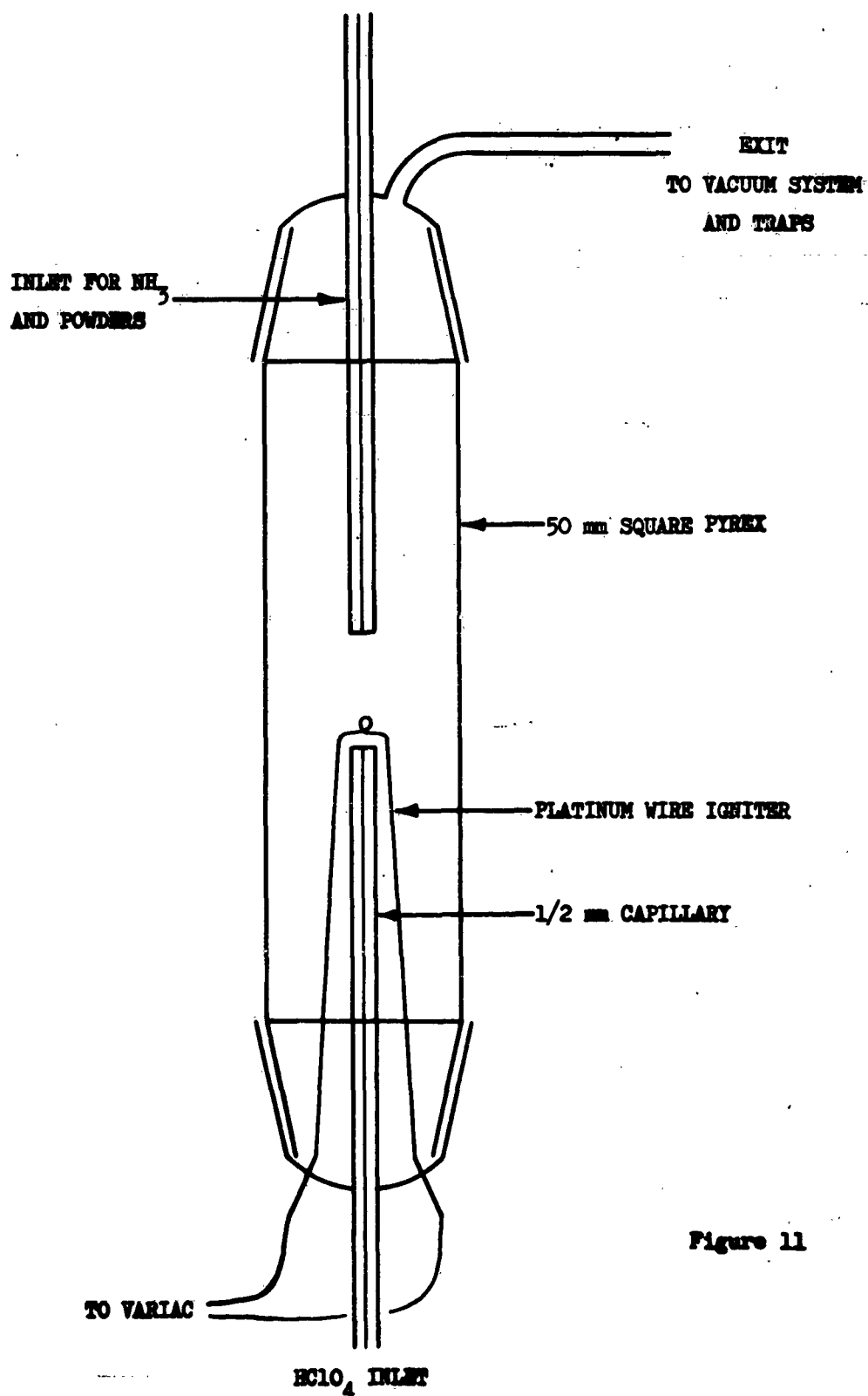


Figure 11

FLOW REACTOR SYSTEM

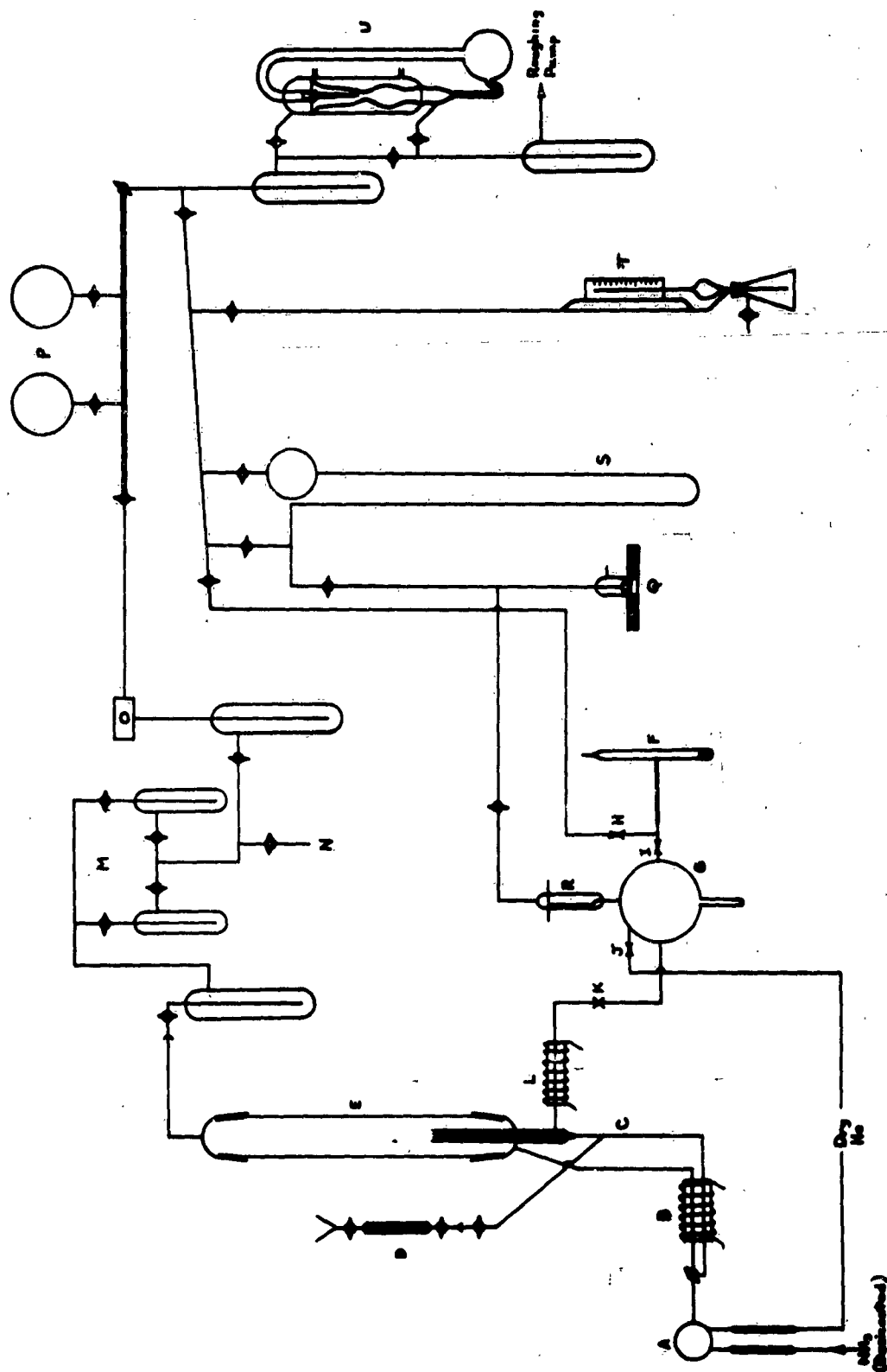


Figure 12

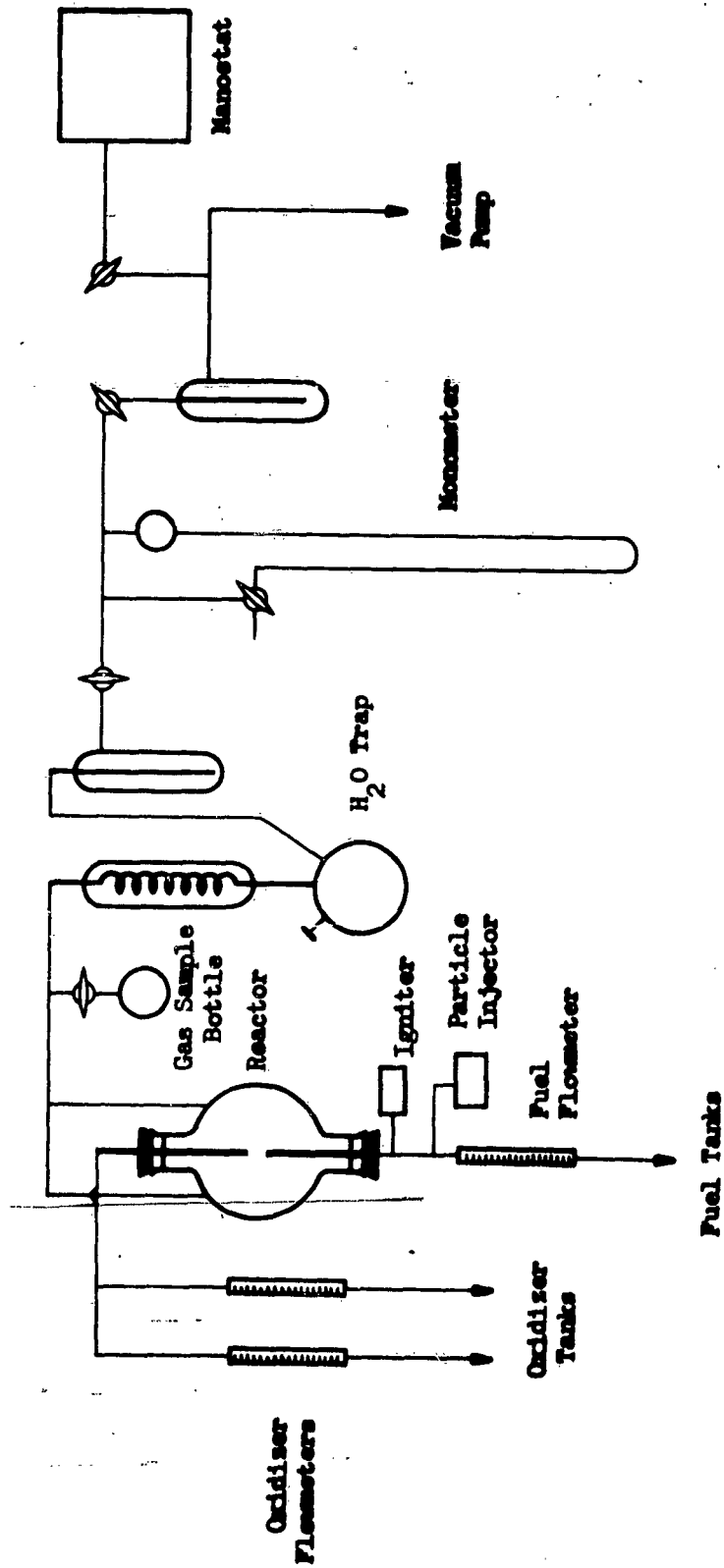
CONDITIONS OF OPPOSED-JET REACTIONS BETWEEN HClO_4 AND NH_3

Run No.	1	2	3	4	5	6	7	8	9	10	11	12
Initial HClO_4 Flow Rate (moles/min)	4.3×10^{-6}	1.7×10^{-5} *	7.5×10^{-6}	9.3×10^{-6}	1.4×10^{-5}	3.7×10^{-5}	6.2×10^{-5} *	8.9×10^{-5} *	1.8×10^{-4}	2.0×10^{-4}	2.5×10^{-4}	2.6×10^{-4}
NH_3 Flow Rate (moles/min)	8.0×10^{-5}	2.8×10^{-5}	9.0×10^{-6}	1.7×10^{-5}	2.0×10^{-5}	2.0×10^{-5}	8.1×10^{-6}	2.2×10^{-5}	2.3×10^{-4}	2.8×10^{-4}	2.8×10^{-4}	2.3×10^{-4}
Mole Ratio ($\text{HClO}_4/\text{NH}_3$)	0.054	0.61	0.83	0.55	0.70	1.9	7.7	4.1	0.78	0.70	0.87	1.1
Mass Ratio ($\text{HClO}_4/\text{NH}_3$)	0.32	3.6	4.9	3.3	4.2	11.4	46.2	24.6	4.6	4.1	5.1	6.6
Nozzle Separation (cm)	5.0	2.0	2.0	2.0	2.0	2.0	2.0	2.0	2.0	2.0	2.0	2.0
Orifice Diam. (mm)	0.5	0.5	0.5	0.5	0.5	2.0	2.0	2.0	2.0	2.0	2.0	2.0
Reservoir Temp. ($^{\circ}\text{C}$)	20 $^{\circ}\text{C}$	20 $^{\circ}\text{C}$	Ambient	Ambient	Ambient	45 $^{\circ}$	82 $^{\circ}$	82.6 $^{\circ}$	Ambient	79 $^{\circ}$	136 $^{\circ}$	180 $^{\circ}$
Reservoir Vol. (ml)	5500	5500	5500	5500	5500	2500	2500	2500	2500	2500	5500	5500
Reactor Pres- sure (torr)	1.0	1.0	1.0	2.0	4.2	9.2	12.0	35.1	60	60	60	60

* Helium diluent used.

Figure 13

OPPOSED-JET REACTOR SYSTEM

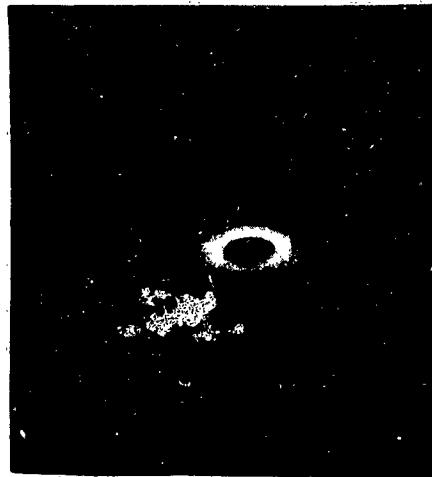


Fuel and oxidant (or oxidant mixture) are metered into the two vertically mounted jets in the reactor and ignited. To make a measurement, the fuel and oxidant flows are alternately increased, keeping the flame centered between the two jets, until a hole is observed at the center of the flame. The average of the mass flows of the fuel and oxidant at flame breaking is divided by the cross-sectional area of the jet to give the mean mass flow per unit area ($\text{gr}/\text{cm}^2\text{-sec}$). This value, when multiplied by the ratio of axial to mean flow velocity (2.0 for laminar flow and 1.22 for turbulent flow) gives the "apparent flame strength" at the jet axis. (Stainless-steel nozzles; 0.77 cm ID app 2.0 cm separation).

Figure 14.

Report 0372-01F

AMMONIA - OXYGEN DIFFUSION FLAME
AT EXTINGUISHMENT



Oxygen inlet at top
Ammonia at bottom

Fig

REACTION CONDITIONS FOR OPPOSED-JET FLAMES BETWEEN
AMMONIA AND OXYGEN

(Nozzle Diameter = 0.77 cm)

	Identification Number							
	1-a	1-b	1-c	1-d	1-e	2	3	4-1
Reactor Pressure, torr	200	300	450	600	745	350	450	650
NH ₃ Flow Rate, * moles/min	0.124	0.282	0.641	1.076	1.935	0.350	0.624	1.474
O ₂ Flow Rate, * moles/min	0.075	0.144	0.344	0.578	1.160	0.203	0.366	0.855
Mole Ratio, * NH ₃ /O ₂	1.65	1.96	1.86	1.86	1.67	1.72	1.71	1.72
AFS**	0.177	0.340	0.482	1.33	2.20	0.449	0.809	1.89
AFS***	0.108	0.208	0.295	0.812	1.34	0.274	0.494	1.154

* Value at extinguishment. Average value for all experiments is 1.77.

** Apparent flame strength (laminar flow).

*** Apparent flame strength (turbulent flow).

AMMONIA-OXYGEN FLAMES

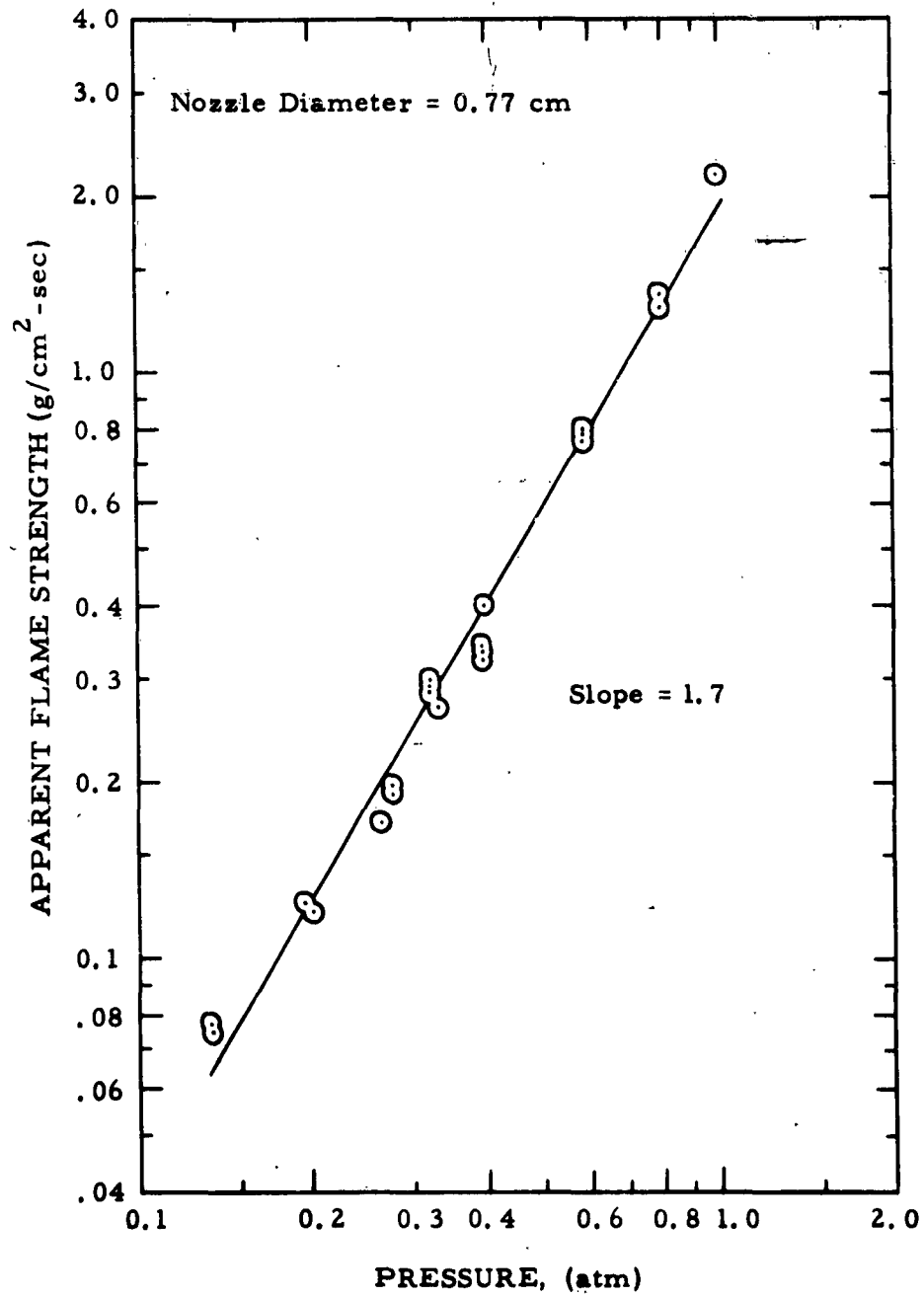


Figure 17

REACTION PRODUCTS FROM AMMONIA-OXYGEN FLAMES

Identification Number	Pressure, Torr	Product Composition, mole %				
		N_2	H_2	H_2O	Trace Materials	H_2/N_2
2	350	63.53	34.67	1.80	NO	0.545
3	450	63.90	32.76	1.01	O_2	0.513
4-1	650	60.49	28.67	10.44	NH_3	0.474

Figure 18

STOICHIOMETRY OF THE AMMONIA-OXYGEN FLAME REACTION IN
THE OPPOSED-JET AT EXTINGUISHMENT

(Nozzle Diameter = 0.77 cm)

Identification Number	Pressure, torr	Based on Product Analyses					Based on NH_3/O_2 Ratio at Extinguishment							
		Moles Reactants, Calculated		Moles Products, Measured			Moles Reactants, Measured			Moles Products, Calculated				
		NH_3	O_2	NH_3/O_2	H_2	N_2	H_2O^*	H_2/N_2	NH_3	O_2	NH_3/O_2	H_2	N_2	H_2/N_2
2	350	2	1.225	1.63	0.545	1.00	2.455	0.545	1.72	1.00	1.72	0.58	0.86	0.674
3	450	2	1.243	1.61	0.513	1.00	2.487	0.513	1.71	1.00	1.71	0.565	0.855	0.661
4-1	650	2	1.263	1.58	0.474	1.00	2.526	0.474	1.72	1.00	1.72	0.58	0.86	0.674
5**	200-745	-	--	--	--	--	--	--	1.77	1.00	1.77	0.655	0.885	0.740
6***	--	-	--	--	--	--	--	--	5.0	3.0	1.67	1.50	2.50	0.600

* Obtained by difference since H_2O analyses are not accurate. Also, the data retain more decimal places than are significant.

** Based upon an average NH_3/O_2 ratio (1.77) obtained for all pressures ranging from 200 to 745 torr.

*** Based upon an assumed NH_3/O_2 ratio of 5/3.

Figure 19

REACTION CONDITIONS FOR OPPOSED-JET FLAMES BETWEEN
AMMONIA AND CHLORINE

(Nozzle Diameter = 0.77 cm)

	Identification Number													
	l-a	l-b	l-c	l-d	l-e	l-f	l-g	l-h	8	9	10	40	41	44
Reactor Pressure, torr	300	350	400	450	500	550	600	745	300	650	450	450	450	300
NH ₃ Flow Rate* moles/min	0.097	0.129	0.165	0.230	0.272	0.322	0.448	0.562	0.087	0.429	0.247	0.259	0.247	0.116
Cl ₂ Flow Rate* moles/min	0.038	0.056	0.073	0.104	0.126	0.147	0.210	0.300	0.035	0.188	0.110	0.123	0.123	0.043
Mole Ratio**** NH ₃ /Cl ₂	2.55	2.30	2.27	2.21	2.16	2.19	2.13	1.87	2.46	2.29	2.25	2.11	2.00	2.70
AFS (g/cm ² -sec)**	0.157	0.214	0.282	0.406	0.490	0.593	0.812	1.301	0.144	0.744	0.433	0.475	0.468	0.180
AFS (g/cm ² -sec)***	0.096	0.130	0.172	0.248	0.299	0.362	0.496	0.795	0.088	0.454	0.264	0.290	0.286	0.110

* Value at extinguishment.
 ** Apparent flame strength (laminar flow).
 *** Apparent flame strength (turbulent flow).
 **** Average mole ratio = 2.25

AMMONIA-CHLORINE FLAMES

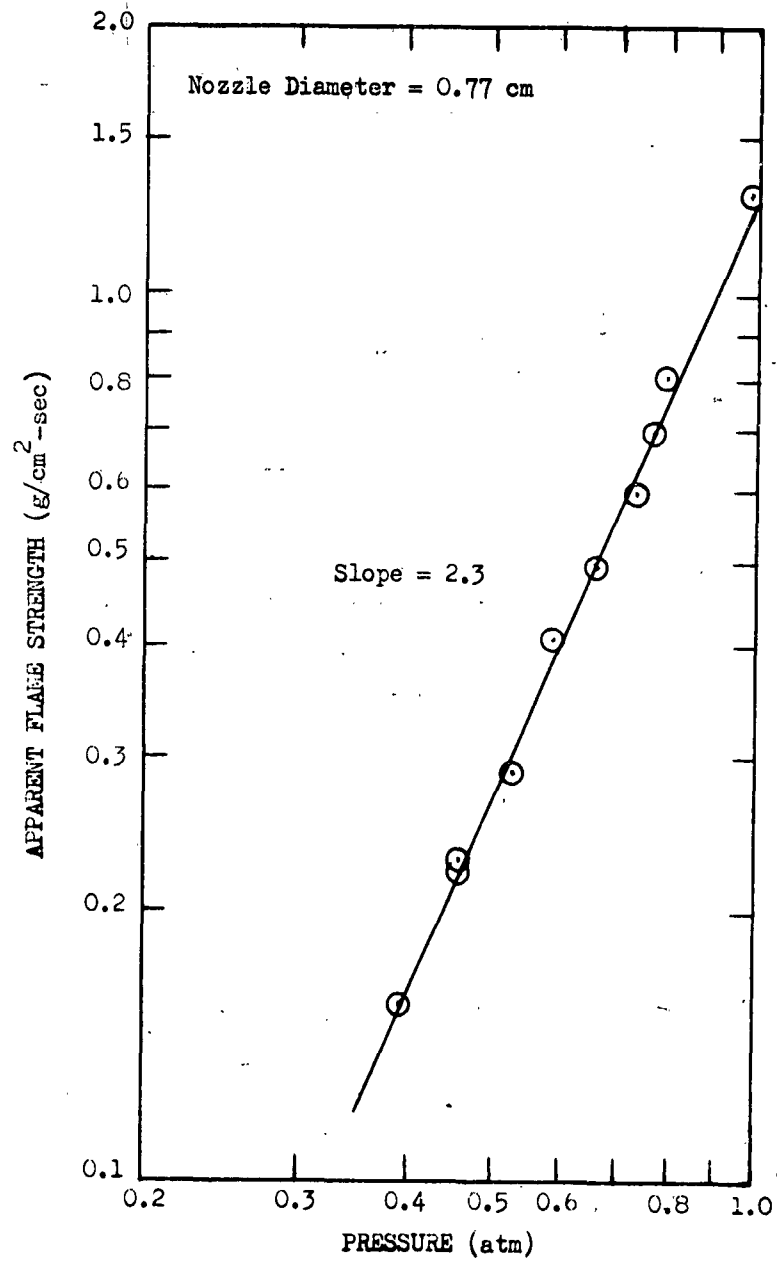


Figure 21

REACTION PRODUCTS FROM AMMONIA-CHLORINE FLAMES

Identification Number	Pressure, torr	N ₂	H ₂	HCl	Cl ₂	H ₂ O*	NH ₄ Cl**	Total	
								N ₂ , NO, NO ₂ ,	NOCl* HCl/N ₂
10	450	44.72	0.50	50.35	1.71	1.7	+	2.03	1.13
40	450	41.0	2.00	55.0	trace	-	+	2.06**	1.34
41	450	35.8	2.00	62.2****	-	-	+	-	1.74
44	300	50.2	-	49.8	-	-	+	0.10***	0.99

* The presence of H₂O and nitrogen oxides is the result of O₂ (air) contamination during the experiment.

** Quantitative data for NH₄Cl not available; + sign indicates white solid deposited in reactor was shown to be NH₄Cl.

*** NO only.

**** This value is uncertain because of leakage in the sample bulb.

AMMONIA-OXYGEN-CHLORINE FLAMES

(Nozzle Diameter: 0.77 cm)

<u>AFS,* Laminar Flow</u> <u>(g/cm²-sec)</u>	<u>Mass Fraction Cl₂</u> <u>in Mixture</u>	<u>Pressure,</u> <u>(torr)</u>
2.01	0.068	745
1.21	0.225	"
0.844	0.300	"
0.717	0.353	"
1.28	0.073	600
0.744	0.222	"
0.516	0.297	"
0.668	0.071	450
0.520	0.124	"
0.446	0.210	"
0.326	0.262	"
0.304	0.051	300
0.254	0.100	"
0.209	0.190	"
0.169	0.257	"

* AFS - Apparent flame strength

AMMONIA-OXYGEN-CHLORINE FLAMES

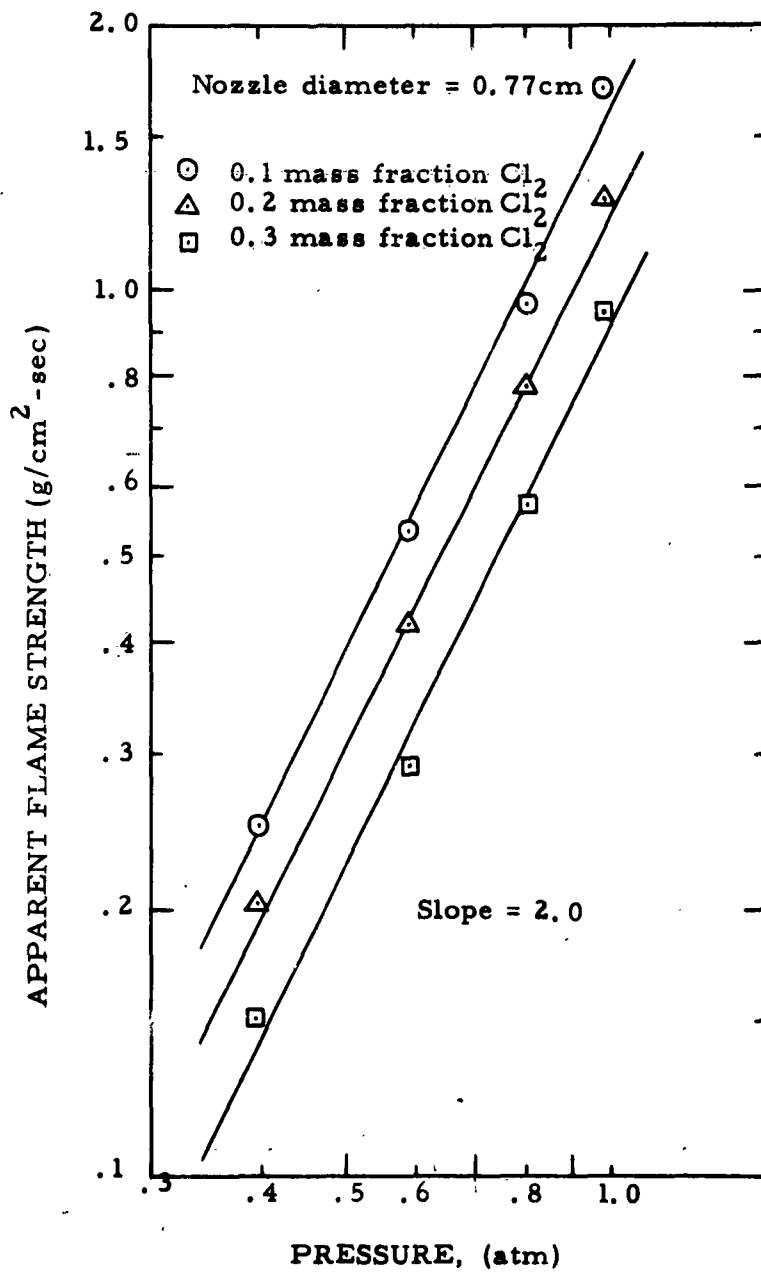


Figure 24

REACTION CONDITIONS FOR OPPOSED - JET FLAMES BETWEEN
AMMONIA AND NITRIC OXIDE

(Nozzle diameter = 0.77 cm)

	Identification Number																		
	20	21	22	23	24	25	26	27	28	29	30	31	32	53	54	55	56	57	58
Reactor Pressure, torr	300	350	400	450	500	550	600	650	700	750	800	850	900	950	1000	1050	1100	1150	1200
NH ₃ Flow Rate,* moles/min	0.106	0.135	0.168	0.188	0.226	0.259	0.315	0.355	0.374	0.459	0.509	0.546	0.640	0.652	0.706	0.756	0.810	0.825	0.866
NO Flow Rate,* moles/min	0.068	0.084	0.108	0.132	0.145	0.165	0.192	0.218	0.245	0.236	0.228	0.231	0.237	0.244	0.251	0.261	0.268	0.277	0.290
Mole ratio,* NH ₃ /NO	1.56	1.61	1.56	1.42	1.56	1.57	1.64	1.62	1.64	1.64	1.64	1.64	1.29	1.40	1.49	1.57	1.62	1.62	1.60
AFS**	0.139	0.173	0.221	0.258	0.296	0.338	0.408	0.462	0.494	0.475	0.458	0.459	0.472	0.486	0.486	0.486	0.486	0.486	0.486
AFS***	0.085	0.106	0.135	0.158	0.181	0.206	0.249	0.282	0.282	0.282	0.282	0.282	0.282	0.282	0.282	0.282	0.282	0.282	0.282

* Value at extinguishment. Average value of NH₃/NO for all experiments in approximately 1.5.
 ** Apparent flame strength (laminar flow).
 *** Apparent flame strength (turbulent flow).

Report 0372-01F

AMMONIA-NITRIC OXIDE FLAMES
Nozzle Diameter = 0.77 Cm
Laminar Flow

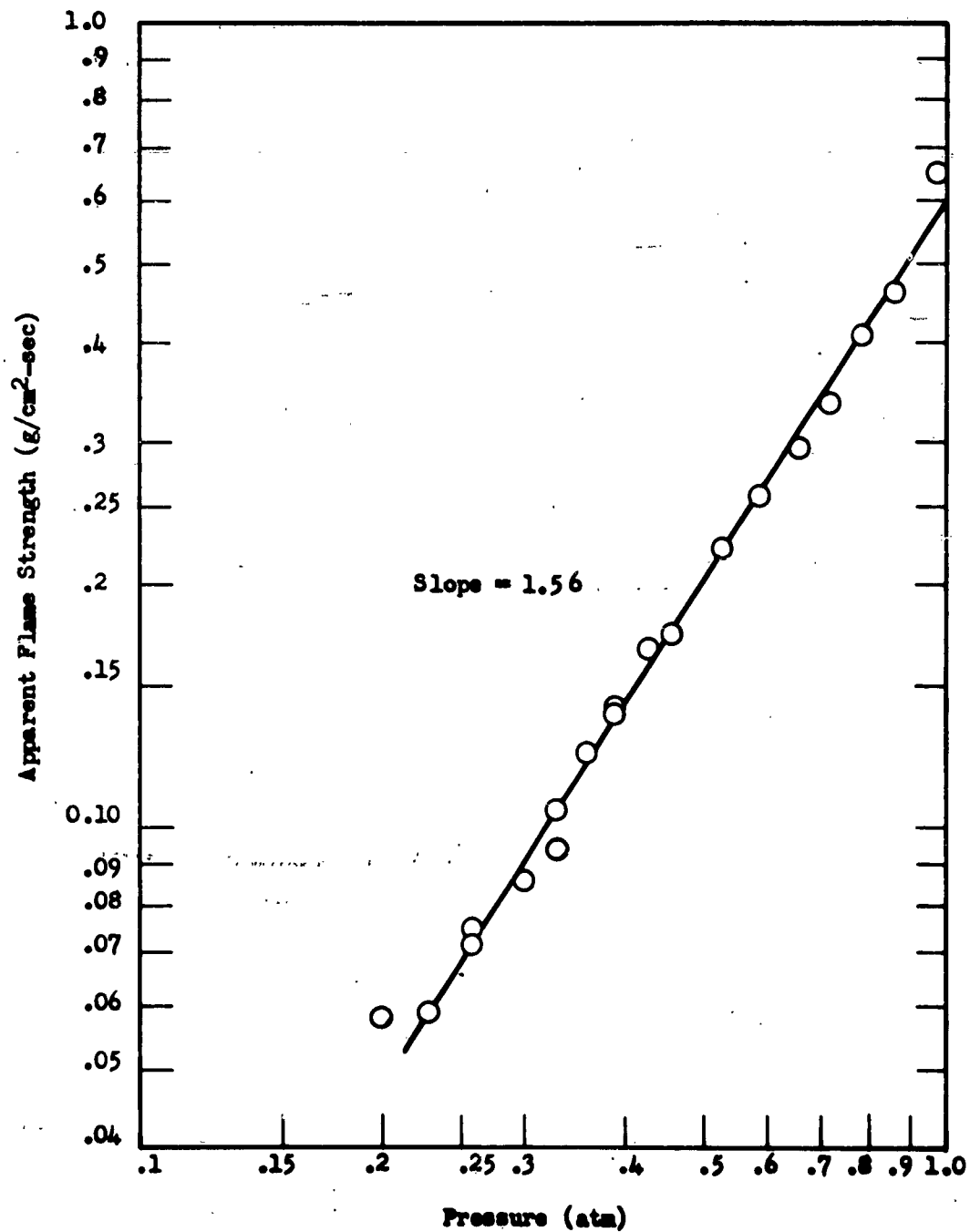


Figure 26

REACTION PRODUCTS FROM AMMONIA - NITRIC OXIDE FLAMES
(MASS SPECTROGRAPHIC ANALYSES)

Identification Number	Pressure, Torr	N_2	H_2	H_2O^*	NO^{**}	NH_3	H_2/N_2
20	300	56.0	41.0	2.97	-	-	0.73
23	450	57.9	40.7	1.40	-	< 0.3	0.70
27	650	53.9	38.4	-	7.7	-	0.71

* These values are inaccurate due to sampling technique.

** Unreacted.

Figure 27

REACTION CONDITIONS FOR OPPOSED - JET FLAMES
BETWEEN AMMONIA AND NITROUS OXIDE

(Nozzle diameter = 0.77 cm)

	Identification Number																
	31	32	33	34	35	36	37	38	39	40	40-1	45	46	47	48	49	50
Reactor Pressure, torr	100	150	200	350	400	450	500	550	600	650	745	175	225	275	250	300	325
NH ₃ Flow Rate,* moles/min	0.048	0.073	0.102	0.344	0.506	0.603	0.724	0.818	0.932	1.050	1.444	0.093	0.124	0.209	0.164	0.262	0.324
H ₂ O Flow Rate,* moles/min	0.026	0.040	0.057	0.204	0.268	0.331	0.417	0.489	0.539	0.764	0.907	0.048	0.075	0.126	0.093	0.144	0.174
Mole Ratio,* NH ₃ /N ₂ O	1.85	1.83	1.79	1.69	1.89	1.82	1.74	1.67	1.73	1.37	1.59	1.94	1.65	1.66	1.76	1.82	1.86
AFS**	0.044	0.108	0.153	0.534	0.735	0.895	1.106	1.278	1.428	1.861	2.326	0.134	0.195	0.328	0.249	0.390	0.476
AFS***	0.027	0.066	0.093	0.326	0.449	0.547	0.676	0.780	0.872	1.137	1.421	0.082	0.119	0.200	0.152	0.238	0.291

* Value at extinguishment. Average value of NH₃/N₂O for all experiments is 1.74.

** Apparent flame strength (laminar flow).

*** Apparent flame strength (turbulent flow).

Report 0372-01F

AMMONIA-NITROUS OXIDE FLAMES
Nozzle Diameter = 0.77 Cm
Laminar Flow

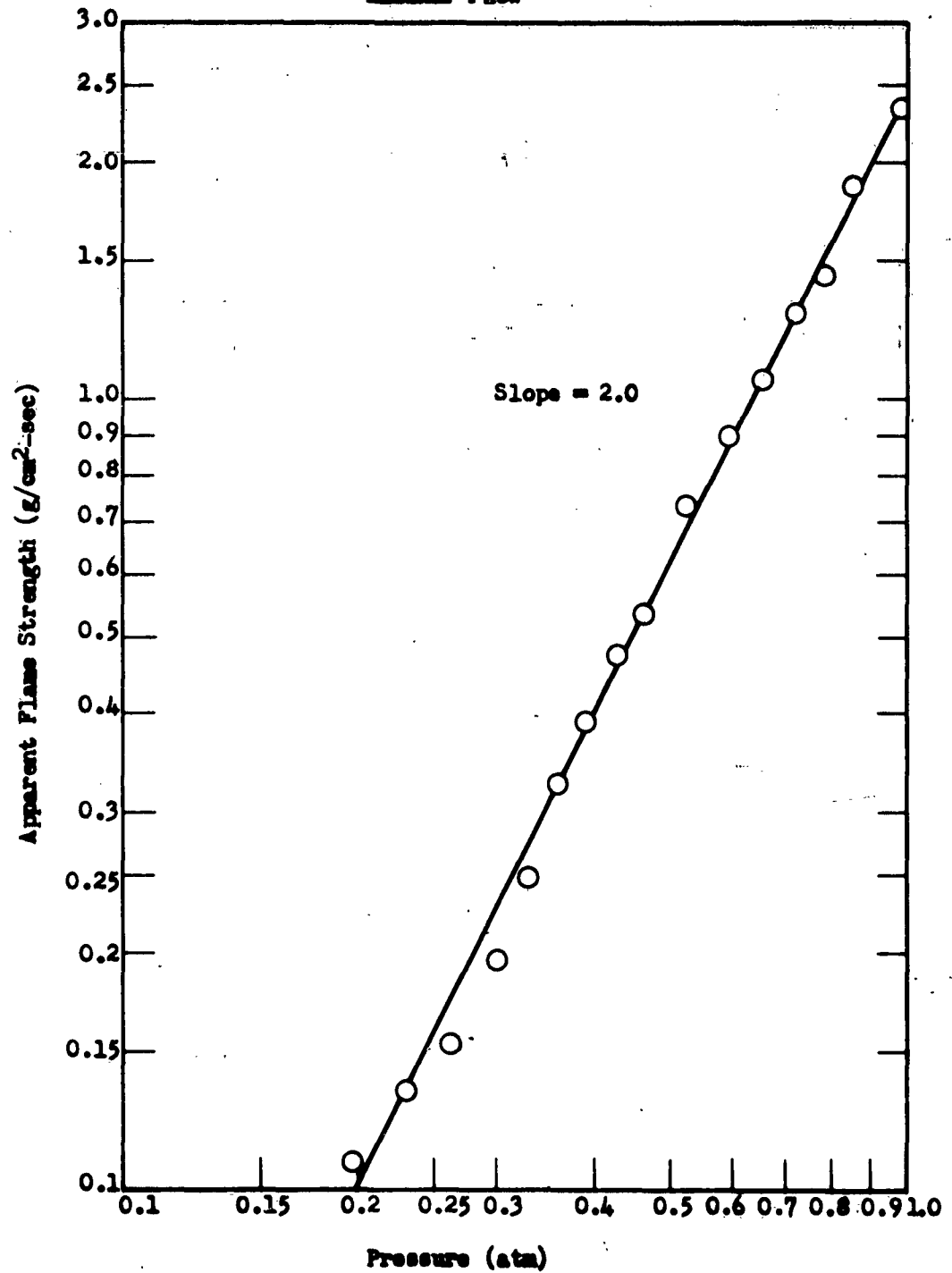


Figure 29

REACTION PRODUCTS FROM AMMONIA-NITROUS OXIDE FLAMES⁽¹⁾
(MASS SPECTROGRAPHIC ANALYSES)

Identification Number	Product Composition, Mole %						
	N ₂	H ₂	H ₂ O ⁽²⁾	NH ₃ ⁽³⁾	N ₂ O ⁽³⁾	H ₂ /N ₂ ⁽⁴⁾	NH ₃ /N ₂ ⁽⁵⁾
FCS-1 ⁽⁶⁾	53.3	14.4	0.8	29.7	1.8	0.27	0.56
FCS-2 ⁽⁷⁾	57.1	16.0	0.8	26.1	-	0.28	0.46
FCS-3 ⁽⁶⁾	56.7	13.8	0.5	27.4	1.6	0.24	0.48

- (1) Pressure = 450 torr
- (2) These values are inaccurate due to sampling technique
- (3) Unreacted
- (4) Average value = 0.26
- (5) Average value = 0.50 (corresponds to 0.75 moles NH₃ in products)
- (6) Samples taken at extinguishment ($\rho_{\infty} U_{\text{ext}}$)
- (7) Sample taken at 0.8 ($\rho_{\infty} U_{\text{ext}}$)

Figure 30

REACTION CONDITIONS FOR OPPOSED - JET FLAMES
BETWEEN AMMONIA AND NITROGEN DIOXIDE

(Nozzle diameter = 0.77 cm)

Identification Number	1-a	1-b	1-c	1-d	1-e	1-f	1-g	17	18	19
Reactor Pres- sure, Torr	400	450	500	550	600	600	745	450	300	650
NH ₃ Flow Rate* moles/min	0.153	0.200	0.276	0.306	0.388	0.382	0.612	0.221	0.100	0.503
NO ₂ Flow Rate* moles/min	0.089	0.130	0.167	0.198	0.248	0.259	0.452	0.166	0.054	0.391
Mole ratio* NH ₃ /NO ₂	1.72	1.54	1.65	1.55	1.56	1.48	1.35	1.33	1.18	1.29
AFS**	0.245	0.339	0.448	0.520	0.650	0.664	1.126	0.412	0.152	0.959
AFS***	0.150	0.207	0.273	0.318	0.397	0.406	0.688	0.251	0.093	0.586

* Value at extinguishment. Average value for all exper. is 1.46

** Apparent flame strength (laminar flow).

*** Apparent flame strength (turbulent flow).

AMMONIA-NITROGEN DIOXIDE FLAMES

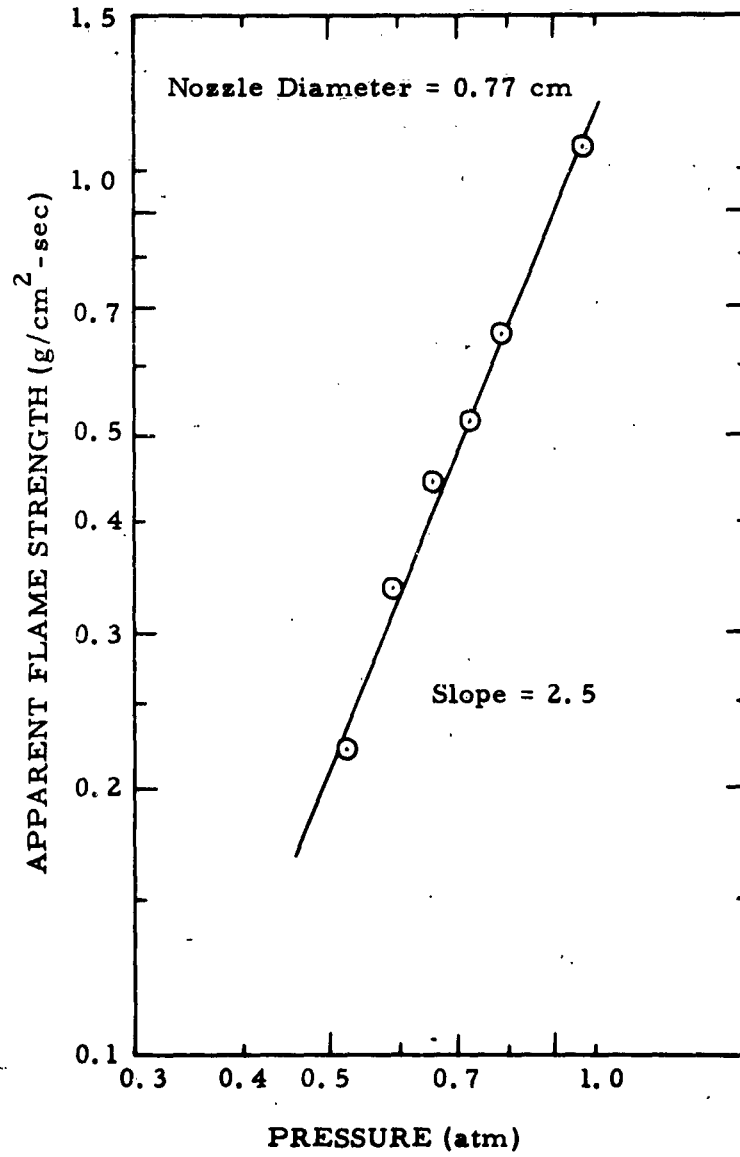


Figure 32

OPPOSED-JET REACTION PARAMETERS (1)
FOR AMMONIA AT 1 ATMOSPHERE PRESSURE

Oxidizer	$AFS(\rho_{\infty} U_{ext.})^{(2)}$ gr/cm ² -sec	$N_{fu}/N_{ox}^{(3)}$ Meas. Theor.	$Y_{st}(\rho_{\infty} U_{ext.}/\gamma_{\infty} D)^{1/2}$	$M_{fu,\infty}$	f_{st}	ρ/ρ_{∞}	r	$\Delta H/gr NH_3^{(4)}$ cal/gr
O ₂	2.20	1.77 1.67	-0.06	1.0	0.47	0.50	1.13	-3410
Cl ₂	1.30	2.25 2.33	-0.256	1.0	0.36	0.58	1.79	-2702
NO	0.65	1.5 1.50	-0.07	1.0	0.46	0.43	1.18	-2464
N ₂ O	2.35	1.74 ⁽⁵⁾ 1.75	-0.17	0.57	0.41	0.33	2.59	-3898

Report 0372-01F

(1) At extinguishment ($U - U_{ext.}$)

(2) AFS = Apparent flame strength; laminar flow

(3) Mole ratio of fuel to oxidizer (meas. = average value of all experiments)

(4) Heat of reaction per gram of fuel for the given stoichiometry

(5) In this reaction, 0.75 moles of ammonia remained unreacted, therefore, parameters are based on $fu/ox = 1.0$

AMMONIA OXIDATION IN OPPOSED-JET DIFFUSION FLAMES
(SUMMARY OF RESULTS)

Oxidizer	Reaction Order	$\dot{m}_{fu, \max}^*$ gr 3 Cm ³ -sec	$\frac{Col}{\dot{q}_{\max}^{**}}$ 3 Cm ³ -sec
O ₂	1.7	7.09	2.42 x 10 ⁴
Cl ₂	2.3	3.39	9.17 x 10 ³
NO	1.56	2.73	6.73 x 10 ³
N ₂ O	2.0	1.95	7.6 x 10 ³

* $\dot{m}_{fu, \max}^*$ = volumetric rate of reaction

$\bar{\psi}_{st}$ used in these calculations approximated to be 0.25

** \dot{q}_{\max}^{**} = volumetric heat release rate

Report 0372-01F

APPENDIX A

SURFACE RATE PROCESSES AND SENSITIVITY
OF HIGH EXPLOSIVES*

R. F. Chaiken** and F. J. Cheselske***

(Submitted for Publication in the Journal of Chemical Physics)

Solid Propellant Research Operations
Aerojet-General Corporation
Azusa, California

*This work was supported by the Advanced Research Projects Agency under Contracts NONr 2804(00) monitored by the Office of Naval Research, and Contract AF 49(638)-851 monitored by the Air Force Office of Scientific Research

**Technical Consultant to Aerojet-General Corporation

***Research Chemist, Combustion Section, Advanced Propellants Department.

Report O372-01F

APPENDIX A

I. INTRODUCTION

In previous papers from these laboratories,^{1,2} it was shown that

-
1. W. H. Andersen and R. F. Chaiken, ARS Journal, 29, 49 (1959).
 2. W. H. Andersen and R. F. Chaiken, ARS Journal, 31, 1379 (1961).

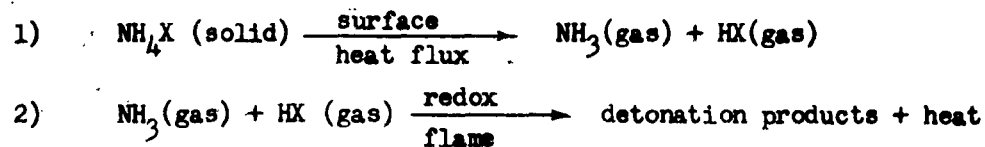
kinetic data for the surface gasification (pyrolysis) of ammonium nitrate and perchlorate could be used in conjunction with the Eyring Grain Burning Theory³ to describe the chemical rate processes occurring during detonation

-
3. H. Eyring, R. E. Powell, G. H. Duffey and R. B. Parlin, Chem. Rev., 45, 69 (1949).

of these low-energy explosives. The linear rates of surface gasification, which were determined as a function of surface temperature by the hot-plate linear pyrolysis technique,^{4,5} suggested the following overall reaction scheme

-
4. M. K. Barsh, W. H. Andersen, K. W. Bills, G. Moe and R. D. Schultz, Rev. Scient. Instr., 29, 392 (1958).
 5. R. F. Chaiken and D. K. Van de Mark, Rev. Scient. Instr., 30, 375 (1959).

during grain burning:



These findings naturally led to the question of whether or not the detonation of high-energy explosives could proceed by a similar reaction

APPENDIX A

scheme, viz., endothermic surface evaporation followed by exothermic gas-phase decomposition.

Toward this viewpoint, the hot-plate linear pyrolysis technique was applied to the four common high explosives TNT, Tetryl, RDX and PETN. It was found that over the range of surface heating conditions imposed (surface heat flux as high as $60 \text{ cal/cm}^2\text{-sec}$), the surface rate process consisted of melt-flow which proceeded at measured linear surface regression rates as high as 0.2 cm/sec . During these experiments, hot-plate temperatures as high as 500°C (well above the isothermal "explosion temperature" for these materials) were recorded. Although the data are not compatible with grain burning detonation rates, they do constitute a measure of the rate at which the surface thermal energy was dissipated. This rate of energy dissipation at the surface of an explosive granule is believed to be of considerable importance in determining the sensitivity of the explosive to initiation by external stimuli (e.g., impact and friction)⁶.

6. F. P. Bowden and A. D. Yoffe, Initiation and Growth of Explosives in Liquids and Solids, University Press, Cambridge (1952).

II. EXPERIMENTAL

The explosives utilized in these studies were of standard military type which were not given any further purification treatment. The explosive in powder form (passed through a U. S. Standard No. 100 sieve) was pressed under 30-40 thousand psi forming pressure into solid strands or pellets for use with the hot-plate apparatus. For PETN and RDX, it was found necessary to incorporate a small amount of binder (polystyrene or nitro-

APPENDIX A

cellulose) into the powder in order to form high-density coherent strands. Solid explosive strands having a density within 88% of crystal density were obtained by these techniques. Figure 1 lists details of the strand characteristics.

Measurements of the linear rate of surface regression of the solid strands under surface heating conditions were obtained with the use of the hot-plate linear pyrolysis apparatus described in detail elsewhere.^{4,5} Briefly, surface heating is accomplished by pressing the end of a sample strand upward against an electrically heated hot-plate. A small Pt (Pt-10% Rh) thermocouple junction, which is imbedded in the hot-plate and positioned at the strand-hot-plate interface, enables the hot-plate temperature (T_h) to be recorded, while the linear rate of regression of the strand surface (B) is measured. For conditions of constant T_h , a constant B is obtained. Varying the electrical power expended in the hot-plate causes a variation in T_h and hence B .

The rate data obtained in this fashion are shown in Figures 2-5 plotted as $\log (B/T_h)$ vs. $1/T_h$ type rate curves. Interestingly, the apparent constant slope of the curves at elevated temperature, corresponding to a linear surface regression rate equation of the form

$$B = AT_h \exp(-E/RT_h) \text{ cm/sec} \quad (1)$$

is reminiscent of what one might expect for a surface decomposition reaction where $T_h = T_s$, the strand surface temperature.^{1,2,7} However, in spite of

7. R. F. Chaiken, W. H. Andersen, M. K. Barsh, E. Mishuck, G. Moe and R. D. Schultz, J. Chem. Phys., 32, 141 (1960).

APPENDIX A

hot-plate temperatures which in some instances reached as high as 770°K, only a slight amount of decomposition was observed in any experimental run. The explosive strands, in each case, seemed to melt and flow away from the strand-hot-plate interface.*

Inspection of the TNT and PETN data indicates that within the experimental data scatter, change in environmental pressure from $\sim 10^{-3}$ to 1 atm has no discernible effect on the melt-flow surface rate. Also, the fact that the surface regression rates for PETN appear to be independent of the type of binder (unreactive polystyrene vs. reactive nitrocellulose) would indicate that the 3% level of binder used in forming the strands, does not influence the inherent surface rate process.

As an aid to interpreting the observed hot-plate surface rate process, the slopes of the straight lines drawn through the upper temperature regime data points of Figures 2-5 were determined to yield "apparent activation energies" and pre-exponential constants corresponding to values of E and A in Equation (1). Surprisingly these values, which are listed in Figure 6, were found to correspond to what might be expected as an energy barrier to a rate process involving melting or viscous flow. According to Eyring's Absolute Rate Theory, the energy barrier to melting and/or viscous flow should be of the order of the heat of fusion.⁸ Unfortunately, data on the heat of fusion

8. S. Glasstone, K. J. Laidler and H. Eyring, Theory of Rate Processes, McGraw-Hill, New York (1941) Ch. 9.

and viscosity coefficient for the explosives of interest are too limited for an

* In the case of TNT, the melt-flow process was verified by high-speed motion pictures of a vacuum run, and recovery of the melt.

Report 0372-01F

APPENDIX A

exact comparison of the results at this time. However, similar melt-flow rate data on benzoic acid, obtained in these laboratories with both the hot-plate and Ostwald viscosimeter techniques (see Figures 7, 8) do allow a precise comparison of results. As seen from Figure 6, the apparent activation energy of 4.1 kcal/mole for the hot-plate surface rate data compares quite favorably with the heat of fusion (4.14 kcal/mole), and the "activation energy" for the temperature variation of viscosity (4.12 kcal/mole).

These correlations are undoubtedly more than fortuitous, thus suggesting that some rate controlling kinetic process related to the explosive itself is occurring at the strand hot-plate interface. If this were so, then Equation (1) can be treated as a surface boundary condition for dissipation of energy under similar surface heat-flux conditions. Bowden,⁶ in his hot-spot treatment of impact and friction initiation of granular explosives, has already suggested that intergranular friction accompanied by melting at the surfaces of the granules could control hot-spot temperatures, and hence, sensitivity to initiation.

This point as well as an analysis of the kinetic processes which are believed to occur is discussed in the following sections.

III. THEORETICAL

A. Analysis of the Hot-Plate Experiment

A proper treatment of the detailed surface rate processes occurring in the hot-plate heating experiment requires consideration of the energy and mass transport in the melt layer separating the hot-boundary, (represented by the hot-plate) and the cold boundary (represented by the strand surface). Solutions to the conservation equations representing such flow phenomena are generally a formidable task requiring numerical methods;

APPENDIX A

however, the simple geometry and steady-state nature of the hot-plate experiment allows for simplifications which render the problem tenable. Cantrell⁹ has demonstrated this for the case of a solid evaporating at a

9. R. H. Cantrell, AIAA Journal, 1, 1544 (1963).

hot-plate surface where the flow velocity in the gas-film layer is subsonic. Solutions have also been presented¹⁰ for the same problem when supersonic

10. R. F. Chaiken, D. J. Sibbett, J. E. Sutherland, D. K. Van de Mark and A. Wheeler, J. Chem. Phys., 37, 2311 (1962).

flow velocities occur in the gas-film layer.

For the melt-flow problem of interest here, flow velocities are undoubtedly subsonic, hence an approach similar to Cantrell's should be applicable.

The model of the hot-plate experiment considered is shown in Figure 9, where cylindrical geometry with radial symmetry is assumed.

The mass balance at steady-state values of the surface regression rate, B , is determined directly by equating the melt flux introduced axially into the melt layer from the surface, to the melt flux passing radially through the melt layer parallel to the strand surface, i.e.,

$$2\pi \int_0^{\delta} \rho_s B r dr = 2\pi \int_0^{\delta} \rho_m u r dz \quad (2)$$

where ρ_s and ρ_m are the densities of the solid and melt respectively; r and z are the respective radial and axial distances in the melt layer;

APPENDIX A

u is the radial flow velocity of the melt, and δ is the thickness of the melt layer.

For constant densities, B can be expressed as

$$B = \frac{2 \rho_m}{r \rho_s} \int_0^{\delta} u dz \quad (3)$$

Now $u(r, z)$ can be readily obtained from the momentum conservation, where it is assumed that 1) the viscosity, η , of the melt can be treated as an averaged constant, and 2) the pressure gradient (ΔP) is zero in the axial direction, i.e., $P = P(r)$. Thus the conservation of momentum is expressed by

$$(dP/dr) = \eta(\delta^2 u / \delta z^2), \quad (4)$$

which can be solved for u under the viscous flow boundary conditions, $u = 0$ at both the strand surface ($z = 0$), and the hot-plate surface ($z = \delta$). Direct integration of Equation (4) gives

$$u = (z/2\eta)(z - \delta)(dP/dr) \quad (5)$$

Substitution of this expression for u into Equation (3) yields the following expression for the radial pressure gradient.

$$(dP/dr) = -(6\eta \rho_s B r) / (\rho_m \delta^3) \quad (6)$$

Taking the pressure at the outer edge of the strand (i.e., at $r = b$) to be the ambient pressure P_0 , integration of Equation (6) defines the pressure explicitly in terms of r , i.e.,

$$P(r) - P_0 = \frac{3\eta \rho_s B(b^2 - r^2)}{\rho_m \delta^3} \quad (7)$$

APPENDIX A

Now since the pressure in the melt layer arises from the strand loading force W , $P(r) - P_0$ is related to W by the expression

$$W = 2\pi \int_0^b (P - P_0) r dr \quad (8)$$

This results in an equation for B in which only the melt layer thickness δ , is unknown, i.e.,

$$B = (2 \rho_m W \delta^3) / (3\pi \eta \rho_s b^4) \quad (9)$$

It now remains to determine δ in terms of the temperature gradient across the melt layer. It is interesting to note that for benzoic acid at $B = 0.1$ cm/sec, reasonable values of the other parameters of Equation (9) give a value for δ of $\sim 2 \times 10^{-3}$ cm, which is larger than the estimated roughness of the hot-plate surface.

The steady-state energy balance at the strand surface can be written as

$$\dot{q}_s = \lambda (\partial T / \partial z)_{z=0} = \rho_s B [L_f + C_s (T_s - T_0)] \quad (10)$$

where \dot{q}_s is the heat flux/unit area at the strand surface; L_f is the latent heat of fusion of the solid; C_s is the specific heat of the solid assumed independent of temperature, λ is the heat conductivity of the melt layer (assumed to be an averaged constant); T_s is the strand surface temperature (assumed to be the melting point of the solid); and T_0 is the ambient initial temperature of the solid.

Assuming the temperature T , in the melt layer to be isothermal in the radial direction, the stationary heat transport in the region $0 \leq z \leq \delta$ is described by

$$w(dT/dz) + K(d^2T/dz^2) = 0 \quad (11)$$

APPENDIX A

where w is the axial component of the melt flow velocity, and $K = \lambda / \rho_m c_m$ is the thermal diffusivity of the melt (assumed to be an averaged constant).

For the conditions of interest here, it is reasonable to neglect the convective term of Equation (11) so that $d^2T/dz^2 = 0$, which leads to the temperature distribution

$$T = (T_h - T_s)z/\delta + T_s \quad (12)$$

This approximation can be justified by considering w to be constant over much of the melt layer. For this condition, the temperature distribution corresponding to Equation (11) is¹¹

11. D. Rosenthal, Trans. Amer. Soc. Mech. Engrs., 68, 849 (1946).

$$\frac{T_h - T}{T_h - T_s} = \exp(-wz/K) = 1 - \frac{wz}{K} + \frac{1}{2} \left(\frac{wz}{K}\right)^2 - \dots \quad (13)$$

For the hot-plate conditions of interest, $|wz/K| \ll 1$ so that second-order or higher terms in the expansion may be neglected.* Thus; dT/dz is approximately constant which justifies the approximation leading to Equation (12).

The melt layer thickness δ can then be derived from Equations (10) and (12) yielding

$$\delta = \left(\frac{\rho_m c_m}{\rho_s c_s} \right) \frac{K (T_h - T_s)}{B [L_f/c_s + (T_s - T_o)]} \quad (14)$$

* A maximum value for $|wz/K|$ would be ≈ 0.1 corresponding to $w = \rho_s B / \rho_m \approx 0.1$ cm/sec, $z = \delta = 10^{-3}$ cm; $K \approx 10^{-3}$ cm²/sec.

APPENDIX A

which when combined with Equation (9), gives the following expression for B.

$$B = \left[\left(\frac{2 \rho_m}{3\pi \rho_s} \right) \left(\frac{\rho_m c_m}{\rho_s c_s} \right)^3 \left(\frac{T_h - T_s}{L_f/c_s + T_s - T_o} \right)^3 \frac{W}{b^4} \right]^{\frac{1}{2}} (\phi K^3)^{\frac{1}{2}} \quad (15)$$

where $\phi = \eta^{-1}$ is the fluidity of the melt.

Now it should be recalled that in the derivation of Equation (15), the transport coefficients K and ϕ , as well as the densities and specific heats, were assumed to be constants averaged over a given region in space. While it might be expected that the ratios ρ_m/ρ_s and c_m/c_s are relatively independent of T_h , the variation of ϕK^3 with T_h should be considered in determining $B(T_h)$. Over the region $0 \leq z \leq \delta$, the average value of a parameter is determined by the expression

$$\langle F(\delta) \rangle = \frac{\int_0^{\delta} F(z) dz}{\int_0^{\delta} dz} \quad (16)$$

or in terms of temperature (see Equation 12),

$$\langle F(T_h) \rangle = \frac{1}{(T_h - T_s)} \int_{T_s}^{T_h} F(T) dT \quad (17)$$

where $\langle F(T_h) \rangle$ is the average value of the function F of interest (i.e., ϕ , K or ϕK^3).

From the Eyring-Absolute Rate Theory treatment of diffusion and viscous flow as rate processes⁸, it can be expected that the energy barriers for thermal conduction, self-diffusion and viscous flow should be very nearly the same. This is reflected in the well known Einstein-diffusion equation, in which the diffusion coefficient is directly proportional to the fluidity, and in

APPENDIX A

the fact that the Lewis Number (ratio of diffusion coefficient to thermal diffusivity) is approximately unity in many flow systems. Thus, in accordance with the Eyring theory it should be possible to represent the temperature variation of ϕ and K as Arrhenius type functions, i.e.,

$$F(T) = F_0 \exp(-E_F/RT) \quad (18)^*$$

where the activation energy E_F is the same for thermal diffusivity and fluid flow.

In this manner, Equation (17) for the average value of $\phi K^3(T_h)$ becomes

$$\langle \phi K^3(T_h) \rangle = \frac{\phi_0 K_0^3}{(T_h - T_s)} \int_{T_s}^{T_h} \exp(-E/RT) dT \quad (19)$$

where $E = E_\phi + 3E_K \cong 4E_\phi$.

While Equation (19) cannot be integrated directly, it can be shown that the appearance of the exponential term in the integrand as a weight factor will result in an average value of ϕK^3 which lies closer to the value of the function at T_h than at T_s . This is particularly true for values of E much larger than RT . For purposes of obtaining a closed solution for the average value $\phi K^3(T_h)$, Equation (19) can be reasonably approximated by

$$\langle \phi K^3 \rangle = \frac{\phi_0 K_0^3 R \langle T \rangle^2}{E (T_h - T_s)} \int_{x(T_s)}^{x(T_h)} \exp(x) dx \quad (20)$$

where $\langle T \rangle = (T_h + T_s)/2$ and $x = (-E/RT)$.

* The symbol F represents either ϕ or K .

APPENDIX A

Integration of Equation (20) yields

$$\langle \phi K^3(T_h) \rangle = \frac{\phi_o K_o^3 R(T_h + T_s)^2}{4 E(T_h - T_s)} \left[\exp(-E/RT_h) - \exp(-E/RT_s) \right]. \quad (21)$$

Replacing ϕK^3 in Equation (15) by $\langle \phi K^3 \rangle$ results in the final expression for $B(T_h)$,

$$B(T_h) = A(T_h^2 - T_s^2)^{\frac{1}{2}} \left[\exp(-E/RT_h) - \exp(-E/RT_s) \right]^{\frac{1}{2}} \quad (22)$$

$$\text{where } A = \left[\left(\frac{2}{3\pi} \right) \left(\frac{\rho_m}{\rho_s} \right) \left(\frac{\rho_m c_m}{\rho_s c_s} \right)^3 \frac{\phi_o K_o^3 R W}{16 E_o b^4 (L_f/c_s + T_s - T_o)^3} \right]^{\frac{1}{2}}$$

It is interesting to note that when T_h approaches T_s , $B(T_h)$ rapidly approaches zero, but as T_h increases above T_s , the expression for $B(T_h)$ approaches

$$B = A T_h \exp(-E_o/RT_h) \quad (23)$$

in agreement with the empirical curve found for the high temperature regime of the hot-plate data (Equation 1).

Using the parameter values listed in Figure 10, $B(T_h)$ was calculated and compared with the experimental hot-plate data for benzoic acid. As can be seen in Figure 7, the theoretical curve represents a reasonably good fit to the experimental data, thus indicating that the assumption of heat transport and forced viscous flow of melt as the rate controlling process at the strand-hot-plate interface is consistent with the experimental data.

B. Application to Explosive Sensitivity

The classical investigations of Bowden and his colleagues⁶ of the impact and friction sensitivity of granular high explosives clearly

Report 0372-01F

APPENDIX A

demonstrate the possible role of melting as a mechanism of degrading the kinetic energy of the external stimuli to heat. Their studies of the sensitization of explosives by high melting ($> 400^{\circ}\text{C}$) grit impurities showed that the effectiveness of a grit impurity in promoting initiation increases directly with its melting point. It was postulated that under the action of impact and friction, hot-spots are induced within the explosive sample by intergranular rubbing. Presumably, the highest temperature achieved by this mechanism of energy dissipation is the melting temperature of the explosive and/or grit; hence, impurities having melting points exceeding the hot-spot temperature necessary for growth of explosion (e.g., $400\text{--}500^{\circ}\text{C}$ for C-H-N-O explosives) will sensitize the explosive to impact and friction initiation.

Unfortunately, this correlation of melting point with sensitivity apparently fails when pure explosives are considered. This is readily seen by comparing the melting point and impact sensitivity of PETN (m.p. = 142°C ; 50% impact height ≈ 15 cm) with that of RDX (m.p. = 204°C ; 50% impact height ≈ 25 cm).¹² Also, it is readily calculated that the rate of isothermal

12. A. D. Little Co., "Punch Card Recording of Data on Explosives,"
Final Summary Report Contract DA 19-020-ORD-173 (March 31, 1954).

decomposition of typical high explosives at their melting point is far too slow to account for a rapid initiation under impact (see Figure 11).

This lack of correlation led Bowden⁶ and Cook¹³ to suggest

13. M. A. Cook, The Science of High Explosives, Reinhold Publishing Corp., New York (1958) p. 180.

Report 0372-01F

APPENDIX A

that in pure C-H-N-O explosives, initiating hot-spots (400-500°C) arise from adiabatic compression of vapor pockets rather than from intergranular rubbing. However, it can be shown on the basis of the current hot-plate data on explosives that melting with viscous flow can also result in initiating hot-spots.

It is assumed, along with Bowden, that in an impact or friction sensitivity measurement, the kinetic energy of the external stimulus (e.g., a falling weight) is converted to heat by the action of explosive particles being pressed and rubbed against each other. It is further assumed that the initial hot-spot temperature will depend upon the endothermic rate processes which occur in the vicinity of the inter-particle contact surface. The analysis of the hot-plate data in the previous section suggests that this type of surface heat generation will result in melting at the particle surface with viscous flow of heated melt in a thin layer separating the actual solid particle surfaces. With this model it might be expected that the rate at which the particles can melt will be given by Equation (1) or (22) where B is now the linear rate of melting of the explosive granule, and T_h the highest temperature in the melt. T_h can also be considered the induced hot-spot temperature.

The energy balance between the rate of energy delivered into the explosive sample per unit of contact area, \dot{Q}_{in} , and the rate of energy dissipated by melt flow at the contact surfaces is then simply

$$\dot{Q}_{in} = \rho_s B [L_f + C_s(T_h - T_0)] \quad (24)$$

where T_0 is the temperature of the explosive before impact, and where it is assumed that the heat capacity of the explosive is independent of temperature and phase. The hot-spot temperature, T_h , can be related directly to \dot{Q}_{in} by expressing B in terms of Equation (1) or (22).

APPENDIX A

A plot of $\log \dot{Q}_{in}$ vs T_h for the four explosives studied is shown in Figure 12.* It is readily apparent that, at any given melt temperature above 250°C, the order in which kinetic energy can be dissipated by melting is given by TNT > Tetryl > RDX > PETN. Likewise, at any given energy input, the induced hot-spot temperatures would be in the order PETN > RDX > Tetryl > TNT, which is just the order of decreasing impact sensitivities of these explosives. Hence, it is suggested that impact sensitivity should be correlated by the rate at which kinetic energy of impact can be dissipated by endothermic surface melting, and not by the melting temperature alone. This consideration is certainly in keeping with the observed sensitivity data as well as with a self-heating type of mechanism for the growth of exothermic reaction (in the melt) to explosion.**

It is interesting to note that below 250°C, the rate of surface energy dissipation by PETN is greater than that of RDX. This would imply that under conditions where hot-spot temperatures less than 250°C are required to cause initiation, RDX may be more sensitive than PETN. However, under most conditions of impact measurements, minimum critical hot-spot temperatures lie in the range of 400-500°C.

In the case of impact sensitivity measurements carried out under standardized procedures it is even possible to use the hot plate data

* In calculating \dot{Q}_{in} , the heat of fusion was taken as being equal to the apparent activation energy for melt flow. The data of Figure 6 indicates that this is probably a reasonable approximation.

** A self heating type of growth mechanism leads to the concept of a critical minimum hot-spot temperature required for initiation of the explosive.

Report O372-01F

APPENDIX A

to estimate relative impact sensitivities. Under standard conditions it might be reasonable to expect that \dot{Q}_{in} will be directly proportional to the kinetic energy of the falling hammer, with a proportionality constant which is the same for the four C-H-N-O explosives under consideration. Also, there is evidence^{6, 13} that the hot-spot temperature required for initiation by impact is approximately the same (400-500°C) for these high explosives. With these conditions, the values of \dot{Q}_{in} should be in the same ratio as the values of the impact heights necessary to initiate the explosive. Figure 13 shows a comparison of these ratios at $T_h = 400^\circ\text{C}$ and $T_h = 600^\circ\text{C}$. It is readily seen that there is reasonably good agreement between the calculated and experimental ratios, and that the ratios are relatively independent of the choice of T_h .

It is perhaps worthwhile to show that the absolute values of \dot{Q}_{in} ($T_h \approx 500^\circ\text{C}$) are of a reasonable order of magnitude on the basis of the initiating kinetic energy of a falling weight. Most standard impact measurements are made with a 2.5 kg hammer with a ~35 mg sample of explosive. It has been estimated¹⁴ that the time duration of the kinetic energy of impact

14. J. Wenograd, "Third ONR Symposium on Detonation," held at Princeton University September 1960; ONR Symposium Report ACR-52 Vol. I, p. 60.

is $\sim 250 \mu\text{sec}$. Assuming spherical explosive granules of radius r_p and a circular contact area of radius r_c , \dot{Q}_{in} can be approximated by

$$\dot{Q}_{in} = \frac{\text{(kinetic energy of impact)}}{(\# \text{ of particles}) \times (\text{contact area/particle}) \times (\text{impact duration})}$$

$$\dot{Q}_{in} = 8 h r_p^3 / r_c^2 \text{ cal/cm}^2\text{-sec}$$

where h , the impact height, r_p and r_c are given in cm.

Report 0372-01F

APPENDIX A

While the value of r_c is not known, it might be reasonable to expect a value of 5μ when $r_p = 50\mu$. Thus an impact height of 50 cm would correspond to $\dot{Q}_{in} \sim 200$ cal/cm-sec, which is within the range of values expected from the hot-plate data.

APPENDIX A

IV. SUMMARY

The nature and rate of linear surface regression of TNT, RDX, tetryl and PETN has been studied utilizing a hot-plate pyrolysis technique over surface temperatures ranging as high as 500°C. The data when compared to similar data for benzoic acid suggests that the primary surface rate process appears to be an endothermic melt-flow having an apparent activation energy suggestive of heat-transfer and viscous flow as a rate controlling step.

These data, when used as a measure of surface heat dissipation, correlate very well with the measured values of impact sensitivity. Also, they offer an explanation for the fact that attempts to correlate impact and/or friction sensitivity with melting point alone could lead to misleading results when PETN and RDX are considered.

Report 0372-01F

APPENDIX A

PHYSICAL CHARACTERISTICS OF EXPLOSIVE STRANDS

	Approx. Strand Dimensions <u>l x w x d (cm)</u>	Forming Pressure (psi)	Strand X-sectional <u>(cm²)</u>	Average Strand Density (gm/cm ³)	X-tal** Density (gm/cm ³)
TNT	3.8 x 0.4 x 0.4	40,000	0.17	1.58	1.65
Tetryl	3.8 x 0.4 x 0.4	30,000	0.16	1.52	1.73
RDX*	4.8 x 0.6	40,000	0.32	1.61	1.82
PETN*	4.8 x 0.6	40,000	0.32	1.57	1.77

* Prepared by cementing 5 cylindrical pellets together with Eastman 910 cement. Pellets formed with 3 wt% of binder, either polystyrene or nitrocellulose.

** W. R. Tomlinson, Jr., "Properties of Explosives of Military Interest" Technical Report No. 1740 Picatinny Arsenal, Dover, N. J., Revised by O. E. Sheffield, April 1958.

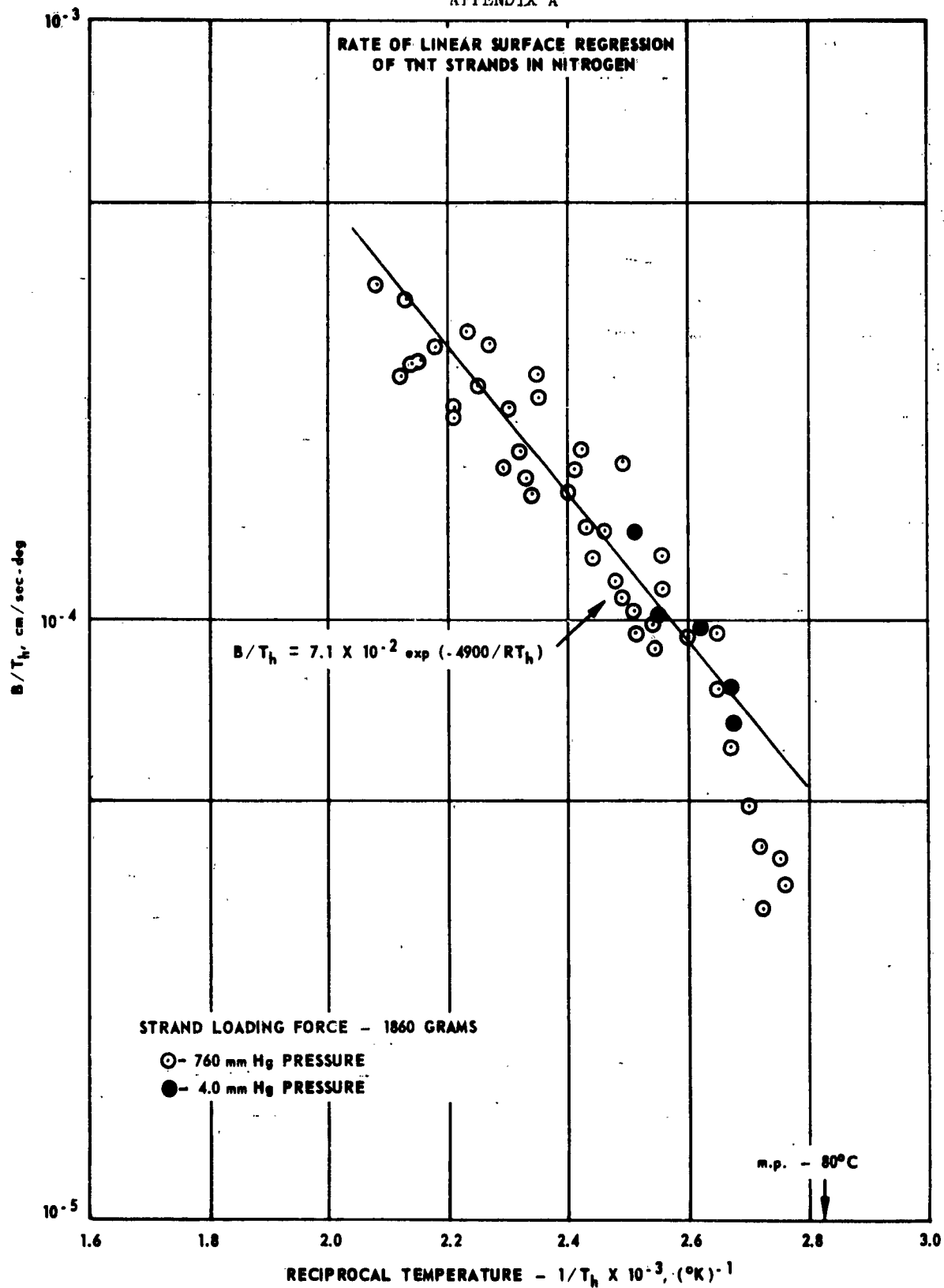


Figure 2

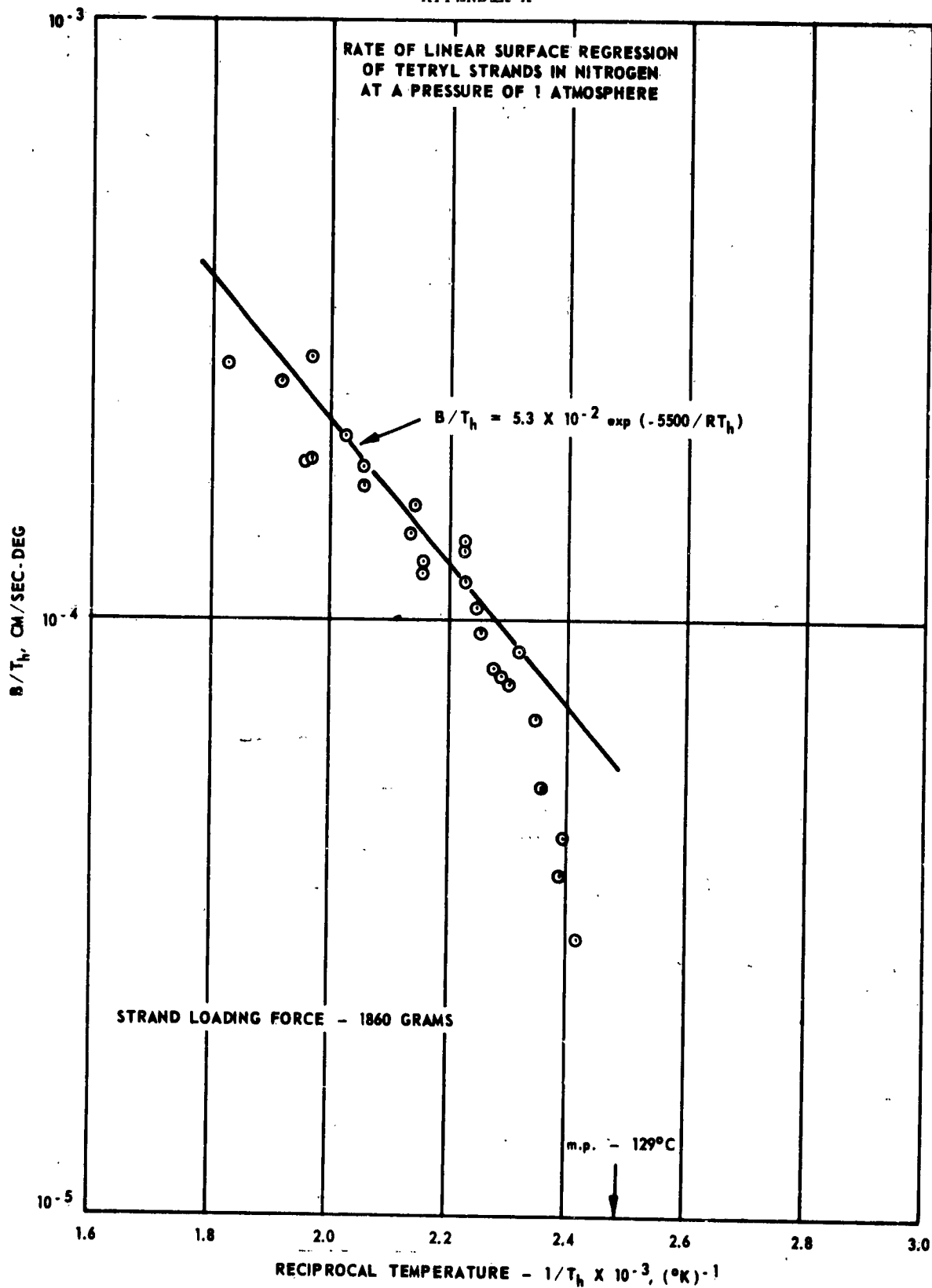


Figure 3

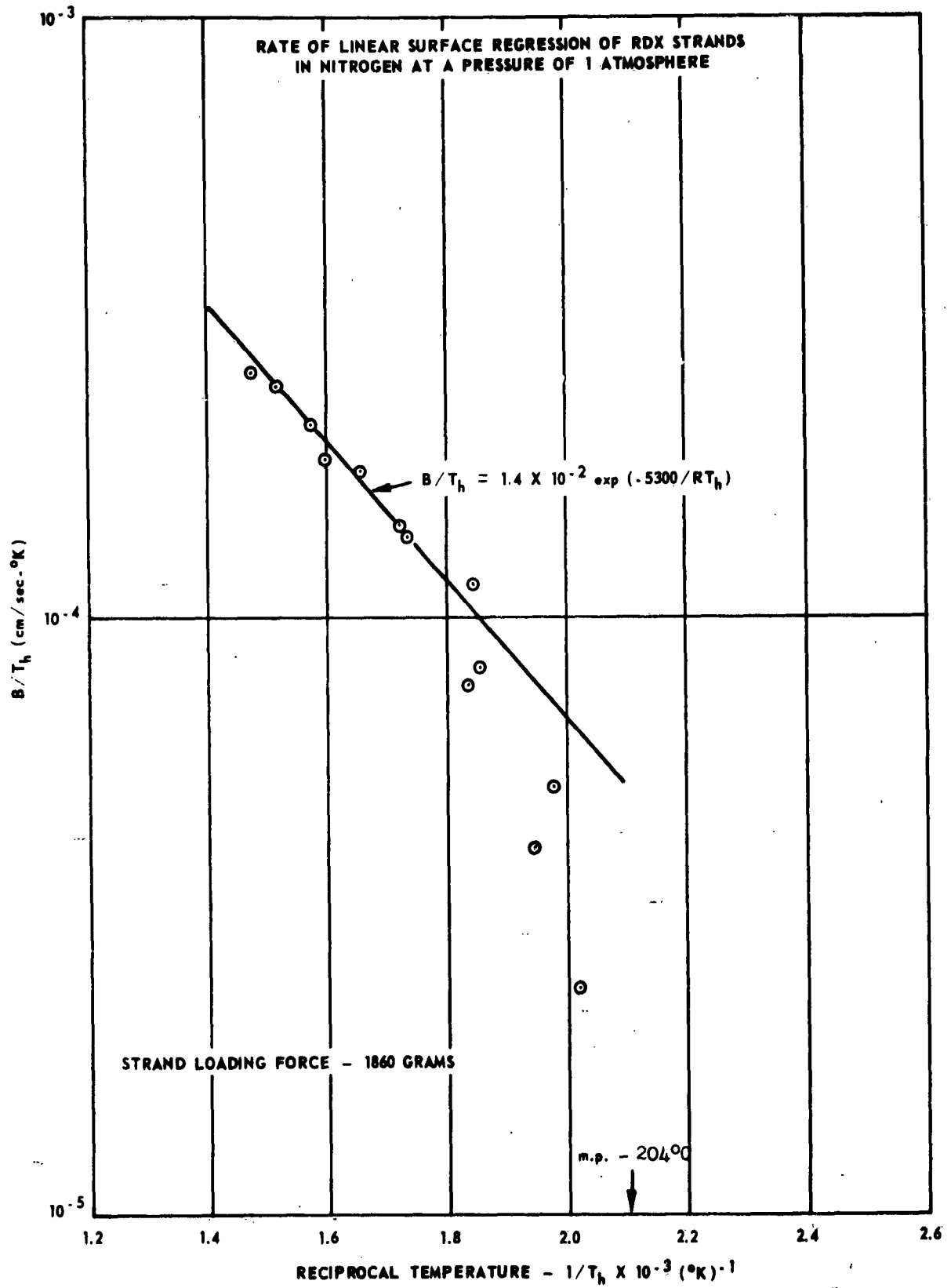


Figure 4

Report O372-01F
APPENDIX A

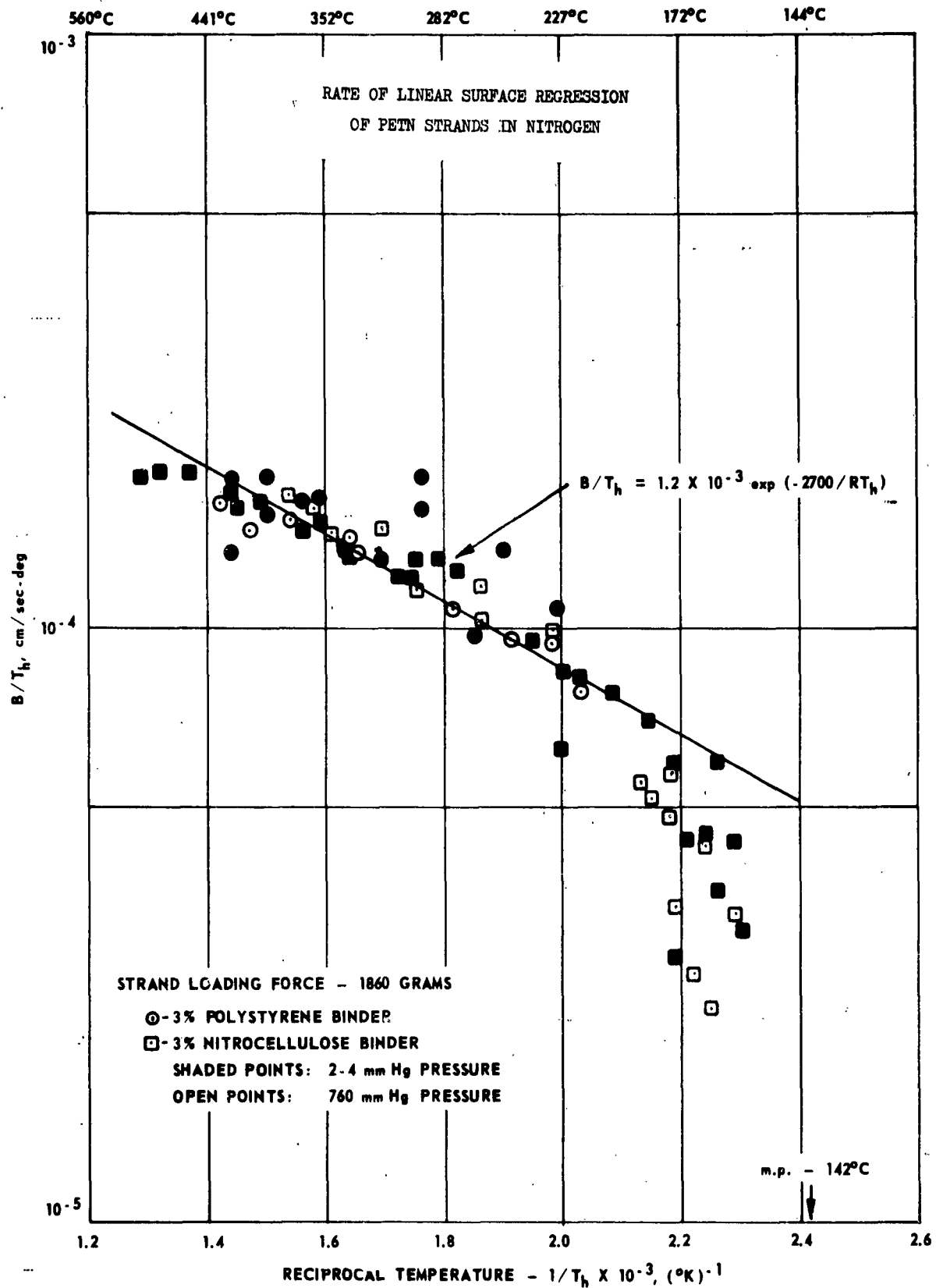


Figure 5

Report O372-01F

APPENDIX A

APPARENT ACTIVATION ENERGIES AND
PRE-EXPONENTIAL FACTORS

	<u>Hot Plate Data</u>		Heat of Fusion (kcal/mole)	Ostwald Viscosimeter Data
	<u>A(cm/sec-°K)</u>	<u>E(kcal/mole)</u>		<u>E_a (kcal/mole)</u>
TNT	0.071	4.9	5.09*	--
Tetryl	0.053	5.5	6.36*	--
RDX	0.014	5.3	--	--
PETN	0.0012	2.7	--	--
Benzoic Acid	0.072	4.1	4.14**	4.12

* W. R. Tomlinson, Jr. Properties of Explosives of Military Interest
Technical Report No. 1740, Picatinny Arsenal, Dover, N. J.,
Revised by O. E. Sheffield, April 1958.

** G. T. Furukawa, R. E. McCoskey and G. J. King, J. Res. Nat. Bur. Stds.,
47, 256 (1951).

Figure 6

Report O372-01F
APPENDIX A
RATE OF LINEAR SURFACE REGRESSION
OF BENZOIC ACID IN NITROGEN
AT A PRESSURE OF 1 ATMOSPHERE

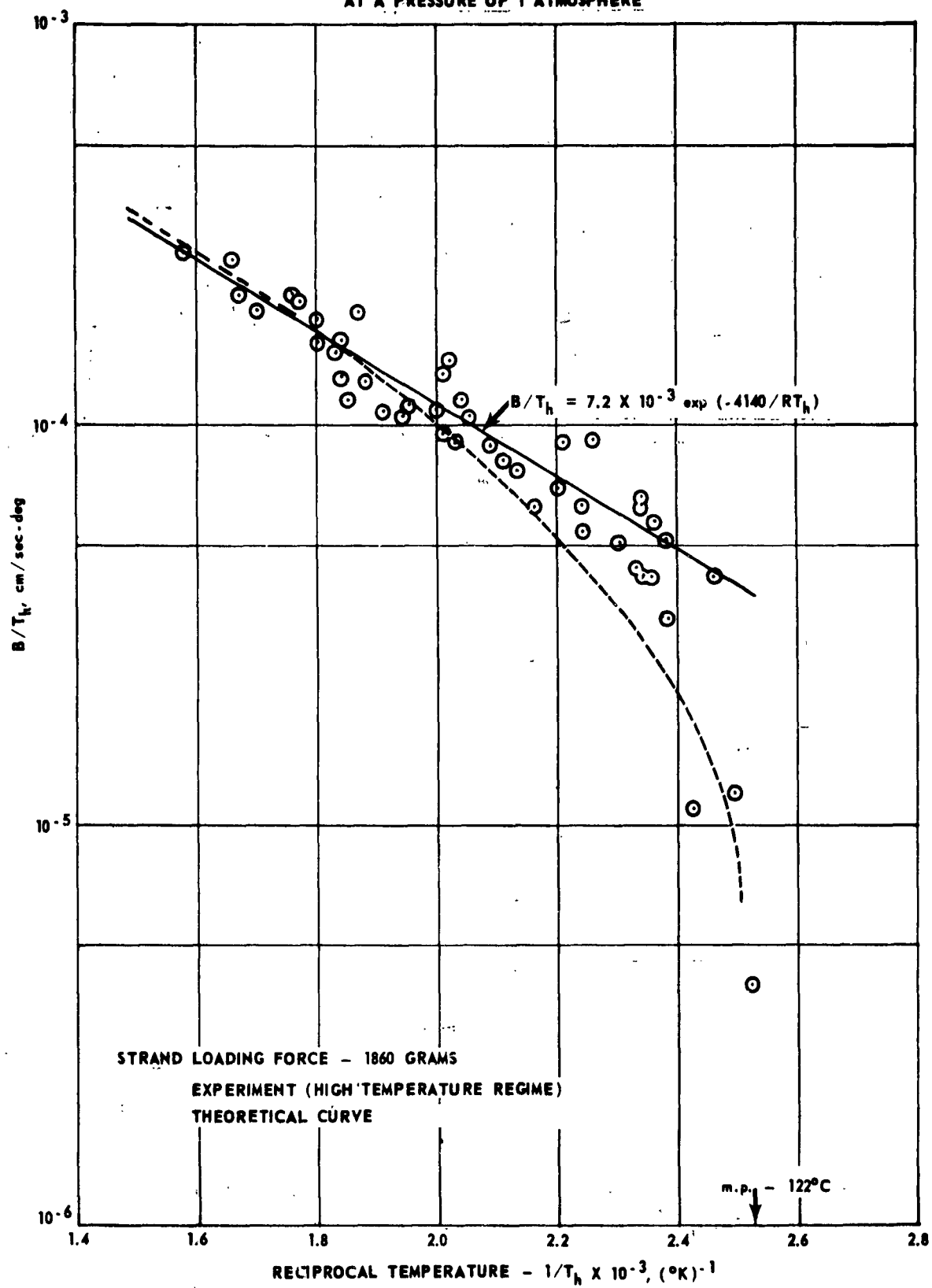


Figure 7

VISCOSITY OF BENZOIC ACID
ABOVE ITS MELTING POINT

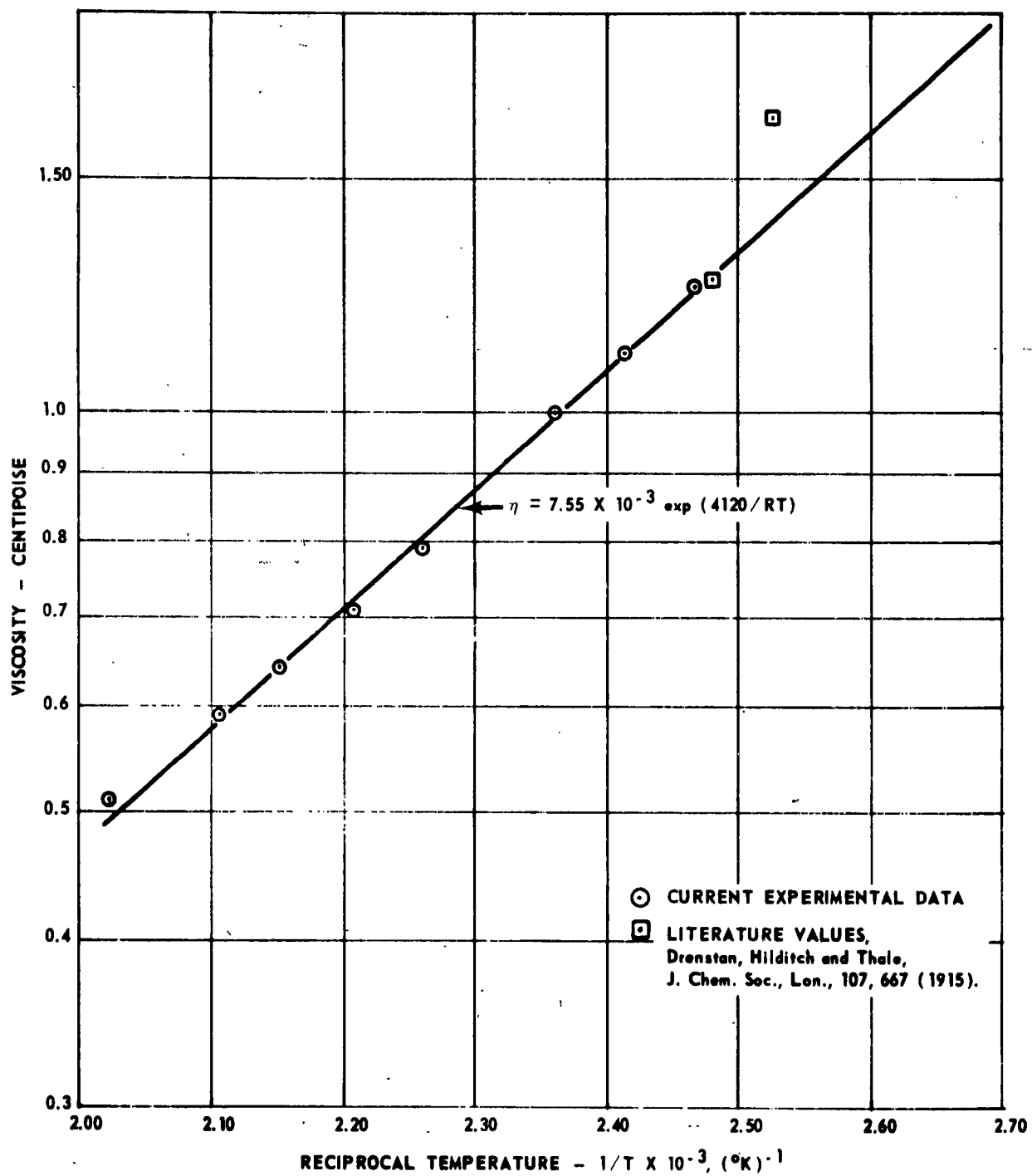


Figure 8

Report 0372-01F
APPENDIX A

CYLINDRICAL GEOMETRY REPRESENTATION
OF HOT-PLATE-STRAND INTERFACE
WITH RADIAL SYMMETRY

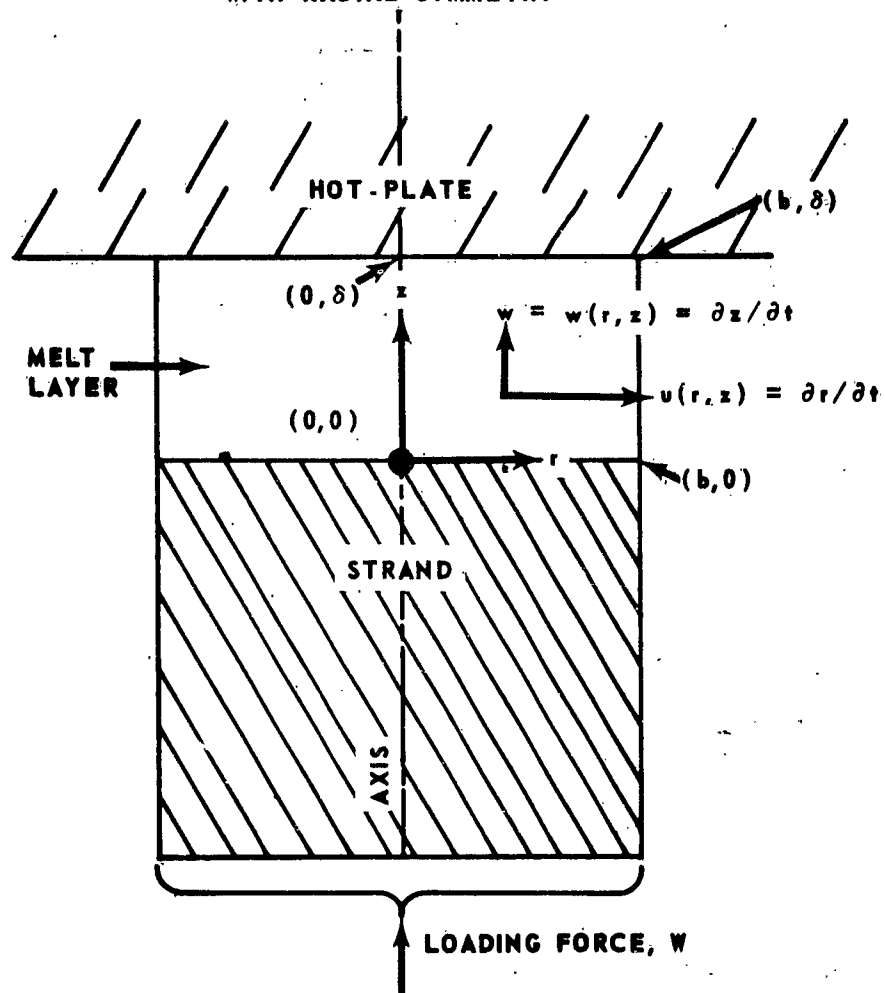


Figure 9

APPENDIX A

BENZOIC ACID PARAMETERS FOR CALCULATING
THEORETICAL SURFACE REGRESSION RATE

$$L_f = 33.95 \text{ cal/gm}$$

$$T_s = 395^\circ\text{K}$$

$$T_o = 300^\circ\text{K}$$

$$\rho_m = 0.95 \text{ gm/cm}^3$$

$$\rho_s = 1.27 \text{ gm/cm}^3$$

$$C_s = C_m = 0.5 \text{ cal/gm}^*$$

$$K_o = 0.8 \text{ cm}^2/\text{sec}; \text{ corresponding to } K(T_o) = 8 \times 10^{-4} \text{ cm}^2/\text{sec}^*$$

$$\phi_o = 1.32 \times 10^4 \text{ poise (cm-sec/gm)}$$

$$W = 1860 \text{ gm-cm/sec}^2$$

$$b = 0.25 \text{ cm}$$

$$E_\phi = 4120 \text{ cal/mole}$$

* Estimated value.

APPENDIX A

ISOTHERMAL DECOMPOSITION RATES AND ADIABATIC EXPLOSION
TIMES OF HIGH EXPLOSIVES AT THEIR MELTING POINT

Explosive	Log Z*	E _a * (Kcal/mole)	Melting Point T _m (°K)	k _r sec ⁻¹	t _{exp} ** sec
TNT(a)	12.2	43.4	353	2.5 x 10 ⁻¹⁵	2.3 x 10 ¹²
TNT(b)	11.4	34.4	353	1.6 x 10 ⁻¹⁰	4.5 x 10 ⁸
Tetryl(a)	12.9	34.9	402	10 ⁻⁶	8.9 x 10 ³
RDX(b)	15.5	41.0	477	6.3 x 10 ⁻⁴	18
RDX(c)	18.5	47.5	477	6.3 x 10 ⁻⁴	16
PETN(a)	15.2	38.6	415	10 ⁻⁵	880
PETN(d)	23.1	52.3	415	4 x 10 ⁻⁵	160

* Decomposition Rate Constant, $k_r = z \exp(-E_a/RT)$.

** Calculated with the heat capacity, $C = 0.5$ cal/gm-deg and heat of decomposition, $Q_d = 500$ cal/gm for all explosives; Adiabatic Explosion Time, $t_{exp} \cong CRT_m^2 / QE_a k_r$

- (a) M. A. Cook and M. T. Abegg, Ind. Eng. Chem., 48, 1090 (1956).
- (b) A. J. B. Robertson, Trans. Faraday Soc., 44, 977 (1948); 45, 85 (1949).
- (c) E. K. Rideal and A. J. B. Robertson, Proc. Roy. Soc. (London), A195, 135 (1948).
- (d) A. J. B. Robertson, J. Soc. Chem. Ind. (London), 61, 221 (1948).

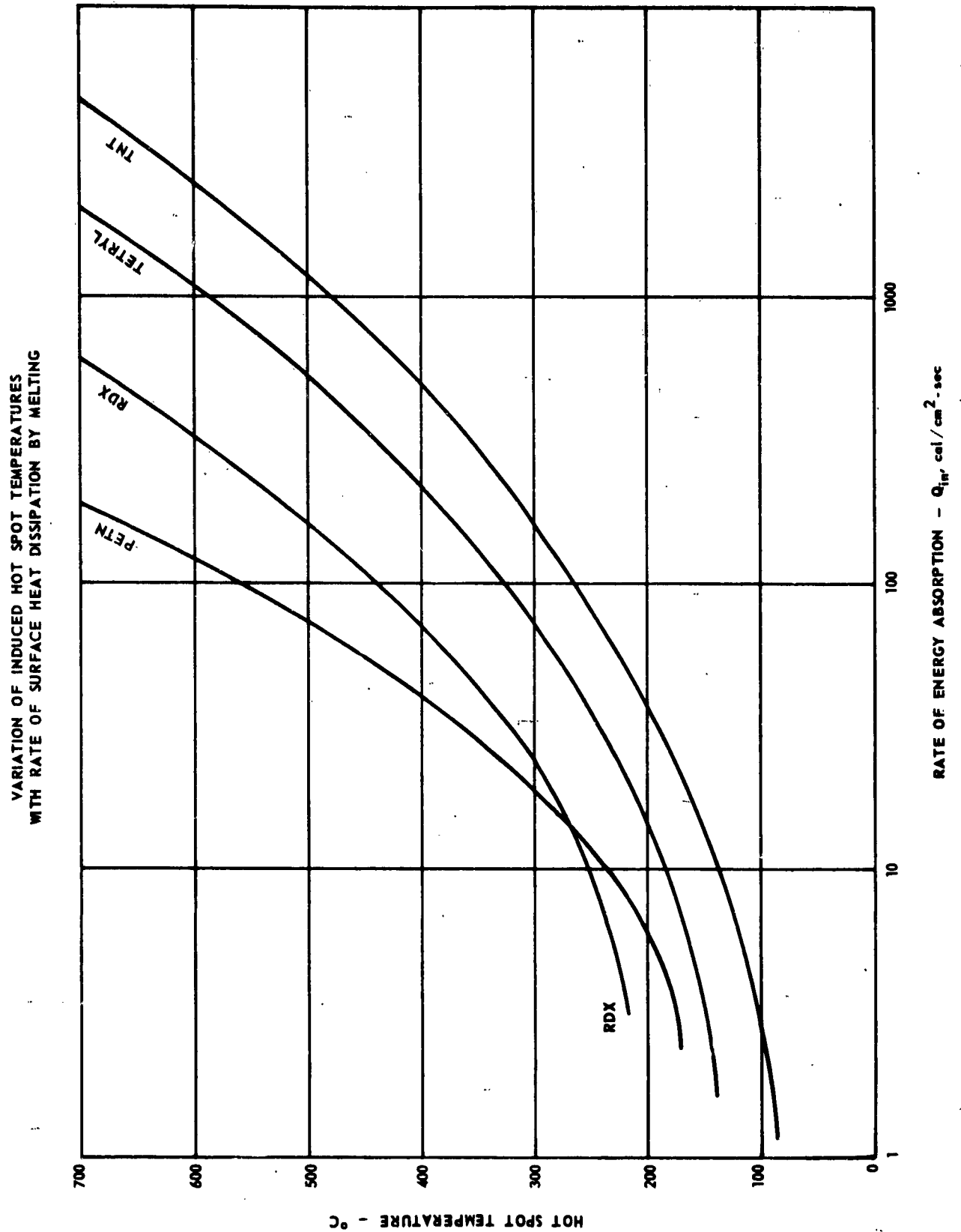


Figure 12

Report 0372-01F

APPENDIX A

COMPARISON OF RATE OF SURFACE HEAT
DISSIPATION AND IMPACT SENSITIVITY

Explosive	Calculated Rates of Surface Heat Dissipation (cal/cm ² -sec)				Impact Sensitivity	
	<u>T_h = 673°K</u>		<u>T_h = 873°K</u>		50%* height (cm)	% Relative to TNT
	<u>Q_{in}</u>	<u>% Relative to TNT</u>	<u>Q_{in}</u>	<u>% Relative to TNT</u>		
TNT	500	1.00	2600	1.00	170	1.00
Tetryl	210	0.42	1100	0.42	40	0.24
RDX	70	0.14	330	0.13	25	0.15
PETN	40	0.08	120	0.05	15	0.09

* Values averaged from several sets of data listed in A. D. Little Co., "Punch Card Recording of Data on Explosives" Final Summary Report Contract DA-19-020-ORD-173 (March 31, 1954) for a 2.5 kg drop hammer on 35 mg of explosive.

APPENDIX B

RATE OF SUBLIMATION OF AMMONIUM HALIDES

By

R. F. Chaiken, D. J. Sibbett, J. E. Sutherland, D. K. Van de Mark,
and A. Wheeler

(A portion of this Appendix was published in the Journal of Chemical
Physics, Vol. 37, 2311, 1962)

I. INTRODUCTION

A. GENERAL BACKGROUND

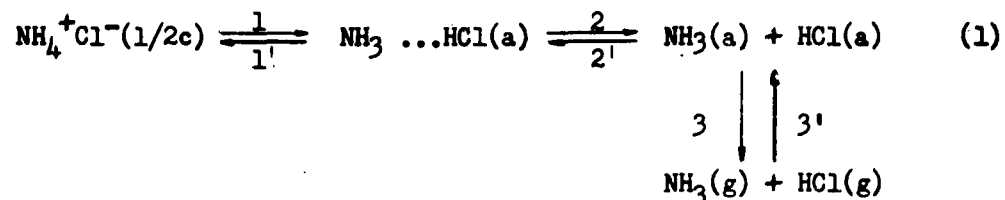
The sublimation of ammonium halides is of special interest in studies of the mechanism of evaporation in that the surface gasification process involves an endothermic dissociation reaction. Also, the measurements of the rate of sublimation of ammonium chloride, by H. Spingler⁽¹⁾ and R. D. Schultz and A. O. Dekker⁽²⁾, have indicated a rate constant which is characterized by an Arrhenius activation energy considerably less than the heat of vaporization, and a frequency factor corresponding to an accommodation coefficient of 10^{-4} (as compared to 0.1 - 1.0 for many non-dissociative molecular evaporations).*

H. Spingler⁽¹⁾ employed M. Volmer's⁽³⁾ concept of step-wise evaporation, and suggested that the rate-controlling step in the gasification process involves the transfer of a molecule from one surface site to another

* The accommodation coefficient for evaporation refers to the constant which appears in the Knudsen-Hertz evaporation rate equation. It should be noted that the physical significance of this coefficient is questionable when applied to substances which dissociate upon evaporation.

APPENDIX B

having less bonding energy. O. Knacke, I. N. Stranski, and G. Wolff⁽⁴⁾ elaborated on this mechanism in further detail. In essence, the reaction steps can be depicted as



where (1/2c) refers to a half-crystal site on the surface (a) to a surface adsorbed site, and (g) to the gas phase.*

The relatively small experimental activation energy (13.5 kcal/mole)⁽¹⁾ led Knacke et al. to consider reaction step (1) as rate controlling.

The small value of the accommodation coefficient is then related to the relatively small concentration of half-crystal surface sites.

O. Knacke and I. N. Stranski⁽⁵⁾ regard the rate of dissociation of ammonium chloride as a "direct proof of Volmer's theory of step-wise evaporation."

The above statement is interesting, since R. D. Schultz and A. O. Dekker^(2,6), who utilized a novel experimental technique (the hot-plate linear pyrolysis technique) to verify Spingler's data, suggested that desorption (step 3 in equation (1)) is the rate-determining step. This assumption implies that the crystal surface is fully covered with an adsorbed layer of (NH₃ ...HCl). By application of transition-state theory to this model, they were able to derive a rate constant in agreement with experiment.

* The half-crystal site (Halbkristallage) is taken as that surface site where the coordination number is one half that for the crystal interior. As such, it is considered that the energy to remove a molecule from that site to the gas phase is exactly the heat of vaporization. An important feature of the half-crystal site is that it is the edge of a surface step, and hence regenerating (i.e., the removal of a molecule from the site forms another filled half-crystal site).

APPENDIX B

B. PURPOSE OF PRESENT STUDIES

In view of the conflicting concepts concerning the details of the sublimation mechanism, it was thought that data on the sublimation of the other ammonium halides, (viz., NH_4F , NH_4Br , and NH_4I) might shed further light on the subject. It is the primary purpose of this paper to describe these rate measurements.

II. EXPERIMENTAL

A. TECHNIQUES

The direct measurement of the sublimation rate as a function of surface temperature is complicated by the fact that considerable surface cooling of the solid can occur during the reaction, and that the reacting surface is continually regressing. Thus, it becomes somewhat difficult to obtain an accurate temperature and area measurement of the reacting surface. In fact, it is probably these difficulties which prompted R. Littlewood and E. Rideal⁽⁷⁾ to make the comment that experimental values of the evaporation coefficient for materials evaporating under vacuum are determined primarily by heat-transfer conditions, and not by other considerations.

In the present vacuum sublimation-rate studies, two separate and independent techniques were employed: (a) a hot-plate linear pyrolysis technique which was initially developed by R. D. Schultz and A. O. Dekker⁽²⁾, and (b) a conventional continuous weight-loss measurements under isothermal-vacuum heating conditions.* In the use of both techniques, careful consideration was given to the measurement of the true reaction temperature.

* H. Spingler's⁽¹⁾ studies were also carried out under isothermal-vacuum heating conditions; however, his rate determinations were based upon an average time-lapsed weight loss.

APPENDIX B

B. ISOTHERMAL VACUUM STUDIES

A continuous weighing method using a quartz spring balance similar to that described by L. L. Bircumshaw and T. R. Phillips⁽⁸⁾ was employed in these studies.

The ammonium halides were of analytical reagent grade obtained from the Baker and Adamson Chemical Company. The chloride was further purified by three recrystallizations from distilled water before use, while the bromide, fluoride, and iodide were used without further purification. All the materials were dried and stored in vacuum over P_2O_5 at all stages of sample preparation. To prepare sublimation samples, the coarse halide crystals were ground in a ball mill to a particle size which would pass through a 100-mesh (149 μ) screen. The dried powder was pressed with a conventional IR-spectrophotometer, KBr window press for 10 min at 10,000 psi into disk-shaped tablets having the dimensions of $\sim 1 \times 12.7$ mm, and weighing ~ 0.2 g. The tablet size quite uniform, and appeared hard and translucent, with no apparent (macro) surface irregularities. Measurements of the tablets' dimensions with a precision micrometer were used to make density calculations. These calculations indicated densities of 0.97, 1.48, 2.36, and 2.47 g/cm³ for the fluoride, chloride, bromide, and iodide respectively. Except for the fluoride, whose crystal density is reported as 1.315⁽⁹⁾, these values are only 2 - 3% below the accepted crystal density values.

The sublimation experiments were carried out in the apparatus illustrated in Figure 1. The apparatus consisted of a quartz helical-spring balance (20 cm long, with a sensitivity of 9.9 mg per mm spring displacement) suspended in an evacuated glass chamber (balance case). The entire lower section of the balance case could be set into an electrically heated vertical combustion furnace. The sample tablet was placed edge up in the small glass bucket attached

Report 0372-01F

APPENDIX B

to the spring in a manner such that a minimum of sample area was in contact with the glass. A thermocouple well allowed a thermocouple junction (Pt - Pt, 10% Rh) to be placed within 1 cm of the sample. This allowed the balance case temperature to be determined as a function of time. The pressure was maintained at $\sim 10^{-6}$ mm Hg during an experiment.

In practice, the furnace was first preheated to the desired temperature and then raised into position around the lower end of the balance case in which the tablet was suspended. Subsequent vaporization in the temperature controlled ($\pm 1^\circ\text{C}$) vacuum chamber was followed by observing the spring contraction with an optical reader. The position of a reference fiber attached to the spring suspension could be read to ± 0.04 mm, leading to weight-loss measurements which were accurate to ± 0.5 mg. Typical weight loss vs time curves which were obtained by this method are shown in Figure 2.

In determining the sublimation temperature, careful consideration was given to the surface cooling effect mentioned previously. In separate experiments, the actual surface temperature was measured as a function of balance-case temperature by comparing the EMF of a thermocouple junction in direct contact with the subliming surface to the reading from the balance case thermocouple. The measured temperature differences served as empirical correction factors (see Figure 3) to account for the effect of surface cooling. (When a non-volatile sample, such as NaCl or NaNO_3 was heated, the two temperature readings agreed to $\pm 1^\circ\text{C}$.) It was interesting to observe that for NH_4F , the surface cooling amounted to as much as 70°C at a balance-case temperature of only 150°C .

C. HOT-PLATE STUDIES

In these studies, direct measurements of the linear rate of surface sublimation of rectangular strands of pressed ammonium halides were obtained by

Report 0372-01F

APPENDIX B

means of the method known as the hot-plate technique⁽²⁾.

The sample strands, measuring 0.5 x 1.0 x 7.5 cm, were prepared by pressing the powdered halides in a special strand mold. The materials used were the same as those employed in the isothermal studies, except for the mesh size of the NH_4F , which was 35 mesh (420 μ).

The strand formation conditions were 20,000 psi, with a 5-min dwell time. It was found that heating the die to $\sim 150^\circ\text{C}$ during the pressing operation was beneficial in obtaining almost uniformly translucent strands; however, the method was only applied to the chloride and bromide. The other two halides were pressed cold in order to minimize the possible formation of ammonium hydrogen fluoride and iodine. Solid-strand densities similar to those listed for the disk-shaped tablets were obtained by this technique.

The hot-plate apparatus employed in the present studies was an improved version of the early apparatus employed by R. D. Schultz and A. O. Dekker.⁽²⁾ The details of this improved apparatus are published elsewhere.^(10,11) Briefly, the surface evaporation is accomplished by pressing the end of a sample against an electrically heated hot plate. A small Pt - Pt, 10% Rh thermocouple junction, which is imbedded in the hot plate and positioned at the strand-hot plate interface, enables the surface temperature to be recorded while the linear rate of regression of the strand surface is measured. The steady-state surface temperature (and hence the linear sublimation rate) is changed by varying the electrical power expended in the hot plate.

Figures 4 and 5 show the data points for the linear sublimation rate of NH_4Cl obtained at different environmental pressures and with different loading pressures (i.e., the force/unit strand area with which the strand is pressed against the hot plate). It is noteworthy that the Arrhenius-rate plot of the

APPENDIX B

vacuum data is linear over a 250°C range of surface temperature, corresponding to sublimation rates which differ by more than a factor of 100. Also, the hot-plate data are in good agreement with the linear surface regression rates obtained from Spingler's data. The significance of the data points which lie below the straight-line curves of Figures 4 and 5 will be discussed in the next section. The vacuum hot-plate data for all the halides are shown in Figure 6. The idealized strand-hot-plate interface for mass transfer analysis is shown in Figure 7.

III. RESULTS

A. ISOTHERMAL VACUUM STUDIES

The problem of determining the rate constant from the experimental weight loss vs time data was apparently greatly simplified by the use of the thin disk-shaped samples, which had a relatively large and well-defined surface-to-volume ratio. As would be expected for a zero-order reaction (i.e., surface reaction with a constant reaction area), the rate of weight loss was essentially constant over a major portion of the reaction (see Figure 2). Since the surface roughness factor was not known, it was assumed that the sublimation rate per unit of area would be determined by the initial geometric sample area, and the slope of the straight-line portion of the weight loss vs time curves. As will be described later, the assumption of unity for the surface roughness factor gives good agreement between the hot plate and isothermal data.

The lower portion of Figure 6 shows a compilation of the rate data obtained in this manner. For convenience, the data have been converted from a mass rate (i.e., mg/cm²-min) to a linear rate (i.e., cm/sec) by dividing by the crystal density and other suitable numerical factors.

B. HOT-PLATE STUDIES

The rate measurements made with the hot-plate technique yield directly

Report 0372-01F

APPENDIX B

the linear sublimation rate, and hence do not require further analysis to determine the reaction area. However, a major assumption in the use of the technique is the identification of the reaction-surface temperature with the hot-plate temperature. It is actually the latter temperature which is measured by the imbedded thermocouple. The assumption implies that the temperature drop across the thin layer of gas separating the strand surface from the hot plate is negligible, which might not be the case.

Evidence for the validity of this assumption lies in the fact that there is a range of vaporization rates where the measured surface temperature is independent of the force used to press the strand against the hot plate (see Figure 5). However, as the gasification rate increases, the thickness of the separation layer must increase in order to maintain steady-state flow conditions. Hence, there will be a vaporization rate above which there will be a significant temperature gradient between the hot plate and the gasifying surface. At this point, the apparent surface temperatures would be fictitiously high, and, in terms of the Arrhenius rate plot of Figure 5, will result in a downward displacement of the data points from a linear curve.

In order to estimate the value of the temperature drop across the interface more quantitatively, an approximation analysis of the heat and mass transfer at the interface was carried out. The details of this analysis are presented in Appendix B-2. It was shown that a temperature difference could be expected to occur within the range of experimental conditions, and that it would vary inversely with the first power of the loading pressure, and directly with the square of the linear regression rate. Thus, one might expect an apparent rate threshold above which the basic assumption concerning the surface temperature measurement would not be valid. As can be seen by comparing the high temperature

APPENDIX B

data points of Figure 5 to the calculated curves (calculated by equation 14A in Appendix B-2), a threshold point does occur at ~ 0.01 cm/sec. Unfortunately, it is believed that the calculated temperature errors are insufficiently certain to warrant their use as correction factors in a manner analogous to the temperature corrections employed in the isothermal vacuum studies.

With regard to the effect of environmental pressure on the rate of sublimation, it is apparent from the data of Figure 4 that increasing pressure causes an apparent decrease in the linear sublimation rate at the lower range of surface temperatures, and that the effect becomes more pronounced as the temperature is decreased.

This environmental pressure effect can be readily understood from consideration of the reverse condensation reaction (see Equation 1). Under environmental pressures which approach the vapor pressure of the NH_3 and HCl in the interfacial layer, the gas flow from the layer becomes diffusion limited rather than sound-velocity limited (see Appendix B-2). This results in an increased residence time for the vapor in close vicinity to the solid surface, thereby enhancing the back condensation reaction. It is this increased condensation which results in measured linear sublimation rates which are less than the vacuum rates.

It can therefore be expected that the measurement of accurate vacuum sublimation rates with the hot-plate technique is limited to surface temperature conditions where the equilibrium vapor pressure is at least twice that of the environmental pressure. For the ammonium halide system and the vacuum conditions employed here (i.e., 1 - 2 mm Hg), this lower limit of surface temperature corresponds to a linear velocity of regression equal to about 10^{-4} cm/sec.

IV. DISCUSSION

The sublimation rate equation can be expressed as a linear surface

APPENDIX B

regression rate,²

$$B = A_s \exp(-E_s/RT_s) \text{ cm/sec} \quad (2)$$

or its equivalent form

$$v = A_s (\rho/M) \exp(-E_s/RT_s) \text{ moles/cm}^2\text{-sec,} \quad (3)$$

where ρ is the crystal density and M the molecular weight.

In Figure 6, the vacuum rate data from both experimental techniques corresponding to Equation (2) have been combined for easy visual comparison. The good agreement between the data of both experiments is quite apparent, particularly when one recognizes the limitations of the techniques.

It is somewhat remarkable to observe from the linearity of the data points, that the experimental data for each halide represent a change in the reaction rate of a factor of about 10^4 , and that a single reaction mechanism appears to be operating over the entire range of temperature.

Figure 8 contains a list of physical constants and constants for the sublimation rate equations as determined by combining both sets of experimental data. Although a complete statistical analysis of variance has not been carried out, it is estimated that the standard deviation of the values for the activation energy E_s , is less than ± 2 kcal/mole.

It should be pointed out that the sublimation rate of NH_4Cl , as determined in the present studies, compares quite favorably with the measurements of Spingler¹ (i.e., $A_s = 87$ cm/sec; $E_s = 13.5$ kcal/mole), and of Schultz and Dekker² (i.e., $A_s = 300$ cm/sec; $E_s = 11.2$ kcal/mole*).

* Reference is also made to the unpublished ammonium chloride hot-plate data by K. W. Bills, M. Therneau, E. Mishuck, and R. D. Schultz OSR-TN-55-117 (1955) in which $A_s = 120$ cm/sec, and $E_s = 13.5$ kcal/mole.

Report 0372-01F

APPENDIX B

Upon examining the experimental rate data of Figure 8, it is interesting to note the following: (1) The values for E_s increase almost linearly with increasing molecular weight, and are approximately one-third the heat of sublimation $\Delta H_{s,sub}$. (2) The values of A_s , except for the case of NH_4F , increase with increasing molecular weight. For NH_4F , the value of A_s is significantly one to two orders of magnitude greater than the other halides. (3) There appears to be no simple quantitative relationship between A_s and the other physical constants listed.

A detailed theoretical discussion of these results in terms of a comparison of the existing mechanisms of evaporation is beyond the intended scope of the present discussion. However, it is interesting to compare the experimental rates with those which can be readily calculated from the Schultz-Dekker transition state treatment of the linear sublimation rate.⁶ From their simplified model of desorption at the reaction surface, the frequency factor of Equation (2) above at $\bar{T}_s = 600^\circ K$ can be expressed* as

$$A_s = 6.98 \times 10^{-16} (m/\rho)^{1/3} \nu_{NH_3} \nu_{HX} m^{1/2}, \quad (4)$$

where $m = M/N$, the molecular mass of the ammonium halide, ρ is the crystal density, ν_{NH_3}, ν_{HX} is the harmonic oscillation frequencies of the NH_3 and HX segments of the physically adsorbed $NH_3 \cdots HX$ complex in the plane of the reaction surface. The apparent activation energy is given by

$$E_a = 1/2 (\Delta H_{m,NH_3} + \Delta H_{m,HX}) + (\Delta H_{s,NH_3} - RT_{s,NH_3}) + (\Delta H_{s,HX} - RT_{s,HX}), \quad (5)$$

where $\Delta H_{m,\alpha}$ is the heat of fusion of component α ($\alpha = NH_3$ or HX), $\Delta H_{s,\alpha}$ is the heat of sublimation of component α measured at temperature T_s , α and R is the gas constant.

* See Equations (18), (19), and (28) of Reference 6.

APPENDIX B

In Equation (5), E_q is taken as the sum of the energy barrier to surface collisions between NH_3 and HX (approximated by the first term), and the energy required for desorption of NH_3 and HX (approximated by the second and third terms). Equation (4) corresponds to a relatively highly localized activated complex which otherwise resembles the adsorbed initial state molecular complex.

Schultz and Dekker⁶ obtained estimates of the harmonic vibration frequencies from the expression

$$\nu_{\alpha} = 1.025 \times 10^5 \frac{(0.5 \Delta H_m \alpha / M \alpha)}{M/N \rho}$$

Thus, Equations (4)-(6) allow almost a completely a priori calculation of sublimation rates.

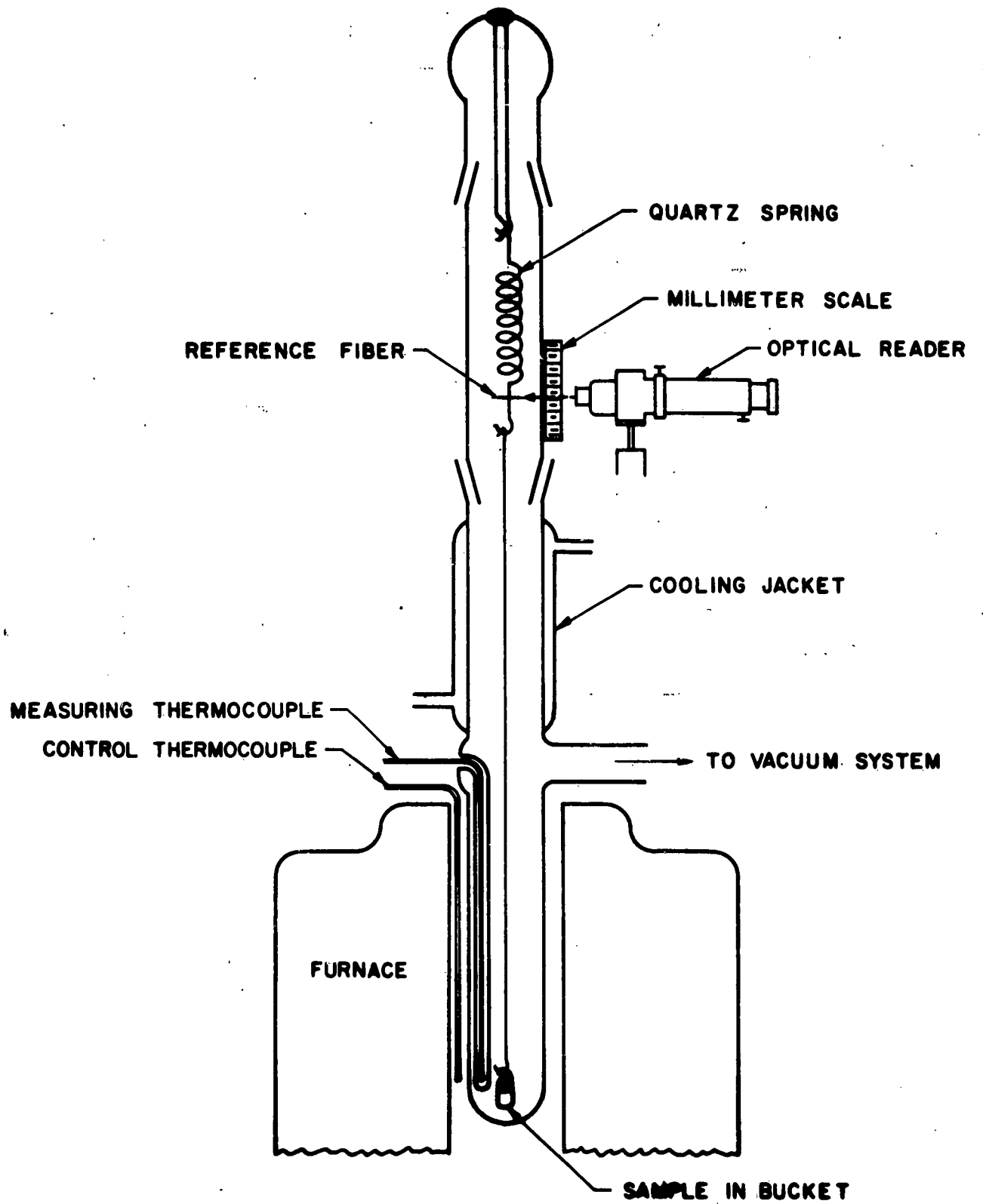
Utilizing thermodynamic data compiled by the U. S. Bureau of Standards,¹² the rate constant parameters for all the ammonium halides were calculated. Figure 9 shows a comparison between the calculated and experimental results. It is readily apparent that the agreement between theory and experiment is quite reasonable. As for the apparent discrepancy between the measured and calculated trend in the variation of A_s with molecular weight, one might argue the significance of this point in view of the uncertain nature of the kinetic rate determinations. However, it is perhaps worthwhile to consider this discrepancy prior to forming any conclusions as to the validity of the Schultz-Dekker treatment.

Report 0372-01F

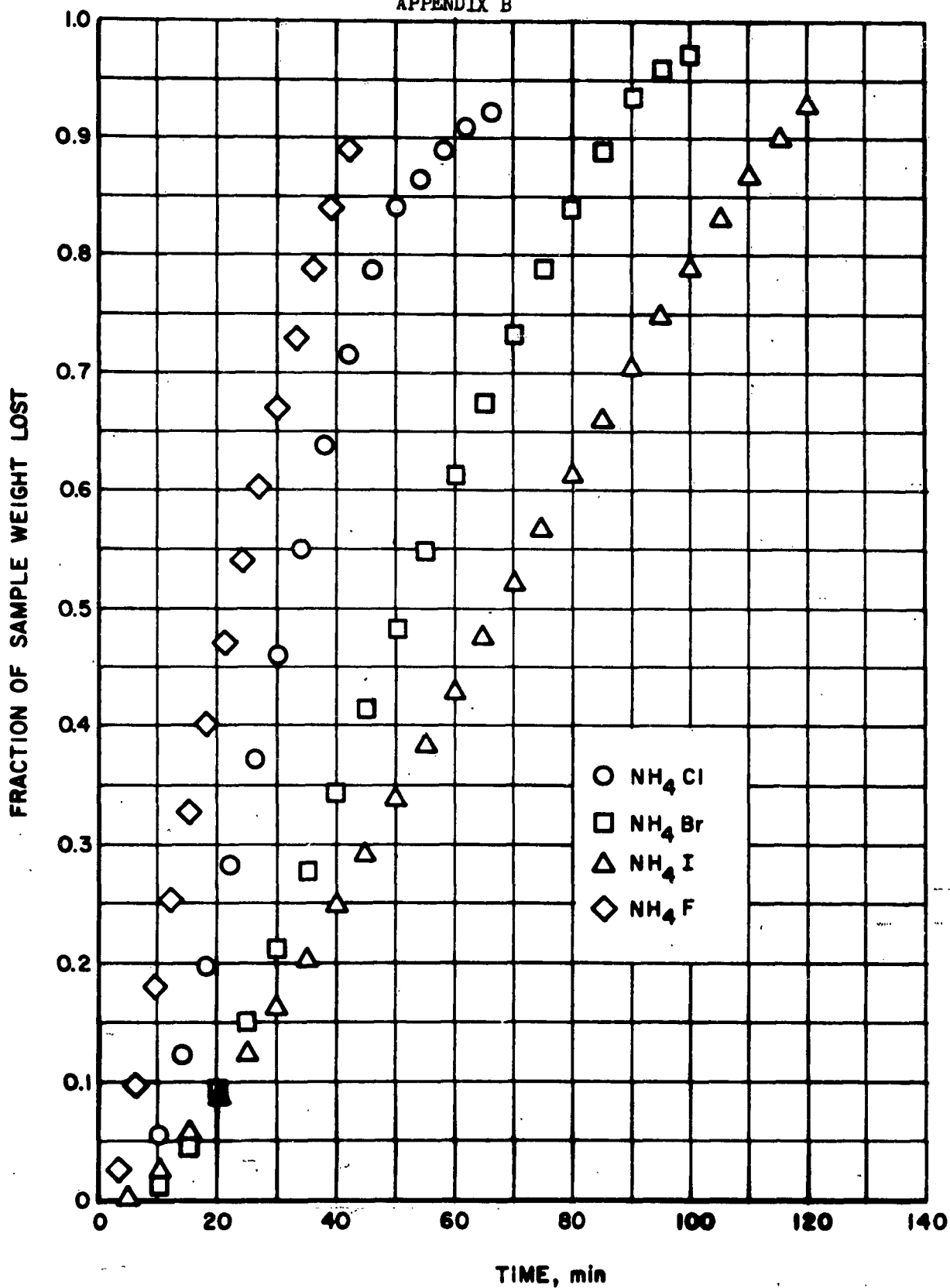
APPENDIX B

REFERENCES

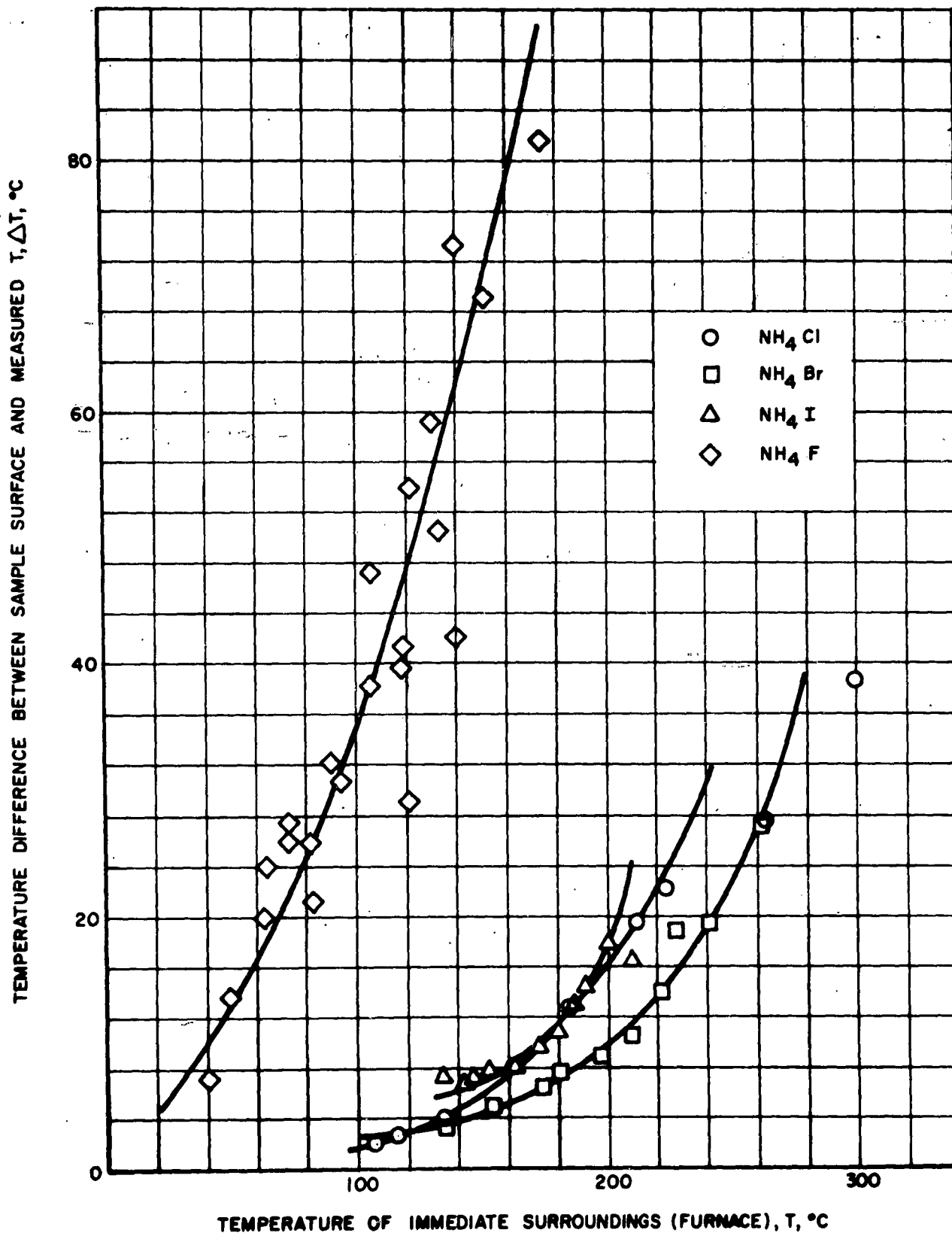
1. H. Spingler, Z. physik. Chem., B52, 90 (1942).
2. R. D. Schultz and A. O. Dekker, Fifth Symposium (International) on Combustion, Reinhold Publishing Co., New York (1955) p. 260.
3. M. Volmer, "Kinetic der Phasenbildung", Dresden and Leipzig (1939).
4. O. Knacke, I. N. Stranski, and G. Wolff, Z. physik. Chem. 198, 157 (1951).
5. O. Knacke and I. N. Stranski, "The Mechanism of Evaporation", "Progress in Metal Physics", Vol. VI, Pergamon Press, N. Y. (1956) p. 181.
6. R. D. Schultz and A. O. Dekker, J. Phys. Chem., 60, 1095 (1956).
7. R. Littlewood and E. Rideal, Trans. Faraday Soc., 52, 1598 (1956).
8. L. L. Bircumshaw and T. R. Phillips, J. Chem. Soc., 4741 (1957).
9. Handbook of Chemistry and Physics, 39th ed., Chemical Rubber Publishing Co., Cleveland (1958) p. 484.
10. M. K. Barsh, W. H. Andersen, K. W. Bills, Jr., G. Moe, and R. D. Schultz, Rev. Sci. Instr. 29, 392 (1958).
11. R. F. Chaiken, and D. K. Van de Mark, Rev. Sci. Instr., 30, 375 (1959).
12. "Selected Values of Chemical Thermodynamic Properties", U. S. National Bureau of Standards, Circ. 500, 1952.



ISOTHERMAL VACUUM SUBLIMATION APPARATUS



SUBLIMATION OF AMMONIUM HALIDES
TYPICAL WEIGHT LOSS VS TIME CURVES



MEASURED SURFACE TEMPERATURE COOLING CURVES

FIGURE 3

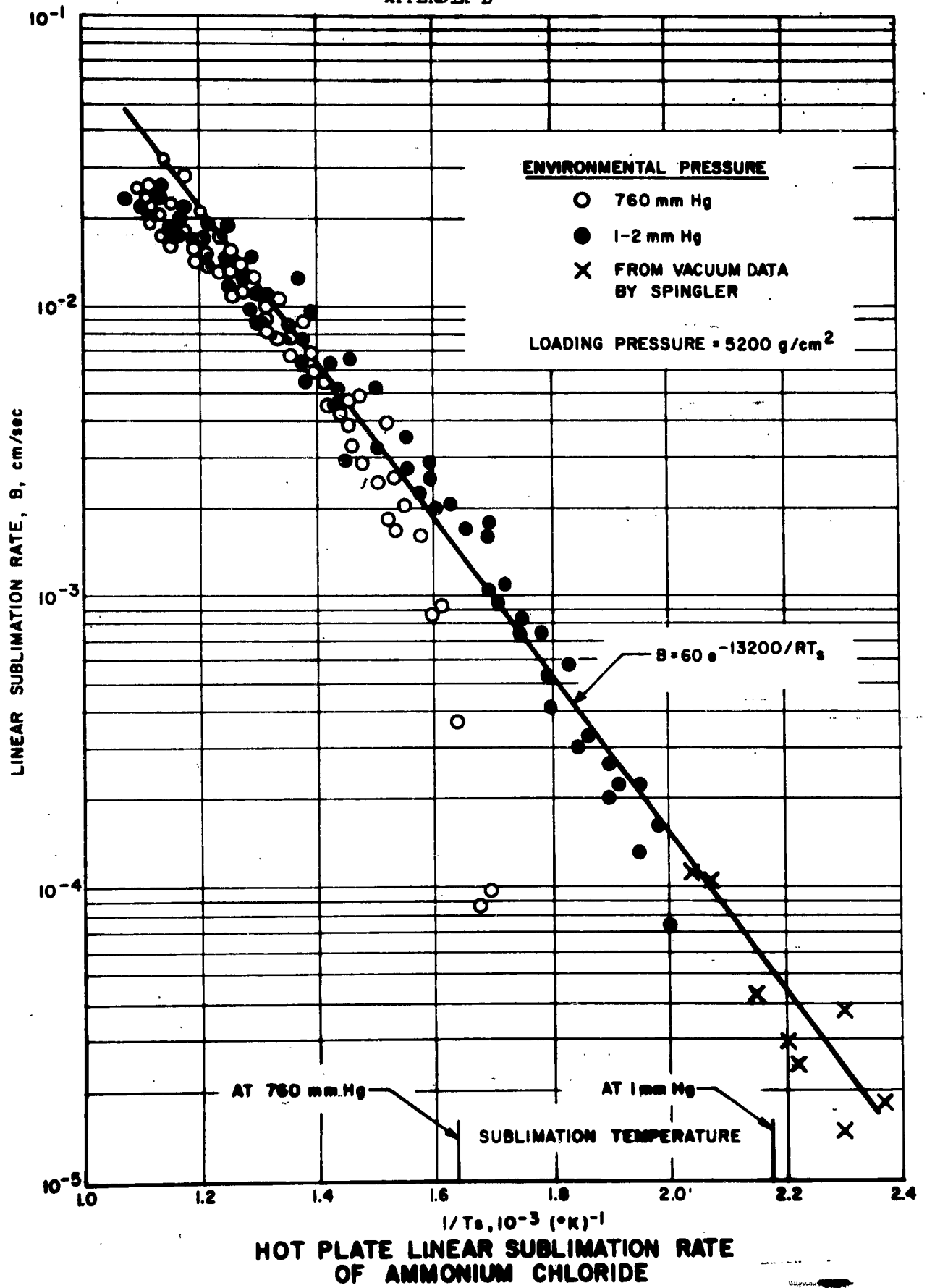
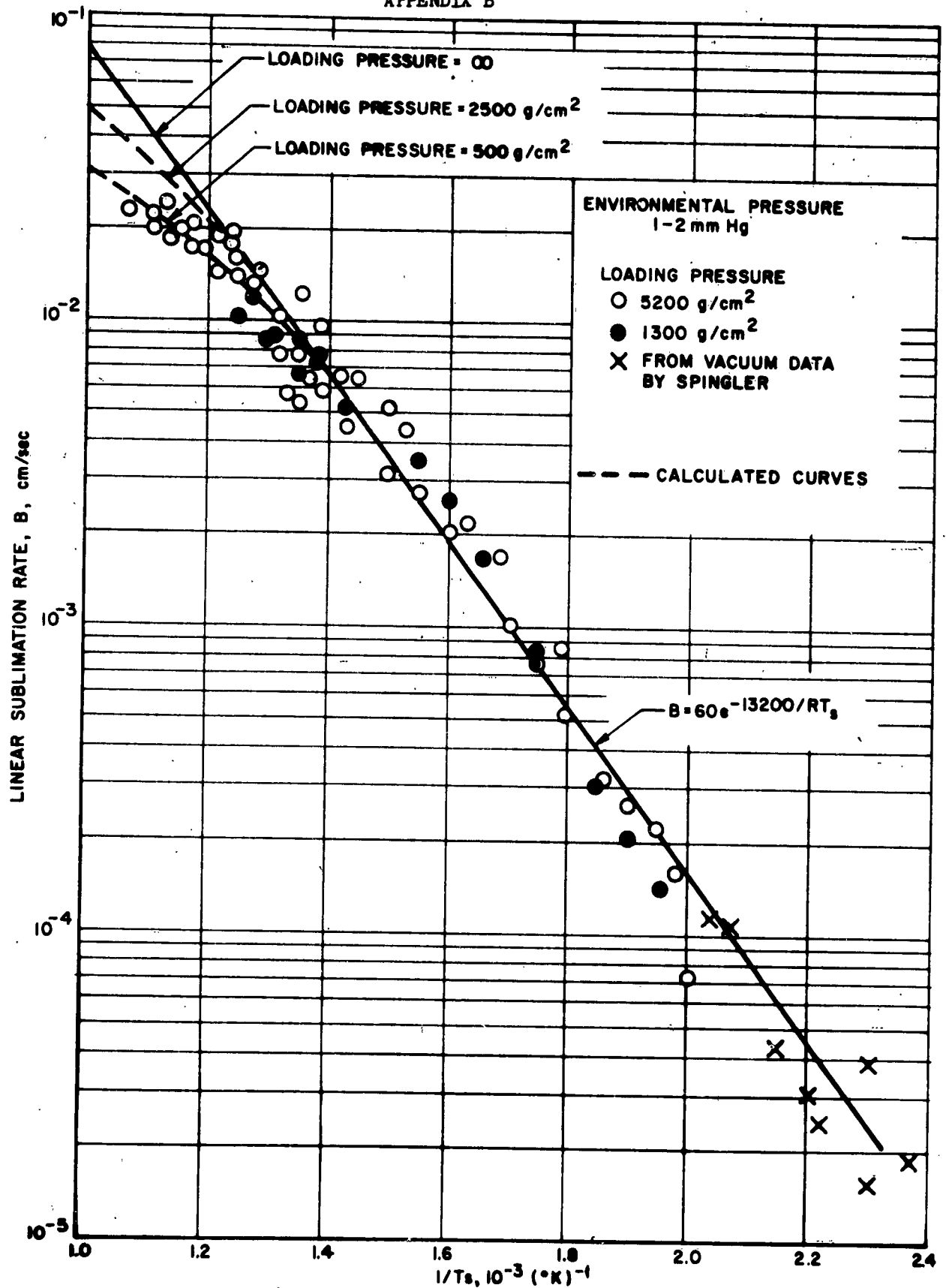
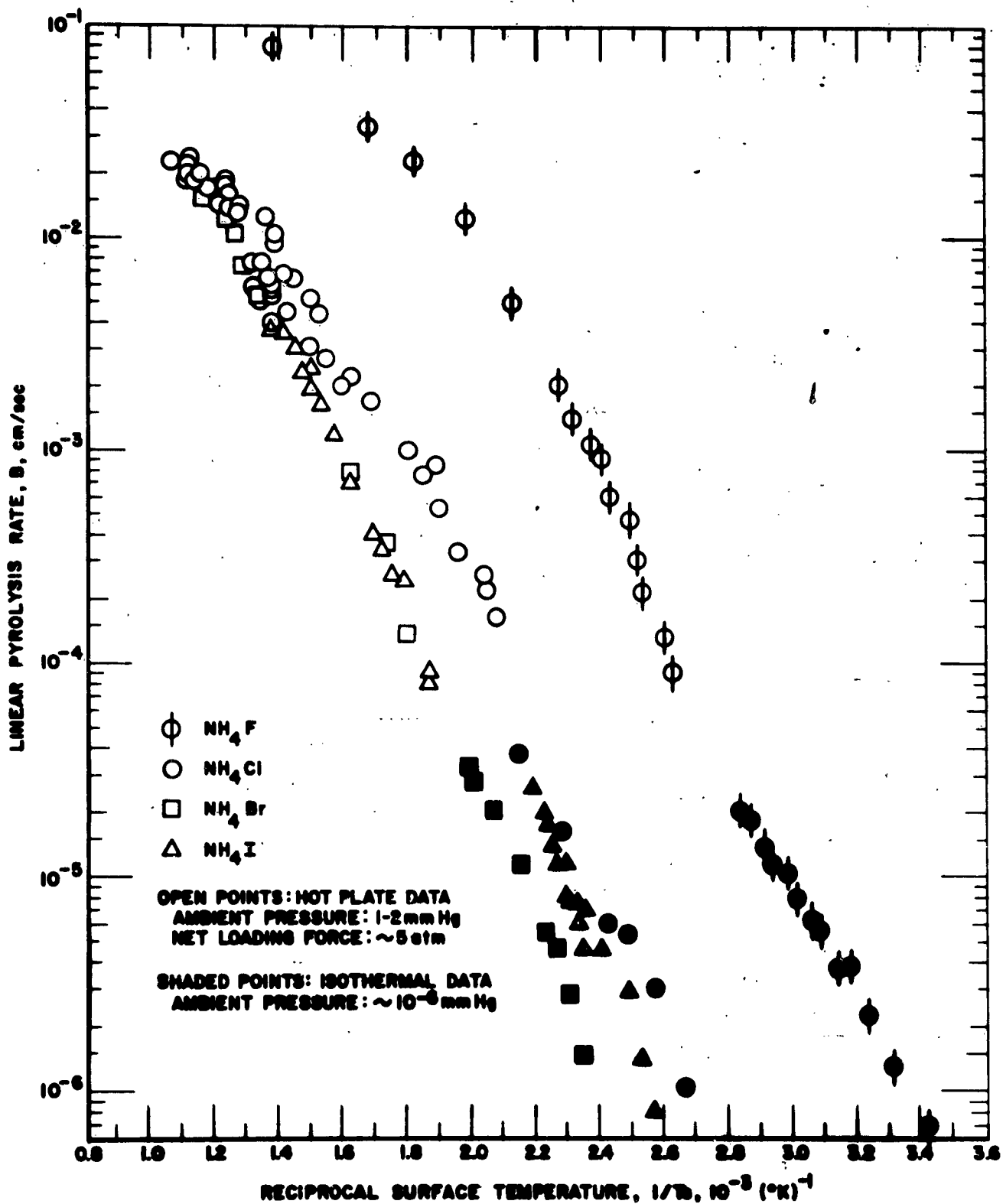


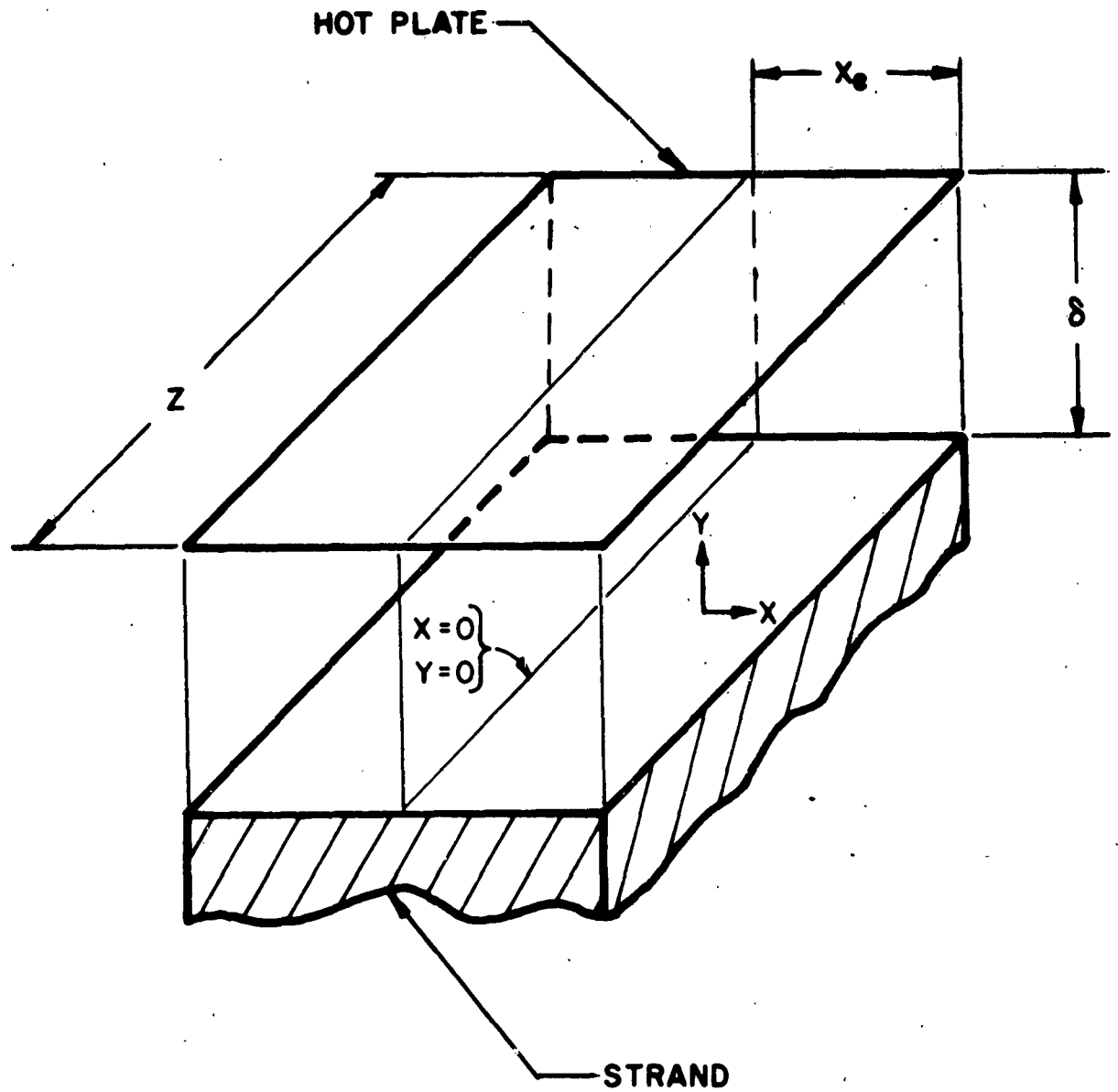
FIGURE 4



EFFECT OF LOADING PRESSURE ON THE HOT PLATE
LINEAR SUBLIMATION RATE OF AMMONIUM CHLORIDE



LINEAR RATE OF SUBLIMATION OF THE AMMONIUM HALIDES



IDEALIZED STRAND-HOT PLATE INTERFACE FOR
MASS TRANSFER ANALYSIS

EXPERIMENTAL ARRHENIUS RATE PARAMETERS FOR THE SUBLIMATION OF AMMONIUM HALIDES

	Crystal Density (*) g/cm ³	Molecular Weight (*) g/mole	Heat of Sublimation (**) kcal/mole	Experimental		
				A _s cm/sec	A _s moles/cm ² -sec	E _s kcal/mole
NH ₄ F	1.315	37.04	36.1	2700	96	12.2
NH ₄ Cl	1.527	53.50	42.3	60	1.7	13.2
NH ₄ Br	2.429	97.96	44.9	130	3.2	15.0
NH ₄ I	2.514	144.96	43.5	900	16	16.6

Report 0372-01F

APPENDIX B

Figure 8

* Reference 9.

** N. W. Luft, Ind. Chemist, 31, 502, (1955).

APPENDIX B

Figure 9

COMPARISON OF EXPERIMENT WITH THE SCHULTZ-DEKKER THEORY

	<u>Experimental Values</u>		<u>Schultz-Dekker Theory</u>	
	<u>A_s</u> <u>cm/sec</u>	<u>E_s</u> <u>kcal/mole</u>	<u>A_s</u> <u>cm/sec</u>	<u>E_s</u> <u>kcal/mole</u>
NH ₄ F	2700	12.2	654	10.04
NH ₄ Cl	60	13.2	362	12.35
NH ₄ Br	130	15.0	312	12.82
NH ₄ I	900	16.6	300	13.50

ANALYSIS

Consider a strand of solid with a cross-sectional area of $2X_e Z$ gasifying at the surface of a hot plate. Under steady-state conditions, a layer of gas of constant thickness, δ , separates the strand surface at temperature T_s , from the hot plate at temperature T_p (see Figure 7). With respect to the actual hot-plate pyrolysis experiment, it should be possible to obtain reasonable estimates of the temperature drop across δ by considering a model of couette type flow between parallel plates, and the following simplifying assumptions*:

1. The mass flow in the z-direction is negligible (this should be a reasonable approximation, since in practice, $Z \sim 4X_e$).
2. The flow velocity in the x-direction, $u(x,y)$, is symmetrical about $y = \delta/2$ and $x = 0$, and is linearly dependent upon x and y , i.e.

$$u = 2 \frac{ax}{X_e}, \text{ for } y < \delta/2 \quad (1A)$$

$$u = 2 ax \frac{(y - \delta)}{X_e}, \text{ for } y > \delta/2 \quad (2A)$$

3. A sonic point exists at $x = X_e$, such that $u(X_e, y) = a$, which is taken as constant. This assumption should be a reasonable approximation, since the pressure, P , in the gas layer is generally greater than twice the environmental pressure, P_0 .

4. The gas moving within the layer δ expands isobarically along x ,

* The authors are indebted to B. L. McFarland of Aerojet-General Corporation for demonstrating the applicability of this approach.

APPENDIX B-2

and isothermally along y ; hence for an ideal gas

$$\rho(x,y) = \frac{P(x)}{RT(y)} \quad (3A)$$

where $\rho(x,y)$ is the gas density at point (x,y) within δ ; $P(x)$ is the pressure at a point x , and is independent of y ; and the gas temperature $T(y)$ is uniform along x , varying only in a direction normal to the surface.

5. The temperature varies linearly with y across δ , i.e. the energy conservation across planes parallel to the surface can be expressed as

$$T = T_s + \epsilon y / \delta \quad (4A)$$

or

$$dT/dy = (T_p - T_s) / \delta = \epsilon / \delta \quad (5A)$$

6. Momentum changes in the gas layer are negligible.

Now the conservation of mass across any plane normal to the surface is simply

$$Z \rho_s B x = Z \int_0^{\delta} \rho u dy = 2Z \int_0^{\delta/2} \rho u dy \quad (6A)$$

From equations (3A) and (4A), we solve for u in terms of y , and integrate (6A) to obtain

$$\rho_s B = \frac{4a P \delta}{R X_e \epsilon^2} \left[\frac{\epsilon}{2} + T_s \ln \left(\frac{2T_s}{T_p + T_s} \right) \right] \quad (7A)$$

Since $2T_s / (T_p + T_s)$ is greater than $1/2$ we can expand the logarithmic term in (7A) in series form, i.e.,

$$\ln \left(\frac{T_s}{T_p + T_s} \right) = -\epsilon / 2T_s + 1/2 \left(\epsilon / 2T_s \right)^2 - \dots \quad (8A)$$

For reasonable values of ϵ and T_s (i.e., $\epsilon < 300^\circ\text{C}$), we can, with negligible error, neglect all terms higher than the square term, and thus obtain the following expression for δ

$$\delta = \frac{2 R X_e T_s \rho_s B}{a P} \quad (9A)$$

Report O372-01F

APPENDIX B-2

Now the heat flux (\dot{q}_s) at the surface is simply that required to raise the solid from a temperature T_0 to a temperature T_s , and to vaporize the solid. Hence

$$\dot{q}_s = \rho_s B \left[\Delta H_v + C_s(T_s - T_0) \right] = \sigma (dT/dy)_{y=0} \quad (10A)$$

where ΔH_v is the heat of vaporization at T_s , C_s is the specific heat of the solid, and σ is the thermal conductivity of the gas layer. From equations (5A), (9A) and (10A), the expression for the temperature drop, $\epsilon = T_p - T_s$, becomes

$$\epsilon = \frac{2R X_e T_s C_s (\rho_s B)^2}{aP} \left[\frac{\Delta H_v}{C_s} + T_s - T_0 \right] \quad (11A)$$

If a is taken as an averaged sound velocity at X_e , then

$$a = (\gamma R' \bar{T})^{1/2} \approx (\gamma R' T_s)^{1/2} \quad (12A)$$

where γ is the ratio of specific heats and R' is the gas constant in cgs units.

Equations (11A) and (12A) allow ϵ to be defined in terms of known parameters, i.e.,

$$\epsilon = (2R X_e C_s / \sigma P) (\rho_s B)^2 (T_s \gamma R')^{1/2} (\Delta H_v / C_s + T_s - T_0) \quad (13A)$$

For the reasonable values of the various parameters shown in the table below, Equation (13A) becomes

$$\epsilon = 3.7 (B^2/P)(1730 + T_s) T_s \quad (14A)$$

VALUES OF PARAMETERS FOR EQUATION (13A)

$\sigma = 2 \times 10^{-4}$ cal/cm-sec/deg	$X_e = 0.25$ cm
$C_s = 0.38$ cal/gm-deg	$\rho_s = 1.6$ gm/cm ³
$M_{av} = 27$ gm/mole	$\Delta H_v = 790$ cal/gm
$R = 82/M_{av} = 3.04$ cm ³ -atm/deg-gm	$T_0 = 350^\circ\text{K}$
$R' = 3.07 \times 10^6$ erg/deg-gm	$\gamma = 1.3$

Report 0372-01F

APPENDIX C

**KINETICS OF THE DECOMPOSITION OF
ANHYDROUS PERCHLORIC ACID***

D. J. Sibbett and I. Geller

(To Be Published in the Journal of Physical Chemistry)

**Solid Propellant Research Operations
Solid Rocket Plant, Aerojet-General Corporation
Azusa, California**

**Research reported in this publication was supported by the Advanced
Research Projects Agency and technically monitored by the Air Force
Office of Scientific Research, Contracts AF 49(638)-566 and AF 49(638)-851.**

KINETICS OF THE DECOMPOSITION OF ANHYDROUS PERCHLORIC ACID

D. J. Sibbett and I. Geller

INTRODUCTION

Study of the decomposition of perchloric acid is of considerable interest as an example of a reaction of the only relatively stable anhydrous oxygen acid of chlorine, because of its importance in the mechanisms of combustion and decomposition of perchlorates which contain hydrogen (such as the hydrazinium and ammonium salts) and because of the use of concentrated solutions in combustion systems.

Thermal decomposition of perchloric acid has been examined in the vapor phase between 200° and 439°C by Levy¹ who has indicated that the reaction appeared to be

¹ J. B. Levy, J. Phys. Chem., 66, 1092 (1962).

heterogeneous between 200° and 350°C and homogeneous in the upper range. Zinoviev, Babayeva and Tsentsiper²⁻⁵ have examined the decomposition of

² V. P. Babayeva and A. A. Zinoviev, Zhur. Neorg. Khim., 8, 567 (1963).

³ A. A. Zinoviev and V. P. Babayeva, Zhur. Neorg. Khim., 6, 271 (1961).

⁴ A. A. Zinoviev and A. B. Tsentsiper, Zhur. Neorg. Khim., 4, 724 (1959).

⁵ A. B. Tsentsiper, Zhur. Neorg. Khim., 4, 1086 (1959).

APPENDIX C

anhydrous acid, hydrated systems and mixtures at temperatures from 60 to 145°C. The present study is concerned with kinetics of the decomposition of gaseous anhydrous acid in the heterogeneous range between 165 and 256°C.

EXPERIMENTALApparatus

Because of the extremely high reactivity of gaseous perchloric acid to most materials, the decompositions were carried out in carefully cleaned all-glass vacuum systems. A series of glass by-passes, capillaries, and break-seals were used in place of stopcocks in the preparation and reactor sections to prevent the perchloric acid from coming into contact with stopcock grease. The apparatus was designed so that the reaction was followed manometrically and in some experiments it was modified to permit the measurement of chlorine formation by a photoelectric colorimetric technique simultaneously with measurement of total pressure.

Manometric System

Figure 1 is a schematic diagram of the apparatus, which consists essentially of three basic sections. The reactor section is shown within the dashed lines on the diagram. The perchloric acid preparation section is located at the left of the reactor. The remainder of the system consists of various cold traps, a diffusion pump, a McLeod gage, storage bulbs, and a differential Mercury manometer equipped with a mercury valve. A description of the sequence of the operations involved in an experiment will explain the functions of the various parts and the manometric technique employed.

To start an experiment, a dry-ice-cooled mixture of three parts of 20% fuming sulfuric acid one part of 72% perchloric acid was introduced into the apparatus through an opening at the top of Section A. The

APPENDIX C

quantity of the mixture was limited to yield a maximum of 0.25 g of gaseous product. After cooling the $\text{HClO}_4\text{-H}_2\text{SO}_4$ mixture to approximately -195°C by placing a Dewar of liquid nitrogen around the base of A, the top of Section A was sealed with a gas-oxygen flame. The entire system was carefully evacuated through side arm, E, to approximately 10^{-3} torr as measured by the McLeod gage, J. The by-pass, E, was removed, with the entire system still under vacuum, to seal the preparatory and reactor parts of the system (Sections A to F) entirely within glass. The gaseous perchloric acid was prepared by removing the coolant from the base of Section A, and allowing the mixture to warm up slowly to room temperature. This process permits the dehydration of the 72% perchloric acid by the fuming sulfuric acid. The dehydrated gaseous product was distilled from Section A through a drying bed of $\text{Mg}(\text{ClO}_4)_2$ located at B into the reactor by cooling the bottom of D with liquid nitrogen. This procedure is a modification of that of Smith⁶ on a microscopic scale. After one to four

⁶ G. F. Smith, J. Am. Chem. Soc., 75, 189 (1953).

hours of distillation the reactor D was sealed off at point C, after first refreezing the mixture remaining in A. This completed the preparation phase.

After warming the reactor to room temperature a silicone oil bath, made opaque by the addition of carbon black, was raised (from behind a plexiglas safety shield by means of a specially constructed, remote controlled elevator) into the position indicated by the dashed lines around sections C, D, E, and F. The temperature of the bath was controlled within 0.1°C . Manometric measurements were commenced when the oil bath was in place.

The system which was used to measure the pressure within the reactor, D, consisted of four parts: F, G, H, and I. F, a glass Bourdon gage was employed to close an electrical circuit when the pressure above the gage exceeded that inside the reactor by more than the gage spring constant. Closure of the circuit through the Bourdon gage actuated a relay and the solenoid surrounding the mercury valve at H. The solenoid was used to depress an iron collar surrounding a sintered-glass air leak. Thus, completion of the circuit through the Bourdon gage raised the mercury level and closed off the air leak. The pressure measuring system was calibrated as a function of pressure at operational temperatures.

Initial pressure measurements at the start of the reaction were obtained by recording the signal from a pressure transducer, indicated at G. A recorder of 20-mv range served to record both time and pressure during the initial rapid pressure changes, which occur as the bath was raised. After the rate of pressure change becomes relatively stabilized measurements were made by means of the differential manometer, I, viewed through a cathetometer.

Calibration of the reactor volume, which includes section D in Figure 1 and the volume of the inner portion of the Bourdon gage and the lower section of the break seal at E, was carried out at the end of each operation after the equilibrated gas samples have been removed through the stopcocks at R. The calibrated volume of bulb N and its stopcock served as the standard for each volume determination. It was carefully calibrated by weighing water volumes prior to the construction of the apparatus. At the end of each decomposition run, before removal of the gas sample, the volume of the glassware extending from the upper manifold to the break seal at E was determined by expansion. After destruction of the break seal, the volume (to the seal at C) was determined. The difference was the volume of the reactor.

Colorimetric System

Figure 2 is a diagram of the colorimeter system used for monitoring the concentration of chlorine in the reactor. The colorimeter operates independently of the pressure measuring system and, consequently, permitted the simultaneous collection of both types of data.

The reactor itself was designed in the same manner as described above, with the exception that a cylindrical Pyrex tube was sealed across the top to give a tee-shaped container. Optical windows of Vycor were fused to the ends of the cross-tube. The glass reactor was mounted in the colorimeter as indicated, seals being maintained with Viton O-rings. These seals prevented any oil from leaking into the tubes and obstructing the optical path. An adjustable front-surface mirror was mounted at each elbow to direct the light beam through the cell. Mirror alignment was obtained by adjustment of a rack and pinion device which operated by means of screwdriver adjustments from the outside of the optical tube.

The photoelectric system consisted of an ordinary 300 watt projection lamp, two collimating lenses, a 1.0 mm pin-hole, a pair of filter systems, and two 1P29 gas-filled photocells. The color filter used for chlorine detection (Gaertner Scientific Corporation, No. L541C) transmitted in the green between 4800 \AA and 5700 \AA with maximum transmission at 5260 \AA . Although its use somewhat decreased the sensitivity of the analysis, its transmission was outside the known absorption range of the chlorine oxides which may have transitory existence during decomposition experiments. The spectral response of the 1P29 photocells was judged satisfactory in the transmitted range although maximum sensitivity occurred at approximately 4200 \AA . The circuit used for amplification and

APPENDIX C

measurement of the output of the opposed photocells was similar to that indicated by Hawes, et. al.⁷ Both the projection lamp and the amplifier

⁷ R. C. Hawes, R. R. Davis, H. H. Gary and A. O. Beckman, Anal. Chem., 23, 503 (1951).

power supply were operated from constant voltage supplies.

In operation, after the oil bath had been raised, signal fluctuations caused by the changing thermal environment were noted. To minimize these effects, constant temperature water was circulated through condensers which jacketed the upright sections of the optical path. A plane ground plate of optical glass was used to close off circulation of hot gases from the optical tube to the detector photocell. With these modifications, stable signals were obtained within a few minutes after the oil bath was raised.

Calibration of the colorimeter was carried out using chlorine gas (Matheson, 99.85% minimum purity) at various pressures with the heated oil bath in the same position and at the same temperatures utilized in the decomposition experiments.

Utilization of the colorimeter was intermittent. The amplifier was operated continuously during each experiment but the air-cooled light source was turned on for five minutes before each reading while the shutter remained closed. It was found that this period was sufficient to establish stable signals. Longer preheating periods did not change the measured readings.

PHYSICAL CHARACTERIZATION OF THE PERCHLORIC ACID PREPARATION

For each decomposition experiment, a fresh portion of anhydrous perchloric acid was prepared. Although the preparation was generally water-white when prepared in a darkened room, some samples which had been

APPENDIX C

exposed to light exhibited yellow coloration. For purposes of characterizing its purity, the vapor pressure of a typical sample was measured. Figure 3 is a plot of the \log_{10} of the vapor pressure against the reciprocal of the absolute temperature from 0° to 61.8°C . The data of these experiments has been compared with the measurements of van Wijk⁸ and Vorlander and von Schilling⁹ at 16.0° and 39°C respectively. These data are considered

⁸ H. J. van Wijk, Zeit. anorg. Chem., 32, 115 (1902).

⁹ D. Vorlander and R. von Schilling, Liebig's Ann., 310, 369 (1900).

to compare satisfactorily.

The extrapolated boiling point for anhydrous perchloric acid as obtained from these measurements is $120.5^{\circ} + 1.3^{\circ}\text{C}$. Hantzsch¹⁰ has

¹⁰ A. Hantzsch, Z. physikal. Chem., 134, 406 (1928).

indicated an extrapolated boiling point of about 130°C . The heat of vaporization as calculated from the slope of the plot between 0° and 61.8°C is $8.13 + 0.06$ kcal/mole. No literature comparison appears to be available.

As a further check on the properties of the initial material and the nature of the decomposition process, infrared spectra were obtained using a Beckman (IR 5) infrared spectrophotometer with sodium chloride windows. The upper section of Figure 4 shows the absorption spectrum of a typical preparation of perchloric acid at 16.8 torr using a path length of 100 mm. This pattern was obtained about ten minutes after the gas was evaporated into the cell.

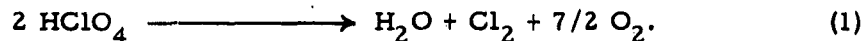
RESULTS AND DISCUSSION

Results of Manometric Experiments

The general form of the pressure-time curves is shown below in

APPENDIX C

Figure 10 where the experimental points are plotted for comparison with a computed curve. These data have been analyzed for all experiments in terms of the established stoichiometry of the decomposition reaction:



The total pressure, P_t is related to the initial pressure P_{A_0} and the pressure of undecomposed acid P_A at time, t by the expression

$$P_A = P_{A_0} - \frac{(P_t - P_{A_0})}{(r - 1)}, \quad (2)$$

where r is the number of molecules formed per molecule of decomposed acid.

On this basis, the amount of perchloric acid remaining unreacted was calculated as a function of time and the data were analyzed in terms of simple first and second order kinetic expressions. Figure 5 is an example of the first order analysis. The ordinate, $\log (P_{A_0} / P_A)$ is plotted against time as the abscissa for two initial pressures of perchloric acid. These experiments were carried out at 200.1°C with a surface to volume ratio of $1.6 \text{ cm}^2/\text{cm}^3$. After the initial 140 minutes the data fitted the simple first order analysis and pseudo first order rate constants (k_2) were calculated for all data from these slopes. An example of the second order kinetic test is shown in Figure 6 for the same experiments. In this case, the ratios of the pressures of perchloric acid decomposed to the pressure of unreacted acid, (P_X/P_A) are plotted against time. The initial portions of the data are linear and these slopes have been used to calculate second order rate constants, k_1 . All of the data collected showed these characteristic linear relations between 156 and 265°C at initial pressures between 8 and 373 torr of HClO_4 . At the higher temperatures, the duration of the second order portion became increasingly short, indicating that it would become undetectable by the manometric method at still higher temperatures.

However, the second order linearity remained valid to values of (P_X/P_A) of 2.0 to 2.5 regardless of experimental conditions. Linearity of the pseudo first order plot commenced at values of $\log_{10} (P_{A_0}/P_A)$ equal to 0.65 to 0.70 and remained valid normally until approximately 95% of the acid was converted. A decreasing slope was noted as equilibrium was approached. These considerations formed the basis for treating the two constants independently.

Effect of Surface on Reaction Rates

Both rate constants were demonstrated to be extremely sensitive to the surface to volume ratios of the pyrex reactors which were utilized. Variation in these ratios was achieved by filling the reactors with carefully cleaned pyrex spheres of varying diameter. Figures 7 and 8 indicate the relationships between the second order and the pseudo first order rate constants and the surface to volume ratios for decompositions carried out at 200°C. The rate constants indicated were averaged values obtained at the indicated surface to volume ratios. Surface areas were calculated on the basis of reactor geometry and the number and diameter of the pyrex spheres required to fill the reactor volume. A roughness factor of 1.3 was used to estimate the surface area of the Pyrex from its geometrically calculated value. Volumes were measured by gaseous expansion from previously calibrated volumes.

The apparent linear dependence of both rate constants on surface to volume ratios indicates that the reactions as studied between 165 and 256°C are surface processes. In addition, the relationship suggests that a meaningful separation of the rate constants has been accomplished. The intercepts on the ordinates of Figures 7 and 8 may indicate the simultaneous existence of a gas phase reaction. Unfortunately, the intercepts may demonstrate a fixed error in the estimate of reactor

surface areas. Since the total surface estimates varied between 126 and 1062 cm² an accurate measurement of the surface area by physical means such as gas adsorption was not attempted. In the absence of actual measurements of surface areas, rate constants have been presented in terms gaseous units at fixed surface to volume ratios.

Measurements of Chlorine Evolution

In order to establish that the stoichiometric reaction (equation 1) existed throughout the full range of measurements and that equation (2) is a valid method for calculating the amount of HClO₄ remaining at any time, simultaneous colorimetric measurements of chlorine and manometric measurements of pressure were carried out. Figure 9 compares the observed chlorine pressures with those computed on the basis of

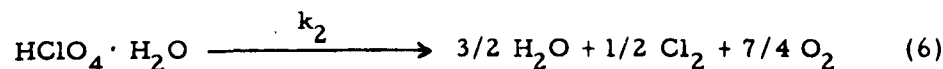
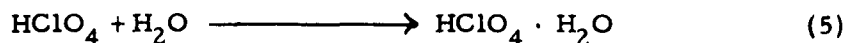
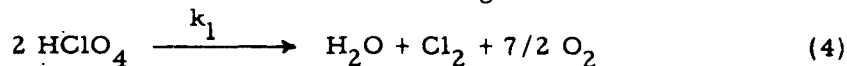
$$P_{Cl_2} = 1/2 P_x \quad (3)$$

where P_x is the pressure of the reacted acid. The points correspond to the direct measurements of Cl₂ pressure. The line is the predicted value.

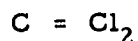
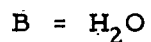
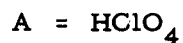
It is evident that the computational methods are supported by these data. By this demonstration, consideration of reaction mechanisms in which the rate of perchloric acid decomposition is not proportional to the rate of chlorine evolution is made unnecessary.

Computer Solution and Comparison with Observed Results

Multiple-trial computations were carried out using a Runge-Kutta-Gill numerical integration program on an IBM 7090 computer system to check the fit of the experimental data with various proposed reaction schemes. The reaction scheme which gave the best fit is:



Let the following letter designations correspond to the pressures of the molecular species in torr.



Based on the assumption that the steps designated in equations (4) through (6) occur on the glass surface, solution to the kinetics was formulated in terms of the following equations:

$$-\dot{A} = 2 k_1 A^2 + \frac{k_2 A \cdot B}{1 + K_B B} \quad (7)$$

$$\dot{C} = \dot{B} = - \frac{\dot{A}}{2} \quad (8)$$

$$\dot{D} = \frac{7}{4} \dot{A} \quad (9)$$

and
$$P_t = A_t + B_t + C_t + D_t \quad (10)$$

\dot{A} , \dot{B} , \dot{C} and \dot{D} are the time derivatives of the species, A, B, C and D.

(The existence of E is limited to the surface of the reactor.) P_t , A_t , B_t , C_t , D_t correspond to the total pressure and component pressures at time, t, K_B is the equilibrium constant for the adsorption of some inhibiting species, presumed to be H_2O on the reactor surface. Implicit in each of the rate constants k_1 and k_2 are equilibrium constants as required by adsorption considerations. Two possible cases where equilibrium constants for

adsorption change the interpretation of these rate constants are indicated briefly below.

k_1 , k_2 and K_B were obtained directly from experimental data. The value for k_1 was the numerical value obtained from the routine second order plot as indicated above.

In order to solve for a value of K_B , the second term of the overall rate equation, (7) was integrated in closed form independently of the first term. That is, the conversion of perchloric acid by the second process may be expressed as

$$\dot{A} = \frac{k_2 A B}{1 + K_B B} \quad (11)$$

This may be integrated to

$$\frac{A_0 t}{\ln(A_0 - A)} = \left(\frac{1 + A_0 K_B}{k_2} \right) \frac{\ln(A_0/A)}{\ln(A_0 - A)} + \frac{1}{k_2} \quad (12)$$

This solution is based on the assumption that as $(A_0 - A)$ approaches zero, $\ln(A_0 - A)$ approaches zero*. Then, the slope, m of the plot of $A_0 t / \ln(A_0 - A)$

* The same result can be obtained by integrating between $A = A_0 - 1$ and $A = (A_0 - A)$ followed by the assumption that $(A_0 - 1) \approx A_0$.

vs $\ln(A_0/A) / \ln(A_0 - A)$ gives

$$m = \frac{1 + A_0 K_B}{k_2} \quad (13)$$

Using the data from experiments at 200°C which have initial values of the perchloric acid pressure ranging from 136.4 to 218.5 torr, three slopes were obtained. A plot of these slopes against the initial pressures of acid yielded values for k_2 and K_B . The slope of the latter plot provided an estimation of

the ratio K_B/k_2 . The intercept was used to evaluate k_2 . The values obtained from the data at a surface to volume ratio of 3.3 were $k_2 = 1.04 \times 10^3$ ml/mole-min and $K_B = 1.55 \times 10^6$ ml/mole.

For the experiment which started at 218.5 torr of perchloric acid, the rate constant for step (4) was, $k_1 = 6.46 \times 10^2$ ml/mole-min.

Using these values, equation (7) was evaluated using the computer program.

Figures 10 and 11 indicate the results of these computations. Figure 10 compares the results of the computations of the total pressure (solid line) with the experimental points. Figure 11 shows the calculated distribution of products during the reaction. The fit of the data with computations indicate that the data are well explained in terms of the three step process, reactions (4) through (6).

Examination of the Adsorption Processes

The form of equation (7) implies that a number of adsorption equilibria may be involved in the surface decomposition processes. If standard Langmuir - Hinshelwood adsorption considerations are accepted, it follows that step (4) occurs by a mechanism in which the perchloric acid is weakly adsorbed and surface coverage is relatively slight. Then, the initial bimolecular process, step (4) can be described by a rate equation such as:

$$v_1 = 2k_1' K^2 A^2 \quad (14)$$

The experimental rate constant, $k_1 = k_1' K^2$ where K is the equilibrium constant for adsorption of perchloric acid on pyrex. This expression requires that the observed activation energy for the process, E_{a_1} be

$$E_{a_1} = E_T - 2 \lambda_{\text{HClO}_4} \quad (15)$$

APPENDIX C

where λ_{HClO_4} is the heat of adsorption of HClO_4 and E_T is the true activation energy for the homogeneous gas phase decomposition of HClO_4 .

Two alternate possibilities exist for explaining the surface processes involved in steps (5) and (6). Either both HClO_4 and the inhibiting reaction product which is assumed to be H_2O , (1) compete for the same sites on the pyrex surface or (2) reaction occurs between the two adsorbed gases but the gases are adsorbed on two different types of surface sites so that they do not displace each other from the surface.

1. Competitive Adsorption

In the case of adsorption of HClO_4 and H_2O on the same sites, the form of equation (7) implies that during the second part of the reaction, water is adsorbed much more strongly than HClO_4 alone. In effect, the reaction takes place between a gaseous HClO_4 molecule and an adsorbed H_2O molecule. The rate expression for the inhibited reaction has the form

$$v_2 = \frac{k_2' K_B AB}{1 + K_B B} \quad (16)$$

This treatment does not necessarily assume that there are no adsorbed HClO_4 molecules, but rather that the role of any adsorbed acid molecules in affecting the rate of HClO_4 (gas)- H_2O (surface) reaction is through their competition with water molecules for the available surface sites. When HClO_4 occupies a site adjacent to H_2O a rapid combination to $\text{HClO}_4 \cdot \text{H}_2\text{O}$ occurs, and the lifetime of $\text{HClO}_4 \cdot \text{H}_2\text{O}$ on the surface is \gg the lifetime of adsorbed HClO_4 . Based upon these considerations, the measured activation energy, E_{a_2} is the difference between the true activation energy for decomposition E_T , and the heat of adsorption of water, $\lambda_{\text{H}_2\text{O}}$

$$E_{a_2} = E_T - \lambda_{\text{H}_2\text{O}} \quad (17)$$

APPENDIX C

2. Non-Competitive Adsorption

The kinetics of the second step may also be explained in terms of a reaction between gases adsorbed on different types of sites so that the gases do not displace each other from the surface. This type of adsorption would give rise to rate expressions of the form

$$v_2 = \frac{k_2' K_A K_B AB}{(1+K_A A)(1+K_B B)} \quad (18)$$

If the adsorption of the acid is small so that $1 \gg K_A A$ then

$$v_2 = \frac{k_2' K_A K_B AB}{(1 + K_B B)} \quad (19)$$

The apparent and true activation energies have the following relationship:

$$E_{a_2} = E_T - \lambda_{H_2O} - \lambda_{HClO_4} \quad (20)$$

where λ_{HClO_4} is the heat of adsorption of $HClO_4$ and the other symbols have their previous significance.

Consideration of the data indicates that the competitive adsorption process is more probable.

Apparent Energies of Activation

Figure 12 is a plot of the second and psuedo first order rate constants, k_1 and k_2 respectively against the reciprocal of absolute temperature for data obtained at a surface to volume ratio of 1.4. These data were obtained at temperatures between 165 and 256°C. The following table summarizes the terms associated with the Arrhenius equation:

$$k = A \exp(-E_a/RT) \quad (21)$$

Report O372-OLF

APPENDIX C

for the two specific reaction rates at surface to volume ratios of 1.4 and 4.7.

Rate Constant	Surface/Volume Ratio	A	E_a (kcal/mole)	Temperature Range ($^{\circ}$ C)
k_1 ($\frac{\text{ml}}{\text{mole-min}}$)	1.4	6.5×10^7	13.4	165-256
k_1	4.7	9.7×10^7	12.3	200-240
k_2 (min) $^{-1}$	1.4	1.0×10^{10}	27.0	165-256
k_2	4.7	7.9×10^{10}	28.7	200-240

When the psuedo first order constant is treated as indicated above to separate k_2 , the second order rate constant and K_B , the equilibrium constant for adsorption of the inhibitor, the following values were obtained at a surface to volume ratio of 4.7

$$k_2' = 1.9 \times 10^5 \exp(-20, 500/RT) \quad (22)$$

$$K_B = 9.8 \times 10^3 \exp(-13, 300/RT) \quad (23)$$

From equation 15 and the value of the activation energy for decomposition of perchloric acid, found by Zinoviev and Babayeva,³ a value for the heat of adsorption of HClO_4 on pyrex may be estimated. On this basis, the estimated heat of adsorption between 165 and 256 $^{\circ}$ C is 9.7 kcal per mole.

Heats of adsorption of water on different glasses have been determined by Rand¹¹ and by Tuzi and Okamoto¹².

¹¹ M. J. Rand, *J. Electrochem Soc.*, **109**, 402 (1962).

¹² Y. Tuzi and H. Okamoto, *J. Phys. Soc., Japan*, **13**, 960 (1958).

Rand found values between 13.5 and 11.6 kcal/mole on vycor as a function of coverage. Tuzi and Okamoto obtained 11 kcal/mole on lead borosilicate glass. These values are in reasonable agreement with the 13.3 kcal/mole estimated for the heat of adsorption of the inhibitor on pyrex. Thus water appears to be the inhibitor.

It is possible to choose between the competitive and non-competitive adsorption mechanisms on the basis of the activation energy values for the processes represented by k_2 and K_B . The competitive adsorption mechanism for which the relationship of equation (17) applies gives rise to a value of the true activation energy, $E_T = 33.8$ kcal/mole. The non-competitive mechanism results in an estimated value of $E_2 = 43.4$ kcal/mole. Thus, the competitive adsorption mechanism appears more probable. The value of 33.8 kcal/mole compares satisfactorily with the activation energy of Zinoviev and Babayeva³, who reported 32.8 kcal/mole. It suggests that the same rate controlling process may be operational as was found by Figini, Coloccia and Schumacher¹³

¹³ R. V. Figini, E. Coloccia and H. J. Schumacher, Z. Phys. Chem., 14, 32 (1958).

for Cl_2O_7 . They obtained an activation energy of 32.9 kcal/mole.

The Effect of Alumina

A few experiments were carried out to determine the effect of alumina on the decomposition rate of perchloric acid at 200°C. The addition of 0.25g of Al_2O_3 (surface area, 75 m^2/g) as a pellet in the bottom of a pyrex reactor which had a 1.4 cm^2/cm^3 surface/volume ratio increased the second order rate constant, k_1 by a factor of 2.9. However, the pseudo first order rate constant, k_2 , remained unchanged within the experimental limits of precision. It may be concluded that the initial second order reaction, which represents the decomposition of the anhydrous acid was considerably accelerated in the presence of alumina. The reason for the unchanged rate of decomposition by the second reaction cannot be clarified without further experimentation. It is possible that stronger adsorption of the inhibiting

species on Al_2O_3 than on glass is a factor. However, since the reactor was not packed fully with alumina, the possible role of diffusion in the reaction rate determination makes an unequivocal conclusion impossible.

Some Geometrical Considerations

The bimolecular nature of the initial reaction gives rise to a number of interesting speculations concerning the form of the activated complex on the surface. Figure 13 shows the calculated dimensions of a possible model which may be similar to a hydrated Cl_2O_7 species. The computations were based on the assumptions of a Cl-O distance of 1.69 \AA in the ClO_4 tetrahedra, 0.96 \AA as the H-O bond length in water and an H-O-H angle of $104^\circ 30'$. Assuming reaction occurs between adjacent adsorbed molecules of HClO_4 , this model requires that the adsorption sites be within 5.46 \AA of each other. A 2.43 \AA minimum distance is required for two point attachments of the undistorted activated species.

In this model it has been assumed that two hydrogen bonds exist between the water molecule and the adsorbed Cl_2O_7 which stabilize the configuration. Figini, Colloccia and Schumacher¹³ have reported an activation energy for decomposition of Cl_2O_7 of $32.9 \pm 1.5 \text{ kcal/mole}$ in the temperature range between 100 and 120°C . The value of $33.8 \pm 3.0 \text{ kcal/mole}$ which has been derived from these data suggests that the same process may be rate controlling in HClO_4 and Cl_2O_7 decompositions.

The hydrogen bonding of the water molecule to the adsorbed Cl_2O_7 which is indicated in the model has been shown to fit reasonably satisfactorily into known bond length requirements. Using a distance between centers of the oxygen atoms of 2.76 \AA such as is found for water, a distortion of the HOH angle from 104.5° to 117.5° would be required. If the water molecule is assumed to remain undistorted, the calculated distance between centers of the oxygen atoms would be 2.99 \AA . The strain

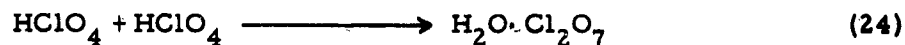
energy for distorting the O-H---O bond would involve only 0.13 kcal/mole according to Pauling.¹⁴

¹⁴ L. Pauling and R. B. Corey, Fortschr. Chem. org. Naturstoffe, 11, 180 (1954).

Thus, it may be considered that such a model satisfies the geometrical requirements for a $\text{Cl}_2\text{O}_7 \cdot \text{H}_2\text{O}$ activated state on the surface.

Reaction Mechanism

On the basis of the results indicated above the decomposition of anhydrous perchloric acid appears to be a surface catalyzed, consecutive step process between temperatures of 165 and 256°C. The initial step appears to be



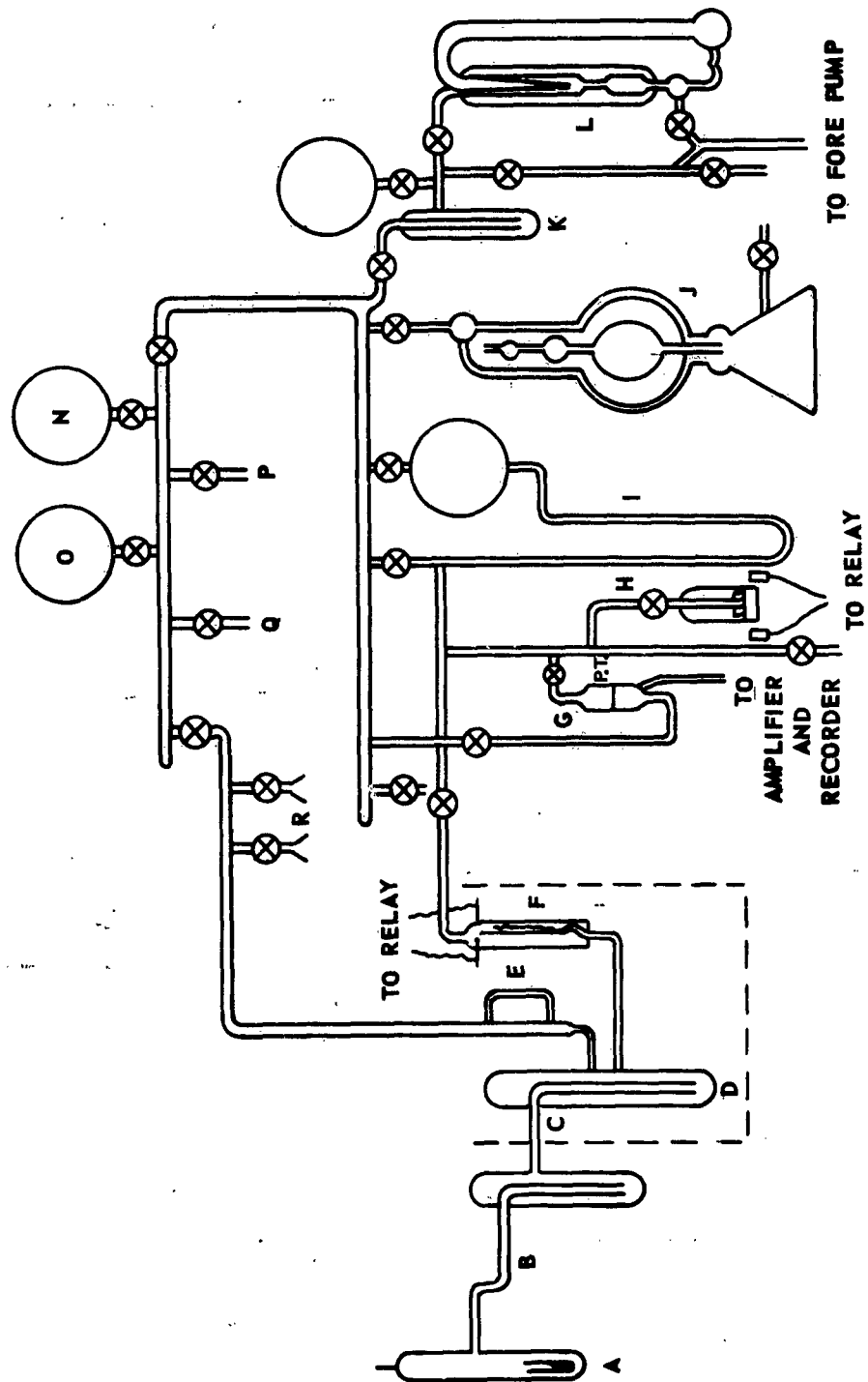
The decomposition of the latter species appears consistent with the mechanism suggested by Figini, Colloccia and Schumacher¹³ for Cl_2O_7 . However, the presence of water is believed to inhibit the surface reaction by competing more strongly for the reactive sites than can HClO_4 . As the concentration of adsorbed water increases the reaction



forms a relatively more stable species than the anhydrous acid. The decomposition of the monohydrate is believed to continue until all of the species, HClO_4 is exhausted. It appears possible that a relatively minor part of the decomposition proceeds by a gas phase reaction under the conditions of these experiments.

ACKNOWLEDGEMENTS

The authors are pleased to acknowledge the fruitful discussions of this work which took place with their colleagues at Aerojet-General Corporation in Azusa, California. Messrs. F. J. Cheselske and R. F. Chaiken were especially helpful with their constructive considerations. A future paper examining the reaction mechanism from a more statistical viewpoint is planned.



APPARATUS FOR GAS KINETICS MEASUREMENTS

**CHLORINE COLORIMETER SYSTEM
FOR PERCHLORIC ACID DECOMPOSITION STUDIES**

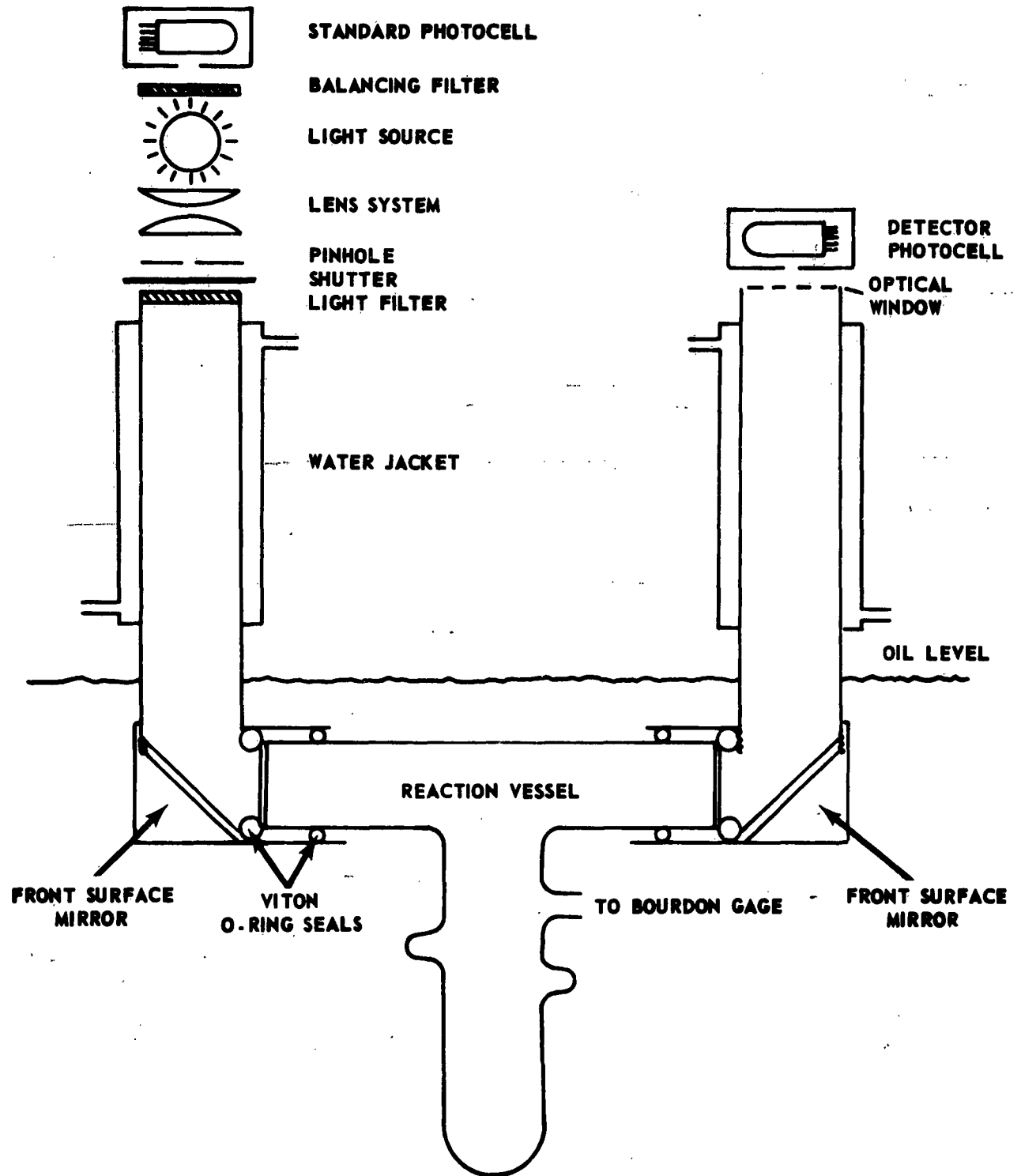


Figure 2

VAPOR PRESSURE OF PERCHLORIC ACID

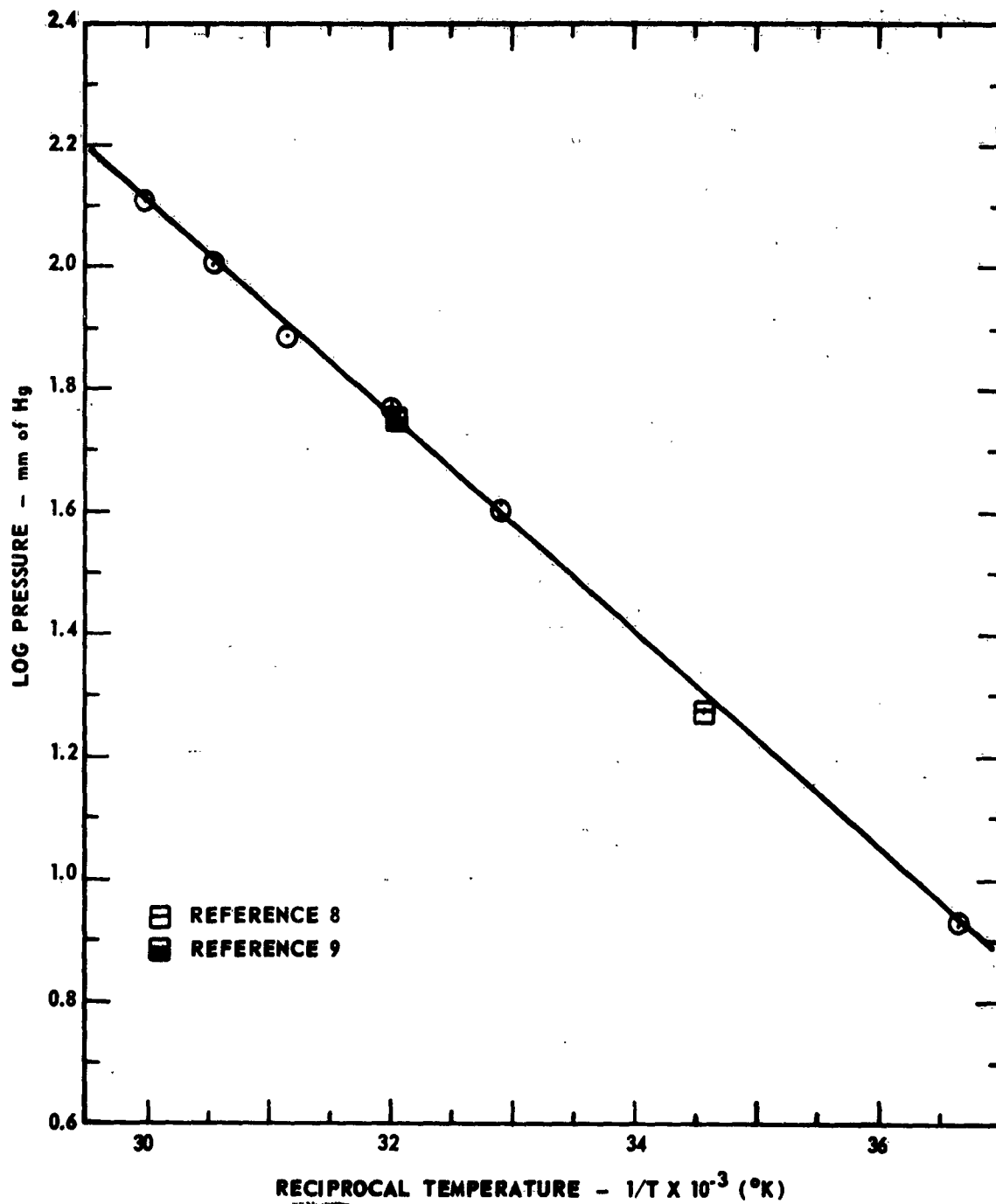


Figure 3

Report 0372-01F
APPENDIX C

INFRARED SPECTRUM OF PERCHLORIC ACID DECOMPOSITION
100 mm PATH - NaCl WINDOWS

UPPER: 16.8 TORR AT 10 MIN AFTER VAPORIZATION

MIDDLE: AFTER 3 HOURS AT 25°C

BOTTOM: AFTER SEVERAL HOURS AT 25°C

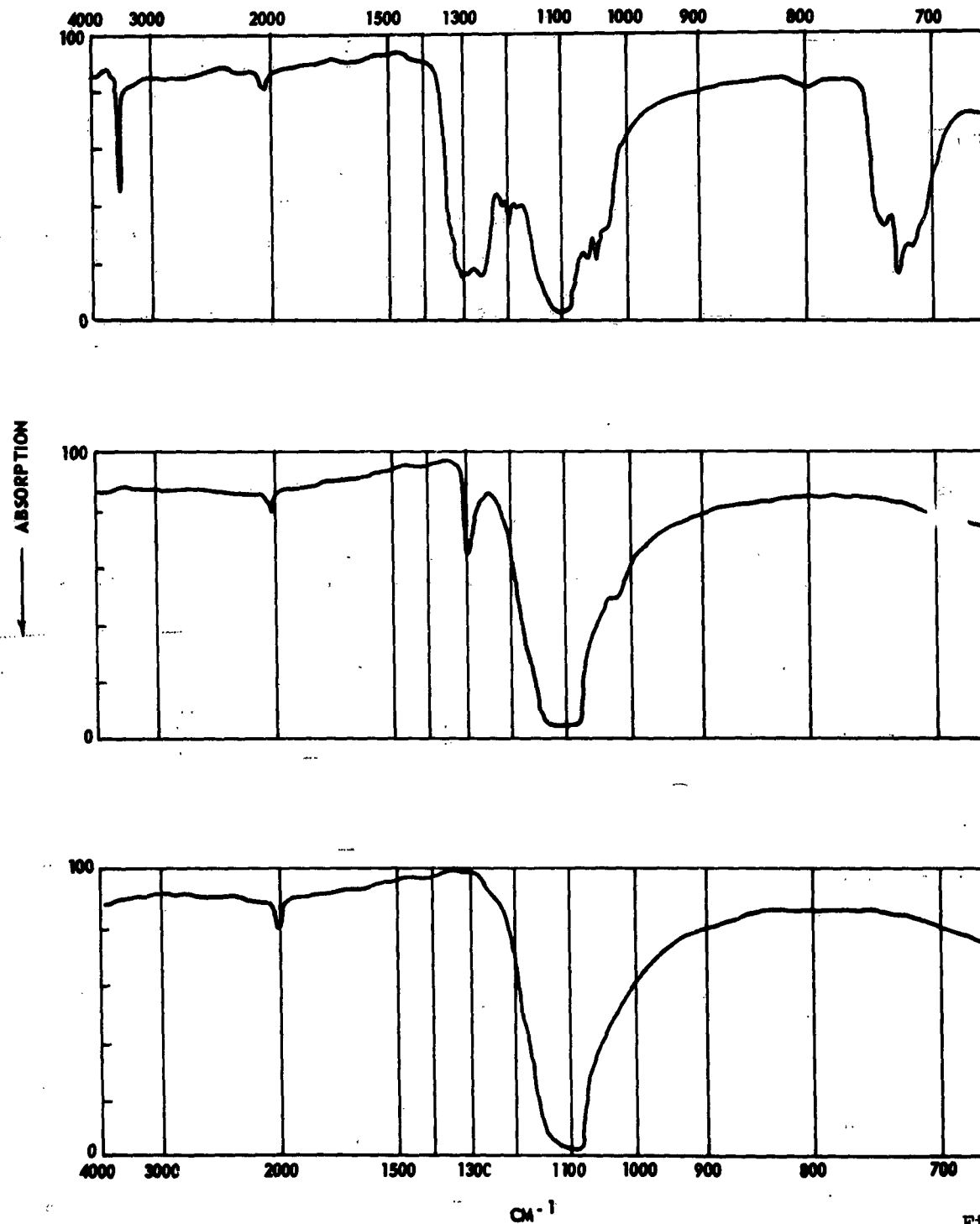


Figure 4

Report O372-01F
APPENDIX C

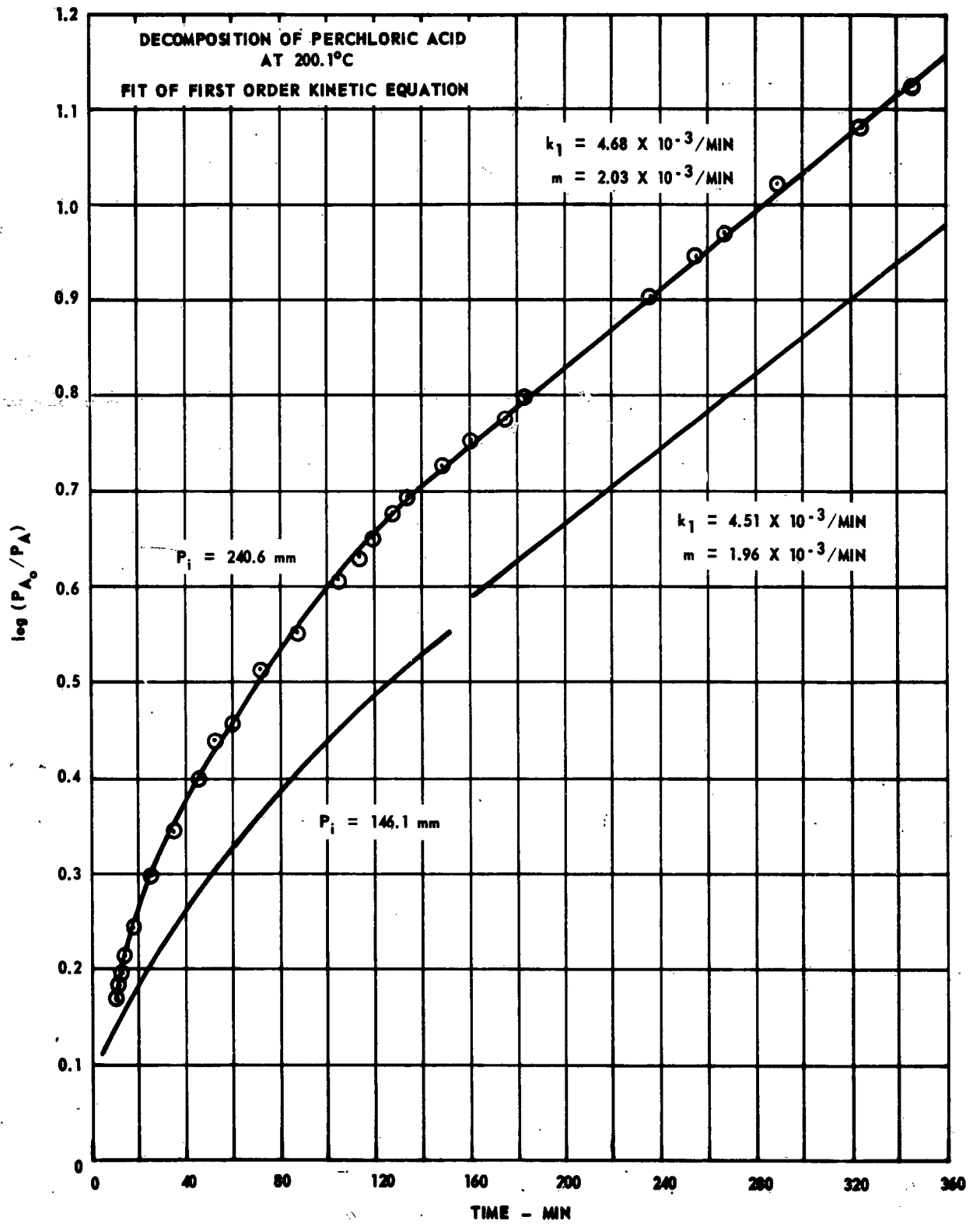


Figure 5

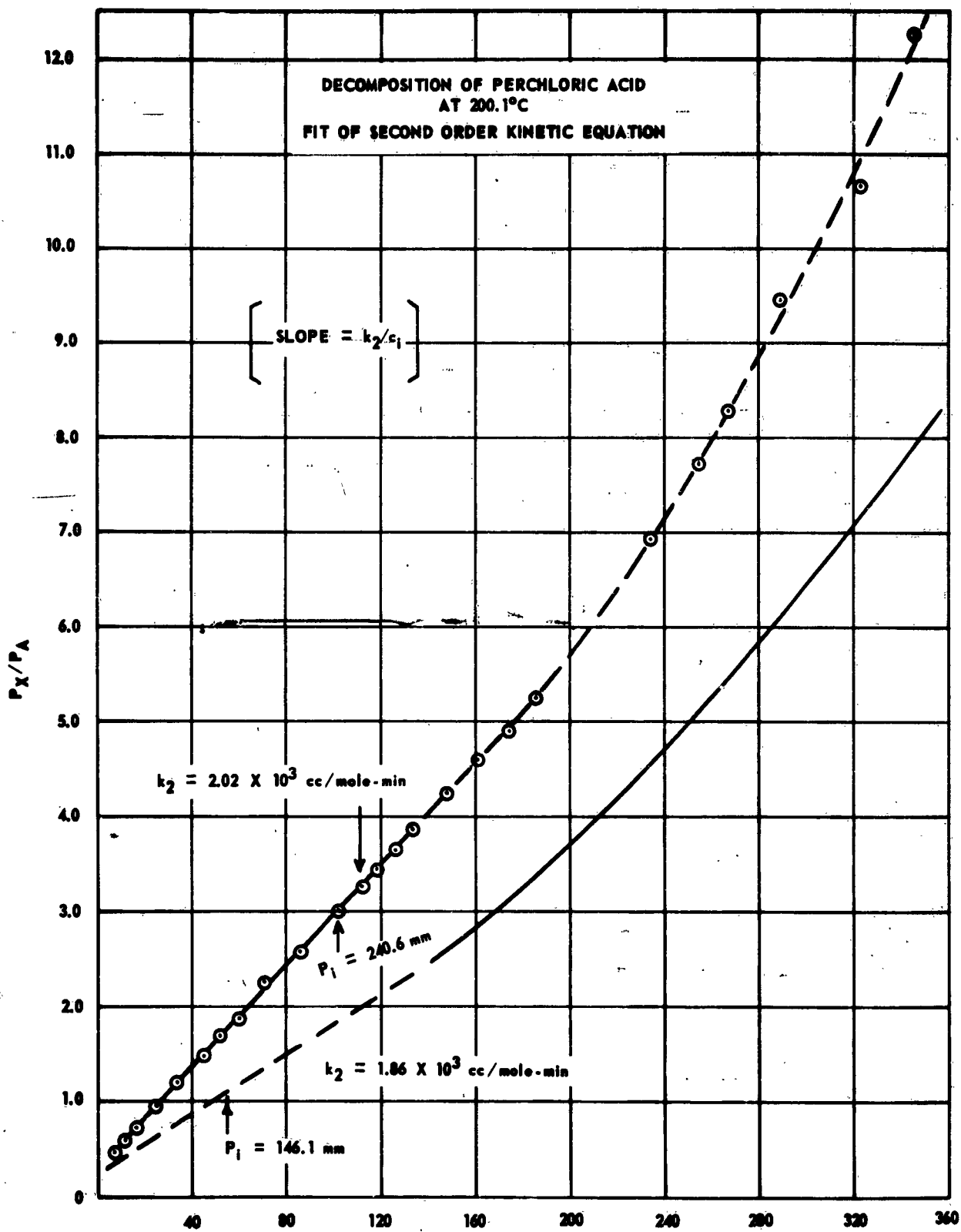


Figure 6

EFFECT OF SURFACE AREA ON PSEUDO FIRST-ORDER
RATE CONSTANTS AT 200°C

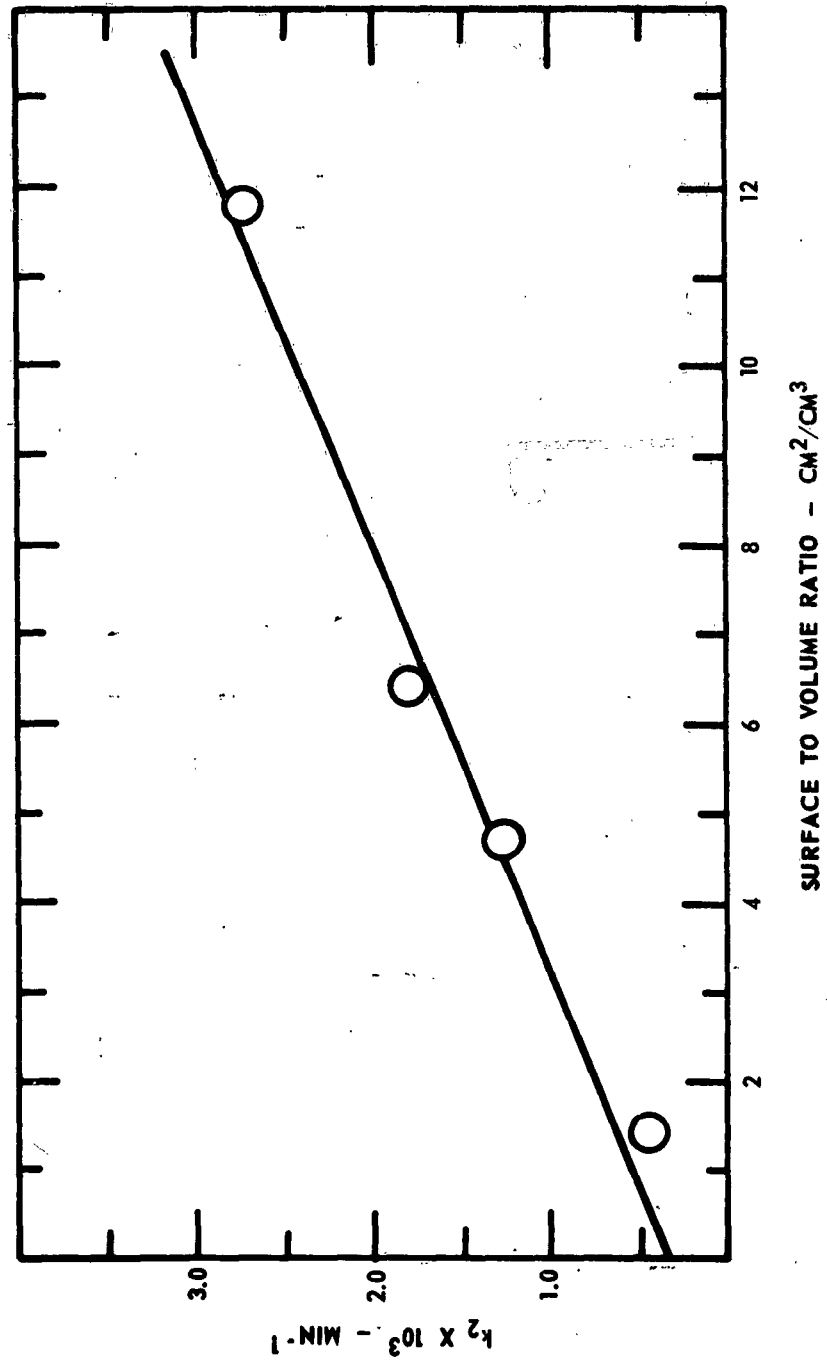


Figure 7

EFFECT OF SURFACE ON
SECOND ORDER RATE CONSTANTS
AT 200°C

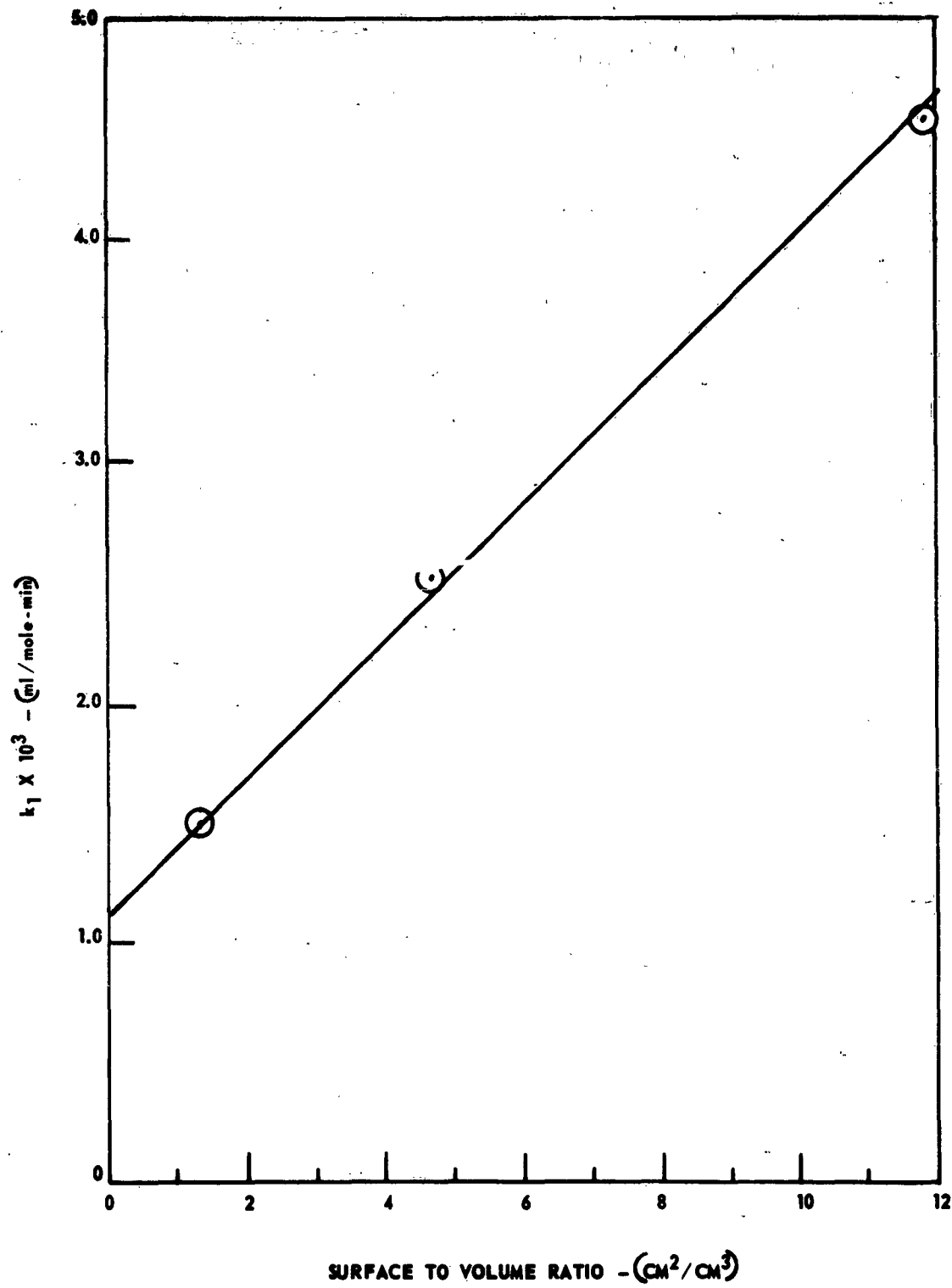


Figure 8

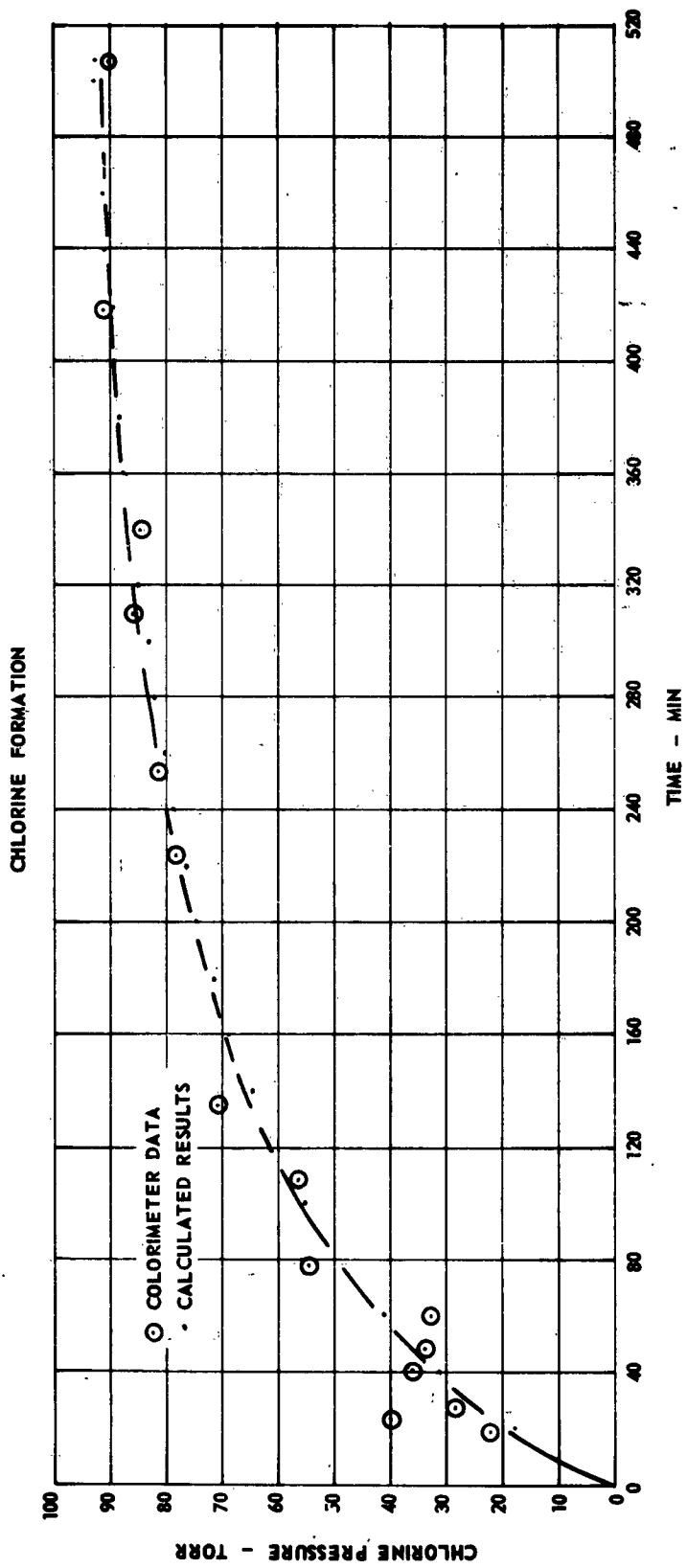


Figure 9

COMPARISON OF COMPUTED AND EXPERIMENTAL PRESSURES

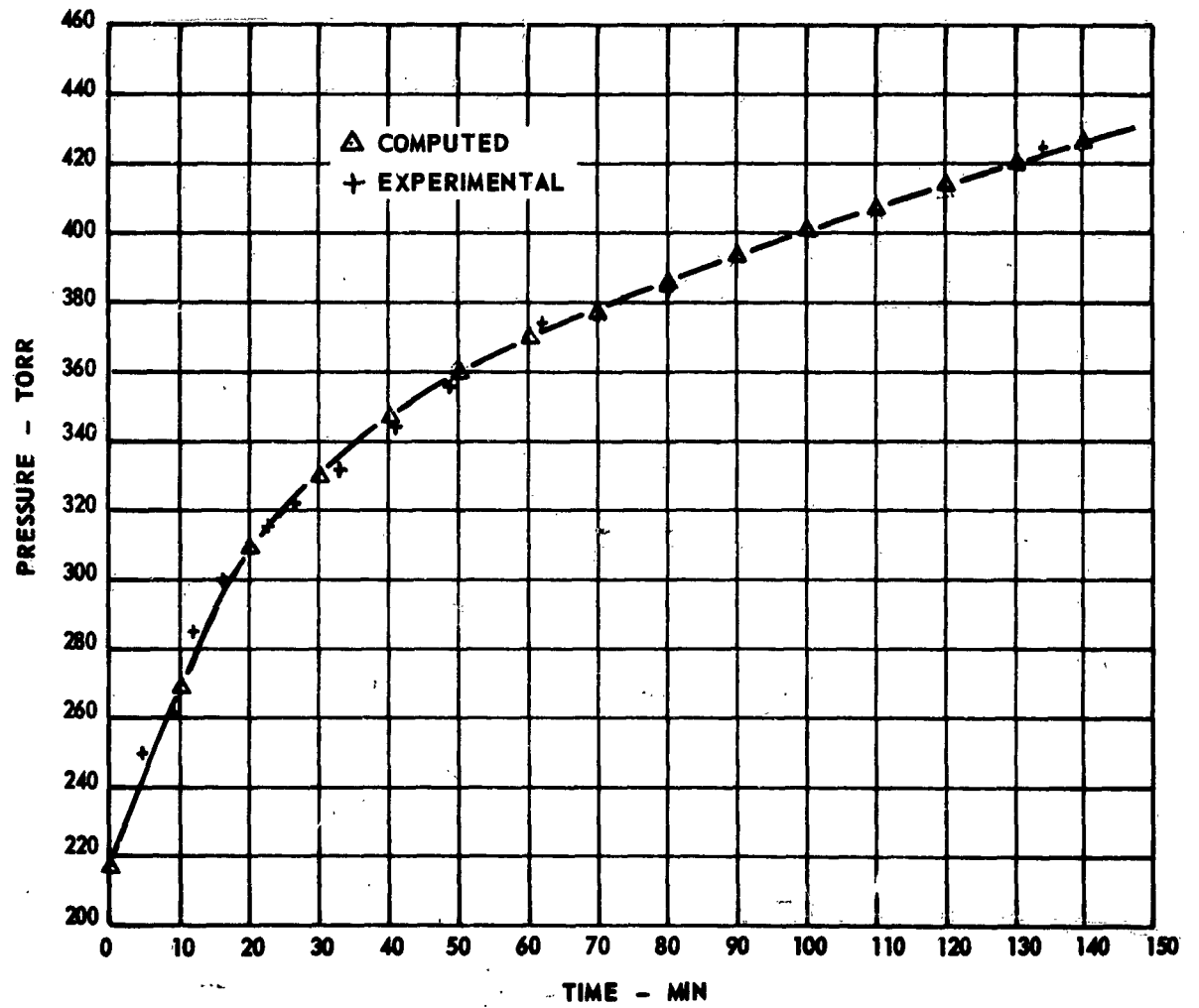


Figure 10

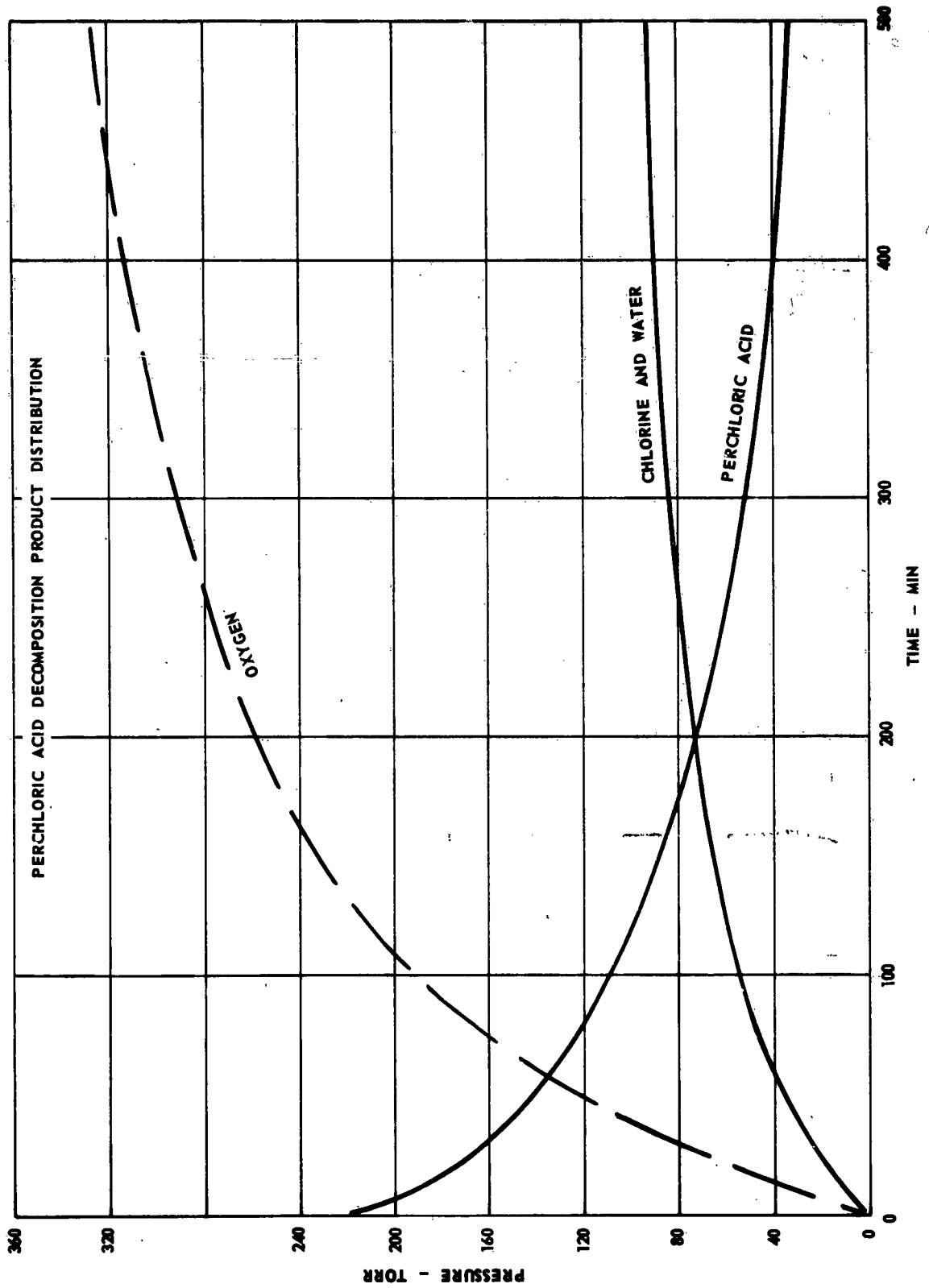


Figure 11

APPARENT ACTIVATION ENERGIES

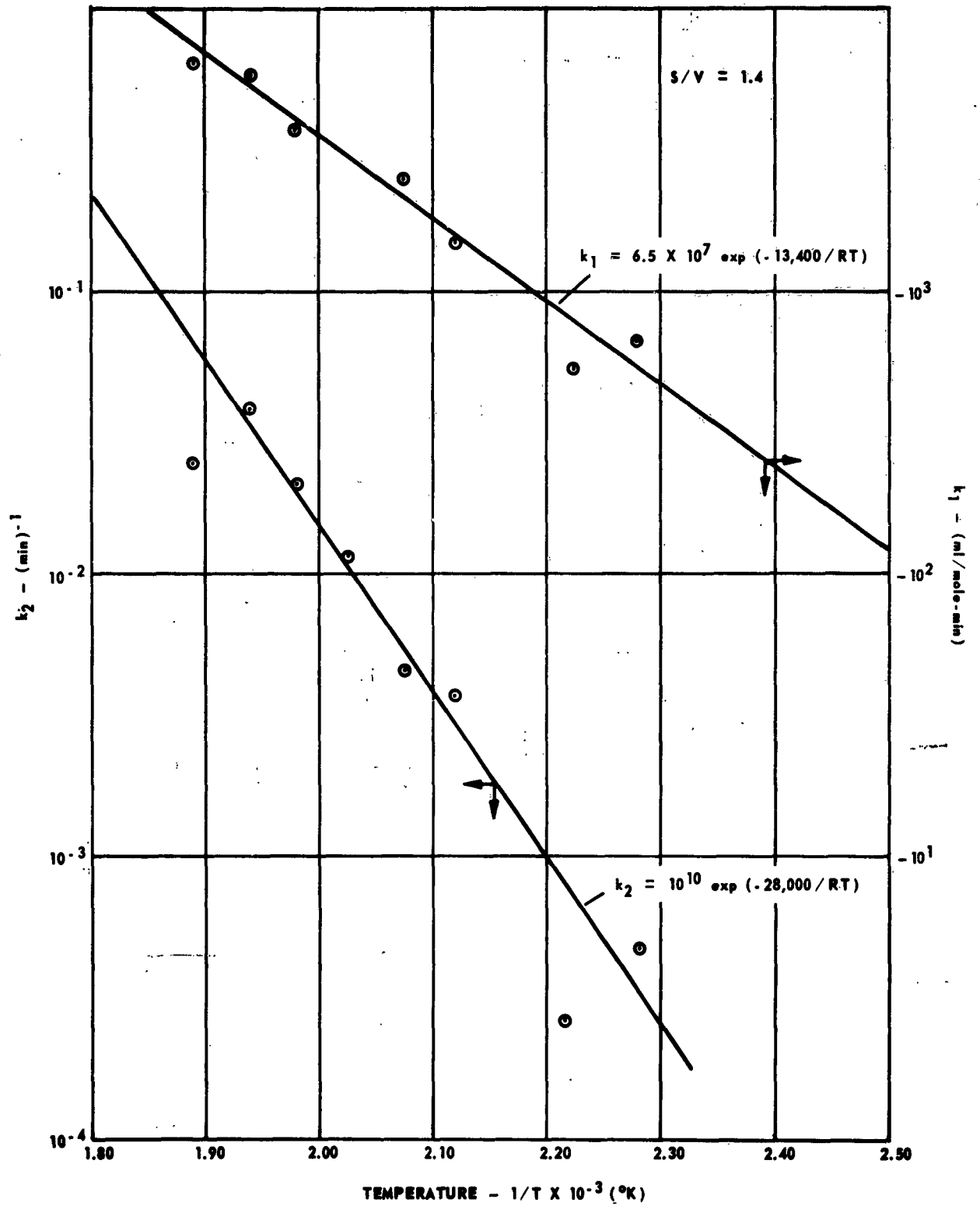
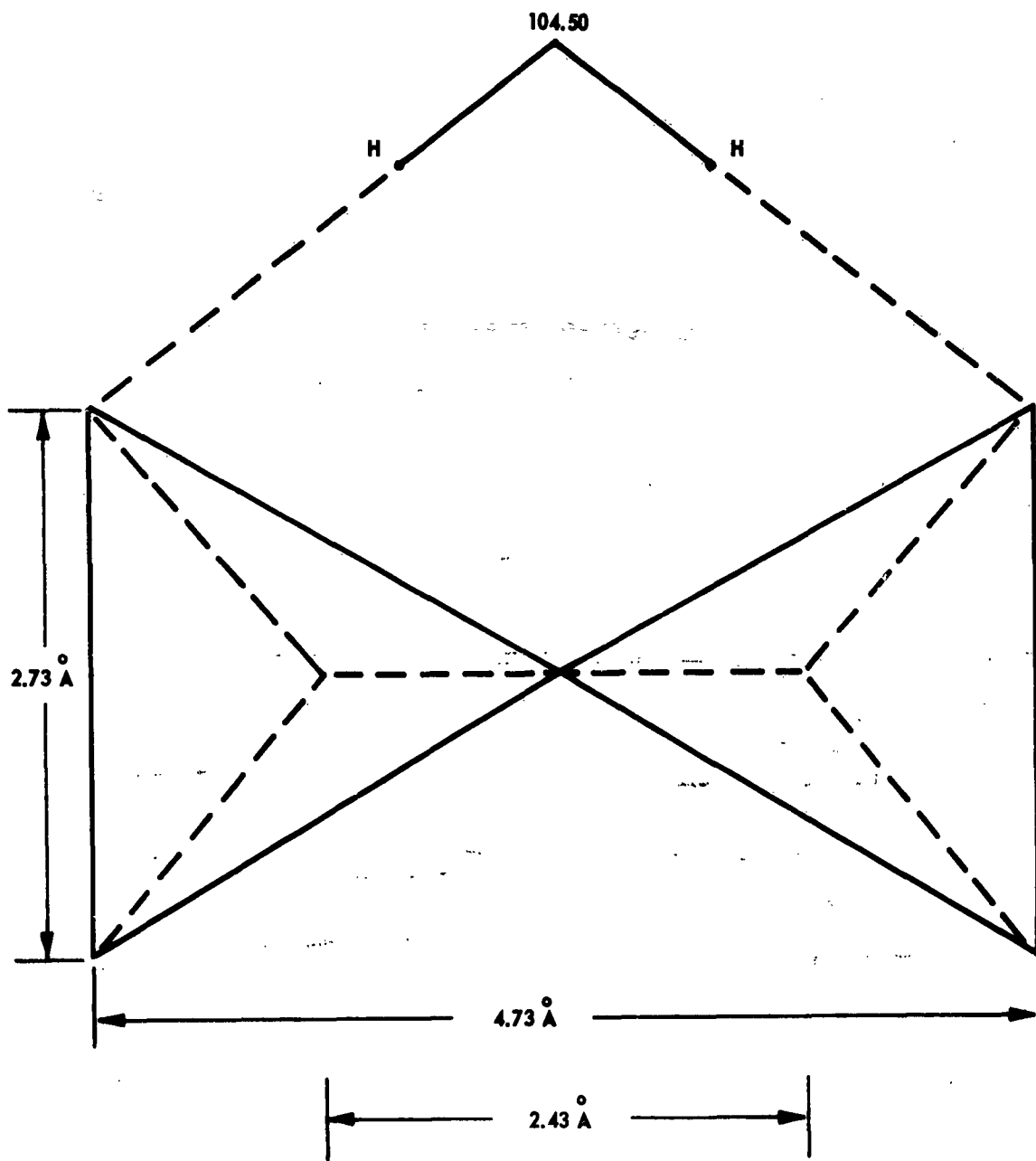


Figure 12



MINIMUM DISTANCE FOR
UNDISTORTED Cl_2O_7

MODEL FOR ACTIVATED STATE IN HClO_4 DECOMPOSITION

APPENDIX D

ON THE EXTINCTION OF OPPOSED-JET
DIFFUSION FLAMES:
A PHYSICAL CRITERION FOR EXTINCTION

By

R. F. Chaiken
Technical Consultant
Aerojet-General Corporation
Sacramento, California

I. INTRODUCTION

The extinction of opposed-jet diffusion flames, which were first investigated by Potter and his colleagues,⁽¹⁻³⁾ and the Spalding theoretical treatment of the phenomena⁽⁴⁾ have demonstrated the potential usefulness of the extinction process as a means for determining chemical reaction rates in flames. In the studies by Potter et. al., the technique involves the extinction of flames which have first been stabilized in the impingement zone between two opposed gas jets, one of which contains fuel, and the other oxidant. Such flames exhibit a well defined "Apparent Flame Strength" or maximum mass flux which can be burned along the axial direction. Gas flow rates which exceed this "Apparent Flame Strength" (referred to hereafter as AFS), results in extinguishment of the axial portion of the flame and its reestablishment in a region encircling the gas jet impingement zone.

According to the Spalding theoretical treatment, the AFS should be directly proportional to the volumetric rate of chemical reaction at extinguishment, and hence, the pressure dependence of the AFS should be the same as the overall order of the chemical reactions giving rise to the flame. These conclusions appear to have been reasonably well verified in flame studies with propane-oxygen⁽³⁾ (reaction order = 2.0), ammonia-oxygen⁽⁵⁾

APPENDIX D

(reaction order = 1.7), and ammonia-nitrogen dioxide⁽⁵⁾ (reaction order = 2.5). Unfortunately, the Spalding Theory requires prior chemical kinetic knowledge (or assumptions) about the flame reactions in order to relate quantitatively AFS data with the maximum volumetric reaction rate at extinction. Thus, it is difficult to interpret comparisons between estimates of flame reaction rates obtained by the opposed-jet technique and those obtained by other methods (e.g., from laminar flame speed data).

Recently, Pandya and Weinberg⁽⁶⁾ have studied the internal structure of flat opposed-jet diffusion flames between ethylene and oxygen utilizing jet flow rates far less than the AFS for this system. In connection with the aerodynamic structure of the impingement zone, these investigators found two types of flow patterns: (1) when the flame zone is displaced from the center of the aerodynamic system, a single plane (the stagnation plane) exists across which no particles can cross. Here, the flame zone is fed by both convective and molecular diffusion of reactant; and (2) when the centers of the flame and aerodynamic systems are made to coincide, two stagnation planes exist across which no particles can cross. In this case, the flame zone, which is bounded by the two stagnation planes, is fed reactants solely by molecular diffusion.

It is believed that the change in reactant flow rate process with different positions of the flame reaction center (relative to the aerodynamic center) offers a possible physical criterion for the extinguishment of opposed-jet diffusion flames. It is the purpose of this paper to describe this physical criterion, and to demonstrate how it can be utilized in conjunction with the Spalding treatment of the mixing of opposed-jets to obtain

Report 0372-01F

APPENDIX D

a quantitative relationship between AFS and chemical reaction rate. This new approach leads to results similar to those obtained by Spalding and does not require prior detailed chemical kinetic knowledge about the flame.

II. SPALDING THEORY OF MIXING IN OPPOSED JETS

The aerodynamic model considered by Spalding⁽⁴⁾ is based on the impingement of two opposed inviscid gas jets of equal strength on a thin, infinite plate held perpendicular to their axes (see Figure 1).

The following conditions were assumed:

- (1) Stationary-state one-dimensional flow in the axial direction.
- (2) The one-half thickness of the impingement region (i.e. distance along the axis measured from the aerodynamic center) is less than 0.1 times the jet diameter.
- (3) The diffusion coefficients of all molecular species are equal at any point along the axis.
- (4) The product of the square of local gas density and the diffusion coefficient is a constant.

For the purposes of this paper it will suffice to just state some of Spalding's results, viz.

$$f = \left(\frac{1}{2}\right) \left[1 + \operatorname{erf} \left(Y \sqrt{\rho_{\infty} U / 2 \gamma_{\infty} r_0} \right) \right] \quad (1)$$

$$\frac{df}{dY} = \left[\frac{U}{2 \pi \gamma_{\infty} r_0} \right]^{\frac{1}{2}} \exp \left[\frac{\rho_{\infty} U Y^2}{2 \gamma_{\infty} r_0} \right] \quad (2)$$

and, $v = - U Y / r_0$

where f = fraction of mass in the local mixture which is derived from the fuel bearing jet.

Report 0372-01F

APPENDIX D

Y = transformed coordinate related to distance along the axis
(y-direction); $Y = \int_0^y (\rho/\rho_\infty) dy$

ρ = local density

γ = local exchange coefficient (equal to the product of the
local density with the diffusion coefficient).

U = initial axial velocity of the jet

v = axial velocity of the jet at point y

r_0 = radius of jet

subscripts $\pm\infty$ refer to conditions at $y = \pm\infty$
(the fuel jet is taken as originating at $y = +\infty$,
and the oxidant jet at $y = -\infty$).

The relationship between f and the composition of the local mixture
can be readily derived from the following considerations. Let the reaction
stoichiometry be independent of y , and such that $\alpha/(\alpha + 1)$ gm of oxidant
reacts with $1/(\alpha + 1)$ gm of fuel to give 1 gm of products. Then the mass
in the local mixture which is derived from the fuel jet is

$$M_{TF} = M_{fu} + M_{infu} + \frac{M_p}{\alpha + 1} \quad (4)$$

where M_{TF} = total mass from fuel jet

M_{fu} = mass of fuel

M_{infu} = mass of inert from fuel jet

M_p = mass of reaction products

likewise for the total mass from the oxidant jet,

$$M_{Tox} = M_{ox} + M_{inox} + \frac{\alpha M_p}{\alpha + 1} \quad (5)$$

Now since the diffusion coefficients of all species are the same, M_{infu}/M_{TF}
and M_{inox}/M_{Tox} are independent of y . Also, $M_p = 0$ at $y = \pm\infty$; $M_{ox} = 0$
at $y = \infty$; and $M_{fu} = 0$ at $y = -\infty$. Normalization of the component

APPENDIX D

masses to the total mass present (i.e. $M_{Tox} + M_{TF}$) leads eventually to

$$f = \frac{m_{fu} = m_{ox}/\alpha + m_{ox, -\infty}/\alpha}{m_{fu, \infty} + m_{ox, -\infty}/\alpha} \quad (6)$$

where the m's refer now to component mass fractions, and the $\pm\infty$ subscripts refer to initial values before mixing of the jets (i.e., at $y = \pm\infty$).

In anticipation of the discussions to be presented, it is of interest to determine the relationship between f and m_{fu} under the limiting condition of infinitely fast reaction occurring. In this case, oxidant cannot exist in regions where fuel exceeds its stoichiometric value; likewise fuel cannot exist in regions where oxidant exceeds its stoichiometric value. Thus, $m_{fu} = 0$ for $m_{ox} > 0$; $m_{ox} = 0$ for $m_{fu} > 0$, and the expression for f on the fuel jet side of the flame front is

$$f \Big|_{\text{side}}^{\text{fuel}} = \frac{m_{fu} + m_{ox, -\infty}/\alpha}{m_{fu, \infty} + m_{ox, -\infty}/\alpha} \quad (7)$$

Also, the position of the flame front (locus of stoichiometry) is determined by $f(m_{fu} = 0; m_{ox} = 0)$ or

$$f_{st} = \frac{m_{ox, -\infty}/\alpha}{m_{fu, \infty} + m_{ox, -\infty}/\alpha} \quad (8)$$

Equation (8) in conjunction with Equation (1) can be solved for the position of the flame front in the transformed axial coordinate system, Y , i.e.,

$$\text{erf} \left(Y_{st} \sqrt{\rho_{\infty} U/2 \gamma_{\infty} r_0} \right) = 2f_{st} - 1 \quad (9)$$

It is noted that, since $\text{erf}(\pm|x|) = \pm \text{erf}(|x|)$, Equation (9) indicates that $\left| Y_{st} U^{1/2} \right|$ must be a constant for a constant flame stoichiometry. Hence as the jet velocity U increases, $\left| Y_{st} \right|$ decreases, and the flame front is

APPENDIX D

established closer to the stagnation plane (at $Y = 0$). This can also be seen from Figure 2* which shows the variation of $Y\sqrt{\rho_{\infty}U/2\gamma_{\infty}r_0}$ vs f .

Now the fuel flow/unit area/unit time along y is given in general by the sum of the diffusion and convective flux, i.e.,

$$\dot{m}'_{fu} = \rho v m_{fu} - \gamma (dm_{fu}/dy) \quad (10)$$

or from Equation (3) and the definition of the transformed axial coordinate, Y ,

$$-\dot{m}'_{fu} = \frac{\rho_{\infty}U}{r_0} Y m_{fu} + \frac{\gamma\rho}{\rho_{\infty}} (dm_{fu}/dY) \quad (11)**$$

From Equation (11), it is noted that the convective flux (given by the first term) is zero at the stagnation plane ($Y = 0$) as well as at points in the flame where $m_{fu} = 0$.

In the case of infinitely fast reaction, Equations (2), (7), and (11) yield the following expression for the fuel flux into the flame front,

$$-\dot{m}'_{fu} \Big|_{Y_{st}} = (m_{fu,\infty} + m_{ox,-\infty} / \alpha) \left[\frac{\gamma_{\infty} \rho_{\infty} U}{2\pi r_0} \right]^{\frac{1}{2}} e^{-\frac{\rho_{\infty} U}{2\gamma_{\infty} r_0} Y_{st}^2} \quad (12)$$

or in terms of Spalding's dimensionless quantities

$$\left[\frac{-\dot{m}'_{fu} \Big|_{Y_{st}}}{m_{fu,\infty} \rho_{\infty} U} \right] \left[\frac{2r_0 \rho_{\infty} U}{\rho_{\infty}} \right]^{\frac{1}{2}} = \Omega_{st} \quad (13)$$

$$\text{where } \Omega_{st} = \frac{\exp[\rho_{\infty} U Y_{st}^2 / 2\gamma_{\infty} r_0]}{\pi^{\frac{1}{2}} (1-f_{st})}$$

* Taken from Spalding's paper (Reference 4).

** A negative value of fuel flux implies a fuel flow towards $y = -\infty$; hence, Equation (11) is written in the sense of fuel flow into the flame front for values of Y on the fuel jet side of the flame.

APPENDIX D

The linear term in brackets on the left-hand side of Equation (13) is equal to the mass rate of fuel burned per unit area of flame divided by the mass flow rate of fuel per unit area of fuel-bearing jet. The square root term is a Peclet number for the jet. In this form, it is more clearly seen that the fuel reaction rate for infinitely fast reactions is independent of the local transport properties of the gas mixture in the region of the flame.

III. FINITE CHEMICAL REACTION RATES

A. DESCRIPTION OF THE FLAME ZONE

In the previous section, the flame zone for infinitely fast reaction rates was represented as a plane of zero thickness at $f = f_{st}$ (see Equation 8). In the model to be considered in this section, it is assumed that finite extent in the axial direction which can be approximated by a definite reaction zone of thickness δ (see Figure 1). It is further assumed that this reaction zone is centered symmetrically with respect to chemical reaction rate on the plane corresponding to $f = f_{st}$. In this connection, it is noted that Pandya & Weinberg⁽⁶⁾ found the profile of heat release rate in the ethylene-oxygen opposed-jet flat flame to be highly symmetrical about the flame center (peak value). This symmetry existed even when the flame was positioned at some distance from the aerodynamic center (within the gas-jet impingement zone).

Now the simple mixing theory of Spalding predicts that a single stagnation plane (at the aerodynamic center, $y = 0$) should occur for all values of $\left| Y_{st} \right|$. However, Pandya and Weinberg found that this conclusion is valid only when the flame zone does not coincide with the aerodynamic center. When these regions do coincide, the flame apparently behaves as a weak gas

APPENDIX D

source which splits the single stagnation plane into two planes across which no particles can cross by convective flow. From these experimental results, it can be inferred that under conditions of flow or stoichiometry where the flame zone is positioned away from the aerodynamic center, at least one of the reactants will be fed into the flame reaction zone (i.e. in the direction of the flame) by both diffusive and convective flow.* However, when conditions prevail where the flame reaction zone and the aerodynamic center coincide, the appearance of two stagnation planes will result in the flame reaction zone being fed both oxidant and fuel solely by diffusive flow.

B. THE EXTINCTION CRITERION

In view of the above comments, it is now possible to develop a physical criterion for the extinction of opposed-jet diffusion flames. First, consider a flame zone whose center at $y = y_{st}$ is initially displaced from the aerodynamic center at $y = 0$ by distance greater than $\delta/2$, which by definition is the half thickness of the effective chemical reaction zone.**

From the relationship between y_{st} and Y_{st} , i.e.,

$$Y_{st} = \int_0^{y_{st}} (\rho/\rho_{\infty}) dy \quad (14)$$

and the relationship between Y_{st} and jet velocity (see Equation 9), it is seen that as the jet velocity U increases, $|Y_{st}|$ decreases, and the flame center will approach the single stagnation plane at $Y = \bar{y} = 0$.

* For the case depicted in Figure 1, oxidant is fed into the flame reaction zone by both diffusive and convective flow, and fuel by diffusive flow alone. The reverse situation would hold for a flame positioned on the fuel side of the aerodynamic center.

** In Figure 1, the initial flame zone is positioned on the negative y -axis, hence, $y_{st} < -\delta/2$. If the initial flame were positioned on the positive y -axis, then $y_{st} > +\delta/2$.

Report 0372-01P

APPENDIX D

Now consider an increase in U to a value where $|y_{st}| = \delta/2$. Then, any further increase in U will cause the finite flame zone to envelop the single stagnation plane at the aerodynamic center. In accordance with the findings of Pandya and Weinberg,⁽⁶⁾ it might be supposed that under these flow conditions the single stagnation plane will be split into two stagnation planes such that the rate of reactant flow into the flame zone suddenly decreases. This decrease in reactant flux will be associated with the sudden change from a combined diffusive and convective flow process to a solely diffusive process.

Now while the rate of chemical reaction (and therefore rate of heat release) within the flame zone must suddenly decrease when $|y_{st}| \leq \delta/2$, there should be no drastic change in the rate of cooling of the flame reaction zone due to radiation and heat conduction to the environment. Hence, it might be expected that the sudden appearance of two stagnation planes could result in complete and sudden extinction of the axial portion of the flame. This physical criterion for extinction would lead to an "Apparent Flame Strength" (i.e., $\rho_{CO} U_{ext}$) which is determined by the value of U for which $|y_{st}| = \delta/2$, or

$$|y_{st}^*| = \int_0^{\delta/2} (\rho/\rho_{CO}) d\xi \quad (15)$$

where $\xi = |y|$

The above expression combined with Equation (9) with $Y_{st} = |y_{st}^*|$ and $U = U_{ext}$ define the physical extinction criterion.

C. RELATIONSHIP BETWEEN AFS AND RATE OF CHEMICAL REACTION

Now the mass flux of reactants into the flame zone at any time will be the flux passing the planes at $y_{st} \pm \delta/2$ which define the effective

APPENDIX D

boundaries of the chemical reaction zone. For the case of fuel flux into the flame depicted in Figure 1, this will be given by Equation (11) evaluated at $Y(y) = Y(y_{st} + \delta/2)$. However, at extinction $y_{st} = -\delta/2$, hence $Y = 0$, and Equation (11) simply becomes

$$\left. \dot{m}'_{fu} \right|_{\substack{y=0 \\ U=U_{ext}}} = \frac{\gamma \rho}{\rho_{\infty}} \left(\frac{dm'_{fu}}{dY} \right)_{\substack{Y=0 \\ U=U_{ext}}} \quad (16)$$

The gradient of fuel mass ratio at $Y = 0$ is readily evaluated from Equations (2) and (6), since it is reasonable to expect that there is little oxidant (i.e., $m_{ox} = 0$) at the flame boundary facing the fuel jet (likewise $m_{fu} = 0$ at the flame boundary facing the oxidant jet). For these conditions, the mass flux of fuel into the flame is a maximum, and Equation (16) can be written as

$$\left| \dot{m}'_{fu} \right|_{max} = (M_{fu, \infty} + M_{ox, -\infty} / \alpha) \left[\frac{\gamma_{\infty} \rho_{\infty} U_{ext}}{2\pi r_0} \right]^{\frac{1}{2}} \quad (17)$$

where the absolute quantity of \dot{m}'_{fu} signifies that the flux is into the flame zone. It should be noted that the AFS (i.e., $\rho_{\infty} U_{ext}$) depends on the flame stoichiometry through Equation (9) which states that $Y_{st} U^{\frac{1}{2}}$ is a constant that is established by the value of f_{st} . At the point of extinction this fact can be represented by the following expressions:

$$\frac{\rho_{\infty} U_{ext}}{2\gamma_{\infty} r_0} (Y_{st}^*)^2 = C^2 \quad (18)$$

or

$$C = \left[\frac{\rho_{\infty} U_{ext}}{2\gamma_{\infty} r_0} \right]^{\frac{1}{2}} \int_0^{\delta/2} (\rho/\rho_{\infty})^{1/2} d\xi \quad (19)$$

Here, C is a positive constant which depends only on the flame stoichiometry and not on jet velocity or flame position alone.

Report 0372-01F

APPENDIX D

Now in terms of a kinetic treatment of the rate of flame reactions, it is considered that the overall reaction consists of



with a mass rate of reaction of fuel/unit volume of flame zone given by

$$R_r = k_r W_{fu} n_{fu}^a n_{ox}^b \quad (20)$$

where R_r = volumetric mass rate of reaction of fuel. R_r is a function of temperature and time through the temperature dependence of k_r and the time dependence of n_{fu} and n_{ox}

k_r = specific reaction rate constant

W_{fu} = molecular weight of fuel

n_{fu} = mole concentration of fuel

n_{ox} = mole concentration of oxidant

$a+b$ = overall order of the reaction

Effecting a mass balance in the opposed-jet geometry between the rate of reaction of fuel in the flame zone and the rate of flow of fuel into the flame zone, it is found that

$$\pi r_o^2 \dot{M}'_{fu} = \pi r_o^2 \delta \bar{R}_r \quad (21)$$

\bar{R}_r = averaged "effective" volumetric mass reaction rate in the flame zone.

Thus, combining Equations (17) and (21), it is seen that the maximum effective volumetric reaction rate at extinction is

$$\bar{R}_{r,max} = \frac{(M_{fu,\infty} + M_{ox,-\infty}/\alpha)}{\delta} \frac{\gamma_{\infty} \rho_{\infty} v_{ext}}{2\pi r_o} \quad (22)$$

From Equation (19), δ is related to the AFS through the constant C , hence the above expression serves to relate the maximum effective volumetric reaction rate to the AFS. However, in order to evaluate $\bar{R}_{r,max}$ from AFS data, it is necessary to determine δ explicitly as a function of AFS, by evaluating

APPENDIX D

the integral of Equation (19). In essence, this requires evaluating the relationship between the real axial coordinate y , and the transformed axial coordinate Y through the flame zone (see Equations 14 and 15). While the exact evaluation of this relationship would require a priori knowledge of the temperature profile through the flame zone, it is possible to show that

$|Y_{st}^*| = \beta \delta$ where β is a constant and should be a relatively good approximation to the integral.

Expressing the local gas density in terms of the perfect gas law and assuming uniform pressure throughout, Equation (15) can be written as

$$|Y_{st}^*| = \int_0^{\delta/2} \frac{R_{\infty} T_{\infty} d\xi}{R T} \approx \frac{R_{\infty}}{R_{st}} \int_0^{\delta/2} \frac{T_{\infty}}{T} d\xi \quad (23)$$

where R/R_{st} is the ratio of the gas constant applicable to the fuel jet to that applicable to the local mixture. This ratio should be far less sensitive to variation than T_{∞}/T . Hence for many flame reactions of interest, it is reasonable to consider $R_{\infty}/R \approx R/R_{st}$, where R_{st} is the gas constant applicable to the flame reaction products.

Now from the Rosenthal treatment of moving heat sources,⁽⁷⁾ it can be expected that the real temperature profile can be approximated by an expression of the form

$$\left(\frac{T}{T_{\infty}} - 1 \right) = \left(\frac{T_{st} - 1}{T_{\infty}} \right) \exp -b(\delta/2 - \xi) \quad (24a)$$

where

$$\left(\frac{T_{st} - 1}{T_{\infty}} \right) \exp(-b\delta/2) \ll 1 \quad (24b)$$

Here, T_{st} and T_{∞} are the temperatures at the flame center and initial fuel jet respectively; b is an adjustable constant with a minimum value such that $T \approx T_{\infty}$ at $\xi = 0$.

Substituting $T(\xi)$ from Equation (24a) into Equation (23), evaluating

APPENDIX D

the integral, and then applying the condition of Equation (24b) yields

$$\left| Y_{st}^* \right| = \frac{R_{\infty}}{R_{st}} \left[\frac{\delta}{2} - \frac{1}{b} \ln \left(\frac{T_{st}}{T_{\infty}} \right) \right] \quad (25)$$

For most flames of interest $\ln (T_{st}/T_{\infty})$ will be relatively constant with a value of ~ 2 ; and b will have some value greater than $10/\delta$ in order to satisfy Equation (24b). Therefore, it is easily seen that the relationship

$$\left| Y_{st}^* \right| = \frac{R_{\infty}}{R_{st}} \beta \delta \quad (26)$$

should be reasonably valid since at most β would be expected to vary between 0.23 and 0.5. In view of the uncertainties in other constants (e.g., averaged transport coefficient), it should be adequate to consider β as having a constant value of $2/5$. Using this value of β , Equations (26) and (19) yield

$$\delta = \frac{5}{2} \frac{R_{st}}{R_{\infty}} C \left[\frac{P_{\infty} U_{ext}}{2\gamma_{\infty} r_0} \right]^{-\frac{1}{2}} \quad (27)$$

which when combined with Equation (22) yields as a final expression for relating effective maximum volumetric reaction rate to AFS:

$$\bar{R}_{r,max} = \frac{R_{\infty} (m_{fu,\infty} + m_{ox,\infty} \sqrt{\alpha})}{R_{st} 5\pi^{\frac{1}{2}} C} \left[\frac{P_{\infty} U_{ext}}{r_0} \right] \quad (28)$$

Since C is determined solely by the flame stoichiometry through Equations (8) and (9), Equation (28) allows $\bar{R}_{r,max}$ to be calculated from AFS and f_{st} data alone. Also, in keeping with the Spalding Theory, Equation (28) implies that the $\bar{R}_{r,max}$ - AFS relationship does not depend upon transport properties in the flame.

It is perhaps worthwhile to point out that the above expression has been derived for a flame which is initially positioned on the oxidant side of the aerodynamic center of the jets (i.e., $y_{st} < 0$), hence the

APPENDIX D

gas constant R_{∞} refers to the fuel jet. Due to the symmetry properties of the flame, Equation (28) will also be valid when the initial flame is positioned on the fuel side of the aerodynamic center (i.e., $y_{st} < 0$); however in this case R_{∞} will be the gas constant applicable to the oxidant jet. This arises from the method by which Equation (15) was evaluated.

IV. COMPARISON WITH SPALDING'S APPROXIMATE THEORY FOR FINITE CHEMICAL REACTIONS

A. THE RELATIONSHIP BETWEEN REACTION RATE AND AFS

Spalding's exact theoretical treatment of finite chemical reaction rate in the flame zone⁽⁴⁾ involves numerical solutions of the differential equation in the m_{fu} - f plane for conservation of the fuel species. It is this exact treatment which requires a priori chemical kinetic knowledge (or assumptions) concerning the flame reactions. However, for high activation energy reactions, Spalding⁽⁴⁾ showed that it is possible to employ the Zeldovich⁽⁸⁾-Spalding⁽⁹⁾ approximation to evaluate the conservation equation in closed form; thereby obtaining an analytic relationship between AFS and chemical reaction rate. This relationship can be written as

$$R_{r,\max} = \frac{\rho}{\rho_{\infty}} \left[\frac{\rho_{\infty} U_{\text{ext}}}{2 r_0} \right] \frac{m_{fu} \Omega_{st}^2}{2 \bar{\Psi}_{st} f_{st}} \quad (29)$$

Here, $R_{r,\max}$ is the local maximum rate of reaction of the fuel in the flame zone just prior to extinction and $\bar{\Psi}_{st}$ is the effective average value of the ratio of local reaction rate to the maximum reaction rate; (i.e., $\bar{\Psi} \equiv R_r/R_{r,\max}$). In the high activation energy approximation, Spalding found $\bar{\Psi}$ to vary between 1/3 and 1/6; hence, he assumed $\bar{\Psi}_{st}$ to have a constant value of 1/4. The ratio ρ/ρ_{∞} was assumed to be given by the initial gas jet density and the density of the reaction products at complete reaction.

A quantitative comparison between Spalding's AFS-reaction rate

APPENDIX D

expression and that given by Equation (28) is not readily discerned since the former, expression relates AFS to the local maximum reaction rate while the latter expression relates AFS to the average effective maximum reaction rate (i.e., $\bar{R}_{r,max}$).

However, since $R_{r,max}$ can be defined for the flame zone depicted in Figure 1 by

$$\bar{R}_{r,max} = \frac{-1}{\delta} \int_{y=0}^{y=-\delta} R_r^* dy \quad (30)$$

where R_r is the local reaction rate and the asterik refers to conditions within the flame zone just prior to extinction, it is readily seen that for thin reaction zones (i.e., high activation energies), $\bar{R}_{r,max}$ should be approximately equal to $R_{r,max}$.

Figure 3 shows a comparison of reaction rates calculated from experimental AFS data several using both equations (28) and (29). It is evident that both expressions yield similar results.

In any case, both expressions predict that the AFS should be directly proportional to the chemical reaction rate, and to the jet diameter. Since the reaction rate is proportional to the pressure raised to a power equal to the overall reaction order (see Equation 20), the AFS will likewise be proportional to the same power of pressure. These predictions are consistent with the experimental data. (3,5)

B. THE RELATIONSHIP BETWEEN AFS AND LAMINAR FLAME SPEED

Spalding⁽⁴⁾ extended his approximate theoretical treatment (i.e., the high activation energy approximation) to derive a relationship between the AFS of opposed-jet diffusion flames and the laminar flame speed

APPENDIX D

of premixed gaseous diffusion flames corresponding to the same stoichiometry (i.e., f_{st}). The laminar flame speed for such a stoichiometric gas mixture is given by the expression

$$\left[m_{fu,\infty} f_{st} G \right]^2 = 2 \int_0^{m_{fu,\infty} f_{st}} \gamma_{R_r} dm_{fu} \quad (31)$$

where G is the mass flux normal to the laminar premixed flame which is propagating steadily through a homogeneous stoichiometric mixture of fuel and oxidant. G relates directly to the flame speed through the expression

$$G = \rho_m S_u \quad (32)$$

where ρ_m is the initial density of the reactant gas mixture and S_u the laminar flame speed.

Evaluation of the integral of Equation 31 in terms of the parameter $\bar{\Psi}_{st}$ led Spalung to predict a quadratic dependence of AFS on laminar flame speed; viz.,

$$\rho_\infty U_{ext} \approx \left[\frac{2r_0}{\gamma_\infty (M_{fu,\infty} \Omega_{st})^2} \right] (m_{fu,\infty} f_{st} G)^2 \quad (33)$$

Now in the present theoretical treatment, the AFS can be related to G through Equation (30), which defines $\bar{R}_{r,max}$. Due to the flame zone symmetry, this definition can also be written as

$$\bar{R}_{r,max} = \frac{2}{\delta} \int_0^{m_{fu,\infty} f_{st}} \frac{\gamma_{R_r}^* dm_{fu}}{\gamma_\infty (dm_{fu}/dY)^*} \quad (34)$$

APPENDIX D

Here, the lower limit of the integral corresponds to $m_{fu}(y = -\delta)$, and the upper limit to $m_{fu}(y = -\delta/2)$, thus, the integration occurs over that portion of the flame zone which faces the oxidant jet.

When the flame zone in the region of interest is relatively thin, a linear relationship between m_{fu} and Y should be a reasonable approximation. Therefore, $(dm_{fu}/dY)^*$ can be replaced by a constant given by

$$(dm_{fu}/dY)^* \approx \frac{m_{fu,\infty} f_{st}}{|Y_{st}^*|} \quad (35)$$

Under this condition, Equation (34), when combined with Equation (31), becomes

$$\delta \bar{R}_{r,\max} \left[\frac{\gamma_{\infty} m_{fu,\infty} f_{st}}{|Y_{st}^*|} \right] = (m_{fu,\infty} f_{st} G)^2 \quad (36)$$

making use of the previously derived expressions for $\delta \bar{R}_{r,\max}$ and $|Y_{st}^*|$, finally yields

$$\rho_{\infty} U_{\text{ext}} \approx \left[\frac{2\sqrt{\pi} r_0 C (1-f_{st})}{\gamma_{\infty} m_{fu,\infty}^2 f_{st}} \right] (M_{fu,\infty} f_{st} G)^2 \quad (37)$$

Thus, the use of the physical extinction criterion also leads to a quadratic dependence of AFS on laminar flame speed.

However, it should be pointed out that the proportionality factor (i.e., the term in the square bracket) is a function of f_{st} ; hence, Equation (37) could be considerably different from Equation (33).

To demonstrate this point, the ratio formed by dividing the right hand side of Equation (37) by the right hand side of Equation (33) is plotted vs f_{st} in Figure 4. It is readily seen that near certain values of

APPENDIX D

f_{st} , the Spalding proportionality factor could be orders of magnitude greater than that given by the present treatment. The zero value of the ratio at $f_{st} = 0$ and 1.0 simply reflects the fact that the proportionality factor of Equation (37) approaches zero faster than that of Equation (33). However, the zero value of the ratio at $f_{st} = 0.5$ reflects the singularity introduced by employing the physical criterion for extinction. For $f_{st} = 0.5$ is initially centered at the aerodynamic center (i.e., $Y_{st}^* = 0$), hence, the flame is unstable at all values of jet velocity.* On the other hand, the Spalding proportionality factor remains finite at $f_{st} = 0.5$. This probably arises from the fact that the Spalding theoretical treatment does not take into account the existence of two stagnation planes when the flame zone is centered on the aerodynamic center.

In Figure 5, Equations (33) and (37) are tested against the experimental data on AFS and G which Potter and Butler⁽¹⁾ first reported. If Equation (33) were obeyed, the quantity tabulated in the next to the last column should have the same numerical value for each flame system.** Likewise, for Equation (37) and the quantity tabulated in the last column of Figure 5. From the results, it would appear that the data conform to Equation (33) somewhat better than to Equation 37. However, it is evident that both theoretical AFS vs G expressions are only approximately obeyed. This could be due, as Spalding suggested, to an unknown experimental variation in f_{st} , or an improper flow pattern in the impingement zone during the AFS determination.***

* It has been tacitly assumed throughout this treatment that the gas jet flow closely resembles Spalding's idealized flow. This automatically requires a fuel jet flow with a Peclet number (i.e., $\frac{2r_0 \rho U}{\mu}$) greater than 1000.⁽⁴⁾ The Peclet number for the jet in Pandya and Weinberg's studies was about a factor of 5 less than this minimum value. Therefore, the fact that they were able to stabilize diffusion flames at the aerodynamic center of their opposed jet flow system does not necessarily contradict the physical criterion for extinction as applied here.

** It is assumed here that the value of γ_{∞} is the same for each flame system.

*** It is interesting to note that in a subsequent study of the propane-oxygen flame with higher velocity jet-streams,⁽³⁾ the AFS was found to be 10 gm/cm²-sec as compared to the 5.1 gm/cm²-sec value shown in Figure 5.

APPENDIX D

Alternatively, the apparent trend to constant values of the tabulated quantities (Figure 5) for the flame systems with higher AFS values (and hence higher reaction rates), suggests that the thin flame zone approximation may not be valid for flames with AFS values less than $\sim 0.2 \text{ gm/cm}^2\text{-sec}$.

In any case, the available experimental data are insufficient to adequately test the validity or comparative merits of the two theoretical AFS vs G expressions. From Figure 4, it is seen that a definitive evaluation of the comparative merits of Equations (33) and (37) should be obtained with experimental AFS and laminar flame speed data at stoichiometric mass fractions near $f_{st} = 0.5$.

V. SUMMARY

The extinction of opposed-jet diffusion flames has been defined in terms of a physical criterion for the extinction process. In essence, it is considered that the stagnation plane at the aerodynamic center of equal strength opposed gas jets is a barrier across which no stable flame can cross.

Although this physical criterion, at present, lacks a theoretical foundation, it does fall within the framework of both the Spalding theory of mixing in opposed gas jets, and the experimental findings by Pandya and Weinberg of the existence of two stagnation planes when counter-flow flat diffusion flames are stabilized centrally between the two opposed gas streams.

The physical criterion, when utilized in conjunction with the Spalding theory of mixing, yields analytic expressions, for relating apparent flame strength with chemical reaction rate and laminar flame speed in equivalent premixed diffusion flames. These relationships differ somewhat from those given in Spalding's approximate theoretical treatment of the extinction phenomena, but do yield quantitatively similar results when both are compared with the available experimental data on hydrocarbon and ammonia oxidation flames.

APPENDIX D

However, it is believed that the available data are insufficient to adequately test the validity or relative merits of either the Spalding approximate treatment or the current treatment of the extinction process. A definitive test will require experimental apparent flame strength data taken under flow conditions which satisfy the requirements of Spalding's mixing theory; i.e., (1) high Reynold's number jet flow, and (2) equal strength oxidant and fuel jets. Also, the apparent flame strength and laminar flame speed for equivalent flame systems should be determined where the stoichiometric mass ratio has values near 0.5.

It is evident from the current and previous analyses of the extinction of opposed-jet diffusion flames, that the technique is an important and useful method for determining chemical reaction rates in flames; particularly for those flame systems where the oxidant and fuel are too reactive to allow a study of laminar flame speed in a premixed gaseous medium.

ACKNOWLEDGEMENT

The many stimulating and helpful discussions with Mr. F. J. Cheselske of the Advanced Propellants Department, Aerojet-General Corporation, Sacramento, California is gratefully acknowledged.

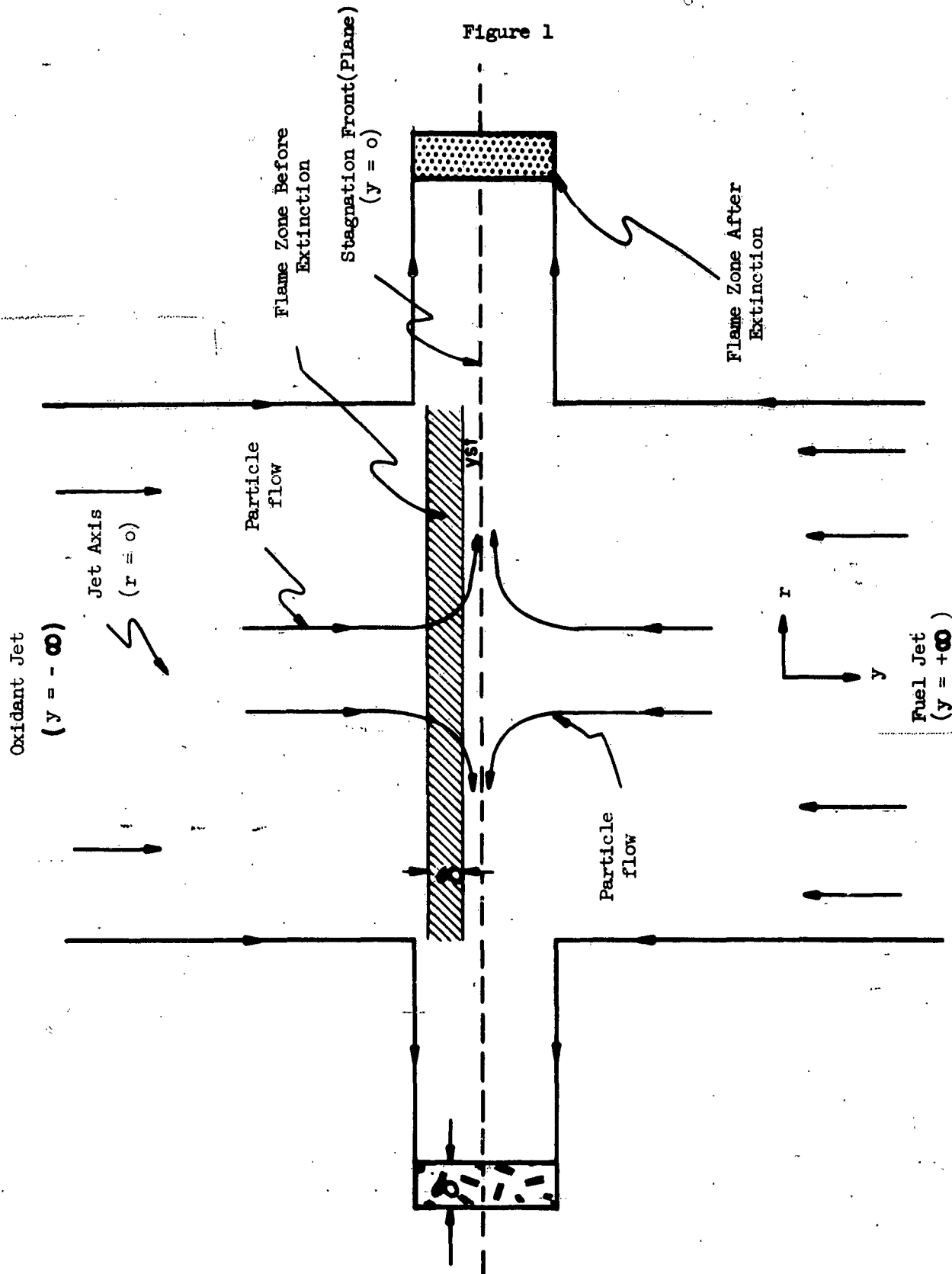
Report 0372-01F

APPENDIX D

REFERENCES

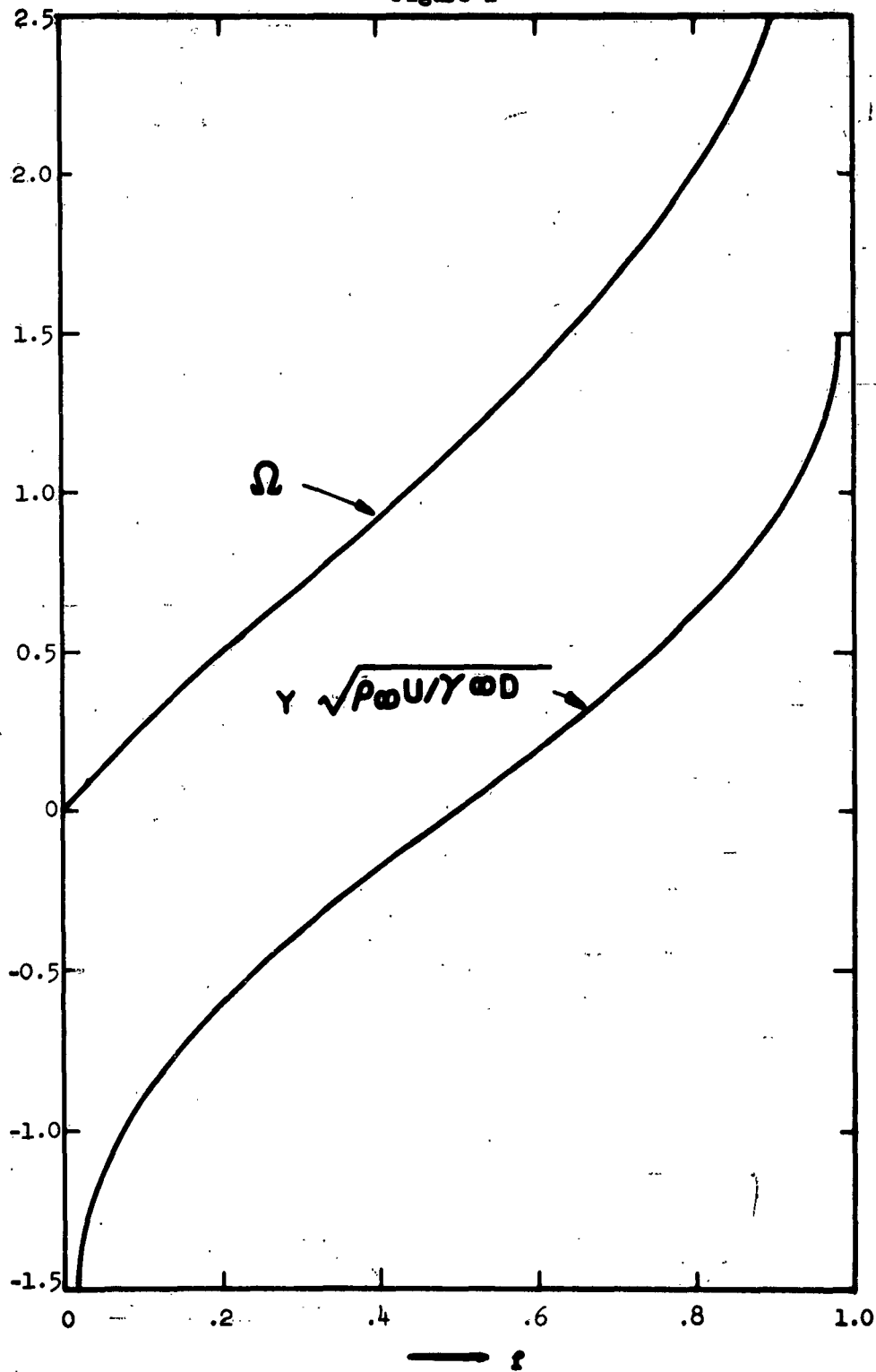
1. Potter, A. E., Jr., and Butler, J. N., "A Novel Combustion Measurement Based on the Extinguishment of Diffusion Flames", ARS Journal, Vol. 29, 1959, pp. 54-56.
2. Potter, A. E., Jr., Heibel, S. and Butler, J. N., "Apparent Flame Strength: A Measure of Maximum Reaction Rate in Diffusion Flames", Eighth Symposium (International) on Combustion, Williams & Wilkins Co., Baltimore, 1962, pp. 1027-1034.
3. Anagnostou, E. and Potter, A. E., "Flame Strength of Propane-Oxygen Flames at Low Pressures in Turbulent Flow", Ninth Symposium (International) on Combustion, Academic Press, New York, 1963, pp. 1-6.
4. Spalding, D. B., "Theory of Mixing and Chemical Reaction in the Opposed-Jet Diffusion Flame", ARS Journal, Vol. 31, 1961, pp. 763-771.
5. Cheselske, F. J., Chaiken, R. F., and Sibbett, D. J., "Oxidation of Ammonia in Opposed-Jet Diffusion Flames", in preparation for publication (1965).
6. Pandya, T. P. and Weinberg, F. J., "The Structure of Flat, Counter-Flow Diffusion Flames", Proc. Roy. Soc., ud. 279A, 1964, pp. 544-561.
7. Rosenthal, D., "The Theory of Moving Sources of Heat and Its Application to Metal Treatments", Trans. Amer. Soc. Mech. Eng., Vol. 68, 1946, pp. 849-866.
8. Zeldovich, Y. B. "On the Theory of Combustion of Initially Unmixed Gases", J. Tech. Phys., Moscow, Vol. 19, No. 1199, 1949; NACA Tech. Transl. 1296, 1951.
9. Spalding, D. B., "A Theory of the Extinction of Diffusion Flames", Fuel, Vol. 33, No. 3, 1954, pp. 255-273.

SCHMATIC REPRESENTATION OF OPPOSED-JET DIFFUSION FLAME



Ω and $\gamma \sqrt{\rho \omega U / \gamma \omega D}$ Plotted Versus r

Figure 2



APPENDIX D

Figure 3

COMPARISON OF CALCULATED MAXIMUM VOLUMETRIC
REACTION RATES IN OPPOSED-JET DIFFUSION FLAMES

Flame	f_{st} (d)	AFS (1 atm) g/cm^2-sec	Maximum Volumetric Reaction Rate, g/cm^3-sec		Volumetric Rate of Heat Release $Kcal/cm^3-sec$
			$\bar{R}_{r,max}$ (Spalding)	$\bar{R}_{r,max}$ (Chaiken)	
C_3H_8 -Air (a)	0.057(-)	0.13	0.036	0.096	1.63
C_3H_8 - O_2 (b)	0.216(-)	10.0	8.1	15.6	265.0
NH_3 - Cl_2 (c)	0.36(-)	1.30	3.67	1.24	3.35
NH_3 - O_2 (c)	0.47(-)	2.20	7.35	16.0	55.0
NH_3 -NO (c)	0.46(-)	0.65	2.93	2.5	6.15
NH_3 - N_2O	0.67(+)	2.35	11.5	12.0	23.4

(a) Reference 1

(b) Reference 3

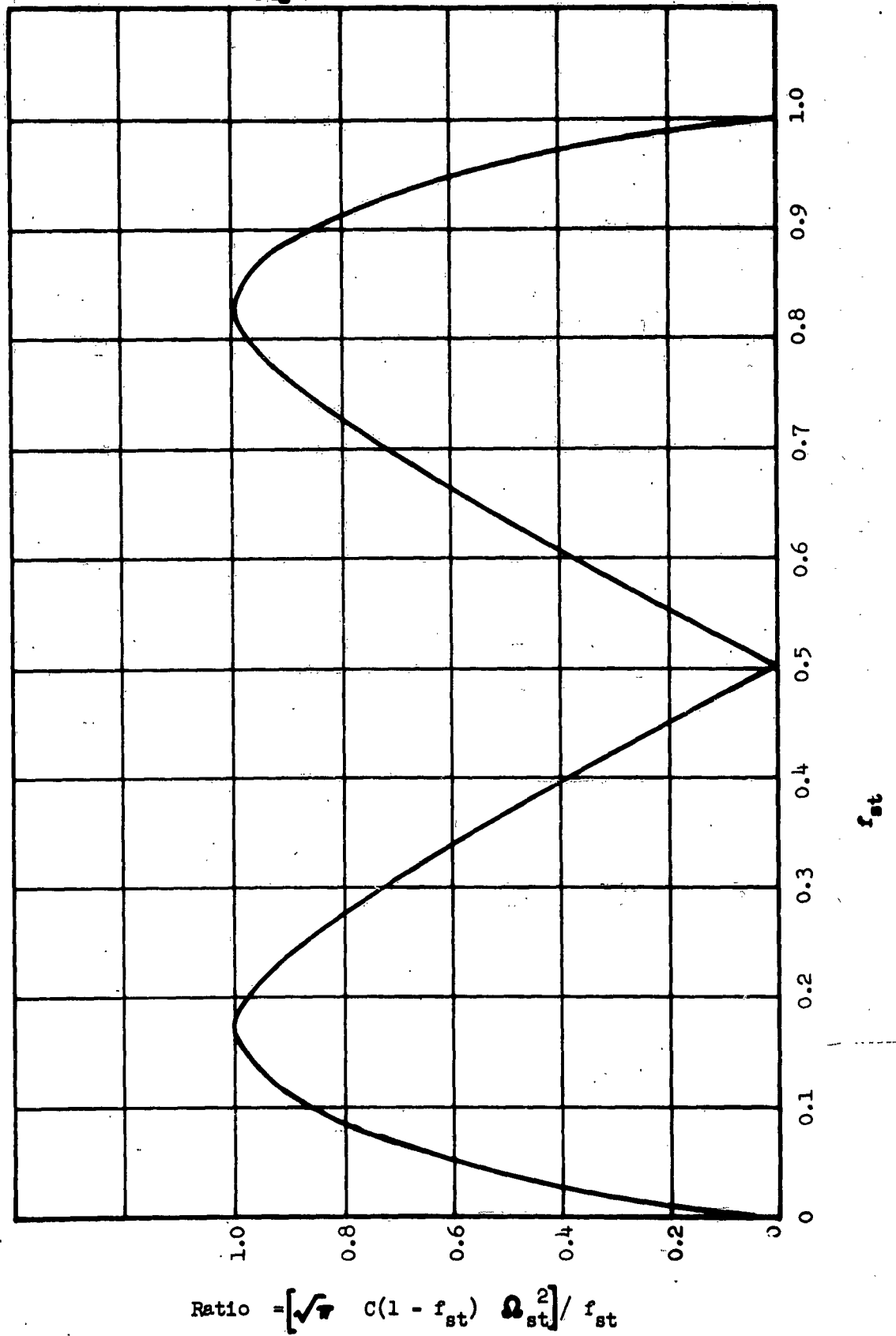
(c) Reference 5

(d) The (+) or (-) notation refers to the position of the initial stable flame; (+) referring to the fuel, jet side of the aerodynamic center and (-) to the oxidant jet side.

(e) Calculated by multiplying $\bar{R}_{r,max}$ by the heat of combustion of the fuel.

RATIO OF PROPORTIONALITY CONSTANTS PLOTTED
VERSUS f_{st}

Figure 4



Report 0372-01F

APPENDIX D

Figure 5

COMPARISON OF AFS VS G RELATIONSHIPS WITH EXPERIMENTAL DATA

Flame System	AFS (a) (1 atm) gm/cm ² -sec	$m_{fu, \infty} f_{st} G^{(a)}$ 10 ⁻³ gm/cm ² -sec	f_{st} (b)	Spalding	Chaiken
				$\left(\frac{AFS}{G^2}\right) \left(\frac{\Omega_{st}^2}{f_{st}}\right)$	$\left(\frac{AFS}{G^2}\right) \left[\frac{1}{C f_{st} (1-f_{st})}\right]$
Propane-O ₂	5.1	100	0.22	140	250
Propane 50 vol% O ₂ 50 vol% N ₂	1.6	30	0.13	200	340
Acetylene-Air	0.6	11	0.067	160	330
Ethylene-Air	0.23	4.7	0.060	210	460
Cyclopropane-Air	0.18	3.9	0.060	320	710
Propane-Air	0.13	2.8	0.057	420	930

(a) Data from Reference 1.

(b) Calculated on the basis of complete reaction to CO₂ and H₂O.

**Report 0372-01F
Appendix E**

**(To be Published in the Journal of the American
Institute of Aeronautics and Astronautics)**

**A MODEL FOR LOW PRESSURE
EXTINCTION OF SOLID ROCKET MOTORS***

**R. F. Chaiken
Technical Consultant
Aerojet-General Corporation
Azusa, California**

*** This work was supported in part by Aerojet-General Corporation,
Solid Rocket Research and Development Division, and in part by the
Advanced Research Projects Agency under Contract AF 49(638)-851
monitored by the Air Force Office of Scientific Research.**

NOMENCLATURE

Rocket Chamber Parameters

A_b - propellant burning area

A_t - nozzle throat area

C_D - nozzle discharge coefficient

P_c - chamber pressure

P_{cr} - critical chamber pressure for onset of "low frequency" instability

P_e - extinction chamber pressure

V_c - chamber volume

$L^* = V_c/A_t$

Propellant Parameters

r - propellant burning rate

n - steady-state burning rate pressure exponent, $r = cP^n$

ρ_p - propellant density

P_{DL} - low pressure stable deflagration limit

M_c - average molecular weight of gaseous combustion products

T_f - adiabatic flame temperature of propellant

T_g - a temperature parameter which is approximated by the adiabatic flame temperature of the ammonium perchlorate monopropellant flame.

k_g = rate constant for the ammonium perchlorate monopropellant flame reactions, $k_g = A_g \exp(-E_g/RT_g)$

Miscellaneous Parameters

g - gravitation constant

R - gas constant

t - time

τ - critical time constant

INTRODUCTION

Anderson, Strehlow and Strand¹ have shown that vacuum firings of solid propellant rocket motors using regressive burning grains exhibit a low pressure burning limit which is generally higher than the low pressure stable deflagration limit of the propellant as determined in a Crawford bomb strand burner. Their studies with ammonium perchlorate composite propellant with varying aluminum content suggest that the extinction pressure (P_e), while independent of burning geometry, is strongly dependent upon Al content and motor L^* (ratio of chamber volume to nozzle throat area). Their data could be curve-fitted by an expression of the form

$$L^* = A(P_e)^{-\alpha} \quad (1)$$

where the constants A and α varied with Al content.

For non-aluminized propellant, the value of the exponent α was approximately twice the value of the steady-state burning pressure exponent (n) at the pressure P_e . In this case, equation (1) becomes almost identical to theoretical expressions derived by Akibo and Tanno,² Sehgal and Strand,³ and Cohen⁴ for describing the critical pressure (P_{cr}) for onset of "low frequency" combustion instability, i. e.,

$$L^* = A'(P_{cr})^{-2n} \quad (2)$$

The theoretical derivations considered the instability as arising from a coupling between the lag of burning-rate response due to the propellant thermal gradient, and the lag in exhausting the chamber due to nozzle flow.

The strong resemblance between the theoretical and empirical expressions suggested to these authors^{1, 3, 4} that the critical pressure for onset of unstable burning (i. e., P_{cr}) should correspond to the observed extinction pressure (i. e., P_e). However, there are two serious discrepancies which arise from this approach:

- 1) The value of α for the case of aluminized propellants (8-16%) is much greater than $2n$; and 2) The extinction pressure is zero for an infinite L^* . Since in a Crawford bomb, L^* can be construed as approaching infinity, it might be expected that P_e should have a limiting value approaching the low pressure stable deflagration limit.

Although it has been argued^{1, 3, 4} that aluminum or its solid combustion product might in some way affect the propellant thermal response or the nozzle exhaust time, no adequate quantitative explanation of these discrepancies has been offered.

It is the purpose of this note to offer a possible explanation in terms of a new model for the extinction process. This new approach suggests that equation (2) defines criteria for possible temporary extinguishment rather than permanent extinguishment, and as such, P_{cr} should not be identified with P_e of equation 1. In addition, the model enables the derivation of a theoretical P_e vs L^* relationship which differs considerably from the form of equation 1.

MODEL OF ROCKET EXTINCTION

It is first assumed that solid composite propellants exhibit a low pressure stable deflagration limit (P_{DL}) which is independent of their extinction under conditions of rocket motor venting. Such phenomena have apparently been noted in strand burners (Crawford bomb) where below a minimum inert gas bomb pressure, strand burning cannot persist. Low pressure deflagration limits have been reported as high as 400 psia for some ammonium nitrate propellants⁵ and as low as 6 psia for some ammonium perchlorate (AP) propellants. Even ammonium perchlorate monopropellant strands exhibit a P_{DL} .⁶

A detailed discussion of the causes for a P_{DL} in solid composite propellants is outside the scope of the present paper, however it can be noted that Friedman⁶ and Nachbar⁷ attempted to explain the P_{DL} of AP strands in terms of radiation heat loss from the burning surface. Also, it would appear that aluminum increases the P_{DL} of AP composite propellant.⁴

Second, it is assumed that during "low" pressure burning in a rocket motor, some inherent combustion instability (perhaps related to the low frequency instability discussed by Sehgal and Strand³) causes the instantaneous burning rate, r , to become zero. The question then arises as to what chamber conditions must be present in order that the instantaneous zero burning rate lead to permanent extinction. On the basis of the first assumption it can be considered that if the rocket chamber exhausts to a value of P_{DL} within a critical time period (τ), then the burning rate will remain zero, and the rocket will be extinguished. Now from the rocket chamber mass balance during propellant burning with sonic nozzle exhaust, the time rate of change of chamber pressure can be described by (e. g., see equation (41) of reference 3 where $L^* = V_c/A_t$),

Report 0372-01F
APPENDIX E

$$\frac{\rho_p A_b g r}{A_t C_D} = P_c + \frac{g ML^*}{C_D RT_f} \left(\frac{dP_c}{dt} \right) \quad (3)$$

Setting $r = 0$, thus gives the rate of chamber exhaust at the instant the burning rate becomes zero. Taking this instant as $t = 0$, the extinction criterion can be stated as: $P_c(t = 0) = P_e$ when during the time interval $0 < t \leq \tau$, the chamber pressure is reduced to the value P_{DL} . Utilizing the above expression with $r = 0$ for $P_c(t)$ over the appropriate time interval, the minimum extinction requirement becomes

$$\int_{P_e}^{P_{DL}} \frac{dP_c}{P_c} = - \frac{C_D RT_f}{g ML^*} \int_0^{\tau} dt \quad (4)$$

or

$$P_e = P_{DL} \exp \left[\frac{C_D RT_f \tau}{g ML^*} \right] \quad (5)$$

It is interesting to note that equation (5) is considerably different from the empirical form used by Anderson et. al. (equation 1), and that if τ is finite and independent of L^* , P_e approaches P_{DL} as L^* approaches infinity. Thus, the new model of extinction would appear to resolve one of the discrepancies as noted in the introduction.

It now remains to describe the physical nature of the critical time constant τ . One possibility that arises is that τ relates to the kinetics of the propellant flame reactions. This might be reasonable from the view point that, at the instant ($t = 0$) when r becomes zero there is no mass efflux from the surface while the propellant surface temperature is relatively unaltered from its value when $r = 0$. At $t > 0$, there is a positive mass efflux with the out-flowing gases requiring τ seconds to react and to supply heat back to the propellant surface. However, if during these τ seconds the chamber pressure drops to P_{DL} , then the gas-phase reactions become quenched, and hence the extinction becomes permanent. In a sense, this extinction process can be likened to the process by which rarefaction waves quench detonation reactions in explosives, giving rise to critical diameter phenomena⁸.

For second order flame reactions, the half-life of the reactions is directly proportional to the reciprocal of the first power of the chamber pressure

(e. g., see reference 9); hence, identifying with the half-life of the flame reactions yields

$$\tau = \beta / P_c \quad (6)$$

For the case where the ammonium perchlorate gas-phase redox reaction controls the flame kinetics ("thermal layer" theory of combustion¹⁰) the constant β can be equated to $2 RT_g/k_g$, where k_g refers to the rate constant of the $\text{NH}_3 + \text{HClO}_4$ flame reaction at the temperature T_g , approximately the adiabatic flame temperature for this reaction.

Using the above expression for τ , equation 4 becomes

$$P_e = P_{DL} \exp \left[E/P_e L^* \right] \quad (7)$$

where $E = C_D RT_f \beta / gM$ is a constant for any given propellant composition.

To test the possible validity of equation 7, the data of Anderson, et. al.¹ have been plotted as $\log P_e$ vs. $(L^* P_e)^{-1}$ in figure 1. It is readily seen that the theoretical expression offers a reasonably good fit to the data. Also, it is noted that for JPL 534 and 540 ($\sim 0\%$ Al), extrapolation to infinite L^* gives a value of $P_{DL} = 8$ psia in good agreement with the reported¹ value of $P_{DL} = 6$ psia.

Similar extrapolations for the propellants containing 8% and 16% Al yield higher values of P_{DL} (29 psia and 42 psia respectively) as might be expected. Unfortunately, Anderson, et. al., did not report P_{DL} values for these propellants so that a more precise comparison of results can not be made at this time.

It is interesting to calculate the expected order of magnitude of E when $\beta = 2 RT_g/k_g$. Although the value of k_g to be used in this expression is quite uncertain, it can be estimated from previous work¹⁰ that a reasonable order of magnitude is $k_g \approx 10^9 \text{ cm}^3/\text{mole-sec}$. Using this value and reasonable estimates of the other parameters, E is approximately 10^2 inch-psia. The slopes of the curves of Figure 1 (i. e., experimental E) lie in the range of 1.6×10^3 to 4.0×10^3 inch-psia (increasing with decreasing Al content), which differ from the theoretical calculated E by less than a factor of 100. In view of the gross uncertainty in k_g , this comparison of theoretical and experimental E can be considered favorable but not necessarily significant. However, assuming the

* $C_D = 7 \times 10^{-3} (\text{sec})^{-1}$; $R = 8.31 \times 10^7 \text{ erg/deg-mole} = 82 \text{ cm}^3\text{-atm/deg-mole}$;
 $M = 30 \text{ gm/mole}$; $g = 980 \text{ cm/sec}^2$; $T_f = 3000^\circ\text{K}$; $T_g = 1400^\circ\text{K}$.

Report O372-01P
APPENDIX B

calculations to be reasonably valid, it would suggest that increasing α may cause an increase in the effective temperature at which the bulk of AP redox flame reactions occur (i.e., T_g)*. Alternatively, it may be speculated, that the nozzle discharge coefficient (C_D) decreases as the amount of solids in the exhaust increases. In either case, there is insufficient data at this time to allow for a more precise account of the effect of aluminum on the L^* vs. P_e relationship.

CONCLUSIONS

The model of solid rocket extinction presented here would appear to resolve some of the difficulties which are apparent when attempting to identify criteria for "low frequency" combustion instability with low pressure extinction criteria. The model also enables a treatment of extinction in terms of the kinetics of the propellant flame reactions, yielding a new form of equation for relating motor L^* and extinction pressure, which is in satisfactory agreement with the available data. However, it is clear that the existing data encompasses only a narrow part of the spectrum of experimental results required for an adequate test of this or any other theoretical treatment.

* In the case being considered $E = 2C_D R^2 T_f T_g / g M k_g$ with $k_g = A_g \exp(-E_g / RT_g)$.
The exponential dependence of k_g on temperature in the denominator will outweigh the linear dependence in the numerator.

REFERENCES

1. Anderson, F. A., Strehlow, R. A. and Strand, L. D., "Low pressure rocket extinction," AIAA Journal 1, 2669-2671 (1963).
2. Akiba, R. and Tanno, M., "Low frequency instability in solid propellant rocket motors," Proceedings of the First Symposium (International) on Rockets and Astronautics (Tokyo, 1959) pp. 74-82.
3. Sehgal, R. and Strand, L., "A theory of low-frequency combustion instability in solid rocket motors", AIAA Journal 2, 696-702 (1964).
4. Cohen, N. S., "Solid propellant extinguishment by pressure perturbation," unpublished work at Aerojet-General Corporation, Solid Rocket Research and Development Division (1964).
5. Andersen, W. H., Bills, K. W., Mishuck, E., Moe, G. and Schultz, R. D., "A model describing combustion of solid composite propellants containing ammonium nitrate," Combustion and Flame 3, 301-318 (1959).
6. Friedman, R., Levy, J. B. and Rumble, K. E., "The mechanism of deflagration of pure ammonium perchlorate." Atlantic Research Corp., AFOSR-TN59-173, Contract AF 18(600)-1502 (February 1959).
7. Johnson, W. E., and Nachbar, W., "Deflagration limits in the steady linear burning of a monopropellant with application to ammonium perchlorate," Eighth Symposium (International) on Combustion, (Williams and Wilkins, Co., Baltimore, Md., 1962) pp. 678-689.
8. Eyring, H., Powell, R. E., Duffey, G. H. and Parlin, R. B., "The stability of detonation," Chem. Rev. 45, 69-181 (1948).
9. Chaiken, R. F., "A thermal layer mechanism of combustion of solid composite propellants: application to ammonium nitrate propellants", Combustion and Flame 3, 285-300 (1959).
10. Chaiken, R. F. and Andersen, W. H., "The role of binder in composite propellant combustion," ARS Progress in Astronautics and Rocketry: Solid Propellant Rocket Research, edited by M. Summerfield (Academic Press, New York, 1960), Vol. 1, pp. 227-249.

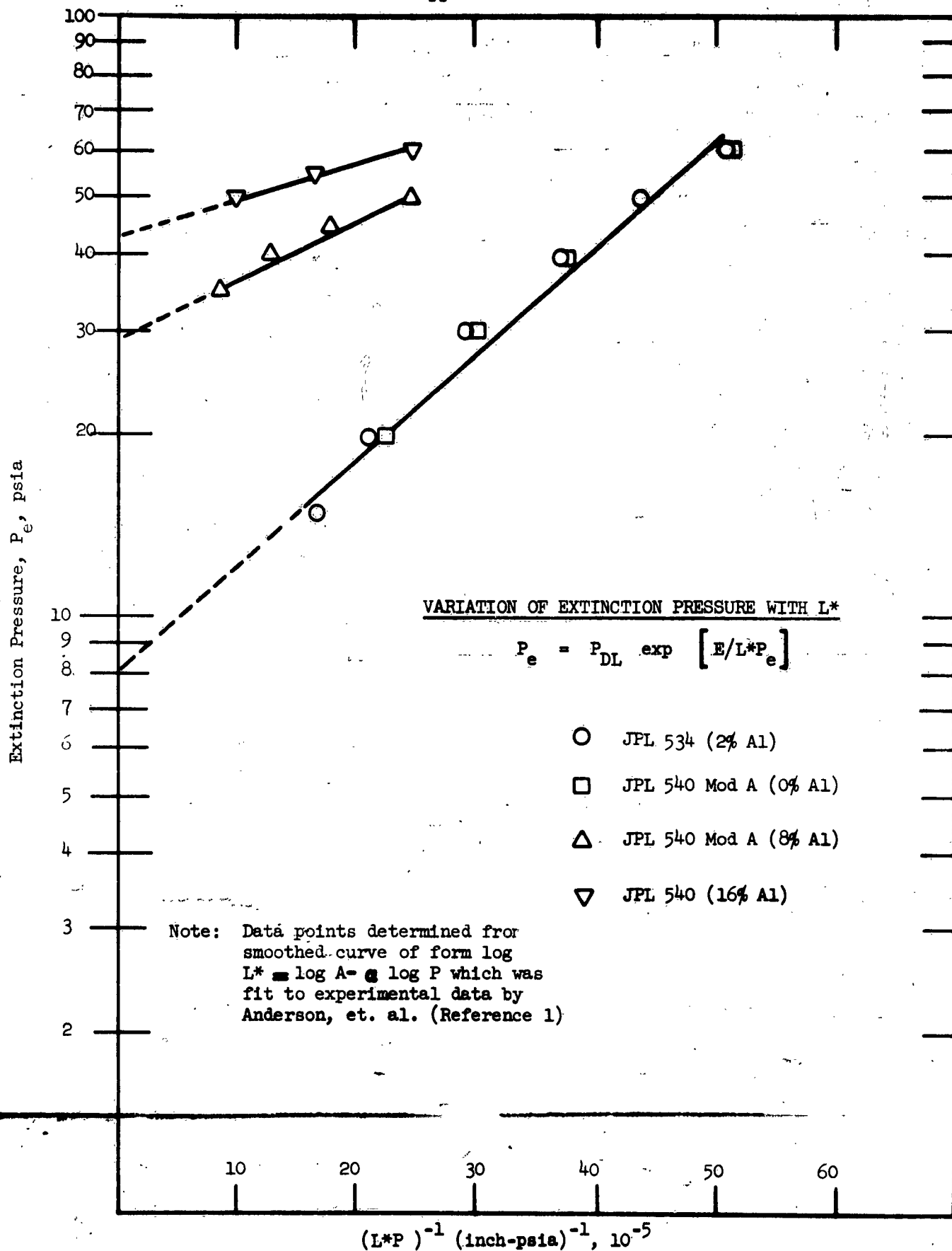


Figure 1

IMPLICATIONS OF A STEADY-STATE SOLID PROPELLANT COMBUSTION
MODEL TO A LOW PRESSURE DEFLAGRATION LIMIT

By

R. F. Chaiken
Technical Consultant
Aerojet-General Corporation
Sacramento, California

I. INTRODUCTION

Many experimental and theoretical studies on solid propellant combustion, have led to a concept of combustion in which the solid ingredients gasify under the thermal influence of a flame to form reactive species which then undergo gas-phase redox reactions to propagate that flame. The mass-flow and energy of each reaction in the burning process is of necessity coupled to each other by the conservation equations. Several mathematical models of varying complexity have been developed to describe the steady-state coupling process⁽¹⁻⁶⁾, but few theoretical studies have been made of extending these models to low pressure deflagration limits.

A notable exception to this is the work of Johnson and Nachbar⁽⁷⁾ in describing the pressure deflagration limit (P_{DL}) of burning strands of ammonium perchlorate (AP) monopropellant. These authors attempted to ascribe the low P_{DL} of AP strand burning to radiation heat losses from the burning surface. Unfortunately, the detailed rigorous treatment given, which requires numerical methods of solution, cannot be readily extrapolated to the problem of low pressure extinguishment of composite propellant combustion.

A somewhat simpler approach to the P_{DL} problem can also be obtained from the two-temperature postulate and thermal-layer treatment

APPENDIX F

of steady-state combustion⁽²⁻⁴⁾. This somewhat heuristic treatment of composite propellant burning yields a generalized burning rate expression in terms of parameters which can be readily related to the chemical kinetic processes occurring during combustion. It is the purpose of this note to show that this treatment also leads directly to a minimum burning rate with implications towards a low pressure deflagration limit.

II. THE TWO-TEMPERATURE AND THERMAL LAYER THEORIES OF SOLID PROPELLANT COMBUSTION

Basically, the "two-temperature" postulate of composite solid propellant combustion, as stated by Schultz and Dekker^(2,8), proposed that the decompositions of oxidizer and binder are nearly independent processes when viewed on a microscopic scale. This concept arose from a consideration of the temperature necessary to achieve equal rates of linear regression for the oxidizer and binder components separately. During steady state burning, the mean rate of linear regression of oxidizer, B_o , is equal to the mean linear rate of consumption of the binder surface B_b , and both are equal to the mean linear rate of burning of the propellant B_p , or,

$$B_p = A_{s,o} \exp(-E_{s,o}/RT_{s,o}) = A_{s,b} \exp(-E_{s,b}/RT_{s,b}) \quad (1)$$

where the linear rates of regression are expressed in terms of Arrhenius rate equations. Since the pre-exponential factors, A and the activation energies, E are generally unlike for the oxidizer and binder respectively, it follows that the surface temperatures at which these components decompose must be different.

In attempting to formulate a mathematical model of the burning process, a steady state has been assumed. The two-temperature concept was applied to make possible the assignment of definitive temperature and heat transfer

APPENDIX F

boundary conditions. As applied to ammonium nitrate composite propellants, the mechanism took the form of four idealized steps.⁽²⁾

- (1) Gasification of the oxidizer by a kinetic rate controlling step which involves surface desorption (endothermic reaction).
- (2) Oxidation-reduction gas phase reactions of the oxidizer pyrolysis products to establish a flame. (exothermic reaction)
- (3) Pyrolysis of binder in the established flame (endothermic reaction).
- (4) Gas phase reactions of oxidizer and binder pyrolysis products (exothermic reaction).

For AN propellants, exothermic reactions between the initial pyrolysis products of NH_4NO_3 (HNO_3 and NH_3) are assumed to occur in the gas phase, establishing a flame zone with a maximum temperature of about 1250°K. Heat from this flame causes gasification of the binder. Eventually, binder and oxidizer decomposition products react in a diffusion flame at some distance from the surface. There is evidence that little heat from the outer diffusion flame gets back to the decomposing surface. For example, substitution of polystyrene binders of drastically different decomposition rates had little or no effect on the burning rates of the propellant. Since large variations in binder decomposition properties should greatly effect the outer diffusion flame, it has been assumed that the surface is heated mainly from the redox flame close to its surface. The inner flame layer which is believed to heat the surface of the propellant, causing decomposition, has been named the "thermal layer".

From considerations of the boundary value problem of steady-state heat transfer by thermal conduction across the thermal layer⁽³⁾, it was

APPENDIX F

shown that the thermal layer thickness, δ , can be approximated as

$$\delta = r_0 / [1 + r_0 \sqrt{\alpha k T}]^{-1} \quad (2)$$

where r_0 is the average particle radius, K is the average thermal diffusivity of the gaseous medium, T is the half life of the gas phase redox reaction, and α is a proportionality constant of the order of unity. Essentially δ is determined by the velocity with which the gas expands away from the surface, which in turn is proportional to the rate at which the gas phase reactions take place.

The thermal layer thickness is a function of pressure, since

$$K = M \sigma / c_p \rho_g \quad (3)$$

where M is the average molecular weight of the gases, σ is the average thermal conductivity of the gas phase, ρ_g is the total density of the gases and c_p is the average molar heat capacity.

If the redox gas reaction is second order

$$T \approx 1/c_g k_g = 2M / \rho_g k_g \quad (4)$$

where c_g is the concentration of one of the gaseous reactants and k_g is the rate constant for the redox reaction. These expressions yield

$$\delta = \frac{r_0}{1 + \frac{r_0 P}{R T_g} \left[\frac{c_p k_g}{2 \alpha \sigma} \right]^{1/2}} = \frac{r_0}{1 + r_0 \phi P} \quad (5)$$

where R is the gas constant, P the pressure and T_g the temperature at which the gases react. ϕ and T_g may be considered as constant for a given gas-phase redox reaction.

APPENDIX F

If the rate of heat conducted into the oxidizer particle surface is set equal to the rate of heat transfer required for steady state linear pyrolysis of the oxidizer:

$$4\pi n r_o^2 \frac{\sigma(T_f - T_{s,o})}{\delta} = 4\pi n r_o^2 \rho_s B_o [\Delta H + C_s(T_{s,o} - T_o)] \quad (6)$$

where a positive value of ΔH is the endothermicity of the oxidizer surface pyrolysis reaction, C_s is the solid heat capacity, ρ_s is the solid density, n is the fraction of the oxidizer particle exposed to the flame, B_o is the linear pyrolysis rate of the oxidizer, and T_o is the initial propellant temperature.

Then, the burning rate of the propellant can be expressed by

$$B_p = \frac{(\sigma / \rho_s C_s)(T_f - T_{s,o})}{r_o (\Delta H / C_s - T_o + T_{s,o})} (1 + r_o \phi P) \quad (7)$$

and

$$B_p = A_{s,o} \exp(-E_{s,o} / RT_{s,o}) \quad (8)$$

A comparison between the experimental burning properties of typical AN propellants and those calculated on the basis of these equations gave very reasonable agreement. (3)

Description of the combustion mechanism for composite propellants which use ammonium perchlorate as oxidizer is still somewhat incomplete. It is postulated that the initial step in such combustion is the decomposition of the oxidizer to give NH_3 and $HClO_4$. (4,5) These products then react to establish a redox flame equivalent to that proposed for AN propellants. However, the surface temperature of AP during combustion should be much closer to that of typical binders than in the case of AN oxidizers. Increased interaction of the binder with the thermal layer envelope may result.

APPENDIX F

Chaiken and Andersen⁽⁴⁾ have discussed the role of binder and its effect on composite solid propellant combustion.

For the particular case where binder diffuses into the thermal layer and reacts suddenly at the temperature T_g , the role of binder can be considered to be one of raising the effective flame temperature, i.e.

$$T_f = T_{f,o} + \epsilon \quad (9)$$

where $T_{f,o}$ is the pure oxidizer flame temperature and ϵ is the effective increase in that flame temperature. It is noteworthy that ϵ should depend upon the diffusion coefficient, and hence be inversely proportional to the pressure. Also, there is a maximum value of ϵ such that T_f should not exceed the maximum adiabatic flame temperature for the propellant composition. This treatment is in good accord with the burning rate data of Bastress et al,⁽⁹⁾. These authors found that at higher burning pressure (~ 1000 psi), AP composite propellant burning rates approached those of pure AP (i.e., $\epsilon \rightarrow 0$ as pressure increased).

It has also been pointed out^(4,10) that preceding the decomposition of AP in combustion, small regions of the crystal undergo partial decomposition by exothermic solid phase reactions. These reactions are believed to occur in the intermosaic (defect lattice) crystal structure. Heat release by such presurface reactions would lower the overall endothermicity of the oxidizer gasification. It is still uncertain as to whether or not this effect is pressure dependent. However, from unpublished studies at Aerojet,⁽¹¹⁾ it would appear that the effect is independent of pressure at normal burning pressures (i.e., < 1500 psi).

APPENDIX F

III. APPLICATION TO A LOW PRESSURE DEFLAGRATION LIMIT

In applying the thermal layer treatment of steady-state combustion to the problem of a low pressure deflagration limit, it will be instructive to first consider the case of a monopropellant oxidizer whose surface temperature is relatively independent of pressure. In this case, the burning rate as a function of pressure is simply

$$B = \frac{b \Delta T (1 + r_o \phi P)}{r_o C} \quad (10)$$

where b , C and ΔT are constant, independent of pressure and oxidizer particle size. The function $B(P)$ represents the entire set of values of B for which solutions to the boundary value problem representing steady-state combustion exist. It is readily seen that as $P \rightarrow 0$, B approaches a minimum finite value greater than zero, i.e.,

$$B_{\min} = \frac{b \Delta T}{r_o C} \quad (11)$$

Thus B_{\min} can be considered the minimum steady-state burning rate of the propellant. Now, if one considers in the heat balance expression of equation (6) the existence of heat loss terms such as radiation, conduction, etc., it is obvious that B_{\min} will occur at some pressure $P > 0$. This pressure, which would be defined by the type of heat loss terms, would be the low pressure deflagration limit, P_{DL} . An expression for P_{DL} can be found by rewriting equation (6) (while keeping the approximations noted above) as

$$4\pi n r_o^2 \frac{b \Delta T}{\delta} = 4\pi n r_o^2 BC + H_L \quad (12)$$

where H_L is the additional heat loss term. Solving for the pressure, we have

APPENDIX F

from equation (5) for δ ,

$$P = \frac{1}{r_o \phi} \left[\frac{r_o C B}{b \Delta T} + \frac{H_L}{4\pi n r_o b \Delta T} - 1 \right] \quad (13)$$

Letting $P = P_{DL}$ at $B = B_{min}$, equations (11) and (13) yield

$$P_{DL} = \frac{H_L^i}{r_o^2 \phi b \Delta T} \quad (14)$$

where $H_L^i = H_L / 4\pi n$

It is interesting to note the P_{DL} will increase with decreasing particle size. This is in agreement with the experimental findings of Friedman and Levy⁽⁵⁾ who studied the burning of pressed AP strands. Their data also indicated that P_{DL} decreased as the initial strand temperature increased. This would be consistent with linear conductive or radiative heat losses where H_L^i would be directly proportional to $(T_s - T_o)$ or $T_s^4 - T_o^4$.

It is a relatively simple matter to extend the above treatment to composite propellants. From the arguments presented in the previous section for AP composite propellant, the expression for B_{min} would be

$$B_{min} = \frac{\sigma (T_{f,o} - T_{s,o} + \epsilon)}{r_o \rho_s [\Delta H + C_s (T_{s,o} - T_o)]} \quad (15)$$

where at $P = 0$, ϵ would be expected to take on its maximum value. If at $P = P_{DL}$, ϵ is still at its maximum value, the following expression for P_{DL} is obtained:

$$P_{DL} = \frac{H_L^i}{r_o^2 \phi (T_{f,o} - T_{s,o} + \epsilon)} \quad (16)$$

This can be easily verified by proceeding in the same manner as demonstrated above for the monopropellant case.

Thus as in the monopropellant case a decrease in oxidizer particle

Report O372-01F

APPENDIX F

size and/or a decrease in initial propellant temperature should cause an increase in P_{DL} .

Now C. Ciapluch⁽¹²⁾ has studied the extinguishment of burning propellant during a rapid pressure decrease. He found that propellants based upon coarse oxidizer particles required more rapid rates of pressure decrease to effect extinguishment than did similar propellants based upon finer oxidizer particles. That is to say, the propellant became more difficult to extinguish as the oxidizer particle size was increased. This might also be interpreted as indicating that burning was more stable at low pressures with propellants based upon the larger size oxidizer particles, and hence such propellants have a smaller value of P_{DL} . This hypothesis is in agreement with the expression derived above for P_{DL} (i. e., equation 16). If we follow the same type of reasoning, we might expect that, since ϕ for AP is believed to be greater than ϕ for AN⁽⁴⁾, AN propellants would be easier to extinguish than AP propellants. It is well known that it is difficult to obtain AN propellants which burn at low pressure.

Another point of interest with regard to the variation of propellant extinguishability with oxidizer type, is the effect of exothermic surface reaction. As indicated previously for AP propellant, such reactions can be considered to effectively decrease the overall endothermicity of the oxidizer surface pyrolysis reaction. Alternatively, exothermic surface (or substrate) reactions can be considered as heat sources within the oxidizer which in effect act in an opposite manner to the heat loss terms, i. e., they will cause a decrease in the value of H_L' in equation 16. Thus, it might be expected that propellants based upon oxidizers (or binders), which will undergo partial exothermic reaction in the solid-phase, will have a low P_{DL} , and hence will

APPENDIX F

resist extinguishment by a rapid pressure decrease.

IV. CONCLUSIONS

The theoretical development of the low pressure deflagration limit in the previous section, and the hypothesis relating extinguishability and low pressure burning stability to P_{DL} appear to be in satisfactory agreement with the available experimental data, and therefore suggests the validity of the approach employed. One might even speculate further that ignitability, being in a sense the opposite of extinguishability, should also be related to P_{DL} in a manner just opposite to that suggested for pressure drop extinguishment of burning propellants. That is to say, that a propellant with a high P_{DL} would be more difficult to ignite than a propellant with a lower P_{DL} . The difficulty in igniting AN propellants relative to AP propellants is certainly in agreement with such a speculation. However, it should be pointed out that a proper theoretical treatment of transient phenomena such as propellant ignition and extinguishment must rightly consider time dependence in the conservation equations, and this might lead to results which are considerably different from those implied in this paper.

Report 0372-01F

APPENDIX F

REFERENCES

1. D. W. Blair, E. K. Bastress, C. E. Hermance, K. P. Hall and M. Summerfield, Progress in Astronautics and Rocketry, Volume I, Solid Propellant Rocket Research, Academic Press, New York, 1960, p 183-206.
2. W. H. Andersen, K. W. Bills, E. Mishuck, G. Moe, and R. D. Schultz, "A Model Describing Combustion of Solid Composite Propellants; Application to Ammonium Nitrate," Combustion and Flame, 3, 301 (1959).
3. R. F. Chaiken, "A Thermal Layer Mechanism of Combustion of Solid Propellants; Application to Ammonium Nitrate Propellants," Combustion and Flame, 3, 285(1959).
4. R. F. Chaiken and W. H. Andersen, "The Role of Binder in Composite Propellant Combustion," Progress in Astronautics and Rocketry, Volume I, Solid Propellant Rocket Research, Academic Press, New York, 1960, p 227-249.
5. R. Friedman, J. B. Levy, and K. E. Rumble, AFOSR-TN-59-173 (February 5, 1959).
6. W. Nachbar, Progress in Astronautics and Rocketry, Volume I, Solid Propellant Rocket Research, Academic Press, New York, 1960, p 206-226.
7. W. E. Johnson and W. Nachbar, Eighth Symposium (International) on Combustion, Williams and Wilkins Co., Baltimore, Maryland, 1962, p 678-689.
8. R. D. Schultz, L. Green and S. S. Penner, Combustion and Propulsion, Pergamon Press, New York (1958) p 367-420.
9. E. K. Bastress, K. P. Hall and M. Summerfield, ARS Solid Propellant Rocket Conference, February 1961, Salt Lake City, Utah, Paper No. 1597.
10. W. H. Andersen and R. F. Chaiken, "On the Detonability of Solid Composite Propellants," ARS Journal, 31, 1379 (1961).
11. Aerojet-General Corporation Quarterly Project Report No. 0372-01-12, Contract AF 49(638)-851, 31 December 1962 (Unclassified).
12. C. C. Ciepluch, NASATN-D1559 (December 1962).

APPENDIX G

LIST OF PERTINENT PUBLICATIONS

I. OPEN LITERATURE

A. CONTRACT AF 18(600)-1026

R. D. Schultz and A. O. Dekker, "The Absolute Thermal Decomposition Rates of Solids", Part I, Fifth Symposium (International) on Combustion, Reinhold, New York (1955), p. 260.

R. D. Schultz and A. O. Dekker, "The Absolute Decomposition Rates of Solids", Part II, J. Chem. Phys., 23, 2133-38 (1955).

R. D. Schultz and A. O. Dekker, "The Effect of Physical Adsorption on the Absolute Decomposition Rates of Crystalline Ammonium Chloride and Cupric Sulfate Trihydrate", J. Phys. Chem., 60, 1095 (1956).

R. D. Schultz and A. O. Dekker, "Transition-State Theory of the Linear Rate of Decomposition of Ammonium Perchlorate", Sixth Symposium (International) on Combustion, Reinhold, New York (1957), p. 618.

B. CONTRACT AF 18(603)-74

M. K. Barsh, W. H. Andersen, K. W. Bills, G. Moe and R. D. Schultz, "An Improved Instrument for the Measurement of Linear Pyrolysis Rates", Rev. Sci. Instr., 29, 392 (1958).

W. H. Andersen, K. W. Bills, A. O. Dekker, E. Mishuck, G. Moe, and R. D. Schultz, "The Gasification of Solid Ammonium Nitrate", Jet Propulsion, 28, 831 (1958).

APPENDIX G

W. H. Andersen and R. F. Chaiken, "Application of Surface Decomposition Kinetics to Detonation of Ammonium Nitrate", AIChE Journal, 29, 49 (1959).

R. F. Chaiken and D. K. Van de Mark, "Thermocouple Junction for Hot-Plate Linear Pyrolysis Apparatus", Rev. Sci. Instr., 30, 375 (1959).

R. F. Chaiken, W. H. Andersen, M. K. Barsh, E. Mishuck, G. Moe, and R. D. Schultz, "Kinetics of the Surface Degradation of Polymethylmethacrylate", J. Chem. Phys., 32, 141 (1960).

C. CONTRACT AF 49(638)-566

R. F. Chaiken and W. H. Andersen, "The Role of Binder in Composite Propellant Combustion", Progress in Astronautics and Rocketry, Volume I, Solid Propellant Rocket Research, Academic Press, New York, 1960, p. 227-249.

D. CONTRACT NOnr 2804(00)

R. F. Chaiken, "Comments on Hypervelocity Wave Phenomena in Condensed Explosives", J. Chem. Phys., 33, 760-761 (1960).

E. CONTRACT AF 49(638)-851

R. F. Chaiken, D. J. Sibbett, J. E. Sutherland, D. K. Van de Mark and A. Wheeler, "The Rate of Sublimation of Ammonium Halides", J. Chem. Phys., 37, 2311 (1962).

APPENDIX G

F. RELATED PERTINENT PUBLICATIONS

R. D. Schultz, L. Green, and S. S. Penner, "Studies of the Decomposition Mechanism, Erosive Burning, Sonance and Resonance for Solid Composite Propellants", Combustion and Premixion, Pergamon Press, New York (1958), p. 367-420.

W. H. Andersen, K. W. Bills, E. Mishuck, G. Moe, and R. D. Schultz, "A Model Describing Combustion of Solid Composite Propellants; Application to Ammonium Nitrate", Combustion and Flame, 3, 301 (1959).

R. F. Chaiken, "A Thermal Layer Mechanism of Combustion of Solid Composite Propellants; Application to Ammonium Nitrate Propellants", Combustion and Flame, 3, 285 (1959).

R. F. Chaiken, "A Kinetic Approach to Detonation of Homogeneous High Explosives", Eighth Symposium (International) of Combustion, California Institute of Technology, Pasadena, Calif., August 29 - September 2, 1960, Paper No. 104.

II. TECHNICAL NOTES AND REPORTS (UNCLASSIFIED)

A. CONTRACT AF 18(600)-1026

R. D. Schultz and A. O. Dekker, "The Absolute Decomposition Rates of Solids"

- a. Part I, OSR-TN-54-127 (1954)
- b. Part II, OSR-TN-54-367 (1954)
- c. Part III, OSR-TN-55-138 (1955)
- d. Part IV, OSR-TN-55-141 (1955)

Report O372-01F

APPENDIX G

R. D. Schultz and A. O. Dekker, "Transition State Theory of the Linear Rate of Decomposition of Ammonium Perchlorate", OSR-TN-55-142 (1955).

K. W. Bills, M. Therneau, E. Mishuck, and R. D. Schultz, "The Linear Vaporization Rate of Solid Ammonium Chloride", OSR-TN-55-117 (1955).

R. D. Schultz and A. O. Dekker, "Advances in the Kinetics of Decomposition, Fusion, and Sublimation of Solids", OSR-TR-55-12; Final Report, Contract AF 18(600)-1026, April 1955.

B. CONTRACT AF 18(603)-74

M. K. Barsh, "An Improved Instrument for the Measurement of Linear Pyrolysis Rates of Solids", AFOSR-TN-57-513 (1957).

W. H. Andersen and R. F. Chaiken, "Application of Surface Decomposition Kinetics to Detonation of Ammonium Nitrate", AFOSR-TN-58-617 (1958).

R. F. Chaiken, W. H. Andersen, M. K. Barsh, E. Mishuck, G. Moe, and R. D. Schultz, "Kinetics of the Surface Degradation of Polymethylmethacrylate", AFOSR-TN-59-619 (1959).

C. CONTRACT AF 49(638)-573

R. F. Chaiken, I. Geller, J. E. Sutherland, and A. Wheeler, "Study of the Kinetics of Solid Phase Reactions", AFOSR-TR-60-44, March 1960; Summary Final Report.

Report 0372-01F

APPENDIX G

D. CONTRACT AF 49(638)-566

R. F. Chaiken and W. H. Andersen, "The Role of Binder in Composite Propellant Combustion", AFOSR-TN-59-540, ASTIA Document No. AD 216-557; Aerojet Report TN-30, July 1959.

D. J. Sibbett, and J. M. Lobato, "Investigation of the Mechanism of Combustion of Composite Solid Propellants", AFOSR-TN-60-64, April 1960; Summary Final Report.

E. CONTRACT NOnr 2804(00)

R. F. Chaiken and K. J. Schneider, "Research on Mechanisms of Detonation Processes", Report No. 1772, Contract NOnr 2804(00), U.S. Navy, Office of Naval Research, Washington, D. C., 15 March 1960; Summary Report.